

INVESTIGATION INTO THE CELLULAR RADIOSENSITIVITY  
OF THE LEC RAT  
AND ANALYSIS OF CANDIDATE GENES

Dissertation  
zur Erlangung des Doktorgrades  
der Fakultät für Biologie  
der Ludwig-Maximilians-Universität  
München  
Vorgelegt von  
Alesia Ivashkevich aus Aspa, Russland  
am 16 Juni 2008

2008

1. Berichterstatter: Prof. Dr. F. Eckardt-Schupp

2. Berichterstatter: PD Dr. Anna A. Friedl

Betreuer: Dr. M. Rosemann

Tag der mündlichen Prüfung: 19 Dezember 2008

## **Ehrenwörtliche Versicherung**

Ich versichere, dass die Dissertation von mir selbständig und ohne unerlaubte Hilfsmittel angefertigt wurde. Die Dissertation habe ich keiner anderen Fakultät oder Universität zur Prüfung vorgelegt. Außerdem habe ich noch nicht versucht, eine Dissertation einzureichen oder mich einer Doktorprüfung zu unterziehen.

Die Arbeit wurde von Dr. Michael Rosemann, Helmholtz Center Munich, Institute for Radiation Biology, Neuherberg, betreut.

Melbourne, May 2008

Alesia Ivashkevich

*The most beautiful thing we can experience is the mysterious. It is the source of all true art and science*

*Albert Einstein (1879-1955)*

*The important thing in science is not so much to obtain new facts as to discover new ways of thinking about them*

*Sir William Bragg (1862 – 1942)*

...dedicated to my family

## ACKNOWLEDGEMENTS

I would like to thank everyone who was involved in the successful completion of this work.

The Institute of Pathology for providing me the possibility to conduct my PhD Thesis and gain a valuable experience in scientific research during this time.

Special thanks to:

Prof. Dr. Friederike Eckardt-Schupp for scientific supervision, many fruitful discussions and encouragement.

Prof. Dr. Michael J. Atkinson, Dr. Michael Rosemann and Prof. Dr. Summer for providing an interesting topic for my project, which attracts great interest in the field of radiobiology and their support during my time at the Institute.

Furthermore, I would like to thank Dr. Anna Friedl, Dr. Beisker, Dr. Maria Gomolka, Dr. Tom Meindl, and Dr. Guido Drexler for many discussions and comments on my work.

Josef Lichtmanneger, Bahar Sanli-Bonazzi for their help with lots of RT-PCR and sequencing and even more important, for cheering me up.

All other colleagues from the Institutes of Pathology, Toxicology and Radiobiology, at the GSF for their collaboration and professional help.

Last but not least I would like to thank my family, and friends for their cordial encouragement and emotional involvement in the process of my experimental work and writing of my thesis.

# OUTLINE

<b>OUTLINE .....</b>	<b>VI</b>
<b>ABSTRACT.....</b>	<b>- 1 -</b>
<b>I. INTRODUCTION.....</b>	<b>- 3 -</b>
1.1 RADIOSENSITIVITY .....	- 4 -
1.1.1 Radiation effects in tissues and organs: stochastic versus deterministic and acute versus chronic effects.....	- 4 -
1.1.2 Effects of acute total body irradiation at the level of the organism. Definition of the Lethal Dose in human and rodents .....	- 5 -
1.1.3 Physical and biological effects of ionizing radiation at the cellular level .....	- 6 -
1.1.4 Experimental end-points to measure cellular sensitivity in vitro .....	- 8 -
1.1.5 Radiotherapy related aspects of radiation sensitivity .....	- 9 -
1.1.6 Molecular basis of radiosensitivity .....	- 10 -
1.1.7 Experimental models of radiosensitivity.....	- 13 -
1.2 LEC RAT – A RODENT MODEL OF HUMAN DISEASES .....	- 14 -
1.2.1 Presence of pathogenic mutations.....	- 15 -
1.2.2 Radiosensitivity in LEC rat.....	- 15 -
1.2.3 Sensitivity to radiation and chemical agents in strains related to LEC rat - LEA and LE rats.....	- 22 -
1.3 THE AIMS OF THE STUDY.....	- 23 -
<b>II. MATERIALS AND METHODS.....</b>	<b>- 24 -</b>
2.1 MATERIALS.....	- 24 -
2.1.1 Equipment.....	- 24 -
2.1.2 Consumable materials and chemicals .....	- 24 -
2.1.3 Rat strains.....	- 26 -
2.1.4 Kits and reagents .....	- 26 -
2.1.5 Length standards .....	- 26 -
2.1.6 Enzymes.....	- 26 -
2.1.7 Oligonucleotides .....	- 27 -
2.1.8 Antibodies .....	- 29 -
2.1.9 Buffers.....	- 29 -
2.1.10 Software.....	- 31 -
2.1.11 Bioinformatic resources .....	- 31 -
2.2 METHODS .....	- 32 -
2.2.1 Rat strains.....	- 32 -
2.2.2 Establishment and cultivation of fibroblasts .....	- 32 -
2.2.3 The experimental systems .....	- 33 -
2.2.4 Growth curves.....	- 34 -
2.2.5 Clonogenic survival assay.....	- 35 -
2.2.6 Pulsed field gel electrophoresis.....	- 38 -
2.2.7 Analysis of $\gamma$ H2AX foci.....	- 47 -
2.2.8 Comet assay .....	- 51 -
2.2.9 Cell cycle analysis.....	- 55 -
2.2.10 General molecular biology methods .....	- 58 -
2.2.11 SYBR Green Real-Time PCR detection .....	- 64 -
<b>III. RESULTS.....</b>	<b>- 70 -</b>
3.1 MORPHOLOGY AND GROWTH OF FIBROBLASTS .....	- 70 -
3.2 CLONOGENIC SURVIVAL ASSAY .....	- 74 -
3.3 PULSED FIELD GEL ELECTROPHORESIS .....	- 78 -
3.3.1 Induction curves.....	- 81 -

3.3.2	Analysis of repair data expressed in FAR.....	- 82 -
3.3.3	Analysis of repair data expressed in Gy-equivalents .....	- 83 -
3.3.4	Analysis of repair kinetics.....	- 85 -
3.4	γH2AX FOCI QUANTIFICATION .....	- 86 -
3.5	COMET ASSAY.....	- 89 -
3.6	CELL CYCLE PROGRESSION .....	- 94 -
3.7.	GENETIC ANALYSIS OF LOCUS OF INTEREST IN LEC VERSUS LE RAT. ESTABLISHMENT OF CANDIDATE GENE(S).....	- 96 -
3.7.1	Sequencing analysis of Rad18, v-Raf-1, XPC and Fancd2 genes .....	- 96 -
3.7.2	Real-time PCR .....	- 101 -
3.7.3	Establishment of further candidate genes.....	- 103 -
3.7.4	Analysis of the Gata-2 gene .....	- 106 -
<b>IV.</b>	<b>DISCUSSION .....</b>	<b>- 112 -</b>
4.1	INVESTIGATION OF GROWTH CHARACTERISTICS IN LEC AND LE FIBROBLASTS.....	- 113 -
4.2	CLONOGENIC ASSAY .....	- 114 -
4.3	INDUCTION OF DNA DAMAGE.....	- 118 -
4.4	REPAIR OF DSB .....	- 118 -
4.5	H2AX PHOSPHORYLATION .....	- 119 -
4.6	COMET ASSAY.....	- 120 -
4.7	REGULATION OF CELL CYCLE PROGRESSION .....	- 120 -
4.8	DISCREPANCY IN OBSERVATIONS OF THE CELLULAR RADIATION SENSITIVITY PHENOTYPE AND CELL CYCLE PROGRESSION OF LEC CELLS .....	- 122 -
4.9	REPAIR CAPACITY AND RADIOSENSITIVITY IN LEC.....	- 122 -
4.10	ANALYSIS OF CANDIDATE GENES .....	- 125 -
	<b>FINAL SUMMARY AND CONCLUSIONS .....</b>	<b>- 128 -</b>
	<b>REFERENCES.....</b>	<b>- 131 -</b>
	<b>ABBREVIATIONS .....</b>	<b>- 144 -</b>
	<b>APPENDIX.....</b>	<b>- 145 -</b>

## ABSTRACT

Recent work has underlined the importance of animal models in discovery and characterisation of molecular mechanisms determining radiosensitivity and radioresistance. Enhanced sensitivity of LEC rats to ionizing radiation in terms of the acute radiation syndrome was investigated in the present work on the cellular level and compared to that of LE rats. To understand the molecular basis for the increased radiation sensitivity a series of studies were performed, which included the classical clonogenic survival assay, investigation of double strand break repair by means of PFGE and  $\gamma$ H2AX evaluation, comet assay for evaluation of repair of single strand breaks and alkaline labile sites, and analysis of cell cycle progression of asynchronous fibroblast population. Survival assay, PFGE, and  $\gamma$ H2AX analysis were performed in a standardised experimental system - confluent fibroblasts, synchronized in G1 phase of cell cycle, and comet assays were performed in G0 lymphocytes. The data suggests a mild radiosensitization of LEC fibroblasts compared to LE. The results of studies using the selected model did not reflect the degree of animal sensitivity on the molecular level, since values of dose modifying factor (DMF) were much lower in fibroblasts (DMF<sub>2</sub> = 1.32) compared to that of animal sensitivity (DMF = 2.36 for bone marrow syndrome (LD<sub>50/30</sub>) and DMF = 1.95 of intestinal death (LD<sub>50/7</sub>)). The investigation of DNA repair and cell cycle did not reveal a significant defect in the studied pathways in synchronized fibroblasts and cell cycle progression was not different from wild type cells. The presented data contradict the published LEC cellular phenotype.

Of the possible candidate genes, which are located in the radiosensitivity locus, several were further analysed. Among those, *Gata-2* appeared to be the most promising of the positional and functional candidates. However, no mutation in the coding sequence could be identified and mRNA expression levels were similar between control and LEC cells. The presented data suggests that radiosensitivity of LEC rats might be attributed to a mechanism specific for certain target tissue, like bone marrow, or enhanced in cell cycle stages other than G0/G1.

## ZUSAMMENFASSUNG

Tiermodelle sind ein wichtiges Instrument zur Erforschung von Strahlensensibilität und Strahlenresistenz. In der vorliegenden Arbeit wurde ein solches Modell mit erhöhter Sensibilität gegenüber ionisierender Strahlung im Hinblick auf das akute Strahlungssyndrom, die LEC Ratte, auf zellulärer Ebene untersucht und mit der LE Ratte verglichen. Um die molekulare Basis für die erhöhte Strahlensensibilität besser zu verstehen, wurde eine Reihe verschiedener Experimente durchgeführt, unter anderem der klassische Clonogenic Survival-assay, die Untersuchung der DNS-Doppelstrangbruch-Reparatur-Rate mit Hilfe von Pulsed-field Gelelektrophorese und Messung von  $\gamma$ H2AX, Mikrogelelektrophorese (Comet-assay) zur Analyse von Einzelstrangbrüchen und alkalilabile Stellen, sowie die Analyse des Zellzyklus in asynchronen Fibroblastenkulturen. Für den Survival-assay, die Pulsed-field Gelelektrophorese und die  $\gamma$ H2AX Messung wurde ein standardisierter Versuchsaufbau verwendet. Dazu wurden konflüente Fibroblastenkulturen, die sich in der G1-Phase des Zellzyklus befanden, benutzt. Die Mikrogelelektrophorese wurde mit Lymphozyten in der G0-Phase durchgeführt. Die ermittelten Daten lassen auf eine leicht erhöhte Strahlensensibilität von LEC Fibroblasten im Vergleich zu LE Fibroblasten schließen. Jedoch konnten mit diesem Versuchsmodell die im Tiermodell erzielten Ergebnisse auf molekularer Ebene nicht bestätigt werden, da der Wert für die dosismodifizierenden Faktoren (DMF) in Fibroblasten (DMF2 = 1.32) im Vergleich deutlich niedriger war als im Tiermodell (DMF = 2.36 für das Knochenmarksyndrom (LD<sub>50/30</sub>) und DMF = 1.95 für das gastrointestinale Syndrom (LD<sub>50/7</sub>)). Die Analyse der DNS-Reparatur-Rate und des Zellzyklus zeigte keinen signifikanten Defekt in den untersuchten Pathways in den synchronen Fibroblasten. Auch der Ablauf des Zellzyklus war unauffällig im Vergleich zu Wildtyp-Zellen. Die in dieser Arbeit gezeigten Ergebnisse widersprechen dem bereits veröffentlichten zellulären LEC Phänotyp.

Mehrere Kandidatengene, die in dem Strahlensensibilitätslocus enthalten sind, wurden näher untersucht. Von diesen erschien *Gata-2* aufgrund seiner Position und beschriebenen Funktion am aussichtsreichsten zu sein. Jedoch konnten weder Mutationen in der proteinkodierenden Sequenz noch Unterschiede der *Gata-2* Genexpression im Vergleich zur Kontrolle nachgewiesen werden. Die in der vorliegenden Arbeit erzielten Ergebnisse bezüglich der Strahlensensibilität der LEC Ratten deuten auf einen bisher nicht entdeckten gewebespezifischen Mechanismus hin. Allerdings kann auch eine verstärkte Sensitivität in anderen als den G0- beziehungsweise G1-Phasen des Zellzyklus nicht ausgeschlossen werden.

## I. INTRODUCTION

By 1900, five years after the discovery of x-rays by Roentgen, most of the medical and scientific community understood that the widespread and uncontrolled use of x-rays caused damage in susceptible organs/tissues of the human body.

Under certain circumstances a person, group of people or even an entire population might be chronically or acutely exposed to ionizing radiation (IR) and suffer from acquired damage. Nuclear bombings of Hiroshima and Nagasaki by the USA during World War II in 1945 are examples for nuclear warfare. Nuclear reactor accidents, such as Chernobyl reactor accident in 1986, affected staff, clean-up workers, and the population of the region. Radiation poisoning can also result from accidental exposure to industrial radiation sources, as it happened in Goiania, Brazil in 1987 [1]. There are also natural sources of IR, such as cosmic and radiation from elements present in the earth's crust (for example radon). Another example, cancer treatment with IR (radiotherapy) is causing damage not only in cancer, but also in healthy tissues of a patient.

However, not all individuals react in the same way to IR. The underlying genetic causes of such variability in one rat model are the subject of this thesis.

THE AIM OF THE STUDY was the investigation of the radiation response pathways in the LEC rat strain, which is highly sensitive to total body irradiation. The work included the characterization of this radiosensitivity at the cellular level. Radiosensitivity, repair, cell cycle response to IR, and candidate genes at the defined locus were all investigated.

## 1.1 Radiosensitivity

Radiosensitivity is the *relative* susceptibility of cells, tissues, organs, or organisms to the harmful effect of IR. The same dose of IR causes differential effects determined by the genetic and functional characteristics of the ‘targeted’ type of cells, tissues, organs or organisms.

Radiobiological research includes investigation of the factors, which cause the different severity of damage induced by the same dose of IR. This knowledge is important in both planning of radiation therapy and in radiation protection.

### 1.1.1 Radiation effects in tissues and organs: stochastic versus deterministic and acute versus chronic effects

IR causes detrimental radiation effects on tissue level [2]. Effects, which occur only if the dose or dose rate is greater than threshold value and affect all individuals in the exposed group equally, are called deterministic (for example cataracts). Other types of effects are stochastic effects, which are not certain to occur, but the likelihood of their occurrence increases with the dose, whereas their timing and severity does not depend on the dose. The most important of such stochastic effects are cancer and heritable germ cell mutations. For most of stochastic effects, such as cancer, radiation is not the only known cause, and it is normally impossible to determine whether an individual condition is the result of radiation exposure or not [2].

Depending on the time of occurrence, an organ or tissue expresses response to radiation damage either as an acute effect or as a late (chronic) reaction. Acute reactions appear within 90 days after exposure to radiation and are characterized by inflammation, oedema, denudation of epithelia, leukopenia and haemorrhage. Late reactions occur after 3 months up to many years. Late reactions may be caused by the absorption of radiation directly in the target tissue, or consequential to acute damage in overlying tissues such as mucosa or the epidermis, which are affected most often. The induction of secondary tumors is also observed [3].

## **1.1.2 Effects of acute total body irradiation at the level of the organism. Definition of the Lethal Dose in human and rodents**

The response of an organism to acute total body radiation exposure is influenced by the combined response to radiation of all organs and cell types. Depending on the actual total body dose, the response in mammals is described as one of three known specific acute radiation (AR) syndromes. The main reason for AR syndrome to occur is damage to the stem cells of bone marrow and intestine. At higher dose the damage becomes so intensive that the organism cannot reconstitute the lost population of stem cells, what leads to secondary effects and death. The three classic AR syndromes are bone marrow syndrome, gastrointestinal and cardiovascular syndromes [3].

The full bone marrow syndrome occurs after a dose between 0.7 and 10 Gy, though mild symptoms may occur after a dose of 0.3 Gy. Onset occurs 1 hour to 2 days after exposure. The primary cause of death is the destruction of the bone marrow stem cells, resulting in infection and haemorrhage. The exact timing of death events varies between species. In humans the death from haematological damage occurs at around 30 days after exposure and happens in further time of 60 days. In smaller animals peak incidence of death caused by bone marrow syndrome occurs starting from 10 to 15 days after exposure and ends by 30 days. That is why in animal models for estimation of death resulting from bone marrow failure (Lethal Dose) LD<sub>50/30</sub> (dose, necessary to kill 50% of animals in 30 days) is applied, and in humans the LD<sub>50/60</sub> (the dose necessary to kill 50% of the exposed population in 60 days) is commonly used. The LD<sub>50/60</sub> is about 2.5 to 5 Gy.

The full gastrointestinal syndrome (GI) happens after a dose greater than approximately 10 Gy although some symptoms may occur after irradiation with a dose of 6 Gy. Onset happens within a few hours after exposure as the result of death of stem cells in the bone marrow and cells lining the gastrointestinal tract. Death usually occurs within 2 weeks of exposure due to infection, dehydration, and electrolyte imbalance. In humans the LD<sub>100/60</sub> (the dose necessary to kill 100% of the exposed population in 60 days) is accepted as measure of death due to GI, and is about 10 Gy [3]. In rodents, the denudation of the intestine (loss of the cells from the upper layer) happens twice as fast as in humans, that is why the estimated LD due to intestinal syndrome is LD<sub>50/7</sub> (dose of IR, necessary to kill 50% of animals in 7 days).

The full cardiovascular / central nervous system syndrome usually occurs after a dose greater than approximately 50 Gy although some symptoms may develop after doses of 20 Gy. Onset happens within minutes of exposure. Death occurs within 3 days due to collapse of the circulatory system as well as increased pressure in the confining cranial vault caused by oedema, vasculitis, and meningitis.

### **1.1.3 Physical and biological effects of ionizing radiation at the cellular level**

When cells are exposed to IR, the interaction between radiation and the atoms or molecules of the cells (energy deposition and ionization events) takes place first and the effect on cell functions and/or cellular death follows later.

Physical effects of IR include direct and indirect action. In direct action the radiation interacts with the atoms (molecules) of the critical target in the cell and induces ionisation or excites it through Coulomb interactions, leading to the chain of physical and chemical events that eventually produce the biological damage. Direct action is the dominant process in the interaction of high Linear Energy Transfer (LET) particles with biological material [2, 3].

In indirect action the radiation interacts with other molecules (mainly water) within the cell. As the result of this interaction, short lived but extremely reactive free radicals such as  $\text{H}_2\text{O}^+$  (water ion) and  $\text{OH}^\cdot$  (hydroxyl radical),  $\text{O}_2^\cdot$  (superoxide radical),  $\text{H}_2\text{O}_2$  (hydrogen peroxide) are produced, which can, through diffusion in the cell, damage the critical targets within the cell. About two thirds of the biological damage by low LET radiations (sparsely ionizing radiations) such as X rays or electrons occurs due to indirect action.

The mechanism of induction of damage in DNA molecules, which are considered the critical targets in the cell, as well as structural changes in bases after exposure to oxidative stress have been comprehensively reviewed elsewhere [4, 5]. More than 20 different types of base damage have been identified after exposure to oxidative stress. It is known that even without action of IR more than  $10^4$  DNA lesions occur in each mammalian cell each day from spontaneous decay, replication errors and cellular metabolism alone [6]. Single strand breaks

(SSB) and double strand breaks (DSB) might be induced directly by IR or may arise as the result of conversion of the base damage [7].

The primary defence against reactive oxygen species (ROS) includes enzymes like superoxide dismutase, catalase, and a large number of other factors such as antioxidant amino acids (e.g., arginine), vitamins (e.g. vitamins A, C and E), thiols (especially glutathione), and polyphenols [8]. As a second line of defence, incorporation of damaged bases into DNA is prevented by enzymes that hydrolyse oxidised dNTPs (e.g. 8-oxoGTP) to the corresponding dNMPs. The third line of defence is repair of oxidative damage, SSB and DSB in DNA by a complex network of DNA repair mechanisms. Base excision repair (BER), transcription-coupled repair (TCR), global genome repair (GGR), mismatch repair (MMR), translesion synthesis (TLS), homologous recombination (HR), and non-homologous end-joining (NHEJ) all contribute to repair of DNA damage [8].

DSB were shown to be the most genotoxic type of damage [9, 10]. Most of the induced lesions in wild-type mammalian cells can be repaired and only a small fraction is non-repairable. It is commonly believed that the majority of the non-repairable lesions are DSB and clustered damage while single-strand lesions are considered to be accurately repaired [9].

A central dogma in radiation biology has been that energy from radiation must be deposited into the cell nucleus to generate a biological effect - 'targeted effect', but recent studies show that damage to the cellular membrane induces signalling cascades, which can cause cellular death [11]. Biological effects of IR occur due to damage to cellular components and result in defect/loss of cellular function, proliferative (clonogenic) death/senescence, cellular death, and mutagenesis.

It is shown [7] that the difference in cellular radiosensitivity results from differences in efficiency and/or accuracy of DNA repair and that DSB is the lesion most likely to be the cause of the lethal effects on cellular level. According to Tounekti *et al.*, 2001 [9] the study of bleomycin (a radiomimetic drug) toxicity demonstrates that DSB are intrinsically 300 times more cytotoxic than SSB. DSB also arise endogenously during DNA replication or as initiators of programmed processes, such as V(D)J recombination and meiotic exchange. If left unrepaired, DSB can result in permanent cell cycle arrest, induction of apoptosis, or mitotic cell death caused

by loss of genomic material; if repaired incorrectly, they can lead to carcinogenesis through translocations, inversions, or deletions. DSB are the precursor lesions for the formation of chromosome aberrations by IR [12]. New arising DSB indicate DNA disintegration, which accompany a necrotic or apoptotic type of cell death [12].

Micronuclei and chromosomal rearrangements result from non-repaired or mis-repaired DNA damage induced by IR [13]. Among chromosomal aberrations dicentric chromosomes are generally not compatible with the survival of normal cells, but other cytogenetic changes (translocations, inversions and insertions) are not so cytotoxic in terms of cell death [14]. Rave-Fränk *et al.*, 2001 [15] have shown that radiosensitivity in fibroblasts was correlated with an increase in radiation-induced excess acentric fragments, which result mostly from unrepaired or misrepaired DSB.

Depending on the damage extent and ability of damaged cell to cope with it, damage may lead to defect/loss of cellular function, senescence, cessation of proliferation, cellular death (apoptosis/necrosis), and mutagenesis, which may cause genomic instability (GI) [16]. GI arises at delayed times after exposure and in the progeny of exposed cells many generations after the original damage. GI usually means chromosomal aberrations, changes in the ploidy, micronuclei formation, gene mutations and amplifications, microsatellite instabilities and/or decreased plating efficiency, and abnormal clonal morphology [16-19]. Recent studies have demonstrated non-targeted genotoxic effects in which the DNA is not directly exposed to radiation [20, 21]. These effects take place in cells that are the descendants of irradiated cells and include GI, or in cells that are in contact with irradiated cells or receive certain signals from irradiated cells, for example the activating cyclooxygenase-2 signalling cascade (radiation-induced bystander effects) [22].

#### **1.1.4 Experimental end-points to measure cellular sensitivity *in vitro***

Different cell functions, such as cell survival, repair capacity, formation of chromosomal aberrations and apoptosis, are affected by individual radiosensitivity. An *in vitro* assay normally measures only one or a few particular cell functions - just a fraction of the possible expression of the underlying susceptibility, even if there are many cellular pathways functioning in radiation response [11]. Burnet *et al.*, 1995 [23] have shown a correlation between intrinsic cellular

radiosensitivity using clonogenic assays and different late tissue reactions. A number of tests have been described and used to assess individual radiosensitivity, which have a practical importance in particular in the radiotherapy field [24].

The existing experimental end-points allow measurement of cellular death, repair of DNA damage and include [11, 24]:

- measurement of induction of cellular death (loss of metabolic activity)
- apoptosis (programmed cell death)
- clonogenic survival assay, which estimates delayed reproductive cell death - progeny of irradiated cells show reduced clonogenic survival compared with unirradiated cells. Several types of chromosomal rearrangements (for example dicentric chromosomes) are generally involved in delayed reproductive death in normal cells
- evaluation of DNA repair capacity applying pulsed field gel electrophoresis (PFGE), neutral and alkaline comet assay, measurement of H2AX phosphorylation
- evaluation of cytogenetic effects, micronuclei, chromosomal aberrations and chromosomal instability.

### **1.1.5 Radiotherapy related aspects of radiation sensitivity**

Cases of hypersensitivity to IR have been known to radiation oncologists for many years. Patients receiving identical radiation treatments develop different reactions in normal tissues, varying from undetectable to severe. Around 5-7% of cancer patients develop adverse side-effects to external radiation therapy within the treatment field in normal tissues [25]. These effects are referred to as 'clinical radiation reactions' and include acute reactions, which appear during or shortly after radiotherapy (e.g. erythema, nausea) and late normal tissue effects, which develop months or years later (e.g. fibrosis, telangiectasia) (see **1.1.1, Radiation effects in tissues and organs: stochastic versus deterministic and acute versus chronic**). Several patient- and treatment-related factors influence the variability of these side-effects, but up to 70% of cases remain unexplained [25]. Study [26] showed that the patient-to-patient variability of

fibroblast radiosensitivity was significantly correlated with the occurrence of subcutaneous fibrosis.

### **1.1.6 Molecular basis of radiosensitivity**

Recent progress in the field of gene identification and expression studies [11] has attracted greater attention to identification and characterization of underlying mechanisms of the genetic and epigenetic susceptibility of normal tissues to radiation damage, which is particularly important in the radiotherapy field for the optimisation of the treatment planning. The molecular pathways, responsible for the increase in sensitivity to the total body irradiation of mouse knock-outs of certain repair genes and genes involved in conservation of genomic stability, sensitivity of their fibroblasts/lymphocytes, have been studied intensively [24, 27-39].

Depending on the investigated system, there are different criteria characterizing radiation induced damage. The sensitivity of animals to the total body irradiation is expressed as LD<sub>50/30</sub>, LD<sub>50/7</sub> (described earlier). There are several classification systems for classification of the extent of side effects in radiotherapy patients [40, 41]. Measurements of cellular sensitivity performed with clonogenic assay result in values of survival fraction (SF) and parameters characterizing the survival curve -  $\alpha$  and  $\beta$ . Outcome of repair assays are kinetics of repair and amount of repaired damage at measured times after irradiation.

Mutations affecting genes, which are involved in DNA repair pathways [27, 42] often lead to an increase in radiosensitivity. The first association between a defect in DNA repair, radiosensitivity and cancer was established by Cleaver in 1968 [43] who showed that xeroderma pigmentosum (XP) is caused by deficient nucleotide excision repair (NER). For approximately 25 years, it was thought that only rare cancer syndromes, such as XP, Cockayne syndrome and ataxia teleangiectasia (AT) are associated with DNA repair defects. Now it is clear that some of the most common hereditary forms of cancer are also associated with defects in DNA repair and radiosensitivity [11]. A number of human genetic disorders, caused by defects in the response to DNA damage, are associated with defects in immune and neurological systems, higher incidence of cancer, and increased sensitivity to IR and ultraviolet (UV) (reviewed in [11]). They result mostly from mutations in genes involved in any of the DNA repair pathways, DNA damage

signalling pathways, cell cycle, and transcription. Examples of such conditions are Nijmegen breakage syndrome (NBS) [44, 45], Fanconi anaemia (FA) [46-48], Bloom's syndrome (BS) [49, 50], and others [11].

So far about 150 human DNA repair genes have been identified, but the real number is probably higher, since function of a significant part of known and putative genes in human genome has not been described yet [51, 52]. DNA repair is integrated within cell cycle regulation, transcription and replication, and may use, in part, common factors [53-55]. Also the role of processes, associated with DNA repair, starts to emerge. Such processes are functioning of chromatin remodelling complexes (changing the access of repair components to damaged sites), cohesins and cohesin-loading complexes (mediating the availability of homologous chromosome in homologous recombination, holding the broken ends together), and the proteasome [56, 57].

Repair of DSB, which are considered the most dangerous type of damage induced by IR [9], is performed by two main repair mechanisms – homologous recombination (HR) and non-homologous end-joining (NHEJ) [27].

HR uses the homologous sister chromatid as a template and is the main pathway for postreplicative repair during the late S/G2-phase, whereas NHEJ is utilized in G1/early S-phase [28]. The relatively high radioresistance of NHEJ-defective mutants is observed in the late S/G2 of the cell cycle when sister chromatids are present and HR pathway is operating. Evidences for a role of HR and NHEJ in the radioresistance of higher eukaryotes were derived from cell survival experiments and studies of knockout mice [27]. There are different phenotypes depending on in which DNA DSB repair pathway the mutated gene is involved. Both HR and NHEJ have important roles in repairing spontaneously arising lesions induced by genotoxic treatment and appear to be crucial for the repair of lesions that arise in certain tissue types, with the consequence that mutation of either of these pathways can lead to developmental defects and embryonic death, increase in tumour induction, and defects in neurogenesis [58-61]. But there are also examples without an obvious phenotype. Knockout mice of *Rad52* and *Rad54* genes (genes, coding for proteins involved in homologous recombination) are viable, fertile, and do not develop tumours [27].

HR mutants also show sensitivity to DNA cross-linking agents [28]. A role for HR in DSB repair is also indirectly supported by cytogenetic investigations, in which, for example, XRCC2- and XRCC3-defective hamster cells show highly elevated levels of spontaneous and IR-

induced chromosomal aberrations. However, investigations with pulsed-field gel electrophoresis (PFGE) or similar approaches that directly quantify DSB repair by determining the molecular weights of broken DNA molecules have not detected a significant role of HR in the repair of radiation-induced DSB [28], because HR play a role in repair of relatively small fraction of DSB, and most of them are repaired with NHEJ. In these assays, in which IR doses of > 20 Gy are used, unsynchronized XRCC2- and XRCC3-defective rodent cells show repair kinetics similar to those of wild-type cells. Although it was concluded from these experiments that XRCC3-dependent HR plays only a modest role in DSB repair and survival of cells irradiated in G1 [28], direct measurements of DSB HR repair using I-SceI nuclease based assays revealed that deficiencies in the HR proteins XRCC2 and XRCC3 produce severe (25-fold) reductions in HR repair [62].

Cell lines defective in any of NHEJ genes are generally highly IR sensitive (> 7-fold) and have marked deficiencies in DSB repair, but, unlike HR mutants, they are not sensitive to crosslinking agents [28]. Mice lacking KU70, KU80 and DNA-PKcs proteins are viable, but, because of their deficiency in V(D)J recombination, show arrested B- and T-cell development [39]. *Ku70* mutant mice have accelerated tumour development, in particular of thymic lymphomas [31]. *Xrcc4* and *Lig4*-null mouse mutants die during embryogenesis [32]. Severe defects in the NHEJ were found for cell extracts derived from *Brca2*<sup>-/-</sup> mouse embryonic fibroblasts (MEFs) [33].

There are known defects in pathways, which do not act directly in processes of DNA repair, but cause radiosensitization, thus showing the functional networking in genome conservation. Such processes include telomere maintenance, transcription, maintenance of the nuclear- and cytoskeleton, signal transduction, regulation of cellular death, and cell cycle. For example radiosensitive phenotype was described recently in the fifth generation of telomerase RNA<sup>-/-</sup> (*mTR*<sup>-/-</sup>) mice [34]. Higher chromosomal damage and increase of apoptosis was found in *mTR*<sup>-/-</sup> mice compared to similarly irradiated wild-type controls [34]. Another example of radiosensitivity, caused by mutation in the gene, which is not directly involved in repair, is mice bearing the autosomal recessive mutation *wasted* harbouring a defect in the transcription elongation factor 1a2 (*Eefla2*) gene [35]. The knock-out of *Eefla2* (*Eefla2*<sup>-/-</sup>) mouse displays a disease pattern including increased sensitivity of lymphocytes to IR, neurological dysfunction, and immunodeficiency [35].

Cdc42 GTPase-activating protein (Cdc42GAP) is a member of the Rho GTPase family known to regulate cell actin cytoskeleton organization, polarity, and growth [37]. *Cdc42GAP* knockout primary cells (*Cdc42GAP*<sup>-/-</sup>) show radiosensitivity with SF at 2 Gy being 30% for mutant and 70% for wild type MEFs. They show reduced survival as determined by survival assays after treatment with methyl-methane sulfonate, mitomycin C, H<sub>2</sub>O<sub>2</sub>, furthermore, increased genomic abnormalities, induction of multiple cell cycle inhibitors, and premature senescence. Gene targeting of Cdc42GAP results in constitutively elevated Cdc42GTP levels in many tissues of adult mice, significantly shortened life span, and multiple premature aging-like phenotypes, including reduction of reepithelialization ability in wound-healing [37].

There are evidences published for radiosensitivity of cyclin-dependent kinase inhibitor *p21* knock-out mice, which clearly show the importance of cell cycle regulating factors in radioresistance [63]. Haemopoietic *in vitro* colony-forming assay revealed increase in radiosensitivity with D0 of 1.25 in *p21* mutants, in comparison to D0 of 1.51 in the respective control [63].

Mice lacking poly(ADP-ribose) polymerase 1 (PARP-1<sup>-/-</sup>) and the cells derived from these mice exhibit hypersensitivity to IR and alkylating agents [36, 38, 64]. PARP-1 catalyzes extensive synthesis of poly(ADP-ribose) (PAR) from NAD<sup>+</sup> and covalently modifies many nuclear proteins. The BER pathway depends on the presence of NAD<sup>+</sup> and was shown to be deficient in *Parp-1*<sup>-/-</sup> mice [65], but repair of DNA strand-breaks in *Parp-1*<sup>-/-</sup> did not differ from the wild type [36, 38].

### **1.1.7 Experimental models of radiosensitivity**

Knowledge about numerous defects causing radiosensitivity and genomic instability comes from studies on cells isolated from radiosensitive patients and from a number of rodent models, yeast and tissue culture systems [11, 27].

Yeasts find application as a very important experimental model in studying the molecular mechanisms of repair defects and radiosensitivity, since many homologue proteins, for example that involved in NHEJ, corresponding to KU70, KU80, XRCC4, and DNA ligase IV (except of DNA-PKcs) also exist in *Saccharomyces cerevisiae* and function to repair DSB in a similar

manner [66]. Mutations in the number of yeast DNA repair genes yKu80, yKu70, Mre11, Rad50, Xrs2, Sir2, Sir3 result in altered telomere length and also in increased radiosensitivities [34].

Mammalian cell mutants, which are hypersensitive to IR or radiomimetic agents, have been isolated and subsequently greatly contributed to the understanding of the mechanisms of DNA repair. Such example are XRCC mutants, which have been shown [67] to be deficient in DSB repair and were classified into at least nine x-ray cross complementation (XRCC) groups. Among them, mutants in XRCC4-7 groups exhibit an extremely high sensitivity to IR and show severe defects in DSB repair and V(D)J recombination. A number of DNA repair genes (*Xrcc4*, *Xrcc5*, *Xrcc6*) were cloned from radiosensitive cells. *Xrs* cells are other mammalian cell mutants with defect in DNA repair [68]. Further examples are the mouse SX9 and hamster V3 mutant cell lines, which exhibit defects in DNA-PKcs and are defective in both DSB repair and V(D)J recombination [69].

Rodent models, harbouring spontaneous or targeted gene mutations are very good tools to study the contribution of specific genes/pathways to the *in vitro* and *in vivo* radiation response [27] (see also **1.1.6, Molecular basis of radiosensitivity**). Such models provide useful information about sensitivity of particular mutants to radiation and other DNA damaging agents, which might be considered in treatment of patients with analogous genetic defects.

## **1.2 LEC rat – a rodent model of human diseases**

The establishment of the Long-Evans Cinnamon (LEC) rat strain dates back to October 1975 when several non-inbred Long-Evans rats were obtained from a closed colony maintained by Prof. Taketoshi Sugiyama, Kobe University (Kobe, Japan) [70]. Two inbred strains selected for coat colour (LEA and LEC) were maintained for further breeding, which in addition to this phenotypic marker also developed various physiological and pathological phenotypes. The Long-Evans Agouti (LEA) has a hooded agoutic coat colour, and the LEC coat colour is hooded brown or diluted agouti, both with a white or creamy belly [70].

### 1.2.1 Presence of pathogenic mutations

Spontaneous hepatitis was noticed for the first time in the offspring of LEC rats at the 23<sup>rd</sup> generation of brother and sister mating [71, 72]. Spontaneous fulminant hepatitis associated with severe jaundice occurs in about 80% of LEC rats between 4 to 5 months of age and most of the affected rats die within two weeks of the onset of jaundice [71, 73]. The clinical signs of such hepatitis of LEC rats resemble those of human fulminant hepatitis. LEC rats provide an animal model for human Wilson's disease and a mutation, causing this phenotype, was found in the copper transporting ATPase gene (*Atp7b*) [72].

The LEC rat has also been reported to exhibit a T-helper immunodeficiency. LEC rat thymocytes show novel maturational arrest from CD4+8+ to CD4+8- thymocytes, resulting in a defect in T helper cell functions [74, 75]. This immunodeficiency is controlled by a single autosomal recessive locus, *thid* [76], which was assigned to chromosome 1. A deletion in the gene encoding a receptor-like protein tyrosine phosphatase k (PTPRK) is causing this phenotype, as was shown recently by Kose *et al.*, 2007 [77].

Another defect, which was identified in the LEC rat [78], is a mutation of aldehyde dehydrogenase-2 (*Aldh2*) gene, which codes an enzyme participating in metabolism of ethanol. This mutation causes high toxicity of ethanol.

Additionally, a locus for susceptibility to renal cell carcinomas induced by treatment with the chemical carcinogen N-diethylnitrosamine in the LEC rat was mapped to chromosome 5 [79].

### 1.2.2 Radiosensitivity in LEC rat

The radiation sensitivity to total body irradiation of LEC rat was investigated by Hayashi *et al.*, 1992 [80], Hayashi *et al.*, 1993 [80, 81], when it was studied in terms of intestinal death and bone marrow failure.

According to the publication of Hayashi *et al.*, 1992 [80], the parental Long-Evans closed colony has expired and therefore observed radiosensitivity phenotype of 8-weeks old LEC rat was compared to that of inbred Wistar strain (WKAH), which is often used in the radiation biology field. The published data about LEC rat radiosensitivity to x-ray irradiation show LD<sub>50/7</sub> (intestinal syndrome) and LD<sub>50/30</sub> (bone marrow death) values of LEC rats to be 7 and 3 Gy,

which is significantly lower than those (13 and 7.8 Gy) of WKAH rats. The histopathological investigations, which were done after LD<sub>50/30</sub> dose application in the bone marrow of WKAH rats, have shown that on 8<sup>th</sup> day after 4 Gy of x-ray irradiation the hemopoietic cells were largely recovered, in contrast, hemopoietic cells were not recovered in LEC rats and fibrous tissues increased [81].

The pattern of heredity of LEC radiosensitivity was studied by Hayashi *et al.*, 1994 [82] and was shown to be autosomal recessive. The further investigations included linkage analysis of radiosensitivity in LEC rat. BN, LEC, (BN x LEC) F1 animals were irradiated in the range of doses and the number of rats not showing somatic effects (moribundity with diarrhea) was estimated. The dose of 13 Gy was applied further to distinguish LEC from BN and F1 rats. The first segregation data of backcross hybrids (BN x LEC) F1 x LEC [83] suggested that the hypersensitivity of LEC rats to the whole body irradiation is controlled by two loci, one of them with high LOD score (LR value 115.4) was mapped to the chromosome 4 and D4Rat49/D4Rat182 were the closest microsatellite markers (**Figure 1.1.**). Another locus was mapped to chromosome 1 with low but significant LOD score (LR value 14.8), very close to the T-helper immunodeficiency (*thid*) locus, described in LEC rat [84].

Fine mapping using LEC backcrossed to another strain (F344) and analysis of F344/LEC congenic lines allowed Tsuji *et al.*, 2005 [85] to narrow the location of the mutation down to a ≈1.3 Mb size region between the D4Got85 and D4Got148 (**Figure 1.2.**) microsatellite markers. This study shows that inheritance of the radiosensitivity trait in LEC rat is controlled by a single, autosomal recessive locus. The authors developed congenic lines (see **Figure 1.3.**) by continuous backcrossing LEC rat to F344 rat and testing radiosensitivity applying 4.5 Gy of X-ray exposure (4 Gy was 100% lethal dose by 30 days postirradiation for LEC, but not for F344 rats) at 4 weeks and observing progenies for 30 days. They have analysed seven positional candidate genes known at this region (*Bmp10*, *Gpr73*, *Gp9*, *Cnbp*, *Copg*, *Rab7*, *Rpn1*) for their coding sequence and expression level (see **Table 1.1.** for summary of their structural features and putative function). Several polymorphisms found between LEC and F344 are presented in the **Table 1.1.** None of the nucleotide polymorphisms resulted in amino acid changes. Significant differences in the basal expression level of *Gpr73* were detected between radiosensitive LEC and radioresistant F344 rats (see **Table 1.1.**), and after irradiation expression of *Gp9* and *Cnbp* significantly differed in LEC from that of F344. Several polymorphisms, identified in the upstream regions of these

genes, could explain the observed changes. The authors [85] did not find clear indication that the shown changes in any of the studied genes are responsible for LEC radiosensitivity. The possibility is present that yet unidentified gene in the locus carries the mutation.

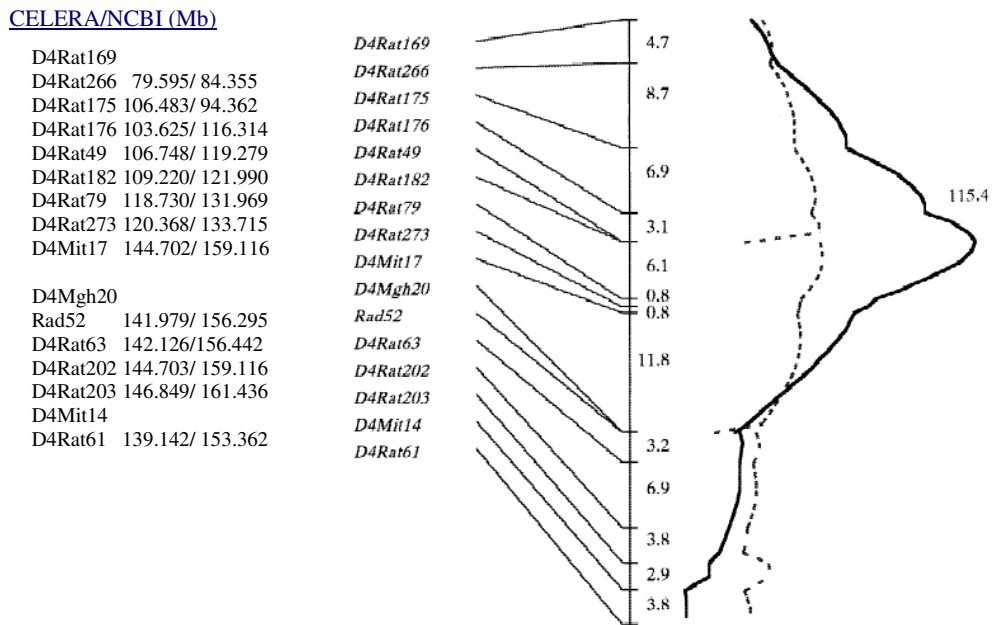


**Figure 1.1. QTL linkage analysis of X-ray radiosensitivity**

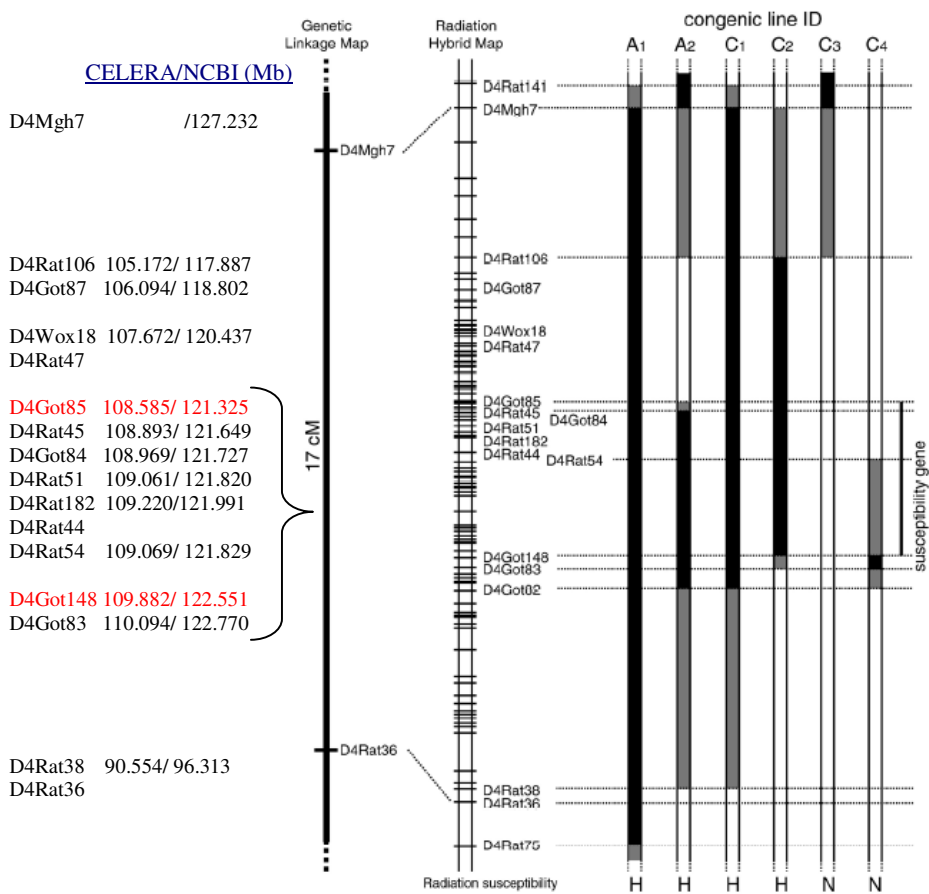
(Modified from [83]). It shows the linkage analysis of radiosensitivity in LEC rat and mapping of the locus of radiosensitivity to chromosome 4. The numbers on the right of the line indicate the genetic distance (cM) between loci. The number above the peak indicates the LR value ( $4.602 \times \text{LOD score}$ ).

The physical location of the markers (which were available) is given additionally according to the latest RGD V3.4, July 2006 (Celera/NCBI).

**Table 1.1. The list of genes investigated by Tsuji *et al.*, 2005**

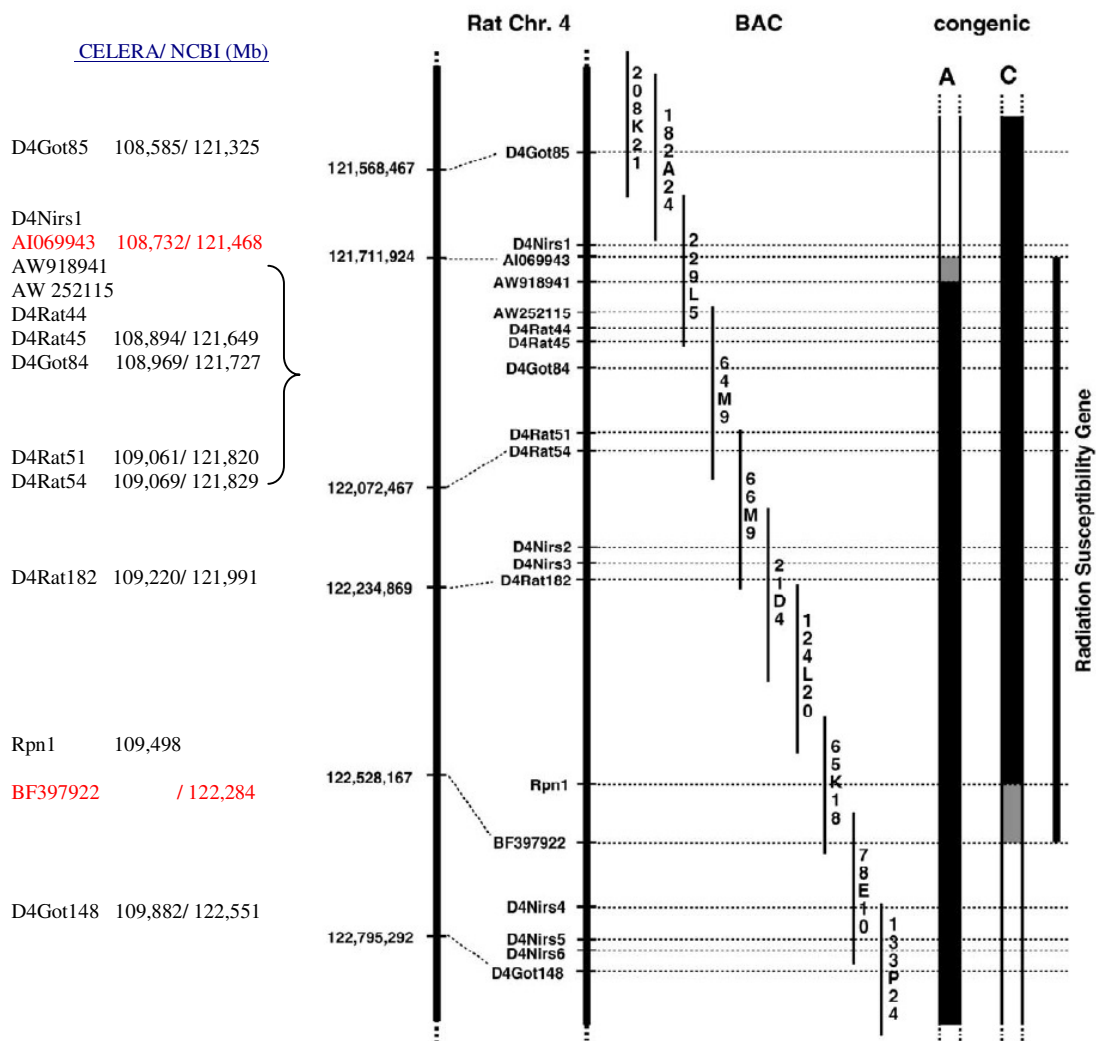
GENE SYMBOL	GENE NAME	STRUCTURE OF THE PROTEIN AND INTERACTIONS	PUTATIVE FUNCTION	DETECTED CHANGES [85]:				
				Sequence	Expression			
					Without IR		After 4,5Gy	
F344	LEC	F344	LEC					
<i>Gpr73</i>	Prokineticin receptor-1	- binds to G-protein-coupled receptors	- potent angiogenic factor; - cardiomyocyte survival [86]	SNP:G789A 5-UTR: C-468T	< (2,7 fold)		no difference	
<i>Bmp10</i>	Bone morphogenic protein 10	- tumor-growth factor- $\beta$ propeptide, known as latency associated peptide in TGF- $\beta$	- heart development [87] - angiogenesis [88]	SNP:G567A	no difference		no difference	
<i>Rpn1</i>	Ribophorin 1	-leucine-reach-repeat-like domain - recognizes the ubiquitin-like domain of RAD23 [89]	- part of the proteasome; - possible involvement into Rad23-mediated protein unfolding [89]	SNP:A1374G T1539C	no difference		no difference	
<i>Rab7</i>		- small GTPase	- acts in the late endocytic pathway [90]	no difference	no difference		no difference	
<i>Gp9</i>	Glycoprotein IX	- membrane glycoprotein	- platelet adhesion [91]	SNP:T240G 5-UTR: T-33C; G-314C; 727ins (TTTT) A-911G	no difference	↓	↑	
<i>Cnbp</i>	Cellular nucleic acid binding protein	- has a zinc fingers domain - binds to ss RNA or DNA	myocytes development? [92]	5-UTR: T-341C; -695del(T)	no difference	↓	↑	
<i>Copg</i>	Coatomer protein complex, subunit gamma	- subunit of COP I coat	- vesicular trafficking in the early secretory pathway [93]	SNP:A1806G	no difference		no difference	

Table contains the summary of function and structural characterisation of the genes identified on the locus of interest and investigated by Tsuji *et al.*, 2005 by means of sequencing and expression analysis. The expression of the candidate genes was analysed in the tail tips of nonirradiated and irradiated with 4.5 Gy of X-ray LEC and WKAH animals (at 6 hrs after IR). The identified changes in the coding sequence, the 5-UTR region, and expression changes are indicated. The signs  $\uparrow$  and  $\downarrow$  reflect detected increase or decrease in expression of studied gene after IR relative to the nonirradiated rat.



**Figure 1.2. Mapping of the locus of interest to the region between D4Rat85 and D4Got148 microsatellite markers**

Genetic linkage (SRHSP x BN intercross in the Rat Genome Database) and radiation hybrid maps of rat chromosome 4 with a schema showing introgressed chromosomal segments for six congenic sublines until the 13<sup>th</sup> generation (modified from [85]). Informative microsatellite marker names are indicated on the radiation hybrid map. Black and white bars indicate chromosomal segments derived from LEC and F344 rats, respectively, and grey bars indicate recombination sites. Radiation susceptibility (H, high; N, normal) was determined by mortality of backcross progeny after X-ray exposure to 4.5 Gy. The physical location of the markers (which were available) is given according to the latest RGD V3.6, July 2006 (Celera/NCBI). The limits of the identified locus, responsible for radiosensitivity in LEC rat are marked in red.



**Figure 1.3. (modified from [94]). Physical map of the radiation susceptibility region on rat chromosome 4**

On the presented map the authors indicated at the left the informative polymorphic markers (SSLP and SNP) by broken lines and the genome positions of six representative markers based on the rat genome version 3.1 (<http://hgse.bcm.tmc.edu/projects/rat/>). The short vertical lines in the middle represent the 10 clones of the BAC contig. At the right, the map shows introgressed chromosomal segments for two congenic lines A and C, which were highly susceptible to X-radiation (see **Figure 1.2.**, [85]). Black and white shaded regions represent chromosomal segments derived from LEC and F344 rats, respectively, and grey shaded regions indicated recombination sites. The genetic location of the markers (which were available) is given according to the latest RGD V3.6, July 2006 (Celera/NCBI). The limits of identified locus are marked in red.

The latest published data [94] (see **Figure 1.3.**) with further linkage analysis of developed LEC congenic lines (described earlier, [85]) narrowed the location of the radiation susceptibility gene down to a region of  $\approx 800$  kb between AI069943 (genomic position starts at nucleotide

121.468 Mb) and BF397922 (genomic position ends at nucleotide 122.284 Mb). Performing *in vitro* rescue experiments by transient transfections of seven BAC clones (covering the region of the interest) into LEC fibroblasts, Tsuji *et al.*, 2006 [94] identified clone CHORI-230-65K18, that maps on the radiosensitivity locus and can revert radiosensitivity of 65K18 BAC-transfected LEC cells after 2 Gy of IR from 60% to 95%. 88% survival after 2 Gy was observed in F344 cells. Irradiation with 4 Gy reduced survival of LEC cells, transfected with 65K18 BAC clone, to 41%, compared to that of 21% in untransfected LEC mutants, and to 75% in F344 cells. According to the authors, this reversion was not complete and there is a possibility that causative mutation happened in another gene located in another BAC. The authors analysed the sequence of the CHORI-230-65K18 clone and found that the region contains only one gene – *Rpn1*. Tsuji *et al.*, 2006 [94] did not find any evidences for *Rpn1* being affected and thus causing radiosensitivity in LEC rat, since there were no changes in the aminoacid sequence, and the transfection of F344 cells with shRNA targeting *Rpn1* did not change survival of the F344 cells.

The radiosensitivity in LEC rat was shown to be independent from the identified mutations in *Atp7b*, *Ptprk*, *Aldh2*, and susceptibility to renal cell carcinomas [77, 79, 95].

Studies on cellular radiosensitivity were done to investigate the cellular phenotype of LEC rat by Hayashi *et al.*, 1994 [82]. The clonogenic assay performed on lung fibroblasts yielded values of survival at 2 Gy being 45% for LEC and 78% for WKAH. The authors [82] have observed an increase of X-ray induced chromosomal aberrations in bone marrow cells and strongly reduced DNA DSB repair in fibroblasts after irradiation with 70 Gy (as shown by PFGE) of LEC rats in comparison to WKAH rats. Hayashi *et al.*, 2002 [96] studied apoptosis induction in thymocytes by X-irradiation and showed increase in apoptosis, which was inhibited by cycloheximide. Using SV40-transformed fibroblasts Hayashi *et al.*, 1997 [97] showed increase of apoptosis induction in LEC fibroblasts, decrease in p53 accumulation and deficiency of G1/S arrest, abnormal accumulation of G2/M phase cells from LEC strain rats after X-irradiation at S phase, as well as radioresistant DNA synthesis. In SV40-transformed LEC fibroblasts the high sensitivity to heat treatment and deficiency in nuclear accumulation of G22P1 and XRCC5 proteins was observed after X irradiation [98], as well as deficiency in fast repair processes of potentially lethal damage induced by X-irradiation [99]. Hayashi *et al.*, 1998 [100] have also found higher sensitivity of LEC and WKAH rat cells to ellipticine, an inhibitor of topoisomerase II.

Large-scale gene expression profiling published by Tsuji *et al.*, 2005 [85] was conducted in tail tips, which were actually not the target tissues, such as intestine and bone marrow, in animal experiments performed by Hayashi *et al.*, 1992, 1993 [80, 81]. They show that without irradiation 31 genes/expressed sequence tags (ESTs) of normally susceptible rats had more than two-fold higher expression than that of LEC and 92 genes/ESTs of normally susceptible rats had more than twofold lower expression compared with LEC. Under irradiation conditions the expression level of 149 genes/ESTs was elevated more than two-fold and expression level of 158 genes/ESTs was reduced more than two-fold compared with non-irradiated conditions in WKAH rats; however, for LEC rats, the expression levels of these corresponding genes did not change significantly upon irradiation. Conversely, under irradiation conditions, the expression of 91 genes/ESTs was elevated more than two-fold in LEC rats and that of 130 genes/ESTs was reduced more than two-fold, and in F344 the expression levels of these corresponding genes did not change significantly upon irradiation [85]. These experiments reflect the large difference in gene regulation between LEC and F344 rats without IR and after irradiation.

### **1.2.3 Sensitivity to radiation and chemical agents in strains related to LEC rat - LEA and LE rats**

LEA rat strain was established from a Long-Evans closed colony together with the LEC rat and has been used as the control strain for several mutant phenotypes seen in the LEC rat. Nevertheless, LEA rat was shown to be more radiosensitive than BN rat strain and linkage analysis identified the radiosensitivity trait on chromosome 4 in the position identical to that of LEC rat (*xhs1*) [101]. This finding may indicate that founder rats in the original LE closed colony all possess this mutant phenotype. Alternatively, the x-ray hypersensitive phenotype might coincidentally be selected in the both LEC and LEA rat strains in the process of inbreeding [101].

The number of aberrations per cell induced by BNU or MMS was significantly higher in bone marrow of both LEA and LEC rats than in Wistar or SD rats [102].

There are no data published concerning the sensitivity of LE rat to IR.

### 1.3 THE AIMS OF THE STUDY

LEC rat is one of the rodent models of radiosensitivity with an as yet unidentified defect.

The present work was initiated to characterize genetically inheritable factors, modifying radiation response, and radiosensitivity in the LEC rat strain.

The fundamental knowledge of pathways, operating in radiation response – signal transduction, repair and stem cells repopulation - is applicable in the field of DNA repair, radiobiology, stem cell biology, and radiotherapy.

The aims of this work were:

- Characterization of *in vitro* radiosensitivity in primary LEC fibroblasts, which have unchanged processes of cellular DNA signal induction and processing
- The investigation of cellular radiosensitivity and repair of LEC primary fibroblasts synchronized at G1 phase of cell cycle applying available methods such as clonogenic assay, pulsed field gel electrophoresis, analysis of  $\gamma$ H2AX, and lymphocytes (at G0) - comet assay
- Comparison of the cellular radiosensitivity phenotype in LEC to a genetically close control – LE outbred rat
- Further analysis of the radiosensitivity locus with establishment and analysis of candidate genes

## II. MATERIALS AND METHODS

### 2.1 Materials

#### 2.1.1 Equipment

Centrifuge, ROTINA 420R	Andreas Hettich (Tüttlingen)
Cell incubator, SW2 JULABO	Labortechnik (Seelbach)
Centrifuge, Biofuge FRESCO	Heraeus Holding (Hanau)
Centrifuge, Sorvall RC-5B Refrigerated Superspeed Kendro Laboratory Products (Hanau)	
Colony Counter	Du Pont Instruments (Wilmington, USA)
Comet electrophoresis unit, HE100 Supersub	Amersham Pharmacia Biotech (Freiburg)
Coulter counter @Z1™ Series	Beckman Coulter, Inc. (Fullerton, USA)
Dissection microscope, 204670 SZ	Olympus (Tokyo, Japan)
Flow cytometer, Becton-Dickinson LSRII	Becton Dickinson (Heidelberg)
Freezer, Stratacooler	Stratagene (La Jolla, USA)
Gel Doc2000 System	Bio Rad (München)
GeneAmp PCR System 9700	PE Applied Biosystems (Weiterstadt)
Horizontal Gel Electrophoresis Chamber	Bio Rad (München)
Irradiation source, HWM D-2000, Cs-137	Wälischmiller (Meersburg)
Irradiation source, Gamma cell 220, Co-60	AECL (Chalk River, Canada)
Inverted Microscope, Axiovert 135	Carl Zeiss (Jena)
Laminar flow hood, UNIFLOW UVUB 180	UNIEQUIP (Martinsried)
Magnetic Mixer, RTC	Labor Schubert&Weiss (München)
Moulds and combs for PFGE agarose plugs	custom designed
PFGE electrophoresis unit CHEF GeneMapper	Bio Rad (München)
pH-Meter CG	Schott Geräte (München)
Semiautomatic pipette, 20, 100, 200, 1000 P/μl	Gilson (Villiers le Bel, France)
SpeedVac Concentrator, Univap 100H	Uniequip (München)
Thermomixer 5436	Eppendorf (Hamburg)
Thermomixer compact	Eppendorf (Hamburg)
Video Camera System, DokuGel	Mitsubishi (Japan)
Waterbath, Julabo SW21	Labortechnik (Seelbach)

#### 2.1.2 Consumable materials and chemicals

##### General

Adhesive PCR Foil Seals	ABGene (Epsom, UK)
Comet glass slides	Menzel (Braunschweig)
Coplin jar	Raymond Lamb Ltd (Eastbourne, UK)

Eppendorf tubes (1,5 ml, 2 ml)	Eppendorf (Hamburg)
Falcon Tubes (25 ml, 50 ml)	Becton Dickinson (Heidelberg)
Fitter Tips	Starlab (Ahrensburg)
Gauge	Braun (Melsungen)
Microscopes Slides SuperFrost	Roth (Karlsruhe)
Pasteur pipette	
Pipette (5 ml, 10 ml, 25 ml)	Nunc (Wiesbaden)
Pipette tips (20 µl, 100 µl, 1000 µl)	Eppendorf (Hamburg)
PCR Plate 96-wells	ABGene (Epsom, UK)
Sequencing 96-wells plate with bar code	ABGene (Epsom, UK)
Single use scalp	Wagner&Munz (München)
Sterile filters for syringe	Sartorius (Göttingen)
Syringe, 5 ml	Braun (Melsungen)

### Chemicals for electrophoresis, gels staining and microscopy

Agarose	Amersham Pharmacia (Freiburg)
Bromphenolblue	SIGMA (Deisenhofen)
LMP agarose (A9414 Comet first layer)	SIGMA (Deisenhofen)
LMP agarose (LMA Comet second layer)	Ameresco (Solon, USA)
Cresol red	SIGMA (Deisenhofen)
DAPI	SIGMA (Deisenhofen)
Ethidium bromide	SIGMA (Deisenhofen)
Glycerine	SIGMA (Deisenhofen)
Kristall violett	Merck (Darmstadt)
LMP agarose Type I (LMP EEOA6013 PFGE)	SIGMA (Deisenhofen)
SYBRGreen	Molecular Probes (Eugene, USA)
Triton X-100	SIGMA (Deisenhofen)
Vectashield	Vector Laboratories (Burlingame, USA)
Xylencyanol	SIGMA (Deisenhofen)

### Cell culture consumable materials and chemicals

Cell culture plates (Petri), 140x20 and 60x10 mm	NUNC (Hessen)
DMEM (4.5 gGlucose, Glutamax, -Purivate)	Invitrogen (Karlsruhe)
Dimethyl sulphoxide (DMSO)	SIGMA (Deisenhofen)
FCS (Foetal Bovine Serum)	Invitrogen (Karlsruhe)
Freestanding Cryogenic Vial (2 ml)	Falcon (Becton Dickinson, San Jose, USA)
Quadriperm	RENNER (Dannstadt)
Penicillin/Streptomycin (10 <sup>4</sup> IU/ml, 10 <sup>4</sup> µg/ml)	GIBCO/Invitrogen (Karlsruhe)
Solo flasks with filter caps	NUNC (Hessen)
Trypsin/EDTA	GIBCO/Invitrogen (Karlsruhe)

### Other chemicals

Absolute Ethanol (C <sub>2</sub> H <sub>5</sub> OH)	Merck (Darmstadt)
Acetic acid (CH <sub>3</sub> COOH)	Roth (Karlsruhe)
Ampuwa (pyrogen-free water)	Fresenius (Bad Homburg)

Ammonium acetate (CH <sub>3</sub> COONH <sub>4</sub> )	Merck (Darmstadt)
Boric acid (H <sub>3</sub> BO <sub>3</sub> )	Merck (Darmstadt)
Chloroform (CHCl <sub>3</sub> )	Merck (Darmstadt)
Citric acid (H <sub>3</sub> C <sub>6</sub> H <sub>5</sub> O <sub>7</sub> )	Merck (Darmstadt)
Diethylester	Merck (Darmstadt)
EDTA	SIGMA-Aldrich (Deisenhofen)
Heparin-Natrium	B.Braun Melsungen AG (Melsungen)
Isopropanol (C <sub>3</sub> H <sub>8</sub> O)	Merck (Darmstadt)
Methanol (CH <sub>3</sub> OH)	Merck (Darmstadt)
Nonidet P40	Merck (Darmstadt)
Phenol	Merck (Darmstadt)
Potassium chloride (KCl)	Merck (Darmstadt)
Sodium chloride (NaCl)	SIGMA-Aldrich (Deisenhofen)
Sodium citrate (Na <sub>3</sub> C <sub>6</sub> H <sub>5</sub> O <sub>7</sub> )	Merck (Darmstadt)
Sucrose (C <sub>12</sub> H <sub>22</sub> O <sub>11</sub> )	Roth (Karlsruhe)
Sodium dodecyl sulfate (C <sub>12</sub> H <sub>25</sub> OH)	SIGMA-Aldrich (Deisenhofen)
Tris, Tris-HCl	SIGMA-Aldrich (Deisenhofen)

### 2.1.3 Rat strains

Long-Evans	Charles-River Wiga GmbH (Sulzfeld, Germany)
Long-Evans Cinnamon	Charles-River Laboratories Japan Inc. (Yokohama, Japan)

### 2.1.4 Kits and reagents

Big Dye Terminator 3.0 Cycle Sequencing Kit	QIAGEN (Hilden)
High Pure RNA tissue Kit	Roche Diagnostic (Mannheim)
LightCycler FastStart DNA Master <sup>plus</sup> SYBRGreenI	Roche Diagnostic (Mannheim)
QIAquick PCR Purification Kit	QIAGEN (Hilden)
SuperScript <sup>tm</sup> II RNase H <sup>-</sup> Reverse Transcriptase	Invitrogen (Karlsruhe)
TRIzol, total RNA isolation reagent	Invitrogen (Karlsruhe)

### 2.1.5 Length standards

DNA-Molecular weight marker (VIII)	Roche Diagnostic (Mannheim)
------------------------------------	-----------------------------

### 2.1.6 Enzymes

Proteinase K	Roche Diagnostic (Mannheim)
Taq DNA Polymerase	Eurobio (Raunheim)
RNase A	QIAGEN (Hilden)
Collagenase 2	Seromed (Berlin)

## 2.1.7 Oligonucleotides

Oligonucleotides (Primers) were synthesised by AG BioDV, GSF, Eurogentec (Cologne) and MWG, Biotech, AG (Ebersberg). In all tables the nucleotide number denotes the position of the 5'-end of the primer; orientation is given as follows: F – for 5' Primer (sense orientation), and R – 3'-Primer (antisense orientation).

**Table 2.1. Rat microsatellite oligonucleotides**

Name	Sequence (5'-3')	Position, bp		Orientation
		Celera	NCBI	
D4Rat38	AATGCCATTGGAAATGTGAG	90553749-	96313186-	F
	CACCCACATGGCCTTTAAAT	90553889	96313326	R
D4Wox18	GGTGGAAGGAGAGAACCAAC	107672487-	120436733-	F
	AAGTTACAGCTAGAGGGGTGTG	107672599	120436845	R
D4Got85	CATACACACAAGCCTGTGCAC	108585845-	121324657-	F
	GATCTTCTCTTAGCCAGCTGGTTA	108585973	121324785	R
<i>D4Nirs1</i>	CCAGGATGGAGGAAAGCATA		121504389-	F
	GCTTGTCTTGGTGCAGAACA		121504601*	R
AW918941	TCCACCCTTCTTTCCATTTG		121603167-	F
	TGGGGACATATTCCTGCTTC		121603362*	R
AW252115	CCGATGCTTAAGGGTTTGTGAG		121621828-	F
	CTTTGAGCACAGCACATGGT		121622028*	R
<i>Rpn1</i> (A64976G)	AGAATTCTGTAGCCACACCCT		976596-	F
	CATCACATGGGCGTTAGGAC		977074*	R
<i>Rpn1</i> (T66167C)	TGCTGTTGAGCCCAGTCCATTA		975335-	F
	GGTCAAGGACAAGTACTCACAA		975757*	R
BF397922 (G165868C)	GAGACACGAGGCCTGCTTAG		122283766-	F
	TAACCTGCTGCTGGCTCTGA		122283969*	R
D4Rat54	CAGGCCAGACGTCTAAGATG		121828906-	F
	GAGCCCCTCATGTGAGGATA		121829076	R
D4Got148	CCTGGAGCTTTTACGGTAGGA	109882384-	122550918-	F
	TCTAACGAGTCCACTCTGCTTTT	109882539	122551073	R
D4Got83	GGTGGGATGAAAATGCCA	110093803-	122770006-	F
	CAGAACCAGGCAAAGGACTTTAC	110094030	122770233	R
D4Got82	GCTCCTTCTCAGCATCTTC	112078071-		F
	GTGTGTGAGTCTGTGTGTGCC	112078189		R

The nucleotide position of primers for selected markers on chromosome 4 was derived from NCBI/Celera Browser RGD V3.4, July 2006 (Celera/NCBI). The position of the markers, which were selected from those published by Tsuji *et al.*, 2005 [85] and which position was not available in NCBI (marked with \*), was defined by BLAT comparison tool, available at USCS site (<http://genome.ucsc.edu/>) of the published oligo sequence against rat genome.

**Table 2.2. Oligonucleotides for amplification and sequencing of candidate genes**

**A**

Name	Sequence (5'-3')	Position	Orientation
Rat-Raf1_40f	GCGAGCTTGAAGCAGGAAGG	40	F-1
Rat-Raf1_738r	TCAGGAACGTTTTCCGAGCA	738	R-1
Rat-Raf1_505f	TCAATGTGCGGAATGGGATG	505	F-2
Rat-Raf1_1198r	CTCAGGTTGTTGGGGCTGCT	1198	R-2
Rat-Raf1_991f	ACTCCACACCCCATGCCTTC	991	F-3
Rat-Raf1_1647r	GCCGGGCAATGTCAATTAGC	1647	R-3
Rat-Raf1_1367f	GGGCTCCTTTGGCACTGTGT	1367	F-4
Rat-Raf1_2041r	TTCATTGCCTTGGGGCAGTT	2041	R-4
Rat-Raf1_1779f	CGCTGGAGTGGTTCTCAGCA	1779	F-5
Rat-Raf1_2436r	TTGGCGGACAGCTTCCATT	2436	R-5

**B**

Name	Sequence (5'-3')	Position	Orientation
Rat-Rad18_14f	CGCGGGGAATTTGAGTAGA	4	F-1
Rat-Rad18_410r	CTTTGAGGTGGAAGACACAGGAGA	401	R-1
Rat-Rad18_261f	CCAATTGTTGCGTGCCAGT	378	F-2
Rat-Rad18_758r	CCCGTGATAAACAACGTCTAAATGC	750	R-2
Rat-Rad18_637f	TGGTCTGTGACACCCTCTACA	629	F-3
Rat-Rad18_1487r	ACAGCCCTGGGGAGTCCA	1317	R-3
Rat-Rad18_994f	GAACATGGAGAAGACCAGGATGC	986	F-4
Rat-Rad18_1762r	CAGGTCACCGTTCAGAAAACTG	1588	R-4

**C**

Name	Sequence (5'-3')	Position	Orientation
Rat-XPC-fwd-49	GAAGCCGAGGACAAGAAAGCA	5-UTR	F-1
Rat-XPC-rev-510	CGCCTGCTCTGGTGTTCAT	510	R-1
Rat-XPC-fwd-287	GGGATGATTTCCGGGACTCA	287	F-2
Rat-XPC-rev-859	AAATGGCGATCCTCCTTTCCA	859	R-2
Rat-XPC-fwd-561	GCGGAGGATGATGAAGCGTT	561	F-3
Rat-XPC-rev-1078	TGGTCTTGGGTTTGTGTGGC	1078	R-3
Rat-XPC-fwd-1359	TTGTAAGCCTGGCCCTCGAA	1359	F-4
Rat-XPC-rev-1951	GGAATTTCAAGAGGTGGCGCT	1951	R-4
Rat-XPC-fwd-1664	ATGCCACCAACCATGACCT	1664	F-5
Rat-XPC-rev-2202	TTTCCGGGCACGGTTAGAGA	2202	R-5
Rat-XPC-fwd-1931	AGCGCCACCTCTTGAAATTCC	1931	F-6
Rat-XPC-rev-2271	CACGTTCCCAAACCTATTCCG	2271	R-6
Rat-XPC-fwd-2047	ACGTGGCTGAAGCAAGCAAGA	2047	F-7
Rat-XPC-rev-2461	AGCCTCCATGGAAATCGAAGC	2461	R-7
Rat-XPC-fwd-2295	CAATGACTTGGGCCTCTTTGG	2295	F-8
Rat-XPC-rev-2761	AGAGTCCGCCTCCTGCATTT	2761	R-8
Rat-XPC-fwd-2413	ATGCCTATCGGCTGTGTCCA	2413	F-9
Rat-XPC-rev-2919	TGGGAAGAGATGGGAAGCCT	2919	R-9
Rat-XPC-fwd-2688	GAAAGGCTGAAACTCCGCTACG	2688	F-10
Rat-XPC-rev-3utr	TGCAGCACAACCTTCTAGTCCCC	3-UTR	F-10

**D**

Name	Sequence (5'-3')	Position	Orientation
rGATA2gen-Ex1f	CCCTTCCCCCTCCCTGAG	89	F-1
rGATA2gen-Ex1r	CTGCACCCCTCCTGCAGAC	94	R-1
rGATA2gen-Ex2f	ATCTGCCGGAGCAGCCAAT	107	F-2
rGATA2gen-Ex2r	CCACAGGAGATCCTGGTTTGA	77	R-2
rGATA2gen-Ex3f	CCTCTGTGAAGCTCCGATGG	108	F-3
rGATA2gen-Ex3r	TTCCTGTGGATCCCACATCC	100	R-3
rGATA2gen-Ex4--1f	TTTTAAAGGGTGGGGCTGCT	109	F-4
rGATA2gen-Ex4--1r	AGGGGACTGCCACCTTCC	457	R-4
rGATA2gen-Ex4--2f	AGCTCCGTAGCCTCCCTCAC	411	F-5
rGATA2gen-Ex4--2r	TAGCCGACCACAACCCCTTT	71	R-5

The position of primers is based on cDNA of candidate genes published under Genbank Accession Numbers:

**A:** *Raf-1*, NM\_012639 **B:** *Rad18*, XM\_342734 **C:** *Xpc*, XM\_232194 **D:** the position of primers for genomic sequence of *Gata-2* is based on sequence given in the ENSEMBL database under gene name ENSRNOG00000012347. The location of forward primers reflects their position to intron/exon boundary, and location of reverse primers reflects their position to exon/intron boundary.

**Table 2.3. Real Time PCR Oligonucleotides**

Name	Sequence (5'-3')	Position	Orientation
GATA-2-1204f	CTGCCTCAGCTCATGAATATGGCAG	1204	F
GATA-2-1409r	CCGATTCTGTCCATTCATCTTGTG	1409	R
Fancd2-2484f	ATGTGACGTGGCACCGTCTG	2484	F
Fancd2-2694r	AGGCCCCAGCTGGACAACCTT	2674	R
RN_PBGD_3_F	GCTGAGAACCTGGGCATCAG	996	F
RN_PBGD_5_R	AGGAGCACAGGGCACTTGAC	1164	R

The position of primers is based on cDNA sequences of investigated genes published under Genbank Accession Numbers: *Gata2*, NM\_033442, *Fancd2*, XM\_232273, *Pbgd*, X06827

### 2.1.8 Antibodies

Mouse monoclonal IgG<sub>1</sub>, anti-phospho-histone H2AX (Ser139)  
Goat IgG, Alexa488, anti-mouse

Upstate (Lake Placid, USA)  
SIGMA-Aldrich (Deisenhofen)

### 2.1.9 Buffers

#### Pulsed field gel electrophoresis

##### *1 x TBE running buffer*

90 mM Tris  
90 mM Boric Acid  
3.2 mM EDTA, pH = 8.0

##### *ESP*

0.5 M EDTA, pH = 8.0  
1% (w/v) Sodium Lauryl Sarcosinate  
0.1% (v/v) Proteinase K

0.5 M EDTA, pH = 8.0

### PCR

#### *1 x PCR Buffer*

0.2 mM of each dNTPs  
1:10 10xPCR buffer  
1.5 mM MgCl<sub>2</sub>  
60 mg/ml Sucrose  
40 µg/ml Cresol red

#### *5 x TBE buffer, pH = 8.0*

0.4 M Tris  
0.4 M Boric Acid  
0.01 M EDTA

### Comet assay

#### *Lysis Buffer I*

2.5 M NaCl  
100 mM NaEDTA, pH = 10.0  
10 mM Tris/HCl, pH = 10.0  
1% (w/v) Sodium Lauryl Sarcosinate  
1% (v/v) Triton-X-100

#### *Neutralization Buffer*

1 M NH<sub>4</sub>Ac

### Cell cycle analysis

#### *Solution I (detergent solution)*

584 mg/l NaCl  
1000 mg/l Na-citrate  
25 µg/l ethidium bromide  
10 mg/l RNase  
0.3 ml/l Nonidet P40

### DNA extraction from cultured cells

#### *Lysis Buffer I*

10 mM Tris pH = 8.0  
10 mM NaCl  
10 mM EDTA pH = 8.0  
1% (w/v) SDS  
100 µg/ml RNase A

#### *Rinsing Buffer*

10 mM Tris/HCl  
10 mM EDTA, pH = 7.5

#### *10 x Loading Buffer*

50% (v/v) Glycerine  
1 mM EDTA, pH = 8.0  
0.2% (m/v) Bromphenol Blue  
0.2% (m/v) Xylencyanol

#### *Electrophoresis Buffer*

300 mM NaOH  
10 mM NaEDTA  
2% (v/v) DMSO

#### *Staining Solution*

5% (v/v) DMSO  
20% (v/v) Vectashield  
0.05% (v/v) SYBRGreen

#### *Solution II (citric acid-sucrose solution)*

1.5% (v/v) citric acid  
0.25 M sucrose  
40 µg/l ethidium bromide

### DNA extraction from tissues

#### *Lysis Buffer II*

50 mM Tris pH = 8.0  
100 mM NaCl  
100 mM EDTA  
1% (w/v) SDS

### Buffer for enzymatical digestion of tissues for fibroblasts preparation

DMEM (without FCS)  
0.3% (v/v) Trypsin/EDTA  
1.5 mg/ml collagenase  
1% (v/v) Penicillin/Streptomycin

### Standard cell culture media

DMEM  
10% (v/v) FCS  
1% (v/v) Penicilline/Streptomycine

### **2.1.10 Software**

FAR3	custom program, developed by D. Kononko (Minsk, Belarus)
Gel Doc2000 System	Bio-Rad (München)
GraphPad Prism 3.03	San Diego (USA)
Quantity One-4.4.0	Bio-Rad (München)
LSM-510 META 3.2SP2	Expert Mode, Carl Zeiss (Jena)
ImageJ 1.36b	NIH (USA) see <a href="http://www.rsb.info.nih.gov/ij/">http://www.rsb.info.nih.gov/ij/</a>
VisCOMET	Impuls GmbH (Gilching)

### **2.1.11 Bioinformatic resources**

Rat Genome Database (RGD) Web Site, Medical College of Wisconsin, Milwaukee, Wisconsin. World Wide Web (URL: <http://rgd.mcw.edu/>). RGSC v.3.4, release July, 2006; RGSC, v3.4, release November, 2004.

The UCSC Genome Browser (URL: [Genome Bioinformatics Group of UC Santa Cruz](http://genome.ucsc.edu/))

ENSEMBL Genome Browser (URL: [http://www.ensembl.org/Rattus\\_norvegicus/index.html](http://www.ensembl.org/Rattus_norvegicus/index.html))

Primer3 (URL: [http://waddlslab3.life.smu.edu/cgi-bin/primer3/primer3\\_www.cgi](http://waddlslab3.life.smu.edu/cgi-bin/primer3/primer3_www.cgi))

ORF Finder (URL: <http://www.ncbi.nlm.nih.gov/gorf/gorf.html>)

## **2.2 Methods**

### **2.2.1 Rat strains**

The Long-Evans Cinnamon and Long-Evans rat strains were purchased from Charles-River Laboratories Japan Inc. (Yokohama, Japan) and Charles-River Wiga GmbH (Sulzfeld, Germany). Rats were maintained and treated according to the German Tierschutzgesetz. Rats were kept in one Macrolon-Standard cage Type 3. Water and food were provided *ad libidum*. The rat facility was maintained at 22<sup>0</sup>C in 22% relative humidity and was lit under a twelve hours Day/Night Rhythm.

### **2.2.2 Establishment and cultivation of fibroblasts**

Primary rat fibroblast cultures were established from LE and LEC newborn rats according to the protocol published by Ungaro *et al.*, 1997 [103].

Five newborn male rats were killed by short exposure to liquid N<sub>2</sub> and subcutaneous level was scraped off from kidneys, peritoneum and skin. The tissues were minced with a sterile scalpel and digested for 16 hours in 20 ml of enzyme solution (DMEM, 0.3% trypsin, 1.5 mg/ml collagenase, 1% Penicillin/Streptomycin) at 37<sup>0</sup>C in a cell incubator with magnetic stirring. 500 µl fractions were seeded in 20 ml of standard cell culture media (DMEM, 10% FCS, 1% Penicillin/Streptomycin), in 140 x 20 mm Petri dishes and incubated at 37<sup>0</sup>C and 8% of CO<sub>2</sub>/air in a humidified cell culture incubator. Media was changed after 24 hours. After several passages only 2 LEC (LEC-1, LEC-2) and 3 LE (LE-1, LE-2, LE-4) cell lines were growing successfully and were used for further experiments.

### **Subcultivation procedure**

The general morphology and growth of a cell population, and presence of any microbial contaminants was checked regularly under an inverted microscope. Primary cells and their descendants were grown in monolayer culture at 37<sup>0</sup>C and 8% of CO<sub>2</sub>/air in standard cell culture

media (DMEM, 10% FCS, 1% Penicillin/Streptomycin) and subcultivated after they reached sub-confluency (every 3-4 days) into three Petri dishes. All growth experiments employed serum from the same lot. Cells were rinsed with 5 ml sterile prewarmed PBS and after addition of 0.7-1 ml prewarmed trypsin/EDTA plates were incubated for 5 min at 37<sup>0</sup>C. Detachment of cells was observed under the inverted phase contrast microscope and was assisted by gentle shaking. 5 ml of media containing FCS was added to inactivate trypsin and to resuspend the cells. Cells were plated with 10 ml of cell culture media (DMEM, 10% FCS, 1% Penicillin/Streptomycin). Next day after plating cells were washed with 5 ml of sterile prewarmed PBS and media was changed the following day.

### **Cell freezing**

Cells were frozen for future use at subsequent passages. Sub-confluent cells were trypsinised as described above, collected in 15 ml Falcons, and centrifuged at 1000 rpm for 5 min. Supernatant was decanted and cells were resuspended at a concentration of 1x10<sup>6</sup> per ml in DMEM media containing 10% FCS, 10% DMSO and 1% Penicillin/Streptomycin. 1.5 ml aliquots of the cell suspension were transferred to sterile 2 ml Cryogenic Vials. For freezing the vials were left at -70<sup>0</sup>C in a Stratacooler filled with iso-propanol and transferred after one day to liquid N<sub>2</sub>. To thaw cells, vials were quickly removed from the freezer, placed in a 37<sup>0</sup>C water bath. Cells were seeded in 60 x 10 mm Petri dishes in 10 ml of pre-warmed medium and reincubated until the cells attached. The following day the medium was changed to remove residual DMSO.

### **2.2.3 The experimental systems**

Fibroblast cell culture for all experiments was performed in standard culture media - (DMEM, 10% FCS, 1% Penicillin/Streptomycin), and cells were incubated at 37<sup>0</sup>C in a humidified atmosphere containing 8% CO<sub>2</sub> in air. Tests of radiosensitivity - clonogenic assay, PFGE,  $\gamma$ H2AX assays - were conducted in the primary embryonic fibroblasts of the lower passages (4-12). Comet assay, after being tested in fibroblasts, was performed in the whole blood. The primary fibroblasts of earlier passages do not carry the genetic alterations, which accumulate

usually during prolonged passaging and are induced by immortalisation in established cell lines, therefore they represent the most adequate experimental *in vitro* system. A particular effort has been provided to perform the repair measurements (PFGE,  $\gamma$ H2AX) and clonogenic survival experiments with cells at early confluency to assure their synchronisation at G1 phase of the cell cycle. The selection of doses for experiments was done to make possible comparison to published literature data about cell cycle progression of LEC cells (5 Gy [97]). 5 Gy of IR was used for investigations of growth curves to have consistency with cell cycle analysis. The dose applied for investigation of DSB repair by means of PFGE (70 Gy) was the same used by Hayashi *et al.*, 1994 [82] in their PFGE experiments on LEC versus WKAH fibroblasts.

#### 2.2.4 Growth curves

The growth curves of LEC and LE fibroblasts were investigated without and after 5 Gy of  $\gamma$ -irradiation. The growth curves were determined by plating 12 dishes of each cell line at initial density of  $4 \times 10^5$  cells per 60-mm<sup>2</sup> dish in standard culture media and were grown for 48 hours until they reached a log growth phase, which was determined experimentally in preliminary experiments. Further, they were irradiated with 5 Gy of  $\gamma$ -irradiation (HWM2000, dose-rate 1.7 Gy/min) and the numbers were counted. 23.5 hours and 54 hours after irradiation two dishes of control and irradiated sample of each cell line were trypsinized, 5 ml of standard culture media containing 10% FCS was added, cells were suspended and microscopic observations with inverted microscope Axiowert 135 were done. If the uniform single-cell suspensions were observed, the cell concentration was determined with Coulter Counter. If there were still clumped cells seen, resuspension was continued and microscopic observations were continued.

The rate of growth and doubling time (generation time) was determined from derived cell number counts. The mean value and standard errors were estimated for LEC and LE cells at 23.5 and 54 hours after irradiation and in controls.

Growth rate was determined according to equation:

$$K' = \text{Ln} (N2 / N1) / (t2 - t1)$$

Number of divisions per day:

$$\text{Div.day}^{-1} = K' / \text{Ln}2$$

Doubling time (generation time):

$$\text{Gen' t} = 1 / \text{Div.day}$$

where N1 and N2 = number of cells at time1 (47.5 hours after plating) and time2 (101.5 hours after plating) respectively. Divisions per day (Div.day) and the generation or doubling time (Gen' t) is calculated from the data of growth rate.

### **2.2.5 Clonogenic survival assay**

The clonogenic survival assay [104] was performed using LEC and LE fibroblasts to investigate their cellular radiosensitivity according to the protocol developed by Munschi *et al.*, 2005 [105] with minor modifications.

#### **Cell preparation and irradiation**

Fibroblasts of passage 5-12 were grown in 60 mm Petri dishes until they reached confluence (monolayer of spindle-shaped cells without visible mitotic activity and without crowding) and were irradiated being in G1 phase of the cell cycle. Cell cultures were trypsinised as described above. Cells were resuspended into single cell suspensions, which were observed under light microscope and in case of clumping, resuspended again, and diluted to get the desired concentrations. Cell concentrations were determined with Coulter Counter. Cells were further placed in 15 ml Falcon tubes, irradiated with 0-4 Gy (HWM2000, dose-rate 1.7 Gy/min) and known numbers of cells were seeded into 60 mm Petri dishes filled with 6 ml of pre-warmed standard culture media to yield 100 to 150 colonies per dish using two different cell inoculum levels ( $10 \times 10^3$  and  $5 \times 10^3$ ). For each dose point, three replicate dishes were used. Dishes were coded to assure independence of counts, each in triplicate, and incubated at standard culture conditions. Cell cycle of the remaining cells was checked to assure accumulation of cells in G1 at the moment of irradiation.

## Staining of plates

Colonies were fixed and stained at variable times during 1-2 weeks depending on their growth rate. The media was aspirated, 5 ml of staining solution (0.5% crystal violet in 70% ethanol) was added to the plate and left for 10 min for staining and fixation of the colonies. The staining solution was discarded, the plates were washed in tap water, and dried on air (see **Figure 2.1.**, which contains the example of the stained plate (**A**) and colony (**B**)).

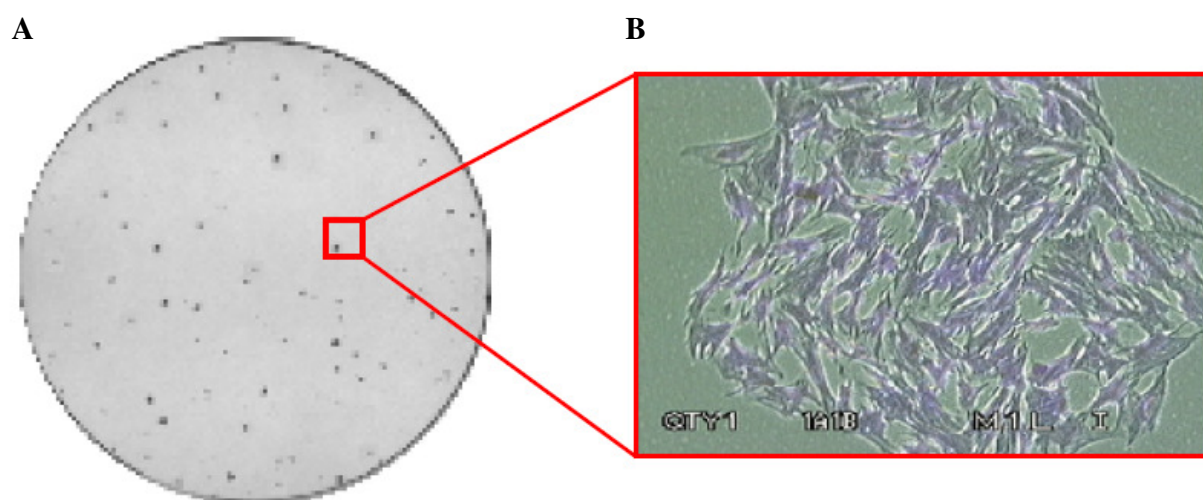


**Figure 2.1. Image of representative plate in one of studied cell line (LEC-1, 1 Gy)**

**A:** The plates were stained with 0.5% crystal violet in 70% ethanol and dried. The colonies containing more than 30 cells were counted under dissection microscope.

**B:** The picture of representative colony of unirradiated LEC-1 fibroblasts was taken with phase-contrast microscope Axiovert, under 40x magnification.

## Counting of colonies

Colonies (see **Figure 2.1.**) were counted under the magnified field of the dissection microscope in each dish to obtain the plating efficiency (PE). The term PE indicates the percentage of cells seeded into a dish that finally grow to form a colony.

A cluster of blue-stained cells was considered a colony if it comprised at least 30 cells (**Figure 2.1., B**). The commonly used threshold is 50 and 30 cells. In case of primary fibroblasts colonies are more sparse and occupying more space on the plate. With the high colony numbers seen in control there is a possibility that colonies fuse, that is why a cut-off of 30 cells was set.

Plating efficiency and survival fractions were estimated. PE was calculated as:

$$\text{PE (\%)} = \frac{\text{Number of colonies counted}}{\text{Number of cells plated}} \times 100$$

Following determination of PE, the fraction of cells surviving a given treatment (SF) was calculated by normalizing PE after a given dose to that of the control unirradiated plates:

$$\text{SF (\%)} = \frac{\text{PE of treated sample}}{\text{PE of control}} \times 100$$

The cytotoxic effect of IR on mammalian cells is generally described by a cell survival curve. The survival curves were evaluated for LEC and LE cell lines irradiated at G1 phase of cell cycle in a range of doses from 0 to 4 Gy. Higher doses of irradiation could not be used, since the number of control colonies became too low for reliable quantification. Increase in number of seeded cells failed to overcome this dose limitation, what led to overgrowing of colonies in controls. For visual presentation of survival after radiation the survival fraction was plotted on a logarithmic scale (y axis), against dose on a linear scale (x axis), resulting in a survival curve.

### **Survival curve fitting. Parameters of survival curves**

The linear-quadratic model is now the model of choice to describe survival curves. The theory behind the shape of the shouldered mammalian cell survival curve fitted to linear-quadratic equation relates the linear and quadratic terms in dose to cell killing. The linear coefficient in dose,  $\alpha$ , describes the part of curve resulting from cell death dominated by single hit kills, while the quadratic term in dose,  $\beta$ , describes cell death requiring multiple interactions [3].

By this model the mathematical expression for the cell-survival is:

$$S = e^{-\alpha D - \beta D^2},$$

where S is the fraction of cells surviving a dose D, and  $\alpha$  and  $\beta$  are the constants, characterizing the curve.

The values of D1, initial slope, were estimated from survival curves. D1 is the mean lethal dose, or the dose that delivers, on average, one lethal event per target and is the dose, which decreases the survival fraction to 0.37 on the initial portion on the survival curve [3].

The dose modifying factor (DMF) for SF at 2 Gy and 3 Gy was determined as:

$$\text{DMF} = \frac{\text{SF(Dose) (LE)}}{\text{SF(Dose) (LEC)}}$$

### **Statistical evaluation**

The data were presented as mean values and SEM of 3-6 independent experiments. According to the work published by Buffa *et al.*, 2001 [106] the distribution of the SF2 can be fitted to Gaussian and log-Gaussian distribution. Therefore, the further statistical evaluation of data included testing for difference of measured SF at different doses (1-4 Gy),  $\alpha$ ,  $\beta$  and D0 applying the Student's t-test.  $P < 0.05$  was considered significant. Additionally two-way ANalysis Of VAriance between groups (ANOVA) was applied for comparison of survival of fibroblasts from LEC and LE rat strains.

### **2.2.6 Pulsed field gel electrophoresis**

#### **The principle of pulsed field gel electrophoresis**

The repair of DSB induced by IR was investigated using pulsed field gel electrophoresis (PFGE).

PFGE is applied to study the mobility of DNA molecules as large as 10 Mb. Intact genomic DNA and fragments longer than 50 kb from mammalian cells are too large to migrate into an agarose gel under the constant field strength. Periodically changing the orientation of the electric field forces the DNA molecules in the gel to relax on removal of the first field and

elongate to align with the new field, resulting in a net migration of DNA fragments in a straight line.

Broken DNA fragments resulting from irradiation, which are shorter than gel-specific threshold, can migrate into the gel. The number of DSB and therefore the number of fragments increases with dose. Therefore the fraction of DNA released from the well can be used as a measure of radiation-induced DSB and their repair.

PFGE was performed in CHEF Mapper gel electrophoresis system according to the protocol developed by Friedl *et al.*, 1995 [107] with some modifications.

### **Preparation of agarose plugs/ DNA extraction**

Cells were grown in cell culture Solo flasks till confluency. Confluent cells were used to reduce the proportion of S-phase cells, because it is known that the percentage of DNA released from the plug for cells irradiated in S-phase is one-third of that for cells irradiated in G1 phase [108]. With the fraction of cells in S phase ranging from 1 to 5% estimated in performed experiments ( $4.32 \pm 1.96\%$  of LEC and  $3.6 \pm 0.71\%$  of LE cells were in S phase,  $n = 6$ ), cell cycle distribution had therefore no impact on DNA migration.

Cells were washed with pre-warmed PBS and harvested by trypsinisation (as shortly as possible, to avoid induction of DSB by the trypsinisation process). Cell suspensions were centrifuged (1000 rpm, at RT, for 5 min), washed in PBS, and resuspended in PBS at the concentration of  $3 \times 10^6$  cells/ml. For a typical experiment at least 2 ml (about  $6 \times 10^6$  cells/ml) were used.

### **Embedding of cells in agarose plugs**

For preparation of agarose plugs, plastic custom-designed moulds were rinsed with 70% ethanol and dried on air. 1.6% low melting point (LMP) agarose was boiled in 20 ml PBS (microwave) and kept at 37°C in a water bath. Cell suspensions were mixed with an equal volume of the agarose solution (ca 37°C), shortly vortexed at low speed, and 200 µl portions were pipetted into the mould (see **Figure 2.2., A, APPENDIX**, page 145). Moulds were left in the refrigerator at 4°C for solidification of agarose plugs. Moulds were opened and plugs were transferred with plastic spatulas into 15 ml Falcon tubes filled with a few ml of ice cold media

(Figure 2.2., B, APPENDIX, page 145). The plugs were then left for equilibration for 30 min on ice.

### **Sample preparation and irradiation**

Agarose plugs for calibration, repair and repair control samples were prepared.

Each plug of calibration (induction) samples was transferred into a 15 ml Falcon Tube filled with 10 ml of ice-cold DMEM standard culture media. The samples were irradiated with 0, 5, 10, 20, 30, 40, 50, 60, 70 Gy of  $\gamma$ -irradiation on the Gammacell I (Co-60) machine operating at a dose rate of 4.2-3.98 Gy/min (the range reflects the decay of the source in the time period when experiments were performed). For repair samples the desired number of plugs (normally 6) was first placed into a 50 ml Falcon Tube containing about 20 ml of ice-cold media and irradiated with 70 Gy. Control samples (6 plugs) were treated like the repair samples, except that they were not irradiated. They served to measure unspecific DNA degradation during 6 hours of post-irradiation incubation. During irradiation, cells were kept on ice to prevent DSB repair; further sample preparation was performed on ice. To allow repair, plugs containing intact cells, were transferred to Petri dishes, filled with fresh, prewarmed media (37<sup>0</sup>C). Since cells may suffer from prolonged incubation within the plugs, the most reliable observations of DNA repair under such conditions were within 6 hours after irradiation.

### **DNA preparation in agarose plugs**

To prepare intact genomic DNA, cells were lysed *in situ* in the agarose plugs. This protects the molecules from both mechanical breakage and nuclease degradation during the isolation process. Cellular materials released by digestion diffuse out of the agarose during the washes while the DNA macromolecules remain trapped. Because cellular enzymes were removed completely, samples prepared in this way are relatively stable and could be stored for 2-3 months. Induction samples were treated directly after irradiation, repair and control samples after time for repair (see above, Sample preparation and irradiation). The plugs were transferred to 15 ml Falcon tubes filled with ice-cold 0.5 M EDTA (pH 8) (Figure 2.2., C, APPENDIX, page 145). After incubation on ice for 30 min, EDTA was decanted and 1 ml of ESP Buffer was given to the plug. In this solution, the plugs were incubated at 50<sup>0</sup>C for about 48 hours. ESP was decanted and

the Falcons were filled with Rinsing Buffer. Rinsing Buffer was changed 3-4 times during the next 2-4 days, and plugs were ready for storage and electrophoresis.

### **Preparation of the electrophoresis gel**

To prepare the gel with plugs for electrophoresis, 0.8 % LE-agarose was boiled in 175 ml 0.5 x TBE and kept at 37<sup>0</sup>. Part of the agarose solution was poured into a gel cast device and left to solidify (**Figure 2.2., E, APPENDIX**, page 145). Formed gel stripe thus contained 10 wells that were 10 mm broad. The calibration sample agarose plugs were placed into these wells: this required to cut pieces of 5 mm x 10 mm x 1 mm out of the 200 µl plugs (these are about 15 mm x 10 mm x 1 mm) using ethanol-rinsed cover slip (**Figure 2.2., D, APPENDIX**, page 145). Once all wells were filled, the well-forming device was placed about 3.5 cm below the gel strip and agarose solution (50<sup>0</sup>) was filled into this space. In the same way wells were filled with repair samples. Finally the device was placed again 3.5 cm below the gel stripe and niches were filled with repair and control samples (**Figure 2.2., E, APPENDIX**, page 145). At the end, remaining agarose solution was poured over to obtain a smooth surface (**Figure 2.2., F, APPENDIX**, page 145). After plugs were embedded in gels their DNA was subjected to PFGE.

### **Electrophoresis conditions**

Electrophoresis was performed in a BioRad CHEF GeneMapper electrophoresis chamber, filled with 2 litre of 0.5 x TBE (Running buffer) at a buffer temperature 25<sup>0</sup>C for 30 hours, with 75 min pulse time, and a voltage gradient of 1.3 V/cm. Under these PFGE conditions fragments which are larger than a certain threshold value remained within the plug during electrophoresis, while smaller fragments 100 kb up to 5 Mbp entered the gel and formed a pseudo-band (about 2 cm below the plug) (A. Friedl, personal communication), (see **Figure 2.3.**).

### **Gel staining and DNA measurement**

The gels were stained overnight in a 0.5 µg/ml of ethidium bromide in Running Buffer. For scanning of the fluorescence intensity the gels were placed on top of a UV transilluminator

(302 nm), and pictures were taken with the Bio Rad Gel Doc2000 System. To avoid fading of fluorescence, the image was taken within 2-3 seconds of UV exposure of the gel [107].

The distribution of the signal was determined by analyzing the images generated using Quantitative One-4.4.0 Software. The line borders were arbitrary defined on each analysed gel (see **Figure 2.3., A**). The Quantitative One-4.4.0 Software measures the pixel intensity and assigns the values for it (Y axis, Intensity) at each point of the defined line (X axis, Distance). For the further analysis a custom program for FAR (fraction of activity released) analysis (FAR3) (see **Figure 2.4., APPENDIX**, page 146-147) was developed on the basis of FAR-ANALYSIS (Anna Friedl, 1995 (Program for two column input data)) by D. Kononko (personal communications, Check Point Branch, Minsk). The program is compact, efficient, user-friendly, and has a number of useful features for data analysis (for detailed description see **Figure 2.4., APPENDIX**, page 146-147). The density profile of the full width of each lane was plotted versus distance of migration (see **Figure 2.3., B**). The profile consisted of the origin of the plug and the pseudoband (composed of fragmented DNA) which was induced by IR and which resulted from spontaneous fragmentation. After a dose of 70 Gy the fragmentation of the DNA resulted in the majority of the DNA migrating out of the origin and without irradiation there was almost no DNA migration observed. If the cells are allowed to repair for 6 hours, most of the DNA no longer migrates beyond the plug, indicating its return to a higher molecular weight (DNA repair).

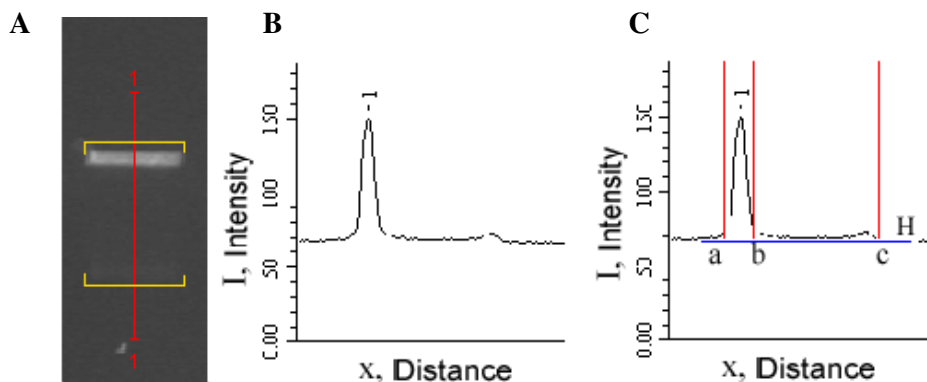


**Figure 2.3. Intensity profile of one of the bands on the PFGE gel (see Figure 3.6.)**

**A:** One of the bands is delineated with QuantityOne-4.4.0 Software

**B:** Distribution of the EtBr signal in the band along the DNA migration lane is shown

**C:** The FAR3 program used for evaluation of FAR estimated amount of DNA between (a) and (c) borders, limiting band. This distance was set the same for all samples on one gel from band to band. The position of the first peak corresponding to the plug (between (a) and (b)) was also set to be same for all samples. The background (H) was corrected considering the values outside of the band (before (a) and after (c)). FAR3 Software allowed to estimate the amount of DNA in the whole lane and find out what fraction of DNA is migrating out of the plug by dividing values of DNA migrated out of plug by whole DNA in the lane limited by a, c borders and background.

## Data analysis and presentation.

### Correction for background and control values

The percentage of DNA migrating from the plugs into the lane (% DNA-extracted, or FAR-fraction of activity released) was used for quantification of DSB.

FAR-fraction was estimated as:

$$\text{FAR (\%)} = \frac{\int_b^c (I(x) - H)dx}{\int_a^c (I(x) - H)dx} \times 100$$

where (see **Figure 2.3., C**):

a - migration distance, at which peak begins (border 1). It is the beginning of the band as well.

b - migration distance, at which peak ends (border 2)

c - migration distance, at which band ends (border 3)

H - background value

$\int_b^c (I(x) - H)dx$  - integral value proportional to the amount of DNA migrated out of the peak, background is subtracted

$\int_b^c (I(x) - H)dx$  - integral value proportional to the amount of DNA in the line, background is subtracted

## Derivation of Gy-equivalents

The percentage of extracted DNA in the PFGE gel not only depends on the DSB frequency within the sample, but also on the conditions of the electrophoresis and the cell cycle distribution of the cells. To avoid the possibility that differences in chromatin structure caused by difference in cell cycle distribution might cause the differences in induction of DNA damage [109] and to facilitate comparisons between different experiments, experiments were performed on cells mostly in the G1 phase of cell cycle ( $89.42 \pm 4.28$  % of LEC fibroblasts - in G1, LE –  $89.25 \pm 0.78$  %;  $4.32 \pm 1.96$  % of LEC and  $3.6 \pm 0.71$  % of LE cells were in S phase, N = 6). The internal standards (induction curves) were performed for different doses and were compared between LEC and LE cells (**Figure 2.5., A**). The calibration of the relationship between irradiation dose (induction samples) (**Figure 2.5., B**) and fraction of DNA released (FAR) (**Figure 2.5., A**) was used to derive Gy-equivalents (Gy-eq) In other words, the data of FAR repair (at 1.5 hours FAR is 24.5%, **Figure 2.5., A**) have been converted into the number of Gy-eq of initial damage (24,5% FAR is converted to 24 Gy-eq, **Figure 2.5., B**). Any damage level remaining after repair was thus expressed in terms of initial damage Gy-eq (i.e. the proportion of DNA eluted is the same as if the sample had been irradiated with dose x).

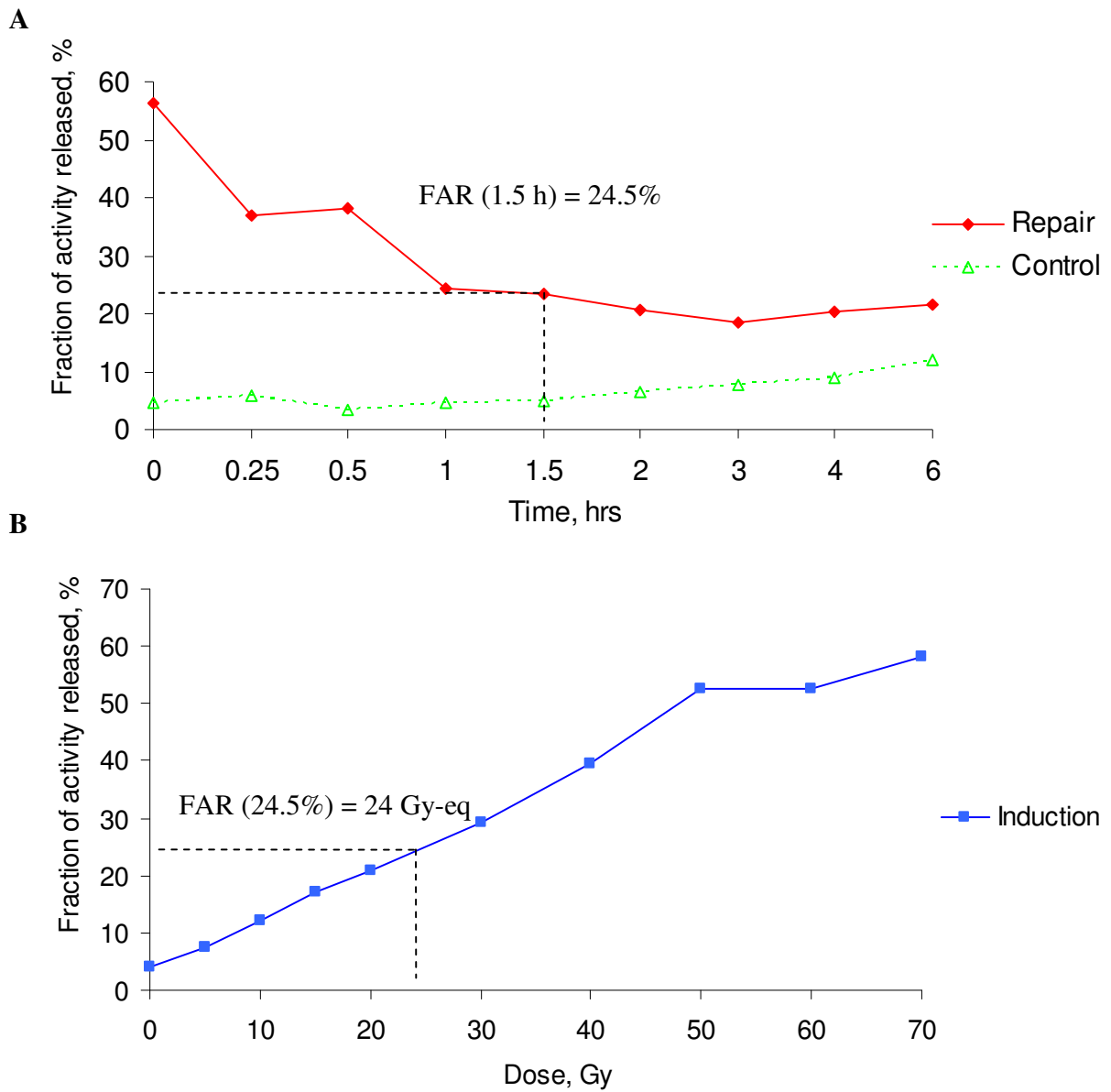


**Figure 2.5. Scheme representing conversion of FAR values into Gy-eq**

One of the experimental data sets is presented.

**A:** Fraction of activity released (FAR) repair values were determined for repair times

**B:** FAR values were converted in Gy-eq applying the measured induction curves

## Correction for DNA degradation

Data for irradiated cells were corrected for background (Gy-eq observed for control (unirradiated) cells). For each experiment the values of Gy-eq for respective control samples were subtracted from respective values of Gy-eq repair. This correction assumes that an additional amount of DNA is released into the lane because of background degradation processes.

## Fitting of data and derived parameters

Fitting of repair curves was achieved using the non-linear regression analysis of the commercially available software package GraphPad Prism 3.03. Repair kinetics data were fitted assuming two exponential components of rejoining according to the equation:

$$FAR = Ae^{-bt} + Ce^{-dt} + R,$$

where:

the first term in the equation ( $Ae^{-bt}$ ) was fitted to the fast, and the second ( $Ce^{-dt}$ ) - to the slow component of rejoining. Parameters A and C describe the amplitudes and parameters b and d are the rate constants of the fast and slow component of rejoining, respectively, R is a residual damage.

From these parameters the half-times for the rejoining of the fast and the slow component was calculated as:

$$t_{1/2, \text{ fast}} = \ln 2/b$$

$$t_{1/2, \text{ slow}} = \ln 2/d$$

where:

$t_{1/2, \text{ fast}}$  is the half-time of DSB rejoining by the fast component;

$t_{1/2, \text{ slow}}$  is the half-time of DSB rejoining of the slow component;

parameters b and d the rate constants of the fast and slow component of rejoining.

The fraction of DSB rejoined by the fast and slow component of rejoining can be calculated as:

$$F_{\text{fast}} = \frac{A}{A+C}$$

$$F_{\text{slow}} = \frac{C}{A+C}$$

where:

parameters A and C describe the amplitudes of the fast and slow component of rejoining, respectively, and  $F_{\text{fast}}$  – fraction of DSB rejoined by the fast component, and  $F_{\text{slow}}$  – fraction of DSB rejoined by the fast component.

### **2.2.7 Analysis of $\gamma$ H2AX foci**

Formation and dissociation  $\gamma$ H2AX repair foci were investigated in LEC and LE primary fibroblasts. The applied protocol was developed by Guido Drexler (personal communications).

#### **Growth of cells on slides and irradiation**

$1 \times 10^4$  cells were plated on glass slides and grown for 4 days in standard growth DMEM media at 8% of CO<sub>2</sub>/air. Cells were either left untreated or exposed to 1 Gy of  $\gamma$ -irradiation and left for repair in the cell incubator for 9 and 24 hours.

#### **Fixation and staining with primary/secondary antibodies**

After the indicated time intervals cells were fixed in 2% Paraformaldehyde, washed once with PBS, permeabilized in PBS containing 0.2% (v/v) Triton X-100, incubated three times with 0.15% Triton (PBS), and blocked another three times for 10 min with PBS+ (PBS, 1% BSA, 0.15% Glycin). All steps were done at RT. Fixed, permeabilized cells were incubated with primary  $\gamma$ H2AX phosphospecific mouse monoclonal antibody diluted 1:300 in PBS+. 75  $\mu$ l was applied to slide and left for 1 hour at 4<sup>0</sup>C in a humidified chamber. Subsequent washing was

conducted at RT as follows: 5 min, PBS; 10 min, PBS/0.15% Triton; 5 min, PBS; 7 min, PBS+. Secondary antibody (anti-mouse IgG-Alexa488), was diluted 1:200 in PBS+, and 75  $\mu$ l of the mixture was applied to each slide and left for 45 min at 4<sup>0</sup>C in darkness. After this, slides were washed with PBS/0.15% Triton twice for 5 min, once for 10 min with PBS, and again once for 7 min with PBS. Nuclei were counterstained with the DAPI - DNA stain for 90 seconds and washed twice for 2 min with PBS. After short air drying 8  $\mu$ l of Vectashield was applied and slides were covered with cover slip. Fluorescence microscopy was performed within 7 days after staining.

## Microscopy

Images were obtained using the LSM510 (Zeiss) confocal laser microscopy system. To allow direct comparison, all samples from one experiment were treated and processed simultaneously and all images were obtained using the same parameters (brightness, contrast). Images were collected by laser scanning of stained cells (filter C-Apochromat, 63 x 1.2 W corr) with parameters for fluorescent dyes: Alexa488 (excitation 488 nm, emission 520 nm) (see **Figure 2.6., H**); DAPI (excitation 350 nm, emission 460 nm) (see **Figure 2.6., G**). 5 z-stack images were taken from consecutive layers of each image (see **Figure 2.6., A-F**) and were further projected into one image (see **Figure 2.6., F**), allowing scoring of all foci at different levels of one nucleus on a single image. Size of the image taken: 512 x 512 x 5 (pixel). Images were further analysed with special application LSM-510 META 3.2SP2, ZEISS, Expert Mode.

## Foci quantification

The number of  $\gamma$ H2AX foci was evaluated in control and irradiated fibroblasts after 1 Gy of  $\gamma$ -irradiation after chosen time (9 and 24 hours).

Considering that manual counting of foci is very laborious, subjective and error-prone, a simplified automatical foci quantification was performed.

For quantitative analysis of foci, the images were further processed with ImageJ 1.36b (NIH) image – analysis program (NIH, USA; see <http://www.rsbl.info.nih.gov/ij/>). The ImageJ 1.36b shows the green and blue channels of the image separately. The images from Alexa488 ( $\gamma$ H2AX) green channel were stacked together and by applying the ‘Montage’ option turned into

one image with the scale factor 0.5 (**Figure 2.7., A, APPENDIX**, page 148-149). The images from all samples were processed in an identical way. The ‘Threshold’ function of ImageJ was applied to subtract background (see **Figure 2.7., A, B, APPENDIX**, page 148-149). The threshold was fixed the same for all images and was set high enough to assure the background elimination. The ‘stacked’ and ‘montaged’ DAPI images were merged with outlines of DAPI images of the same sample (**Figure 2.7., C, D, APPENDIX**, page 148-149) using the ‘RGB merge’ plugin of ImageJ Software. The quantification of  $\gamma$ H2AX foci was done automatically using ImageJ 1.36b Software on the montaged images of  $\gamma$ H2AX, which counts foci in the whole image. Number of cells in the image was counted from the DAPI staining and number of foci was averaged per number of cells in the sample.

### **Statistical evaluation**

All experiments were performed at least three times in independent tests. Differences between LEC and LE respective data groups for analysed time-points were compared using two-tailed Student’s t-test and  $P < 0.05$  was considered significant.

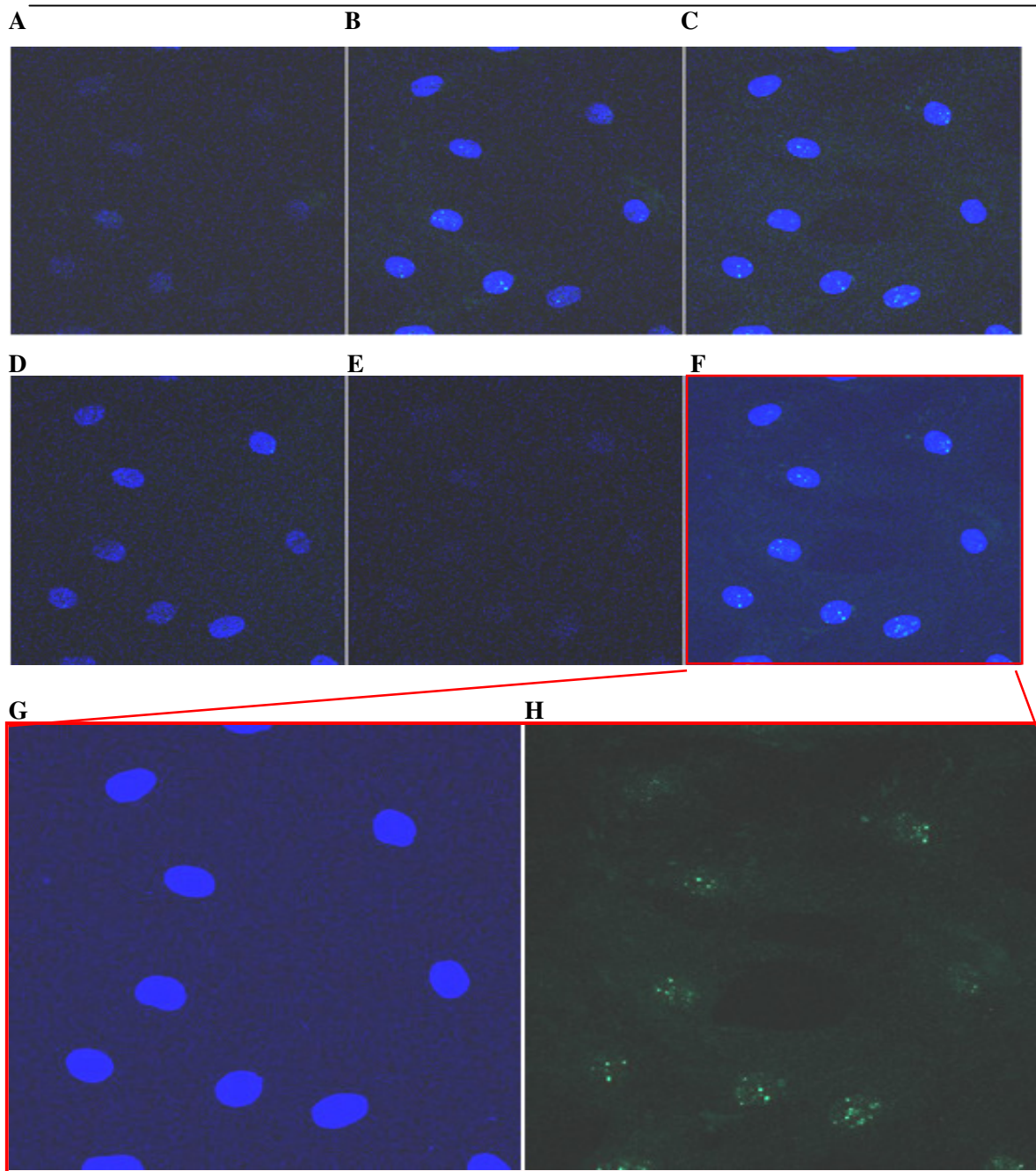


**Figure 2.6. Sequence of scanned images of  $\gamma$ H2AX staining. z-stack processing**

**A-E:** 5 images were taken from subsequent levels of thickness of one region of the slide with LSM510 (Zeiss) confocal scanning laser microscope. Cells were stained with primary mouse antibody against  $\gamma$ H2AX, and secondary antibody was linked to Alexa488

**F:** The 5 images (**A-E**) were further projected into one, applying z-stack techniques

**G:** The blue (DAPI) channel is shown

**H:** The Alexa488 signal ( $\gamma$ H2AX) is shown

### **2.2.8 Comet assay**

The alkaline version of the comet assay [110] was performed to assess repair capacity of SSB, alkaline labile sites (ALS), and DSB in LEC and LE cells. At alkaline pH (pH > 13) increased DNA migration results from conversion of ALS into SSB. The method was performed at the facilities of BFS (Institute for Radiation Hygiene, Neuherberg), following the protocol developed by Singh, 1995 [111] with modifications introduced by Maria Gomolka [112].

Preliminary experiments, which were conducted using fibroblasts, showed large heterogeneity in measured values and it was decided to measure repair in lymphocytes of whole blood. Investigations of Chuang *et al.*, 2004 [113] show that the use of whole blood creates comet images, which were not different from those obtained from isolated lymphocytes. Three animals were bled and repair capacity was evaluated at 0, 15, 30 and 60 min after 4 Gy of IR.

### **Collection of blood and irradiation of samples**

The blood samples were taken from the sublingual vein of rats following the protocol developed by Zeller *et al.*, 1998 [114]. Unfasted rats were anaesthetized with isoflurane in an inhalation chamber. One person held the unconscious animal and the second person pulled forward the tongue and punctured one of the sublingual veins with a gauge. Blood samples of volume about 0.5 ml were collected into tube containing anticoagulant (heparin).

20 µl of the whole blood was aliquoted in 1.5 ml Eppendorf tubes and irradiated on ice with 4 Gy of  $\gamma$ -irradiation. Irradiation was performed with HWM D2000 (Cs-137) at dose rate of 1.7 Gy/min).

### **Repair incubation, cell lysis and slides preparation**

Immediately after irradiation the samples were placed in an incubator at 37°C. At 0, 15, 30 and 60 min after irradiation 10 µl of an irradiated and for chosen time points of a control sample was removed and embedded in a second layer of agarose, prepared as the first layer (described later) and stored at 50°C until use. The irradiated samples (10 µl) were mixed gently with 100 µl of the liquid agarose, placed on the slide and covered with a cover slide (dipped

before in 0.1% Triton-X/H<sub>2</sub>O and dried) to create a uniform surface without included air-bubbles. The slides were placed for 5 min on a cold plate (4<sup>0</sup>C), before removing the cover slip.

After removing the cover glass, the slides were placed in 50 ml of freshly prepared Lysis Buffer I and were incubated overnight at 4<sup>0</sup>C. To remove proteins slides were placed in 50 ml of Lysis Buffer II and incubated at 37<sup>0</sup>C for 1 hour.

Glass slides were prepared in advance. Slides were covered with a first layer of 0.1% low-melting agarose (Serva). 0.1% low-melting agarose was suspended in 0.9% NaCl, vortexed and permitted to rest for 10 min at 50<sup>0</sup>C. Afterwards, the suspension was vortexed and microwaved briefly until boiling, checked for clumps. The process of vortexing and microwaving was repeated three times and agarose was aliquoted into Eppendorf tubes, which were agitated at 50<sup>0</sup>C for 1 hour. Slides were put onto a warming plate at 45<sup>0</sup>C and 200 µl aliquots of liquid agarose were pipetted onto the slides and evenly distributed with a spatula. The slides were dried completely at least for 1 hour.

### **Electrophoresis. Neutralization, dehydration and precipitation**

1 litre of Electrophoresis Buffer was set up prior to electrophoresis and was precooled at 4<sup>0</sup>C. Before electrophoresis slides were placed and fixed in a special modified electrophoresis chamber to allow DNA unwinding for 20 min at 4<sup>0</sup>C. Slides were exposed to electrophoresis at 4<sup>0</sup>C, for 30 min, at 24 V with stirring of buffer in the electrophoresis chamber.

For neutralization, dehydration and precipitation slides were placed in 50 ml of the neutralization buffer in Coplin Staining Jar and incubated for 30 min at RT in the dark. For further dehydration slides were placed in absolute EtOH overnight at RT.

Before drying slides covered with agarose were rehydrated in 70% EtOH for 5 min at RT preferably in the darkness. Dried slides were stored in a closed box until staining.

### **Staining of slides**

For staining slides were placed twice into H<sub>2</sub>O<sub>dist</sub>, and 50 µl of the staining solution were applied. The staining steps were performed in the dark as SYBRGreen is sensitive to light. Evaluation of results was done immediately following the staining.

## Image acquisition

60-120 SYBR Green stained electrophoregrams (comets) in the central part of each slide were examined under epifluorescence microscope (Axiovert 135, Zeiss, Germany; 40 x air objective) equipped with filters for SYBRGreen and a monochromator (T.I.L.L. Photonics, Munich, Germany) as a light source for the image analysis with excitation at 461 nm and emission at 510 nm. Images were acquired with a Sony Video Camera (XC-7500) and evaluated by VisCOMET Software. Acquisition was done with preliminary adjustment of image saturation.

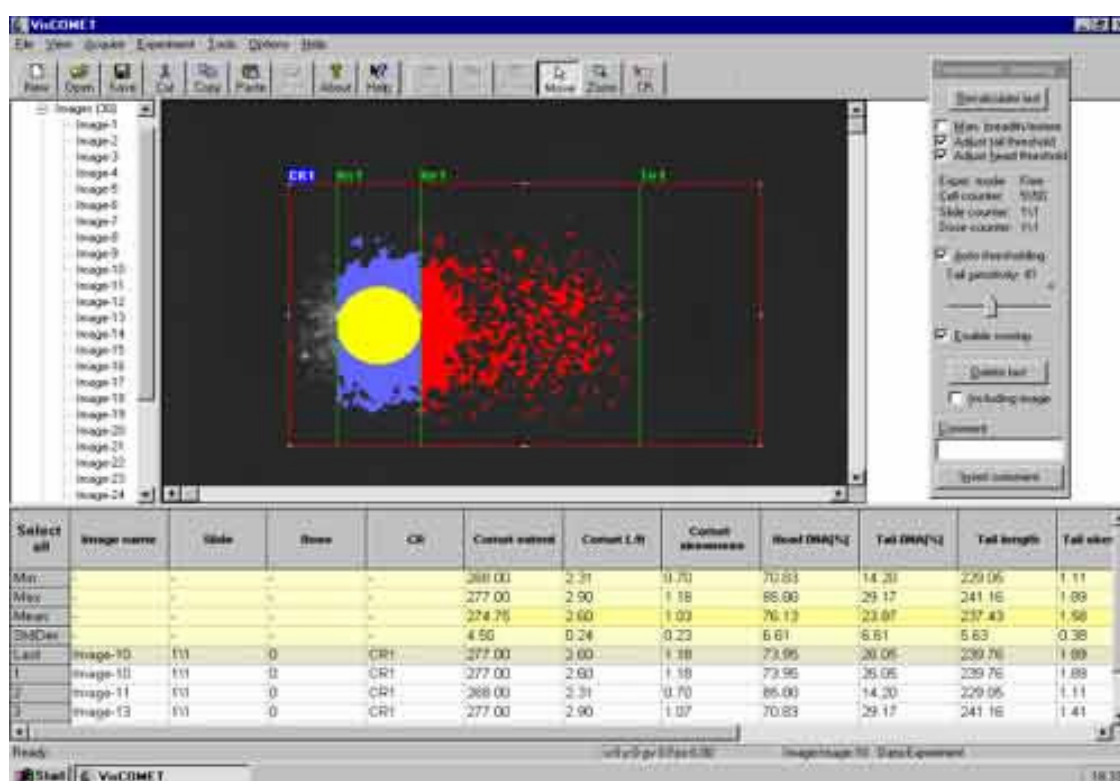


**Figure 2.8. VisCOMET program interface with pictured example of acquired comet with defined regions of interest - tail, head, background**

The image pictured by VisCOMET represents an electrophoregram of the single cell DNA with extended 'tail' containing DNA fragments of different size, stained with SYBR Green. The program features for comet analysis include automatic and manual settings of head and tail regions, adjusting exposure and image parameters. The measured values include 24 characteristics of the acquired comet with statistical evaluation within the sample (mean, maximum, minimum, standard deviation).

## Comet analysis

The regions of interests (head and tail) were determined automatically by VisCOMET from comet images (see **Figure 2.8.**). The list of evaluated parameters included eleven parameters characterizing comet in total, eight parameters – head of comet, and six - % of tail DNA. From all comet characteristics measured the Tail (Olive) moment as commonly measured representative parameter was selected for further analysis.

Tail (Olive Moment) is defined as the product of the tail length and the fraction of total DNA in the tail. Tail moment incorporates a measure of both the smallest detectable size of migrating DNA (reflected in the comet tail length) and the number of relaxed / broken pieces (represented by the intensity of DNA in the tail):

$$\text{Olive Tail Moment} = (|CG - CG_H|) \times \text{DNA}/100$$

where:

CG = center of gravity of the tail or body weighted by gray values

CG<sub>H</sub> = center of gravity of the head weighted by gray values

DNA = tail or body DNA

## Statistical analysis

Tail Olive Moment values were estimated in 3 animals in 60 – 120 cells each at each time point and data were presented in box and whiskers plots. A box and whiskers plot shows quartiles: One quarter of the values lie between the top whisker and the top of the box; one quarter (25<sup>th</sup> percentile) in above the median line (the 50<sup>th</sup> percentile) within the box; one quarter below the median line within the box (75<sup>th</sup> percentile); whiskers show the +/- 1.5 x IQR (interquartile range). The outliers are pictured too.

The values of Tail (Olive) moment for repair were compared at different times. Tail moment is known to have a non-Gaussian distribution [115]. In this case comparison between groups was done with Mann-Whitney U-test and nonparametric Kruskal-Wallis ANOVA rank model, using the Prizm 3.0 Software [116]. The work of Duez *et al.*, 2003 [115] on statistical evaluation of comet data show that commonly used Mann-Witney test and Kruskal-Wallis

statistics are oversensitive and show the statistical significance even when the difference is not relevant biologically because of the large number of measurements in one sample (100). They recommend reduction of data to representative non-parametric statistics (medians, 75<sup>th</sup> percentiles) for further statistical analysis. Considering these recommendations, the statistical analysis of produced data included firstly testing for a difference between samples taken from different animals of one rat strain and measured at one time point applying Mann-Whitney U-test. Further statistical analysis included comparison of the means, medians and 75<sup>th</sup> percentiles, estimated for each measured animal, applying ANalysis Of VAriance (ANOVA).

### **2.2.9 Cell cycle analysis**

Analysis of cell cycle distribution was performed in exponentially growing LEC and LE fibroblasts after 5 Gy of  $\gamma$ -irradiation at different time points by means of flow cytometry analysis.

#### **Choice of protocol for DNA content analysis**

Generally methods, which utilize detergents and/or hypotonic solutions to permeabilize cells and produce free nuclei, provide much more accurate estimates of DNA content compared to measurement of fixed cells. Two-step method developed by Nusse *et al.*, 1984 [117] which allows cell lysis and separation of nuclei, was used for DNA content analysis.

#### **Preparation of samples**

$4 \times 10^5$  cells were plated per Petri dish and left to attach and grow. At 24 hours after plating medium was changed and after additional 24 hours growing cells were irradiated with 5 Gy of  $\gamma$ -irradiation (HWM2000, 1.7 Gy/min). At various time points cells were washed with PBS, trypsinized, and collected in 15 ml Falcon tubes. About  $5 \times 10^5$  cells were centrifuged, most of supernatant was decanted, only a small volume of approximately 50  $\mu$ l of media was left. The pellet was resuspended in the remaining media and 1 ml of the detergent solution I, containing 40  $\mu$ g/l ethidium bromide (EtBr) (See **2.1 Materials**, **2.1.9 Buffers**) was added, and mixed by shaking. 1 ml of citric acid-sucrose solution II (25  $\mu$ g/l EtBr) was added after 60 min incubation at RT to

the cells treated with detergent. After this second treatment released nuclei and micronuclei were simultaneously measured in a flow cytometer.

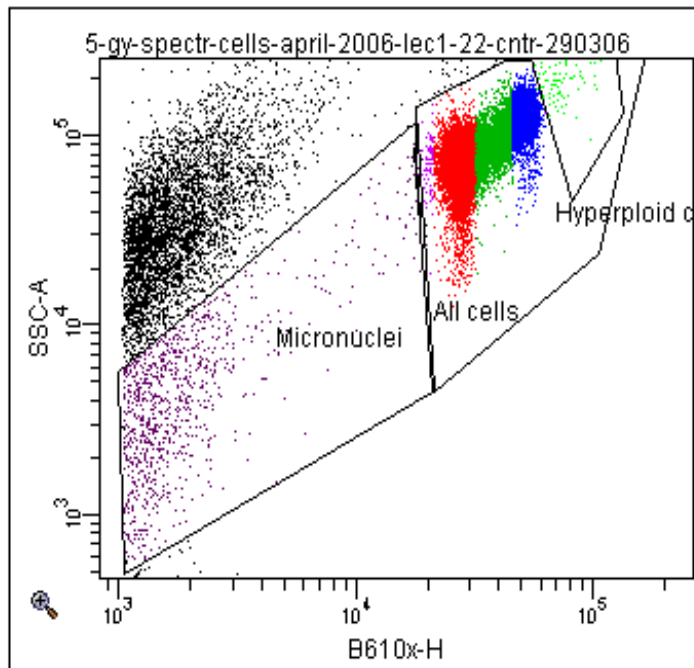
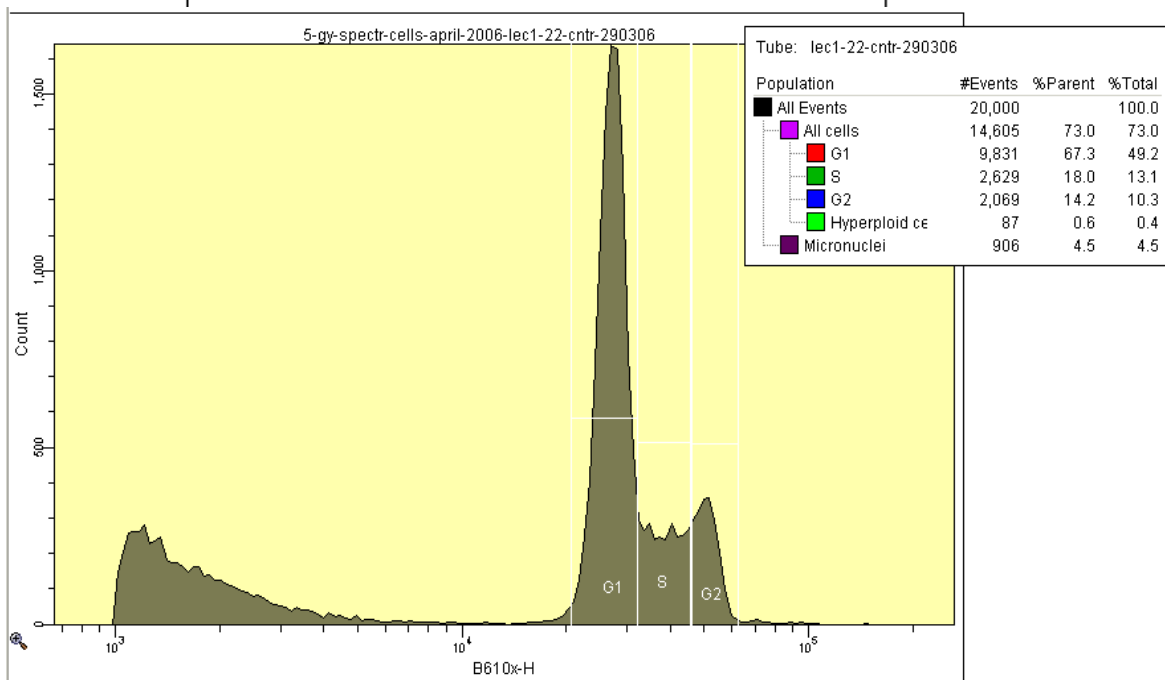
### **Measurement and data collection**

EtBr fluorescence (pulse height and pulse area) and side scatter as well as forward scatter of nuclei and micronuclei were measured simultaneously using a Becton Dickinson LSR II Flow Cytometer (see **Figure 2.9.**). Excitation of EtBr was provided by the 488-nm line of an argon laser; EtBr fluorescence was detected with a long-pass filter.

### **Presentation of cell cycle data**

The data were further analyzed with FACSDiva Software. The **Figure 2.9.** shows the dot-plot and histogram graphs. The cells at %G1, %S, and %G2/M phases were gated with help of the FACSDiva Software according to their EtBr staining (G2 phase cells had twice the amount of DNA compare to G1 cells, S phase cells had intermediate amount). Due to high resolution of DNA histograms the % of cells in the different cell cycle phases was derived directly from histograms by arbitrary gating of cells in G1, S and G2/M phases of cell cycle (see **Figure 2.9.**).

The time course of the kinetics of a cell population is usually represented either by showing the sequence of DNA histograms or by time plots of percentages of cells in the different phases of the cell cycle - G1, S and G2/M (%G1, %S, and %G2/M).

**A****B**

**Figure 2.9. Presentation of cell cycle distribution on the DNA content histogram**

**A:** Figure depicts the dot-plot graph of the measured sample. Intensity of EtBr staining is plotted against side scatter. The gating of the cells, micronuclei, and hyperploidy cells is performed.

**B:** The histogram representation of DNA content distribution is shown. Intensity of EtBr staining is plotted on log scale against measured number of cell counts. On the image cells are gated in G1, S, and G2/M phase of cell cycle and the percentage of cells in each phase of the cell cycle relative to the total number of cells is shown.

## 2.2.10 General molecular biology methods

### Isolation of DNA and RNA from animal tissues (liver, heart, brain, tail tips) and cultured fibroblasts

Genomic DNA extraction from cultured cells. About  $1 \times 10^9$  cells were washed with PBS, trypsinized, and centrifuged. The supernatant was discarded and pellet was resuspended. 10 volume of lysis Buffer I (100  $\mu\text{g}$  /ml Proteinase K was added shortly before use) was added with a subsequent incubation at  $55^\circ\text{C}$  for 5 hours. 1 volume of Phenol/Chloroform (1:1) was added and centrifuged at 12000 g for 10 min. The upper fraction, which contains DNA, was collected and the Phenol/Chloroform extraction repeated. Then 1/10 vol of 3M Sodium-Acetate (pH 5.2) was added and the DNA precipitated with 2.5 volume of 100% Ethanol. The DNA pellet was centrifuged at 12000 g for 10 min, and washed twice for 2 hours with 80% Ethanol. After partial air drying the DNA was dissolved in 0.5 ml TE (pH 7.2).

Genomic DNA extraction from tissues (liver, brain, tail tips) was performed with tissue size of about 0.5 cm, or tail tip of length less than 1 cm. The tissues/tail tips were incubated with 750  $\mu\text{l}$  of lysis Buffer II (0.5 mg/ml protein kinase K was added shortly before use) over night at  $55^\circ\text{C}$ . The following day 250  $\mu\text{l}$  6M NaCl solution was added and the mixture was vortexed. After centrifugation at 10000 rpm for 30 min 800  $\mu\text{l}$  volume was taken from the middle of the solution and transferred to a new Eppendorf tube. 700  $\mu\text{l}$  of Isopropanol was added, mixture was shaken, and centrifuged for 10 min at 13000 rpm. The pellet was washed twice for 15 min with 75% EtOH, air dried and dissolved in 200  $\mu\text{l}$  TE.

170  $\mu\text{l}$  of 6 M NaCl was added and mixed. The samples were centrifuged for 30 min at 10000 rpm, at  $4^\circ\text{C}$ . 500  $\mu\text{l}$  of isopropanol was added, and mixture was further centrifuged at 13000 rpm for 10 min.

Isolation of RNA was performed with TRIzol Reagent. TRIzol Reagents are ready-to-use, monophasic solutions of phenol and guanidine isothiocyanate suitable for isolating total RNA, DNA, and proteins. During sample homogenization TRIzol Reagent maintains the integrity of the RNA, while disrupting cells and dissolving cell components.

For RNA isolation from cells Petri dish cell cultures with growing cell cultures were washed with PBS, 1 ml of TRIzol was added at RT. The lysate was scrapped into a 1.5 ml Eppendorf, resuspended with a pipette, and left for 10 min at RT until lysis was finished. 200  $\mu\text{l}$

Chloroform was added to the sample, which was vortexed and left for 5 min on ice. The mixture was further centrifuged for 10 min at 12000 rpm. The upper phase was transferred to another 1.5 ml Eppendorf tubes, 1 volume of ice-cold isopropanol was added and mixed. The solution was left at RT for 10 min, and centrifuged for 15 min at 12000 rpm. The supernatant was discarded, and the RNA pellet washed with 75% EtOH and centrifuged at 7500 rpm for 5 min. After drying the pellet 100 µl RNase free water was added and was incubated at 42<sup>0</sup>C for 10 min.

### **Quantification of DNA and RNA concentration**

DNA/RNA yield and purity were determined by spectrophotometric measurement. The absorbance at A260, A280 and the ratio A260/A280 were determined. DNA and RNA concentration was estimated according to equations derived from Beer's Law:

$$\text{RNA } (\mu\text{g/ml}) = A_{260} \times 33 (\mu\text{g/ml}) \times \text{Dilution factor}$$

$$\text{DNA } (\mu\text{g/ml}) = A_{260} \times 50 (\mu\text{g/ml}) \times \text{Dilution factor}$$

where:

33 is the concentration of single-stranded RNA (µg/ml) corresponding to an A260 absorbance of 1, and 50 is the concentration of double-stranded DNA (µg/ml) corresponding to an absorbance A260 of 1.

### **Reverse transcription**

The isolated RNA was reverse transcribed to produce cDNA templates required for PCR amplification and for Real-Time PCR expression analysis. Reverse transcription was performed with the SuperScript™ II Reverse Transcriptase Kit according to supplier protocol. 1 µg RNA was incubated together with a mixture of 1 µl of (pT) primer, 50 – 250 ng Random Hexamer Primer, 10 mM dNTPs, and water to 12 µl for 5 min at 65<sup>0</sup>C and transferred immediately onto ice. After this incubation the 1<sup>st</sup> strand buffer, 1 mM DTT, and RNase inhibitor was added and the mixture was incubated for 10 min at 25<sup>0</sup>C and 2 min at 42<sup>0</sup>C. After adding 1 µl of Reverse Transcriptase the reaction mixture was incubated for 50 min at 42<sup>0</sup>C and inactivated for 15 min at 72<sup>0</sup>C. 1 µl of RNAase H is added and left for 20 min at 37<sup>0</sup>C.

## PCR amplification

In the process of Polymerase Chain Reaction (PCR) a defined fragment of genomic DNA or reverse transcribed RNA, can be selectively amplified using specific oligonucleotides (primers) (Mullis, 1986). Repetition of the denaturation, annealing, and extension reactions in presence of 1 U thermostable Taq DNA Polymerase (from *Thermophilus aquaticus*), 5 pM primers, 0,2 mM dNTPs, and 1X Buffer (see **2.1 Materials, 2.1.9 Buffers**) during 30 – 40 cycles increases exponentially the amount of amplicon (initially 20 ng) for molecular analysis. Negative controls (PCR without DNA template) were performed to make sure there was no contamination of the enzymes and buffers with the template. PCR products were electrophoresed as described later.

## Primers design and preparation

Primers for amplification of genomic and/or cDNA were designed using known DNA sequence available with Primer selection program Primer 3. Parameters of the primers were chosen according to the experimental requirement (primers length, T<sub>m</sub>, GC%, product size). Lyophilised oligonucleotides were diluted in 400 µl of water for 2 hours at 40<sup>0</sup>C, quantified by spectrophotometer, and mixed in primer pairs (L + R) to give a working concentration of 5 pM/µl of each primer.

DNA microsatellite markers were amplified by PCR. To compare the genotype of cultured cell strains and conduct haplotype analysis (compare LEC haplotype to that of LE) the microsatellite markers (simple sequence repeats) were chosen for further analysis. The information about the markers on the region of interest on chromosome 4 was derived from the published data about LEC rat [83, 85, 94]. The primers sequence and position are listed in the **Table 2.1**. Genomic DNA was amplified following the program shown in **Figure 2.10**.

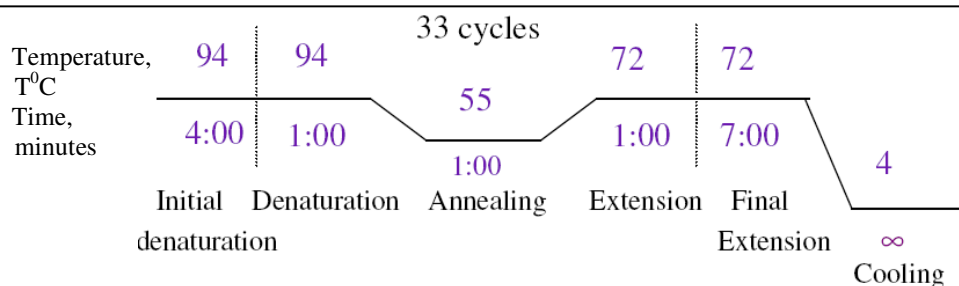


**Figure 2.10. The program for PCR amplification of microsatellite markers**

---

Amplification of cDNA produced by reverse transcription PCR was performed for mutation analysis by sequencing. Using the data of linkage analysis of x-ray hypersensitivity published [83], the candidate genes were selected for further analysis: *Raf-1*, *Ogg-1*, *Rad18*, *XP-C*, *Fancd2*, *Gata-2*. Choice of candidate genes was done based on knowledge of the function of particular gene and described phenotype.

cDNA of chosen genes was amplified with designed primer pairs (see **Table 2.2.** for list of primers). The program for PCR amplification is shown in **Figure 2.11.** The coding sequence of candidate genes was further analysed by means of sequencing.

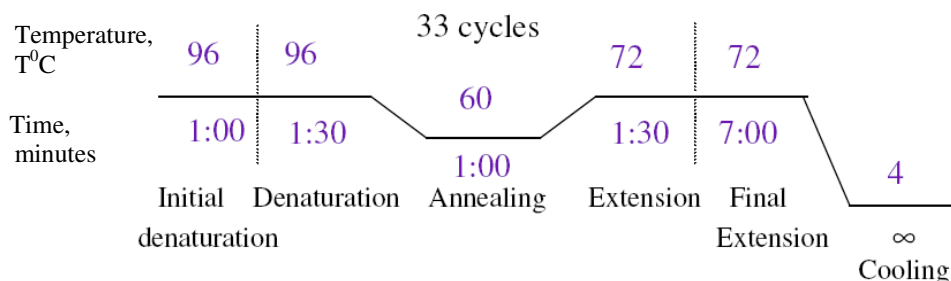


**Figure 2.11. The program for amplification of cDNA for sequence analysis**

---

## **Electrophoresis of the DNA extraction products and PCR amplification products**

For visualisation of quality of the nucleic acids the DNA/RNA extraction products and PCR amplification products were separated by agarose gel electrophoresis and stained with EtBr.

Depending upon PCR product size agarose gels were prepared by dissolving 2.0-3.0 g agarose powder in 100 ml of 1 x TBE buffer prepared from 5 x TBE buffer stock. For longer products (500 bp-1500 bp) of gene amplification 2% agarose was prepared. For separation of

products of microsatellite markers (100 -300 bp) 3% agarose was used. Agarose was dissolved by boiling for 2 -3 min in the microwave. After cooling till 60<sup>0</sup>C of EtBr was added to the gel with final concentration of 0.5 ug/ml to enable fluorescent visualisation of the DNA fragments in UV light. The warm mixture was poured into a gel tray and a well-forming comb was applied. The gel was allowed to solidify, the comb was taken out, and the gel was placed in an electrophoresis chamber and covered with 1 x TBE buffer.

The samples were loaded into the gel wells. The loading buffer prevented escape of the mixture from the slot and served as a visible co-migrating marker. 1 µl of DNA molecular marker VIII was mixed with 8 µl of distilled water and 1 µl of 10 x loading buffer and loaded at the same time together with DNA samples to allow size determination of the fragments. Electrophoresis was run till the samples were good separated at a constant voltage of 60 V for bigger fragments (300-1500 bp) and 90 V for smaller fragments (300 -100 bp). Cresol Red, added to the PCR buffer, served as additional migration marker with a size equivalent to 125 bp, Bromophenol Blue added to the size marker migrated at size equivalent to 300 bp.

### **Purification of the PCR product for sequencing reaction**

After electrophoresis PCR amplification products were cut out from the gel and purified from the agarose. Single bands were cut out with a scalpel from the agarose gel under UV light. DNA was extracted from isolated gel slices by QIAquick Gel Extraction Kit. The chaotropic salt containing Buffer QG dissolved solid agarose at 50<sup>0</sup>C, and the released DNA was purified on a QIAquick column using elution Buffer EB (10 mM Tris-HCl, pH 8.5). For optimal DNA yield the columns were incubated in elution buffer for 5 min at RT. Isolated DNA was used for sequencing.

### **Sequencing of the PCR product and mutational analysis**

Quiagen purified PCR product was further sequenced for mutational analysis. Automated fluorescent sequencing utilizes a variation of the Sanger chain-termination protocol [118].

The cycle sequencing reaction was set up as shown in **Table 2.1.**, and template was amplified and fluorescently labelled for further detection applying the program, which is described in **Figure 2.12.** Reaction mixture composed of dNTPs, fluorescently labelled ddNTPs,

Polymerase enzyme, buffer, oligonucleotide primer (forward or reverse). During the sequencing reaction, when ddNTP is incorporated, further chain elongation is blocked and this results in a population of truncated products of varying lengths, which are separated with electrophoresis and dyes are detected with laser.

**Table 2.4. Set-up for sequencing reaction**

	Volume
Big Dye terminator Mix v3.1	1 $\mu$ l
5X Buffer	1 $\mu$ l
Template	1 $\mu$ l
Primer (10 pmol/ $\mu$ l)	1 $\mu$ l
HPLC-Water	1 $\mu$ l

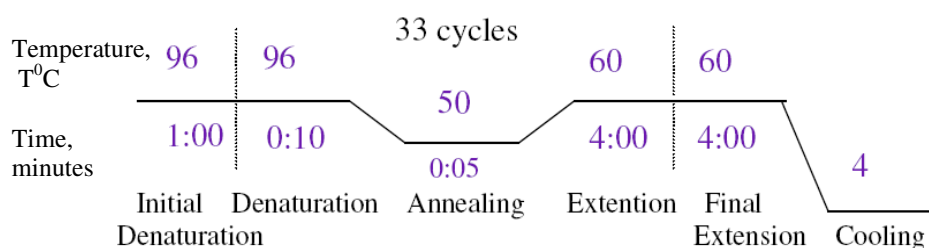


**Figure 2.12. Amplification steps during sequencing reaction**

Sequencing products were kept in darkness and frozen before precipitation.

The reaction product was further precipitated as following. The sequencing reaction plate was centrifuged down shortly (the centrifugation at 4600 rpm was only started and stopped) in the Sorvall centrifuge, 5  $\mu$ l of the sequencing reaction was transferred into a new sequencing plate with a bar code (ABGene). To a 5  $\mu$ l of reaction 15  $\mu$ l of 100% Ethanol was added, the plate was sealed with aluminium foil and mixed by vortexing slowly. The plate was shortly centrifuged and incubated at RT for 15 min in the dark. After incubation plate was centrifuged in the Sorvall centrifuge for 30 min at 4700 rpm at 4°C. The supernatant was discarded by spinning up-side-down the plate in the centrifuge at very low speed for few seconds. 15  $\mu$ l of 70% Ethanol was added and plate was spun in the Sorvall for another 30 min at 4700 rpm at 4°C. The supernatant was again discarded by spinning up-side-down the plate for few seconds. The plate was dried at RT in the dark for 30 min and pellet was resuspended in 50  $\mu$ l of HPLC- water. The information about plate and analysed samples was entered online as a sample sheet. The fluorescence labelled sequencing products were analysed on an ABI 3730 capillary sequencer. After sequencing data were available in seq (txt) and abl (electrophoregram) formats for further analysis.

The sequences were further analysed. For this the resulted sequences were compared to wild type sequences applying BLAST (Basic Local Alignment Search Tool (BLAST)), which is the most frequently used tool for calculating sequence similarity <http://www.ncbi.nlm.nih.gov/blast/bl2seq/wblast2.cgi>.

### **2.2.11 SYBR Green Real-Time PCR detection**

Real-Time (RT) quantitative PCR was applied to investigate the steady-state expression of candidate genes, *Gata-2* and *Fancd2*, in primary LEC and LE fibroblasts. Reverse transcription followed by the polymerase chain reaction (PCR) was used to analyse mRNA expression. The detection technique for the PCR products in RT-PCR used SYBR Green I fluorescence dye that binds specifically to the minor groove of double-stranded DNA (dsDNA). The unbound dye exhibits very low fluorescence; however, fluorescence (wavelength, 530 nm) is strongly enhanced upon binding to DNA. The increase in SYBR Green fluorescence during each round of PCR amplification is directly proportional to the amount of dsDNA generated during the PCR.

### **RNA extraction from cells**

$4 \times 10^5$  cells were plated per 60 mm Petri dish in standard culture media (media was changed in 24 hours after plating) and left to grow until confluency. After irradiation of cells with 5 Gy and incubation cells were collected at 4 and 24 hours and RNA was extracted from cell pellets with the High Pure RNA tissue Kit, Roche.

### **Primer design**

Primers for the amplification of cDNA by RT-PCR were designed, using the Primer selection program Primer3 ([http://waddl3lab3.life.smu.edu/cgi-bin/primer3/primer3\\_www.cgi](http://waddl3lab3.life.smu.edu/cgi-bin/primer3/primer3_www.cgi)). The primers were designed to span one or more introns to avoid false signal resulting from amplification of genomic DNA in case of contamination with genomic DNA. Parameters of the primers were chosen according to the experimental requirement (primer length, primer  $T_m$ ,

primer GC%), for amplification of products with size of 100-120 bp. Primer oligonucleotides were ordered and prepared as described (see above, **Primer design and preparation**). Porphobilinogen deaminase (*Pbgd*) was used as reference gene in expression analysis.

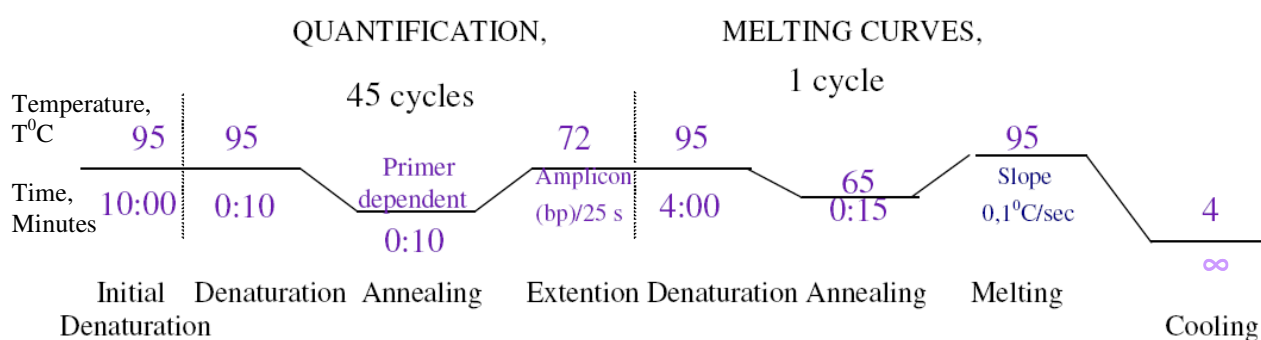


**Figure 2.13. Amplification program for Real-Time PCR**

### Master Mix preparation and Real-Time PCR amplification

The ready-to-use RT-PCR Kit LightCycler FastStart DNA Master<sup>plus</sup> SYBR Green I was purchased from Roche Diagnostic Applied Science. A Master Mix is prepared for use by pipetting of 14 µl of FastStart Taq DNA polymerase to Master Mix (5x concentrate), containing reaction buffer, dNTP mix, SYBR Green I dye, MgCl<sub>2</sub>, PCR primers with concentration of 0.5 µM each and diluting with supplied water to get the necessary concentration.

For the LightCycler reaction 18 µl of ready-to-use hot-start PCR reaction mix was filled in the LightCycler glass capillaries and 2 µl of template cDNA was added. Capillaries were closed, centrifuged and placed into the LightCycler rotor. The LightCycler experimental run protocol, described in **Figure 2.13.**, was used for amplification reaction.

### Evidences of specificity of chosen primers. Melting curve analysis.

#### Confirmation on agarose gel

Specificity of the RT-PCR products was documented using agarose gel electrophoresis and showed a single product with the predicted length (**Figure 2.14.**). A negative control, in which template DNA was replaced with PCR-grade water, was included in the run. To prove that only the desired PCR product has been amplified, a melting curve analysis after PCR was performed.

In the melting curve analysis the reaction mixture was slowly heated to +95<sup>0</sup>C, which caused melting of dsDNA and a corresponding decrease of SYBR Green I fluorescence. The instrument continuously monitors this fluorescence decrease and displays it as melting peaks (**Figure 2.15**). Each melting peak represents the characteristic melting temperature (T<sub>m</sub>) of a particular DNA product (where the DNA is 50% double-stranded and 50% single-stranded). The most important factors that determine the T<sub>m</sub> of dsDNA are the length and the GC-content of the fragment. If PCR generates only one amplicon, melting curve analysis will show only one melting peak. If primer-dimers or other non-specific products are present, they will be shown as additional melting peaks.

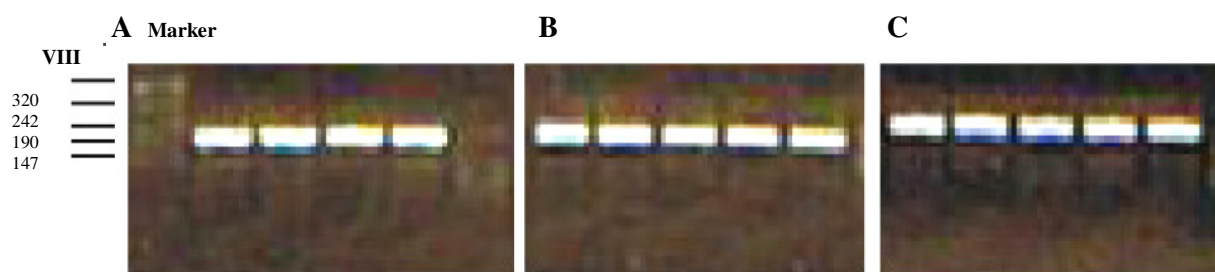


**Figure 2.14. Agarose gel with amplification products of *Pbgd* (A), *Gata-2* (B) and *Fancd2* (C) specific primers**

The Real-Time amplification products of samples with primers specific for the reference gene *Pbgd* (A), target *Gata-2* (B) and *Fancd2* (C) were electrophoresed on a 2% agarose gel to prove the primer specificity. The amplification was specific, since it gave only one band of expected size with each of the selected primer pairs.

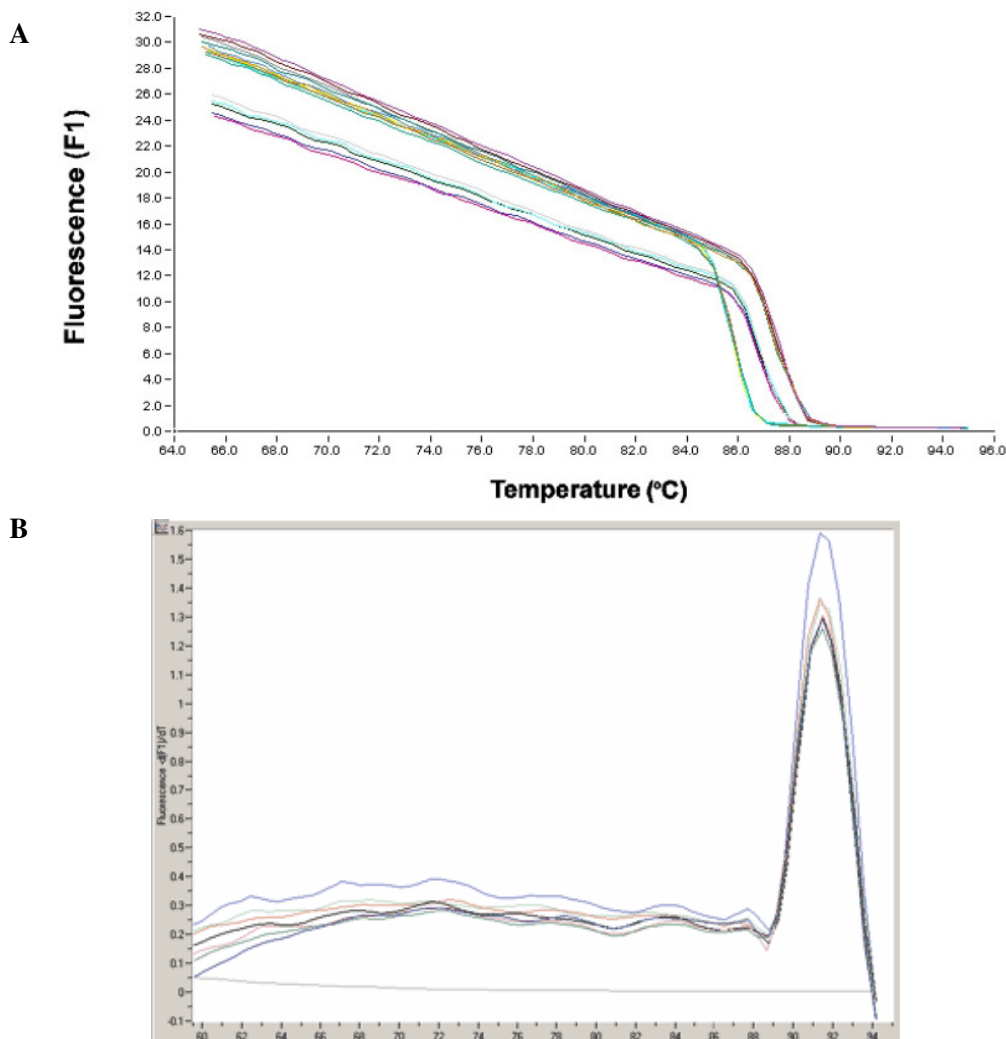


**Figure 2.15. Melting curve analysis**

**A:** Real-time RT-PCR SYBR Green I fluorescence of amplified samples is plotted against temperature.

**B:** The software plots the rate of change of the relative fluorescence units (RFU) with time (T) ( $-d(RFU)/dT$ ) on the Y-axis versus the temperature on the X-axis. The value of ( $-d(RFU)/dT$ ) will peak at the melting temperature ( $T_m$ ).

### Crossing point calculation. Quantification of reaction products

Crossing point (CP) was defined from amplification curve analysis (**Figure 2.16.**) by the Second Derivative Maximum Method applied automatically by the Light Cycler Data Analysis Software. CP is defined as the point, at which the fluorescence rises above the background fluorescence for each amplified transcript. The less copies of the cDNA were in the sample, the higher CP is, the larger number of copies were present – the lower CP.

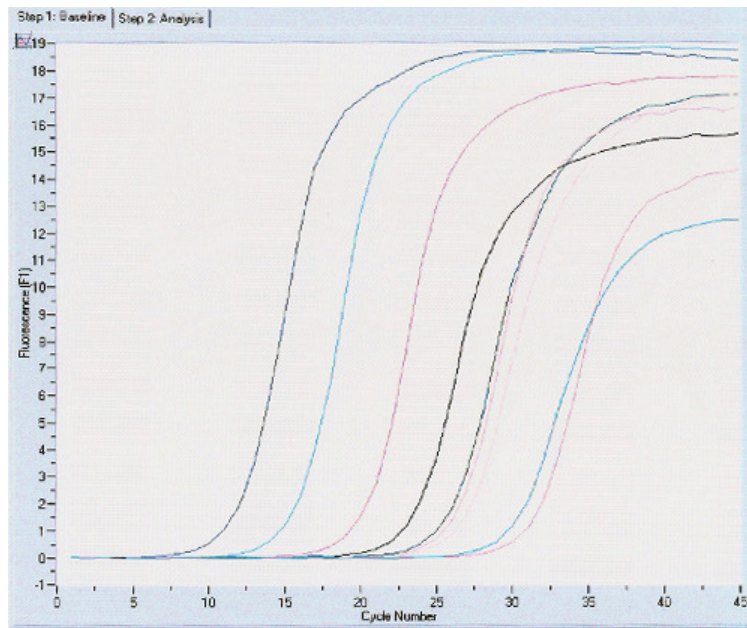


**Figure 2.16. Example of amplification curves obtained using Real-time RT-PCR SYBR Green I.**

Fluorescence is plotted against cycle number of amplified samples. The graph reflects increase in fluorescent signal over cycles in PCR reactions depending on the amount of initial DNA template. The CP values were determined by Light Cycle Data Analysis Software by Second Derivative Maximum Method. The fluorescence values versus cycle number are displayed.

---

### **Quantification of gene expression**

Generally two quantification methods are possible in real-time RT-PCR:

1. A relative quantification based on the relative expression of a target gene versus a reference gene.
2. An absolute quantification, based either on an internal or an external calibration curve.

Relative quantification is easier to perform than absolute quantification because a calibration curve is not necessary. It is based on the expression levels of a target gene versus a reference gene and in theory is adequate for most purposes to investigate physiological changes in gene expression levels [119]. Relative quantification relates the PCR signal of the target transcript in a treatment group to that of another sample such as an untreated control [120]. Non-regulated genes or housekeeping genes like porphobilinogen deaminase (*Pbgd*), which was used in performed experiments are used as reference genes.

## **$2^{-\Delta\Delta CT}$ method**

Expression of *Gata-2* and *Fancd2* was evaluated applying the  $2^{-\Delta\Delta CT}$  method.  $2^{-\Delta\Delta CT}$  is the method of relative quantification developed by K.J.Livak and T.D.Schmittgen, 2001 [120]. It allows compare expression of the target gene in the studied sample to that of the control (calibrator).

1. The first step is the normalization to the endogenous control:

$$\Delta C_T = C_T \text{ Target gene} - C_T \text{ Endogenous control},$$

where  $C_T$  is the threshold value, indicating the fractional cycle number, at which the amount of amplified target reaches a fixed threshold (Crossing Point, CP is another name).

2. Further follows normalisation of  $\Delta C_T$  in the sample to the calibrator:

$$\Delta\Delta C_T = \Delta C_T \text{ Sample} - \Delta C_T \text{ Calibrator}$$

3. Estimation of target, normalized to an endogenous reference and relative to a calibrator:

$$2^{-\Delta\Delta CT} = \text{Target/Calibrator}$$

Before applying the  $2^{-\Delta\Delta CT}$  method, it is necessary to validate it. It is possible to use  $2^{-\Delta\Delta CT}$  method only assuming the same efficiencies of the used primer pairs. To prove this, the pooled cDNA was serially diluted and amplified with chosen primers. The absolute value of the slope of log input amount vs.  $\Delta C_T < 0.1$  shows the same efficiencies of used primer pairs.

For quantitative analysis data of  $C_T$  values were exported to an Excel program. The relative expression ratio (R) of the target genes (*Fancd2*, *Gata-2*) was determined as described above.

### III. RESULTS

#### 3.1 Morphology and growth of fibroblasts

According to the study of Daas *et al.*, 2002 [121] cell morphology (rounded or rhomboidal shape, elongated or spindle), was not a reliable marker for the growth capability of fibroblast subpopulations. Nevertheless, attention was paid to potential differences in morphology of the established LEC and LE cell lines. **Figure 3.1.** shows that there was no significant morphological difference between LEC and LE cell lines 24 hours after plating (left panel images) and at subconfluence/confluence (right panel images (passage 8-11)).

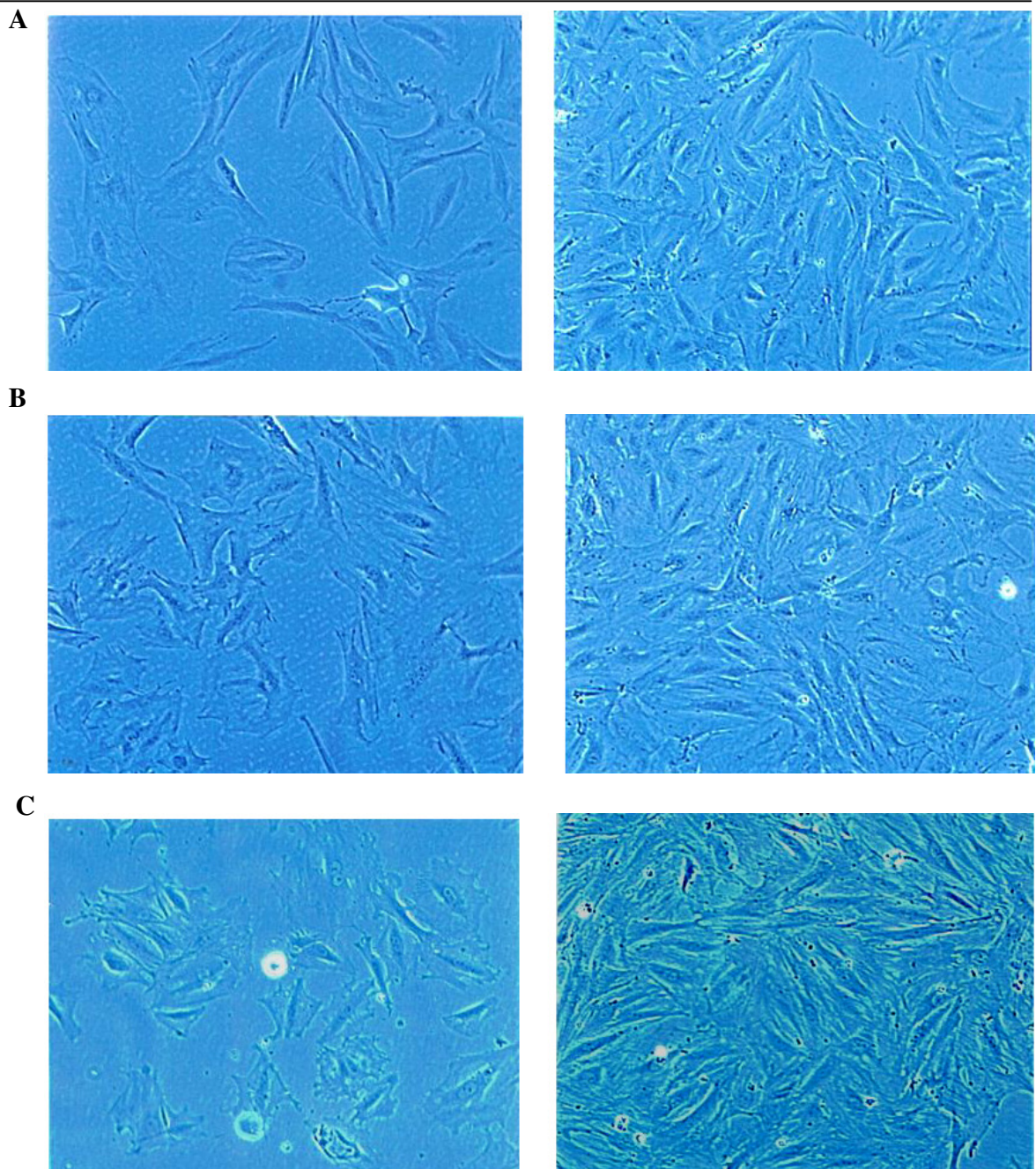
It is important that cell lines used in comparative cell biology studies are characterized relative to their population doubling time (DT), since knowledge of these cell kinetic parameters is necessary when defining cell lines as model systems for *in vitro* studies and might be affected by a carried genetic defect. To define the growth characteristics of LEC and LE fibroblasts their growth curves (**Figure 3.2.**, APPENDIX, page 150) were analysed without and after 5 Gy of IR (**Figure 3.3.**, **Table 3.1.**).

Growth curve measurements did not reveal a difference in growth between non-irradiated LEC and LE fibroblasts. Cell lines from the same rat strain differed in their DT (see **Table 3.1.**), and DT was increasing in fibroblasts of higher passages (passage 11) comparing to lower passages (passage 7). An increase of population DT with further passaging reflected that the cell culture approached the growth minimum (crisis). After this, it was still possible to culture cells (the culture was done till passage 20), but the experimental data were produced on cells from earlier passages (6-12). With further passaging rat fibroblast cell lines also acquired the morphological changes.

Generally there was no difference in growth patterns observed between cell lines of the LEC and LE strains.

A dose of 5 Gy  $\gamma$ -radiation caused suppression of fibroblasts growth (see **Figure 3.2., APPENDIX**, page 150). Cell numbers did not increase 24 hours after irradiation and became only slightly higher at 54 hours after IR in both LEC and LE cells (**Table 3.1.**).

Cell counts in irradiated cells were normalized to that of the respective controls (matched cell line and time) (**Figure 3.3.**). Normalized values did not reflect a significant difference between LEC and LE fibroblasts (see **Figure 3.3., A, B**). DT values were compared before and after normalization and were found to be similar between LEC and LE cell lines (**Table 3.1.**).



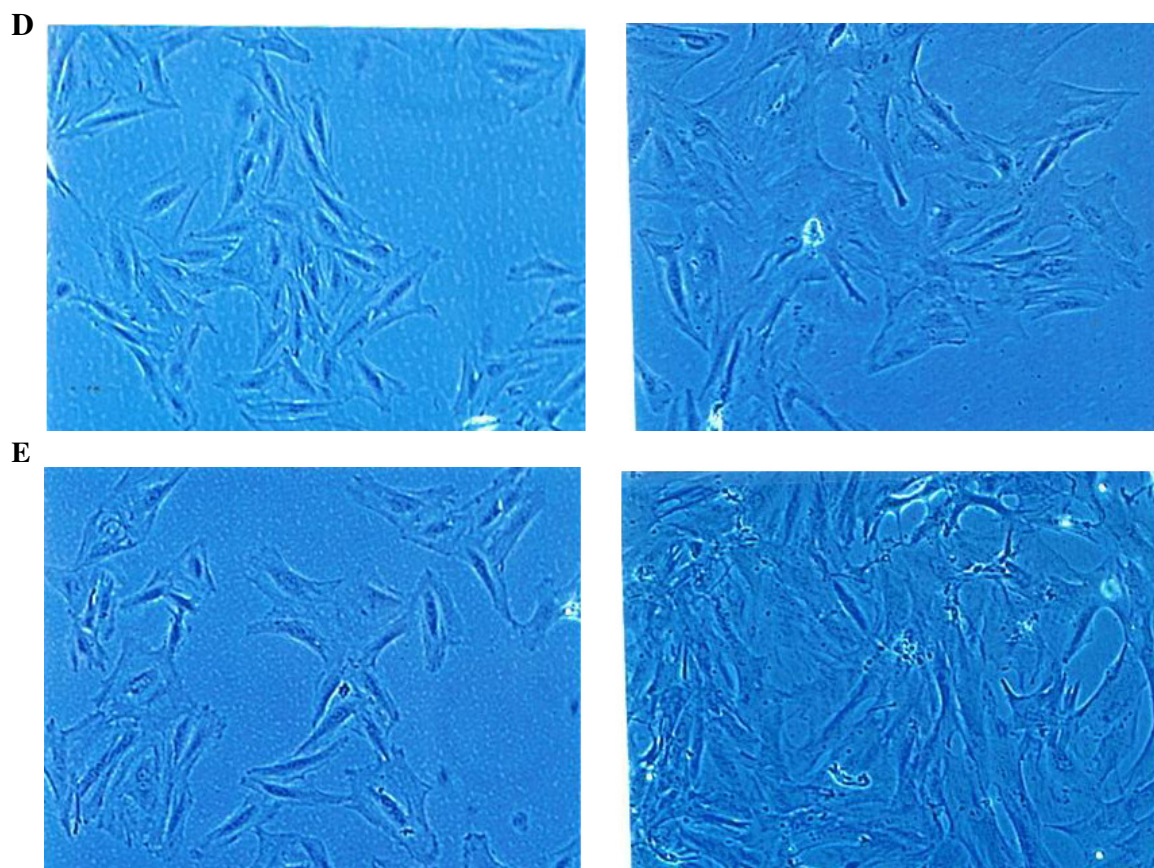


**Figure 3.1. Representative images of cultured fibroblasts**

The images of growing cells were taken 24 hours after replating (left panel), and of sub-confluent cultures (right panel). Pictures were done with the phase-contrast microscope Axiovert under 40x enhancement.

- A:** LE-1, passage 9, LE-1, passage 11
- B:** LE-2, passage 10, LE-2, passage 11
- C:** LE-4, passage 11, LE-4, passage 11
- D:** LEC-1, passage 9, LEC-1, passage 8
- E:** LEC-2, passage 8, LEC-2, passage 9

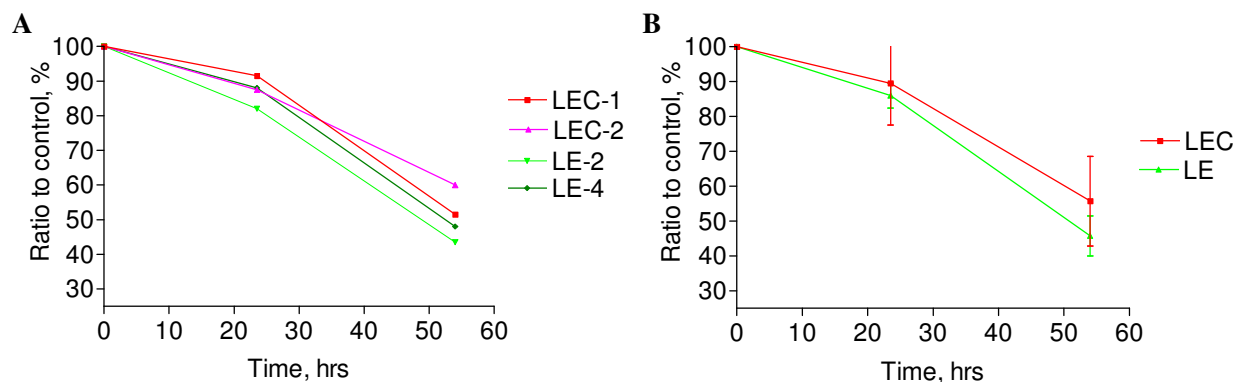


**Figure 3.3. The percentage of irradiated cells at measured time point relative to controls**

The growth curves of LEC and LE fibroblasts were evaluated. The numbers of cells in irradiated samples were normalized to the numbers of cells in controls. Diagram shows measured percentage of every cell line at each time point from two experiments, mean values  $\pm$  SEM of LEC (n = 4) and LE (n = 3) cell lines.

**Table 3.1. Doubling time of cell lines**

	CELL LINE						
	LEC1 (p7)	LEC1 (p11)	LEC2 (p6)	LEC2 (p12)	LE2 (p7)	LE4 (p9)	LE4 (p12)
Control	19,4	53,4	20,6	81,9	23,4	39,9	25,9
5 Gy	38,7	692,1	45,6	104,7	42,2	200,1	79,4
Ratio 5 Gy / Control	1,9	12,9	2,2	1,3	1,8	5	3,07
SUMMARY	LEC				LE		
Control, Mean $\pm$ SEM	43.9 $\pm$ 14.9				29.8 $\pm$ 5.13		
5 Gy, Mean $\pm$ SEM	220.3 $\pm$ 157.9				107.2 $\pm$ 47.7		
Ratio 5 Gy / Control, Mean $\pm$ SEM	3.29 $\pm$ 0.93				4.61 $\pm$ 2.78		

The doubling times were estimated for two LE and two LEC cell lines for control (sham-irradiated) and irradiated with 5 Gy of IR. The ratio of values of irradiated cells to controls was calculated. Mean  $\pm$  SEM values were summarised for LEC (n = 4) and LE (n = 3) cells. In parentheses the passage number (p6-12) of investigated cell line is indicated.

### 3.2 Clonogenic survival assay

The clonogenic assay was performed to compare the radiosensitivity of LEC and LE cells. Cells accumulated in G1 phase of the cell cycle were investigated. Such synchronization allowed eliminate the variation in radiosensitivity caused by differences in cell cycle stage, since it is well known that cells in middle to late S phase and G1 are radioresistant, while G1/S, and G2/M transitions are more sensitive to IR.

After irradiation different changes were observed:

1. some cells were remaining single and did not divide. In some cases they showed evidence of nuclear deterioration as the result of cellular death induction;
2. some cells went through one or two divisions and formed small colonies of just a few cells;
3. some cells formed large colonies (**Figure 3.4.**), indicating that the cells have survived the treatment and have retained the ability to reproduce indefinitely.

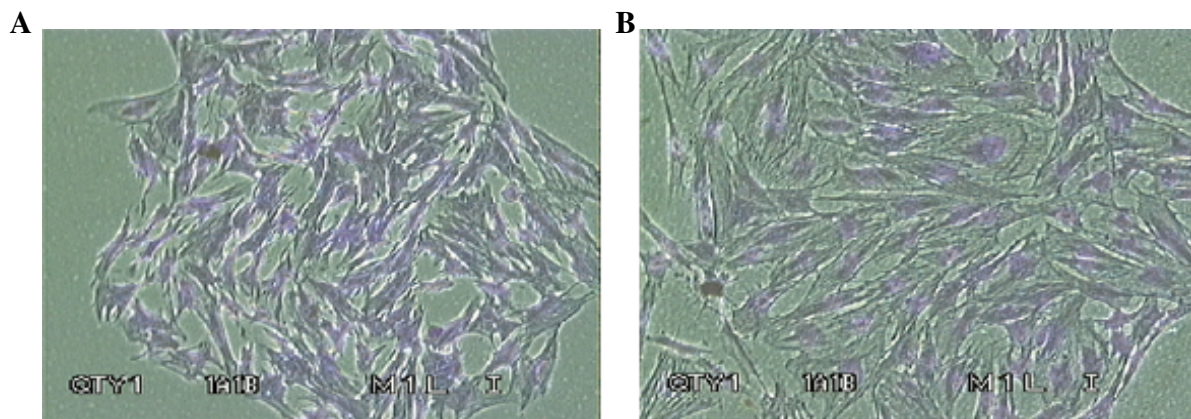


**Figure 3.4. Images of representative non-irradiated colonies of LEC-1 and LE-4 fibroblasts**

The colonies were stained with 0.5% crystal violet in 70% ethanol and dried. The colonies containing more than 30 cells were counted under a dissection microscope. The pictures of representative colonies of unirradiated LEC-1 (**A**) and LE-4 (**B**) fibroblasts were taken with a phase-contrast microscope Axiovert, under 40x enhancement.

LEC and LE fibroblasts did not differ in their plating efficiencies (PE) (see **Table 3.2.**). Without irradiation the PE (%) of LEC cells was  $1.28 \pm 0.44$ , and LE cells-  $1.5 \pm 0.35$  (mean  $\pm$  SEM, n = 6).

**Table 3.2. Measured plating efficiency (PE) for LEC and LE cell lines**

	LEC-1	LEC-2	LE-1	LE-2	LE-4
PE (%)	0.82	0.84	1.28	1.59	1.54
	1.67	0.61	1.16	0.42	n.d.
	0.42	3.30	3.02	n.d.	n.d.
Mean $\pm$ SEM	$0.97 \pm 0.37$	$1.58 \pm 0.86$	$1.82 \pm 0.6$	1	1.54
	LEC		LE		
Mean $\pm$ SEM	$1.28 \pm 0.44$		$1.5 \pm 0.35$		

**Table 3.3. Measured survival for LEC and LE cell lines**

Dose,Gy	LEC-1	LEC-1	LEC-1	LEC-2	LEC-2	LEC-2	Mean (%) $\pm$ SEM
0	1.00	1.00	1.00	1.00	1.00	1.00	<b>100.0</b>
1	0.69	0.54	n.d.	0.49	0.73	0.53	<b>59.6 <math>\pm</math> 4.7</b>
2	0.25	0.23	0.23	0.33	0.29	0.19	<b>25.3 <math>\pm</math> 2</b>
3	0.08	0.14	n.d.	0.11	0.08	n.d.	<b>10.3 <math>\pm</math> 1.3</b>
4	0.016	n.d.	n.d.	0.05	n.d.	n.d.	<b>3.5</b>
Dose,Gy	LE-1	LE-1	LE-1	LE-2	LE-2	LE-4	Mean (%) $\pm$ SEM
0	1.0	1.0	1.0	1.0	1.0	1.0	<b>100.0</b>
1	0.81	0.86	0.75	0.70	0.77	0.43	<b>72 <math>\pm</math> 6.2</b>
2	0.35	0.35	0.39	0.41	0.34	0.23	<b>34.5 <math>\pm</math> 2.5</b>
3	0.14	0.21	0.17	0.097	0.19	0.18	<b>16.5 <math>\pm</math> 1.6</b>
4	n.d.	0.01	0.03	0.03	n.d.	n.d.	<b>2 <math>\pm</math> 0.8</b>

Table includes measured survival fraction of LEC and LE fibroblasts, p7-11, in the dose range from 0 to 4 Gy, between 2 and 6 replicates per time/dose point, mean percentage of survival  $\pm$  SEM (where n  $\geq$  3)

The survival data (**Table 3.3.**) were plotted against dose and further fitted to the linear-quadratic curve (see **Figure 3.5.**) according to the equation  $S = e^{-\alpha D - \beta D^2}$ .

The terms  $\alpha$  and  $\beta$ , which characterize the curves, were compared (see **Table 3.4.**). The mean values were different between LEC and LE cells, the p-value of t-test was at the borderline of 0.058 for the  $\alpha$  component and non-significant for the 0.72 for  $\beta$  component of cell killing. Such a borderline t-test value might reflect that the mode of cell killing had trend of increase in  $\alpha$ - values in LEC cells, what means that LEC cells died more from single-hit cell killing events than LE cells.

**Table 3.4. Parameters characterizing the fitting of survival data**

<i>Best-fit values</i>	LEC	LE	P value of t-test
$\alpha$ , Mean $\pm$ SEM	0.39 $\pm$ 0.08	0.19 $\pm$ 0.08	0.058
<i>95% confidence intervals</i>	<i>0.23 to 0.55</i>	<i>0.03 to 0.34</i>	
$\beta$ , Mean $\pm$ SEM	0.14 $\pm$ 0.04	0.16 $\pm$ 0.04	0.72
<i>95% confidence intervals</i>	<i>0.05 to 0.23</i>	<i>0.08 to 0.24</i>	

The survival data were fitted to the linear-quadratic function. Table contains mean  $\pm$  SEM of  $\alpha$  and  $\beta$  values,  $n = 6$  and 95% confidence intervals, estimated from survival curves fitted to linear-quadratic equation.

Additionally, the values of D1 were estimated from each single survival curve, the mean values and SEM were derived and tested for significance applying Student's two-tailed t-test.

**Table 3.5. The evaluation of D1**

<i>D1</i>	LEC	LE	P value of t-test
Mean $\pm$ SEM, N=6	1.61 $\pm$ 0.06	1.91 $\pm$ 0.12	0.056

Although the mean values were different between LEC and LE – 1.61  $\pm$  0.06, for LEC and 1.91  $\pm$  0.12 (mean  $\pm$  SEM,  $n = 6$ ) for LE fibroblasts - the t-test did not reveal a statistically significant difference between them, returning a borderline p value of 0.056, which reflects the statistical trend, as in the case of  $\alpha$ .

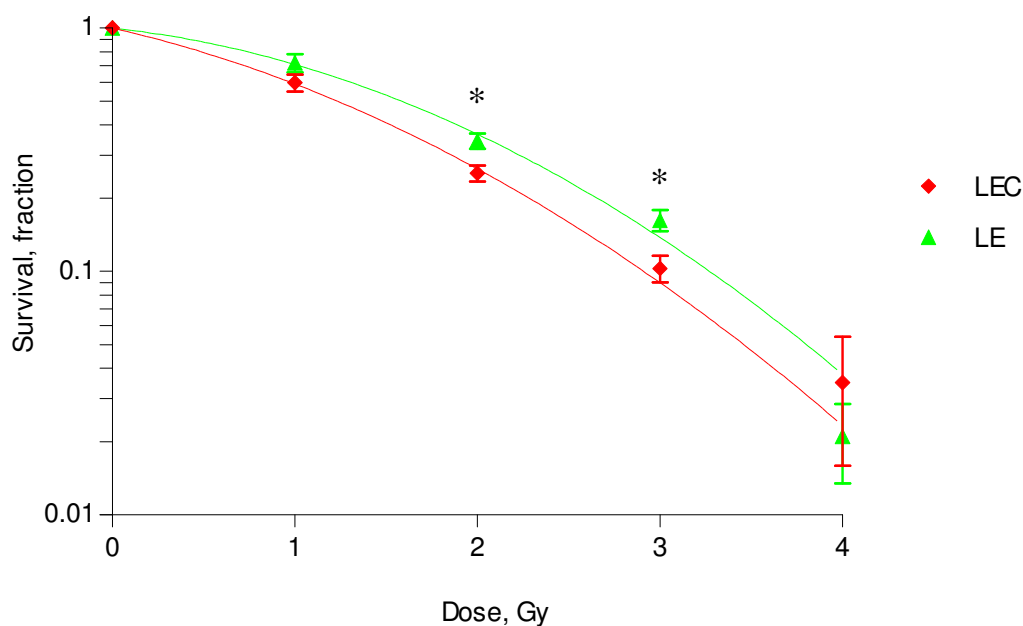


**Figure 3.5. Experimental data of survival are fitted to a linear-quadratic function  $y=\exp(-\alpha*x - \beta*x^2)$**

Survival was measured for LEC and LE fibroblasts (passage 7-11), in G1 phase of cell cycle in 2-6 experiments after 1, 2, 3 and 4 Gy of  $\gamma$ -radiation (see **Table 3.3.** for single values of survival fraction). Estimated mean of survival fraction  $\pm$  SEM plotted against dose. The fitting of data was done with Prism3.03 Software. Student's t-test shows significant difference at 2 and 3 Gy (marked with\*) with p-values being 0.018 and 0.029 respectively.

Survival measured for LEC and LEC fibroblast cell lines for a dose range from 0 to 4 Gy (**Table 3.3.**) was further tested for statistical difference at each dose with Student's t-test. The results of the t-test showed significant difference between LEC and LE fibroblasts at clinically relevant doses of 2 and 3 Gy (see **Figure 3.5.**) with p-values being respectively 0.018 and 0.029. Two-way ANOVA test showed significant difference in survival of fibroblasts between rat strains (p-value 0.019).

The dose modifying factor (DMF) for SF was determined as the ratio of survival at 2 and 3 Gy in LE cells to the respective values of LEC cells and was 1.3 after 2 Gy and 1.58 after 3 Gy in primary fibroblasts (see **Table 3.6.**). The DMF of acute radiation syndromes after irradiation of LEC rat *in vivo* were derived from animal survival data published by Hayashi *et al.*, 1992, 1993 [80, 81]. It was determined as ratio of LD<sub>50/30</sub> and LD<sub>50/7</sub> of WKAH to that of LEC rat and its

values were 2.36 for bone marrow death and 1.9 for intestinal syndrome. The DMF estimated from published survival experiments, conducted *in vivo*, was higher than *in vitro* survival assay.

**Table 3.6. The evaluation of DMF**

	2 Gy	3 Gy	LD <sub>50/7</sub> *	LD <sub>50/30</sub> **
DMF	1.3	1.58	1.9	2.36

The values of DMF were estimated for SF at 2 and 3 Gy for LE *versus* LEC fibroblasts

\*The DMF of LD<sub>50/7</sub> was derived from data published by Hayashi *et al.*, 1992 [80].

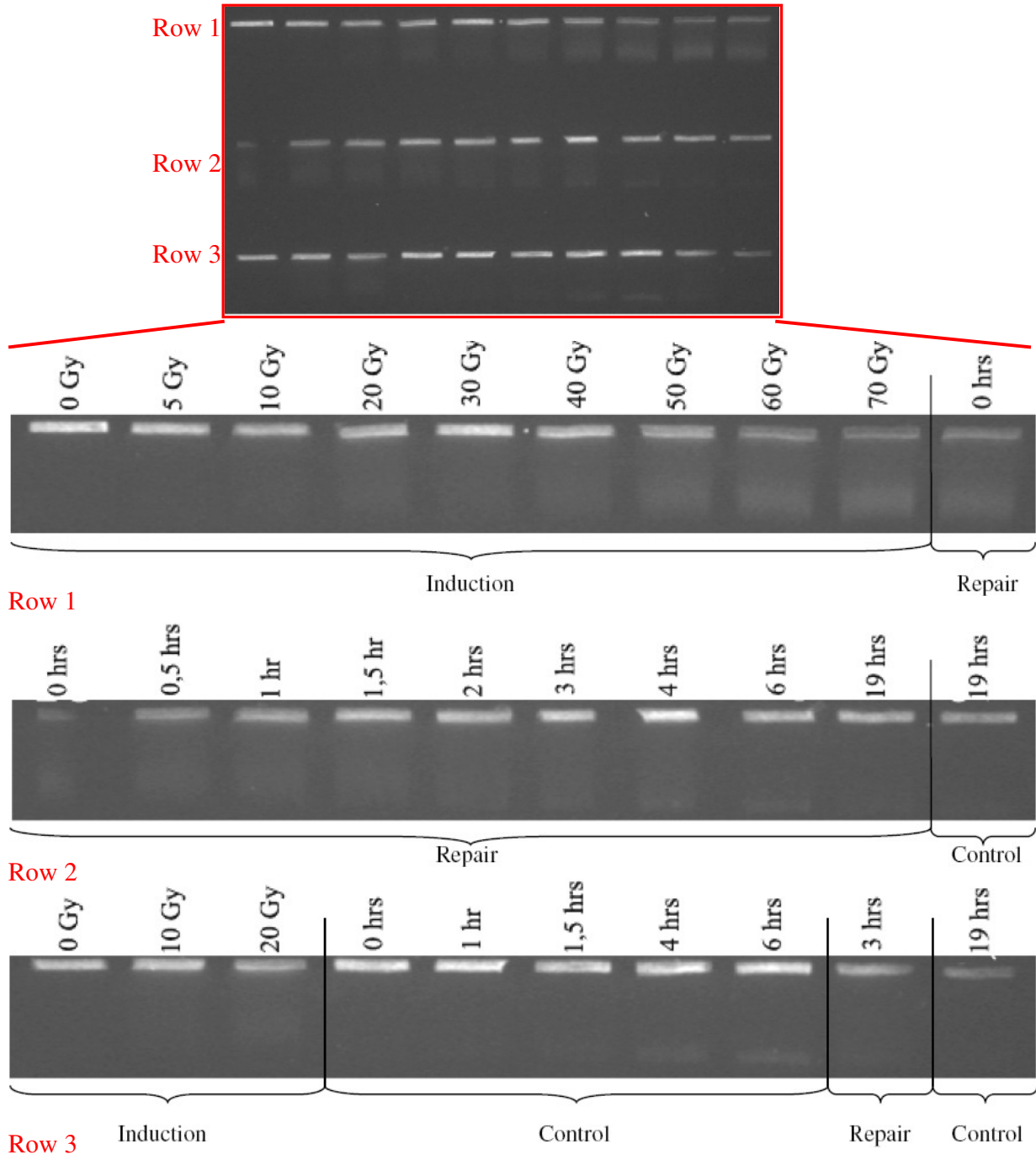
\*\*The DMF of LD<sub>50/30</sub> was derived from data published by Hayashi *et al.*, 1993 [81].

### 3.3 Pulsed field gel electrophoresis

In many cases sensitivity of mutants to cell killing by radiation has been related to their ability to repair DSB [122]. Non-repaired and mis-repaired DSB are particularly genotoxic and are precursor lesions for the formation of chromosome aberrations. Therefore the ability of LEC and LE fibroblasts to repair DSB at G1-phase was investigated applying the PFGE method. These investigations included evaluation of dose-dependent damage (induction curves), investigations of the repair capacity, characterizing the amount of repaired damage at times between 0 and 6 hours after 70 Gy of  $\gamma$ -irradiation, and kinetics of DSB repair.

Two examples of images taken from two PFGE gels are presented in the **Figure 3.6**. The induction samples (Row 1) reflect the dose-dependent increase in DNA damage. The amount of extracted DNA in repair samples was highest at time 0 after IR and was decreasing over time. Controls had a small increase in DNA fragmentation during incubation. The amount of DNA in the pseudo-band in repair samples at 6 hours was close to that in the respective control, but was still present at higher level, what means that repair was not completed. The amount of damage was expressed as fraction of activity released (FAR) (intensity of DNA migrated out of the plug was divided to the whole DNA in the band on the gel). For quantification of DSB induction, repair efficiency, and kinetics the FAR values and subsequently Gy-equivalents (see **Methods, 2.2.6, Pulsed field gel electrophoresis**) were estimated (see **Table 3.7., APPENDIX**, page 151-152).

A



**B**

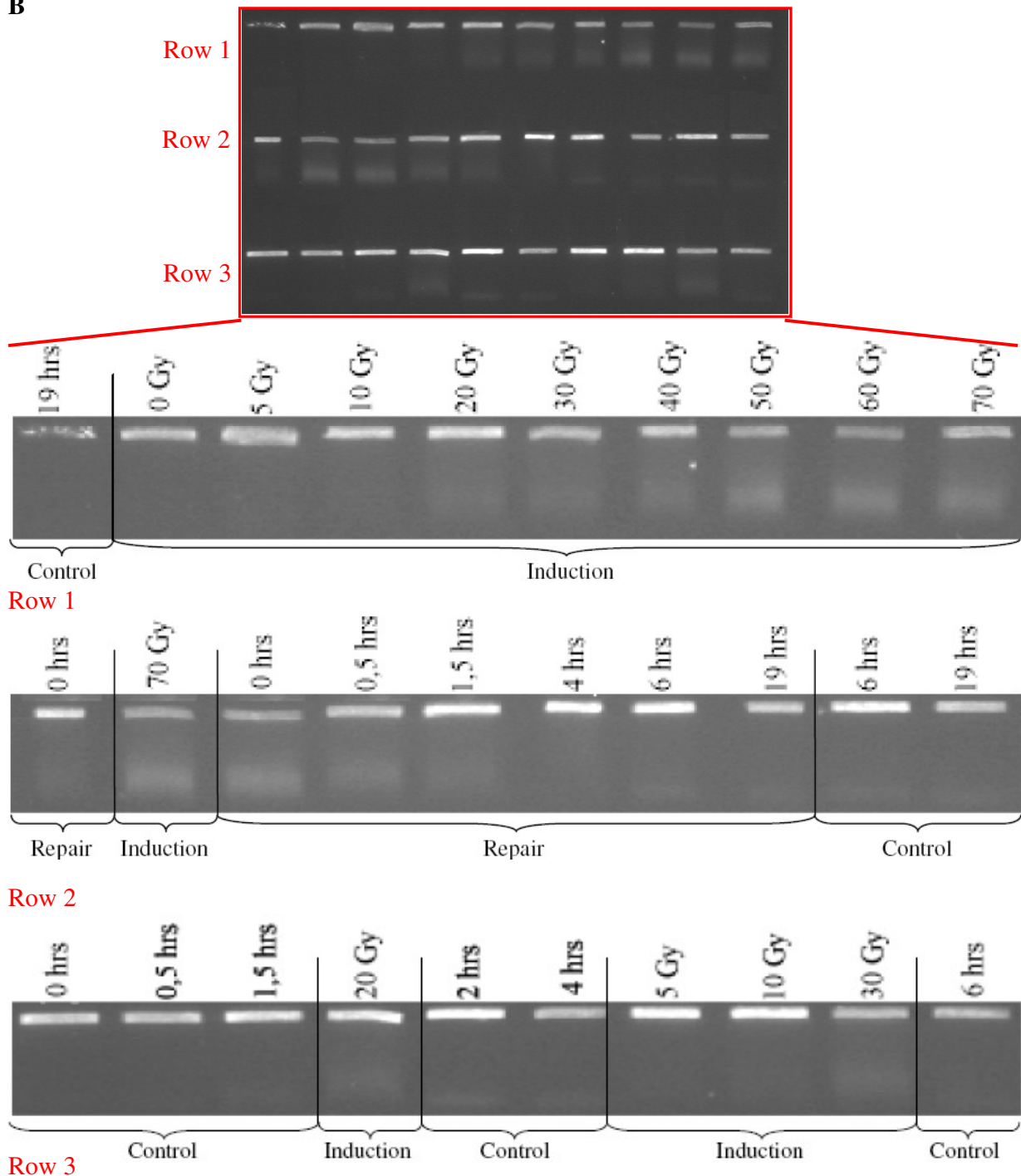


**Figure 3.6. The images of representative PFGE gels are shown**

**A:** LEC-1, p12, experiment 5

**B:** LE-1, p12, experiment 5.

As described in Methods (see 3.4) the PFGE gels were loaded with Induction, Repair (70 Gy), and Control samples of one experiment to simplify further quantification. Replication of samples in different rows (gel A contains for example Induction of 0 and 10 Gy in the first and third rows) allowed more exact evaluation.

### 3.3.1 Induction curves

To check whether the defect in LEC cells is caused by induction of DNA damage, the induction of DSB in LEC and LE fibroblasts was measured by PFGE in the dose range from 0 to 70 Gy. After a dose of 70 Gy, more than 50% of DNA (LEC  $59.1 \pm 4.7\%$  ( $n = 3$ ), LE  $60.4 \pm 6.1\%$  ( $n = 3$ )) migrated out of the well, indicating a high amount of induced damage (see **Figure 3.6., A, B**, Row 1 in both gel images).

The results indicate that induction curves (dose-response curves) do not differ between LEC and LE fibroblasts, accumulated in G1 phase of cell cycle (see **Figure 3.7.**).

The induction curves for a dose up to 50 Gy showed a linear shape, as was shown by linear regression analysis (see **Figure 3.7.**). According to Foray *et al.*, 1999 [123], the threshold effect might be observed in the range of doses from 0 - 10 Gy region of the FAR curve, when the number of DNA fragments, which are small enough to be able to migrate into the gel is very low, since only fragments smaller than a certain size are able to enter gel. In the performed induction experiment no threshold effect was observed (see **Figure 3.7.**). Difference from observations of Foray *et al.*, 1999 [123] might be explained by the different PFGE methodology and conditions, and also the detection system.

At a dose above 50 Gy, the increase of FAR becomes more flatten, thus causing a deviation from linearity at higher doses. This might be due to the induction of additional DSB in DNA that is already damaged. After high doses the large number of DNA fragments induced, therefore is a higher probability that breaks occur in the same fragments. That is why the amount of fragmented DNA entering the gel does not change significantly, but the average size of fragments decreases, and the amount of induced damage by 70 Gy is lower than that expected from the linear regression analysis (see **Figure. 3.7.**).

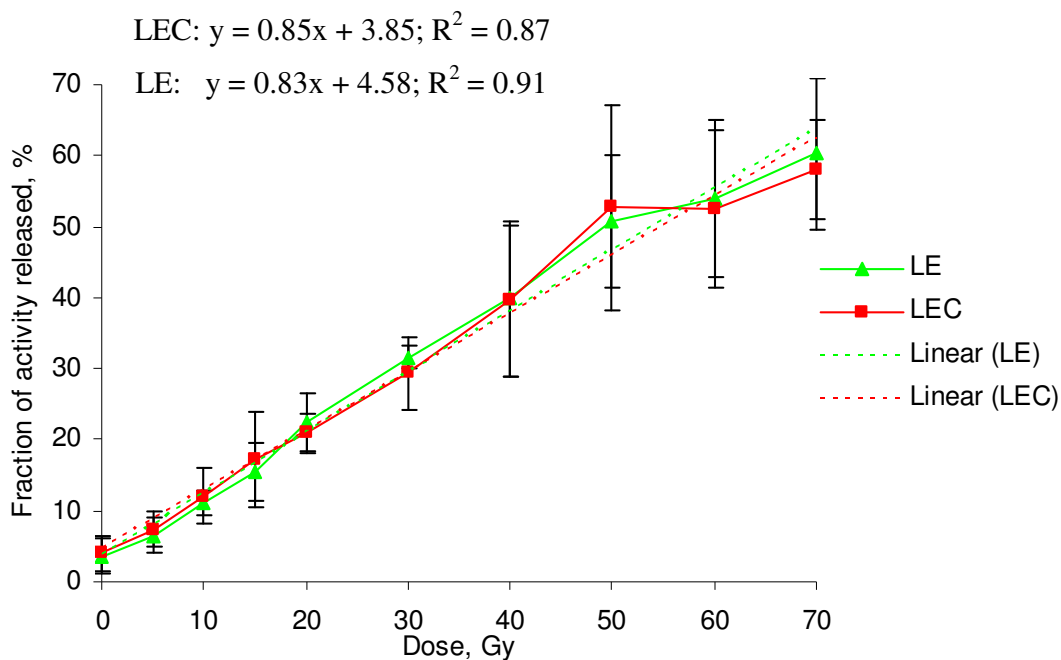


**Figure 3.7. Induction (dose-response) curves are summarised for LEC and LE primary fibroblasts**

The values of FAR (amount of DNA released out of plug) were measured for doses of  $\gamma$ -radiation in the range of 0 to 70 Gy. PFGE of induction, repair and control samples was performed in one experiment. The mean values of FAR  $\pm$  SEM (n = 3-6) are plotted against dose and linear regression analysis of the curve was done using Excel.

---

### 3.3.2 Analysis of repair data expressed in FAR

Analysis of DSB repair expressed in FAR suggests the presence of a minor decrease in repair efficiency in LEC cells, since the mean values of non-repaired damage in LEC were higher than in LE after 1 hour, when the slow component of repair is operating (see **Figure 3.8**). Comparison of data with Student t-test showed a statistically significant difference only at 4 hours after irradiation with 70 Gy, with p-value of 0.023.

DNA repair was studied during incubation of cells embedded in low-melting point agarose. This avoids artefacts related to this particular experimental design. The DNA degradation in controls was investigated in parallel with repair (See **Figure 3.6**). DNA degradation did not change over the investigated time and only slightly increased at 4 hours (LEC  $9.6 \pm 1.3\%$ , n = 5; LE  $6.8 \pm 1.2\%$ , n = 4) and 6 hours (LEC  $11.0 \pm 2.0\%$ , n = 4; LE  $8.8 \pm 1\%$ , n = 3) of repair incubation compare to time 0 (LEC  $4.3 \pm 0.8\%$ , n = 6. LE  $5.4 \pm 0.6\%$  (n = 6) (**Figure 3.6**, **3.8**), where somehow slightly higher DNA degradation was observed in LEC cells. This

means that studied fibroblasts were able to function normally in applied conditions and did not acquire significant DNA damage/degradation, which otherwise could evidence apoptosis.

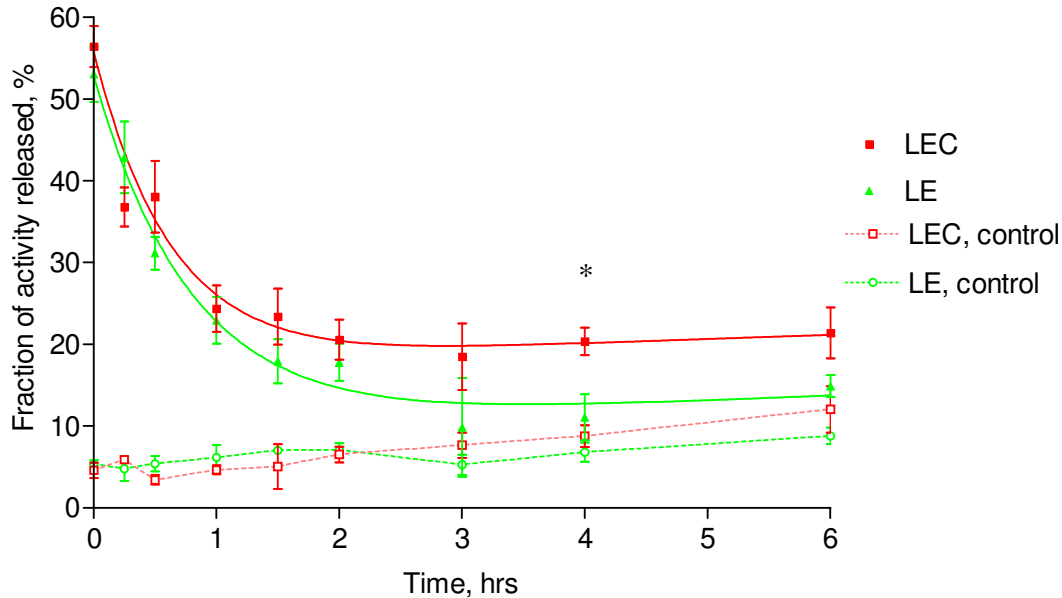


**Figure 3.8. Repair curves and controls expressed in FAR (fraction of activity released)**

The amount of DNA released from the plug (FAR) was estimated using FAR3 program for each sample from the gels stained with EtBr. The mean FAR repair values  $\pm$  SEM of 3-7 experiments are plotted against dose for repair and control curves. Student t-test had a p-value of 0.023 for the 4 hours time-point (marked with \*), results of the test for other time points were not significantly different. Fitting of repair data to two phase decay equation was performed with the commercially available software GraphPad Prism 3.03.

### 3.3.3 Analysis of repair data expressed in Gy-equivalents

The conversion of FAR repair values into Gy-equivalents using the induction curves and subtraction of background Gy-equivalents from respective repair values revealed no major difference in repair between LEC and LE (**Figure 3.9**). Although the mean values of repair in LEC cells were slightly higher than that of LE, possibly indicating a slight deficiency, statistical tests did not confirm it.

The mean FAR values measured at 4 hours had a difference of 8.5% between LEC and LE cells ( $19.6 \pm 1.8\%$  for LEC, and  $11.07 \pm 2.8\%$  for LE cells, Mean  $\pm$  SEM, n = 4 and 3 for LEC and LE cells respectively) (see **Figure 3.8**). After converting them into Gy-equivalents and subtracting control (background) Gy-equivalents from repair Gy-equivalents the difference became statistically non-significant ( $9.3 \pm 0.8\%$  for LEC and  $5.2 \pm 3.8\%$  for LE cells, Mean  $\pm$

SEM, N = 4 for LEC and 3 for LE cells). It might be explained by observing induction curves in the region of smaller damage (see **Figure 3.7.**). Induction of damage seems to be a bit higher in the region between 0 to 20 Gy in LEC cells, and conversion of the same amount of damage then produce higher values of Gy-equivalents in LE cells than in LEC. Summarising this difference and background subtraction might cause such an effect. Also considering that at the later times (4 and 6 hours) the amount of damage is very small (10-5 Gy-equivalents) even if the difference in repair of 2-3 Gy-equivalents between LEC and LE takes place it is difficult to confirm it statistically due to the methodological variation (staining of the gels, background variation). Additionally, the analysis of induction curves was conducted only for these experiments, from which the 4 hours repair time point was derived (n = 4 for LEC and n = 3 for LE) (see **Figure 3.10., Table 3.7., APPENDIX**, page 151-152). The induction in LEC cells seems to be higher than in LE, what might explain the higher FAR repair values in LEC.

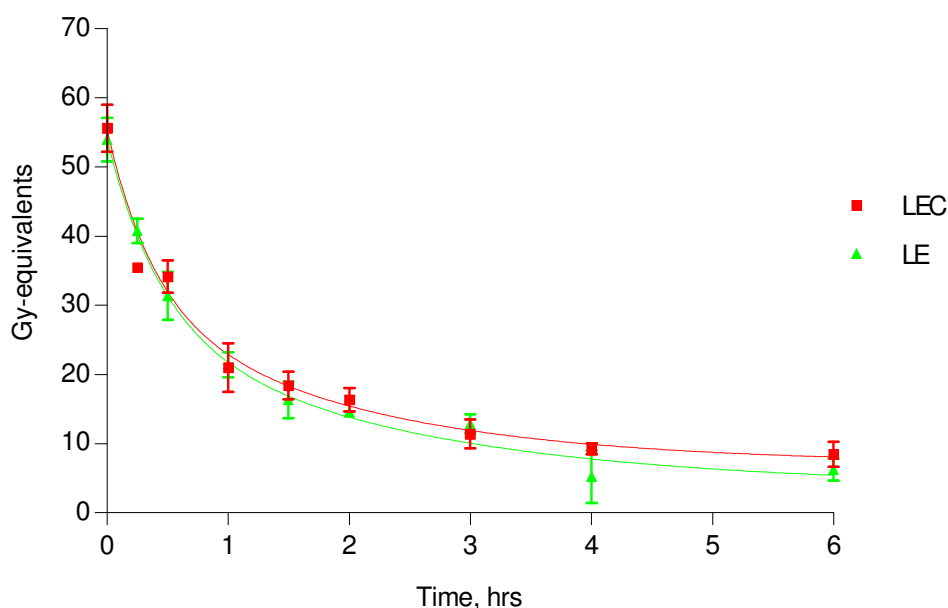


**Figure 3.9. Repair of DSB induced by 70 Gy of IR in LEC and LE fibroblasts was expressed in Gy-equivalents and fitted to two-phase exponential decay equation**

One run of PFGE included induction, repair, and control samples of one experiment. The gels were stained with EtBr and intensity of staining was measured in each line. The amount of DNA released from the plug (fraction of activity released - FAR) was estimated for each sample and compared to the respective induction curve. The Gy-equivalents were estimated for each experiment, and Gy-equivalents of controls were subtracted from irradiated samples. The mean values  $\pm$  SEM plotted against time and fitting of data to two-phase exponential decay was achieved using the non-linear regression analysis of a commercially available software package GraphPad Prism 3.03. Student t-test did not show statistically significant difference in repair between LEC and LE cells.

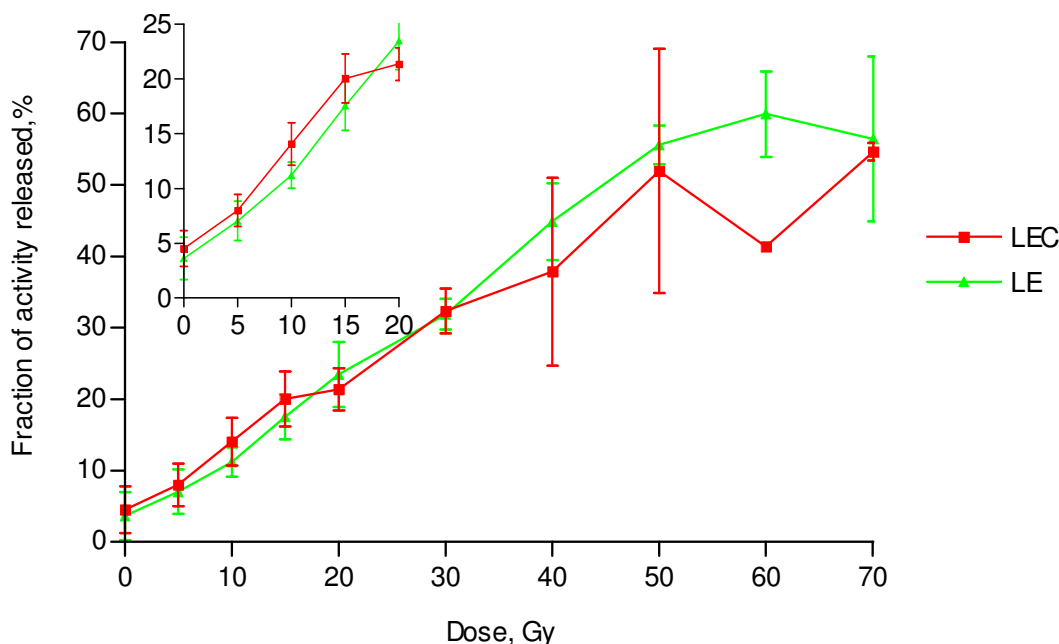


**Figure 3.10. The induction curves of the experiments, which showed statistically significant difference at 4 hours after irradiation**

The experimental data were summarized for LEC (n = 4) and LE (n = 3) repair curves (see **Table 3.7., APPENDIX**, page 151-152), where FAR analysis reflected a statistically significant difference at 4 hours after IR (see **Figure 3.8.**). The inset graph reflects the repair in the dose region between 0 to 20 Gy.

### 3.3.4 Analysis of repair kinetics

To characterise the kinetics of repair, the Gy-equivalent repair values were further fitted to a two-phase exponential decay equation. The kinetics of repair can be described by three components: the fast and slow components of repair and the repair plateau, which is a constant component of non-repairable DSB. The band intensity almost reached the control level within 4-6 hours (see **Figure 3.6.**), although repair values were still higher than in the respective controls (for estimated FAR repair see **Figure 3.8.**).

According to the data derived from the fitting (see **Table 3.8.**), the half-times of the fast component was 0.28 hours in LE and 0.27 hours in LEC cells. The amount of damage repaired with the fast component was 53% in LE cells and 49% in LEC cells. The calculations of the half-times of the slow component showed values of 1.38 hours for LE cells and 1.29 hours for LEC cells. LEC cells had a higher plateau value of 7.14% comparing to that of LE – 3.8%, what means

that repair was not completed in LEC cells. However, statistical evaluation of the parameters, characterizing kinetics of repair curves (slope, half-time of fast, and slow components of repair, plateau) did not reveal significant difference between LEC and LE Gy-equivalent repair curves.

**Table 3.8. List of parameters, characterizing the repair of DSB in LEC and LE expressed in Gy-equivalents, resulted from fitting of repair curves to two phase exponential decay equation**

<i>Best-fit values</i>	LEC, Mean $\pm$ SEM	LE, Mean $\pm$ SEM	P value of t-test
A	24.1 $\pm$ 22.1	26.6 $\pm$ 26.3	0.94
b	0.54 $\pm$ 0.71	0.50 $\pm$ 0.7	0.97
C	24.2 $\pm$ 26.1	23.7 $\pm$ 30.9	0.99
d	2.6 $\pm$ 2.7	2.4 $\pm$ 2.97	0.95
PLATEAU	7.14 $\pm$ 5.6	3.8 $\pm$ 6.2	0.68
$t_{1/2, \text{ fast, hrs}}$	0.27	0.28	
$t_{1/2, \text{ slow, hrs}}$	1.29	1.38	
$F_{\text{fast}}$	0.49	0.53	
$F_{\text{slow}}$	0.50	0.47	

The experimental data of DSB repair as evaluated with PFGE and converted into Gy equivalent units, were fitted to the two-exponential decay equation using GraphPad Prism 3.03 Software (see **2.2.6, Pulsed field gel electrophoresis. Fitting of data and derived parameters**). Parameters A and C describe the amplitudes and parameters b and d are the rate constants of the fast and slow component of rejoining, respectively. The curves are characterized by their half-time ( $t_{1/2}$ ) of slow and fast components of repair and amount of breaks repaired by fast and slow components ( $F_{\text{fast}}$ ,  $F_{\text{slow}}$ )

### 3.4 $\gamma$ H2AX foci quantification

Histone H2AX is phosphorylated after exposure to IR, forming microscopically visible foci, each containing thousands of phosphorylated H2AX (denoted as  $\gamma$ H2AX) molecules covering about 2 Mb of DNA flanking the DSB. Formation of  $\gamma$ H2AX is observed within a few minutes, causes changes in chromatin conformation, and may serve as a signal for recruitment of DNA repair enzymes [124].

Despite its highly coordinated regulation, the precise role of  $\gamma$ H2AX in DSB repair is not completely understood.  $\gamma$ H2AX is reported to mediate the recruitment of numerous DSB-

recognition and repair factors to the immediate area of the break, including many chromatin modifiers, DNA checkpoint proteins, and cohesion [124]. The number of foci per cell was shown to be equivalent to the number of DNA DSB [125].

The kinetic of DSB repair differs from that of  $\gamma$ H2AX dephosphorylation and occurs significantly faster. It was shown that half-time of dephosphorylation is less than 3 hours and fraction of phosphorylated histone H2AX foci, which is higher than that of unrepaired DSB persisted for a long time after irradiation [126]. Additionally, at later time points the acquired images of  $\gamma$ H2AX foci do not overlap as it happens at earlier times when phosphorylation of  $\gamma$ H2AX is maximal. Since loss of  $\gamma$ H2AX has been proposed to reflect cellular radiosensitivity and/or DNA repair of the DSB, the number of foci per cell and size of foci were evaluated at 9 and 23 hours after 1 Gy of IR by immunofluorescent staining (see **Table 3.9.**) and further image analysis (**Figure 3.11.**). At 9 hours the number of foci was higher in LEC cells compared to LE and unexposed controls, what means that the damage was not completely repaired yet. The results of the paired t-test comparison gave a p-value of 0.18, which was not statistically significant and did not prove the observed difference in  $\gamma$ H2AX foci formation between LEC and LE cells. The number of  $\gamma$ H2AX foci at 23 hours reached the control values in both LEC and LE cells (see **Table 3.9.**). For further evaluation the number of foci per cell measured in the control was subtracted from values in irradiated cells (see **Table 3.9.**) and a two-tail t-test comparison of the resulted values was performed, which gave a non-significant p-value (0.2).

The background number of  $\gamma$ H2AX in the control was similar for LEC and LE fibroblasts. It is known that S- and G2 phase cells have a higher background  $\gamma$ H2AX than cells in G1 phase, but radiation-induced phosphorylation is higher in G1 than in S and G2 cells ([127], [128]). To avoid the cell cycle phase effects on the results of the experiment, the cells were grown till confluency, therefore getting synchronized in the G1 phase of cell cycle. The same approach was applied in all cell survival and PFGE experiments.

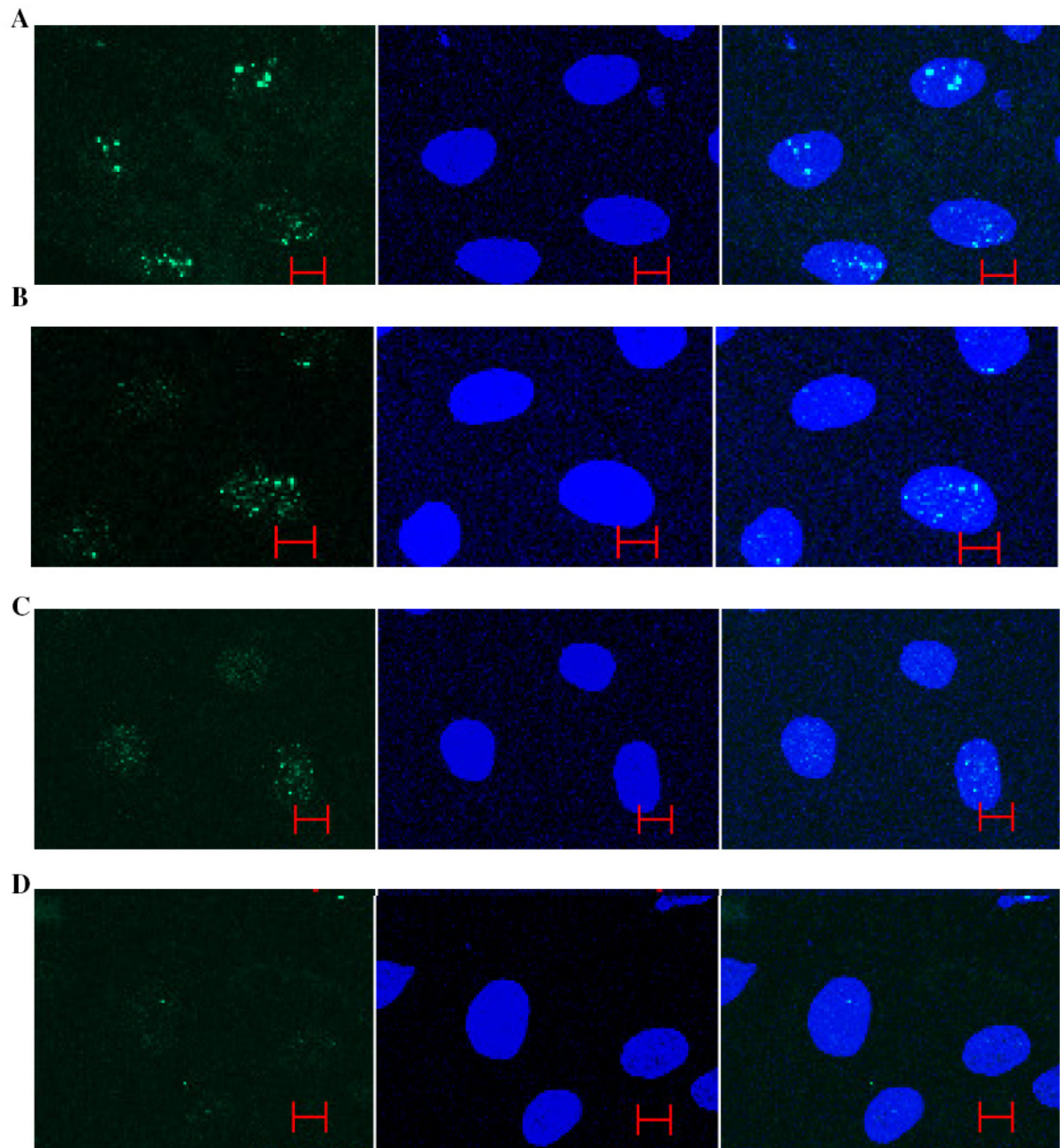


**Figure 3.11. Immunofluorescent staining of H2AX phosphorylation in 9 hours after 1 Gy of  $\gamma$ -irradiation**

Representative images of  $\gamma$ H2AX staining are shown.  $\gamma$ H2AX was detected with mouse monoclonal primary antibody; the secondary goat anti mouse was labelled with Alexa488; the nuclei were counterstained with DAPI. Microscopy was performed with LSM510, filter C-Apochromat, objective 63 x 1,2 W. Bar size 10  $\mu$ m.

**A, B:** LEC and LE cells after 1 Gy of  $\gamma$ -irradiation, 9 hours

**C, D:** LEC and LE cells, mock-irradiated controls, 9 hours. Left panel images depict green channel for detection of  $\gamma$ H2AX foci; middle panel - DAPI stain of nuclei; right panel - merged image of  $\gamma$ H2AX foci on DAPI field.

**Table 3.9. Evaluation of  $\gamma$ H2AX foci in LEC and LE fibroblasts**

Time, hrs	Experiment	LEC			LE		
		N of cells	Mean N of foci/cell	Mean size of foci	N of cells	Mean N of foci/cell	Mean size of foci
9	1	40	2.28	0.364	51	1.7	0.55
	2	46	3.5	1.097	81	1.88	0.90
	3	218	6.97	0.65	82	2.95	0.59
	<b>MEAN <math>\pm</math> SEM</b>		<b>4.25 <math>\pm</math> 1.4</b>	<b>0.7 <math>\pm</math> 0.21</b>		<b>2.04 <math>\pm</math> 0.26</b>	<b>0.68 <math>\pm</math> 0.11</b>
Control	1	72	0.55	0.51	76	0.91	0.32
	2	99	1.43	1.65	85	1.07	1.37
	3	90	0.82	1.67	61	1.17	1.16
	<b>MEAN <math>\pm</math> SEM</b>		<b>0.93 <math>\pm</math> 0.26</b>	<b>1.05 <math>\pm</math> 0.08</b>		<b>1.28 <math>\pm</math> 0.38</b>	<b>1.02 <math>\pm</math> 0.35</b>
<b>Subtracted</b> (1 Gy, 9h - control, 9h)	<b>1</b>		<b>1.73</b>			<b>0.79</b>	
	<b>2</b>		<b>2.07</b>			<b>0.81</b>	
	<b>3</b>		<b>6.15</b>			<b>1.78</b>	
	<b>MEAN <math>\pm</math> SEM</b>		<b>3.3 <math>\pm</math> 1.42</b>			<b>1.13 <math>\pm</math> 0.32</b>	
23	1	n.d.	n.d.	n.d.	n.d.	n.d.	n.d.
	2	70	0.73	0.58	143	0.99	0.49
	3	122	1.27	1.04	147	1.77	0.96
	<b>MEAN</b>		<b>0.99 <math>\pm</math> 0.27</b>	<b>0.81 <math>\pm</math> 0.23</b>		<b>1.38 <math>\pm</math> 0.39</b>	<b>1.02 <math>\pm</math> 0.52</b>

Table summarizes data of evaluation of  $\gamma$ H2AX foci from three independent experiments. It contains the number of cells evaluated in each experiment, number of foci per cell as obtained with ImageJ Software and mean size of foci in LEC and LE fibroblasts at 9 and 23 hours after irradiation with 1 Gy and in controls. At 9 hours after IR the mean number of  $\gamma$ H2AX foci in control was subtracted from that of irradiated cells.

### 3.5 Comet assay

The repair of single strand breaks (SSB) and alkaline labile sites (ALS) was investigated by means of the alkaline comet assay in lymphocytes of blood of LEC and LE rat strains.

The induction of damage was studied in both LEC and LE lymphocytes, since there are some indications that some mutants (FA cells, ATM [129]) show higher levels of initial DNA damage in alkaline comet assays. According to conclusions made by Djuzenova *et al.*, 2002 [129], such observations mean the presence of changes in their chromatin structure. No difference

was seen in the dose-response of SSB and ALS damage induction between LEC and LE lymphocytes after irradiation with 4 Gy (see **Figure 3.12. -3.14.**).

At the first instance the data of all animals of one strain for one time point were compared as box and whiskers plots (**Figure 3.12.**). Statistical analysis applying Kruskal-Wallis test has shown the difference between medians with  $P < 0.0001$ . This evaluation of comet assay data indicated that LEC lymphocytes have a tendency of suppression of repair of SSB and ALS. But taking into consideration the studies of [115] on statistical evaluation of comet data, which show that commonly used Mann-Witney test and Kruskal-Wallis statistics are oversensitive, the Mann-Whitney test was applied to find out whether there is also a difference observed between measurements at one time point of different animals of one rat strain (see **Figure 3.12.**). The results indicated that measurements of different animals of the same rat strain at one repair time point reporting significantly different values, for example, Mann-Whitney test returned a value of 0,0033 when samples taken from two LEC rats and measured at 15 min after 4 Gy of  $\gamma$ -irradiation were compared. As the rats were of the same age and genetically identical the observations are probably due to experimental variation. Considering these results and the recommendations of [115], the data were further reduced to representative means, medians and 75<sup>th</sup> percentiles of each measurement in a set of animals ( $n = 3$ ) analyzed from each rat strain (see **Figure 3.13.**) at each repair time point. These data were further tested for significance with the Student t-test at each time point and with ANOVA test for the whole data set, which did not show statistical difference in repair of SSB and ALS between the two strains.

Additionally, the estimated tail (Olive) moments of one sample were arbitrary classified in 6 size groups (see **Figure 3.14.**). The mean frequencies of comets in the size groups were compared. Irradiation caused an increase in number of cells in size fractions 200-1400 (TOM), what reflects the damage induction, in parallel with a decrease of cell number in the group size 0-200. After the repair time the distribution changes and becomes similar to that of controls, although at measured time points some damage still remained unrepaired (see **Figure 3.14.**). Cells derived from LEC rat showed a tendency towards slower repair comparing to those of LE rat.

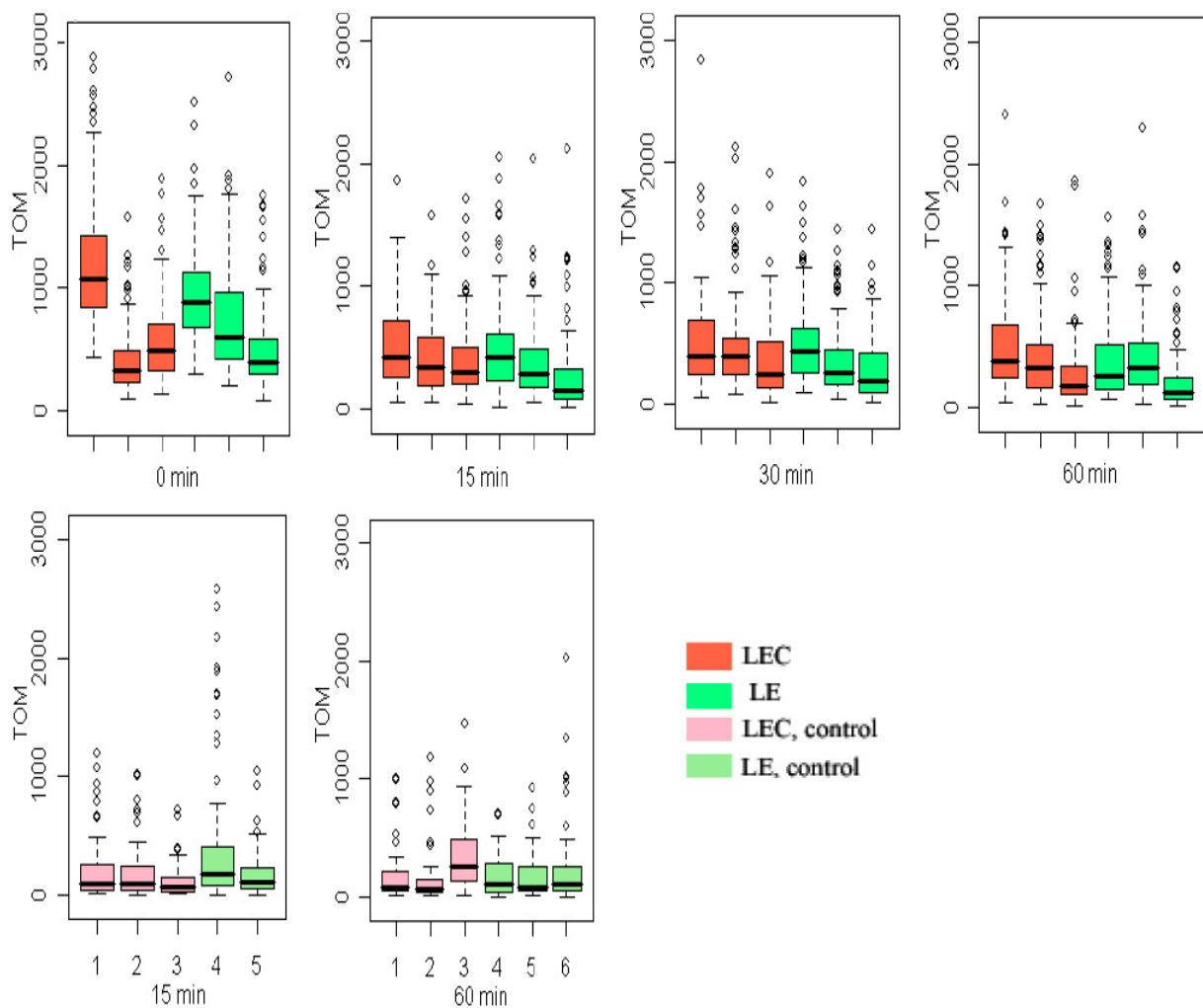


**Figure 3.12. Repair of DNA damage is shown as Tail (Olive) moment plotted against time**

The values of Tail (Olive) moment were measured at several time points (0, 15, 30, 60 minutes) after 4 Gy of  $\gamma$ -irradiation in lymphocytes of whole blood from 3 LEC and 3 LE animals, from 60-120 comets each. The data of repair and background damage are presented as box and whiskers plots for every repair time point. Every box and whisker plot reflects highest, lowest values in the sample, sample mean, 25<sup>th</sup> and 75<sup>th</sup> percentiles (lower and higher limits in the box). Altogether 3600 comets were measured. Statistical evaluation with Kruskal-Wallis test showed the statistically significant difference between medians with  $P < 0.0001$ . Further statistical analysis has shown that this difference was not biologically significant.

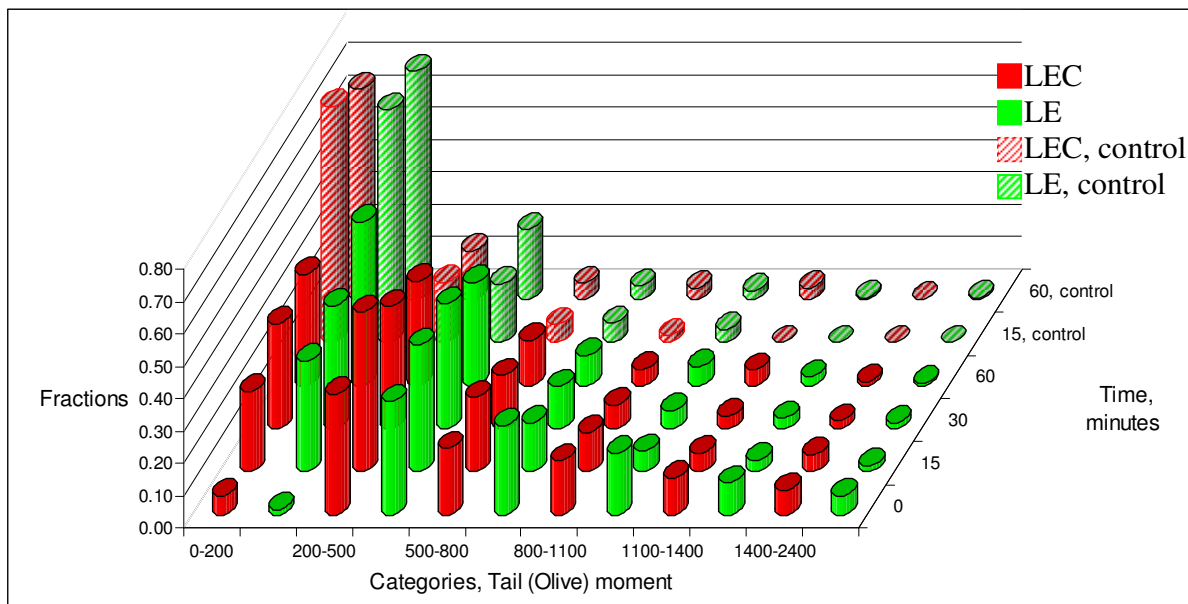


**Figure 3.13. Distribution of mean Tail (Olive) moments in size groups**

Comets depending on their size were classified in size groups and their frequency (fraction) per sample (number of comets in particular group/number of comets measured) was estimated. The mean values of fractions were calculated from samples taken from different animals and per time points and plotted as distributions in 3-D plot. The graph shows induction of damage at time 0, which is not different between LEC and LE animals. The fraction of cells in group with less damage (0-200) is very small and distribution is shifted to the right. With further repair incubation the distribution gets close to the background level, but complete repair of induced damage is not observed during the measured time. Tail (Olive) moments of LEC cells were shifted to the groups with higher tail moment, although statistically it was not significant (Anova test).

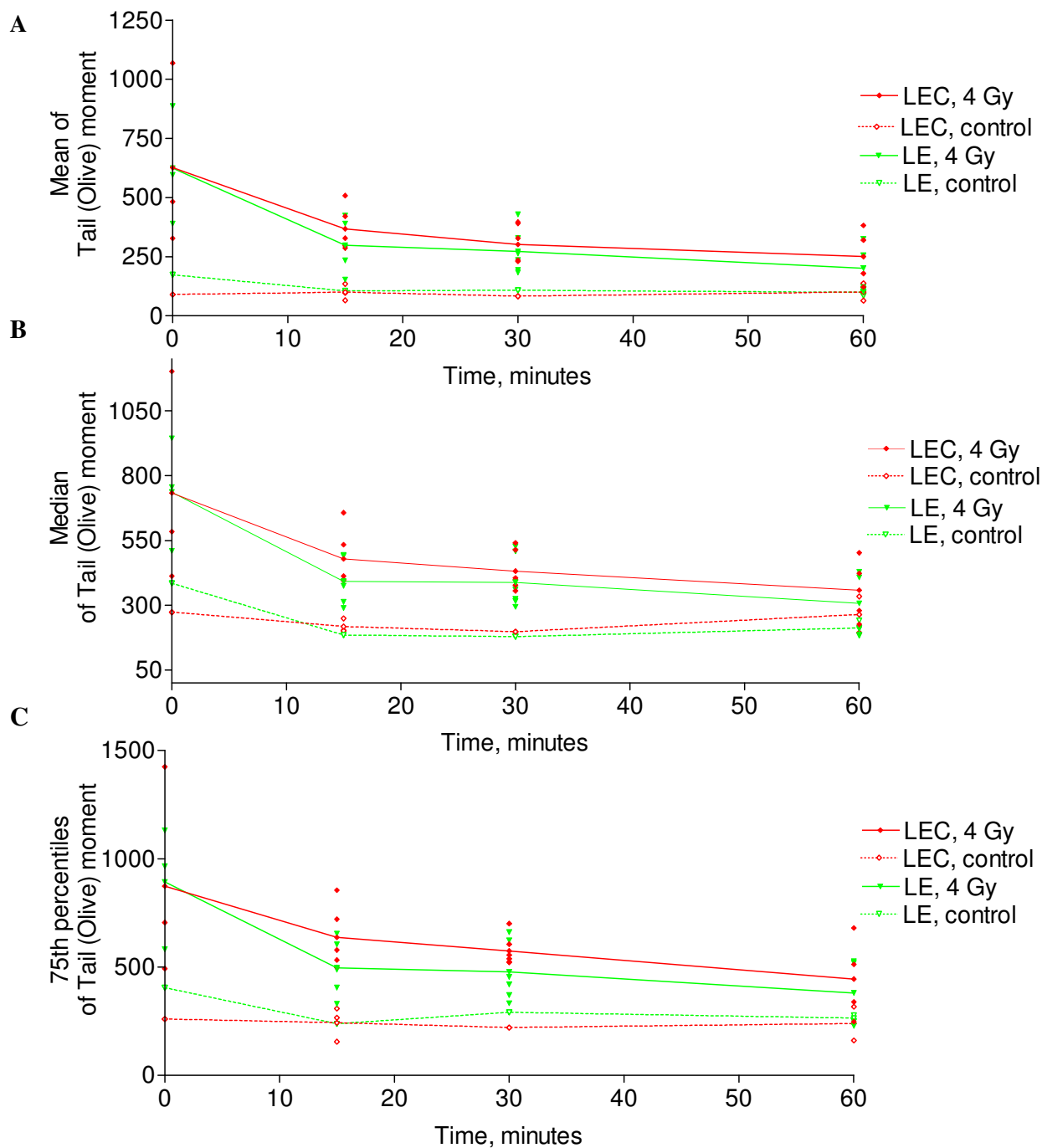


**Figure 3.14. DNA damage induction and repair profiles measured in lymphocytes by the comet assay after *in vitro* irradiation with 4 Gy of whole blood. The extent of DNA damage was measured quantitatively as comet tail moment and expressed as means, 75<sup>th</sup> percentils and medians in each of 3-6 animals**

The values of Tail (Olive) moment were estimated from single cell electrophoregrams of 60-120 cells from each of 3-6 animals at different times after 4 Gy of  $\gamma$ -irradiation. The single values of means (A), 75<sup>th</sup> percentiles (C) and medians (D) of tail (Olive) moment measured for each animal were plotted and means of measurements LEC and LE rat strains were connected. Statistical evaluation with Student t-test did not show significant difference.

### 3.6 Cell cycle progression

To identify radiation-induced changes in cell cycle progression, the analysis of DNA distributions in asynchronously growing fibroblasts was performed after 5 Gy of IR. The plots (see **Figure 3.15.**) reflect numbers of cells in different phases of the cell cycle derived from respective histograms (see **Figure 3.16., APPENDIX**, page 153).

The percentage of cells in S phase decreased 6,5 hours after irradiation from 13.5% (LEC) and 10% (LE) to 5% (LEC) and 8% (LE), and fall further to till 2% (LEC) and 4% (LE) at 23.5 hours and stayed at low levels at investigated later time-points (34 and 54 hours) (see **Figure 3.15., B**). Percentage of S-phase cells in controls (sham-irradiated) also decreased over time and lowest numbers (10-6%) were observed at 54 hours after irradiation. After irradiation cells accumulated at G2 phase of the cell cycle at 6.5 hours (G2-phase arrest) and exited it at 24 hours (see **Figure 3.15., C** and **Figure 3.16., APPENDIX**, page 153). The number of G2 cells in controls also decreased over time after plating.

The estimated percentage of cells in G1 falls initially at 6.5 hours, reflecting G2 phase arrest. 24 hours after IR percentage of G1 cells increased in both LEC and LE.

Cells in control accumulated over time in G1, with a decrease of cells in S- and G2-phase, what reflects normal contact growth inhibition of primary fibroblasts, when they reach confluency (**Figure 3.15.**).

The progression of LEC and LE cells through phases of cell cycle was similar with and without IR.

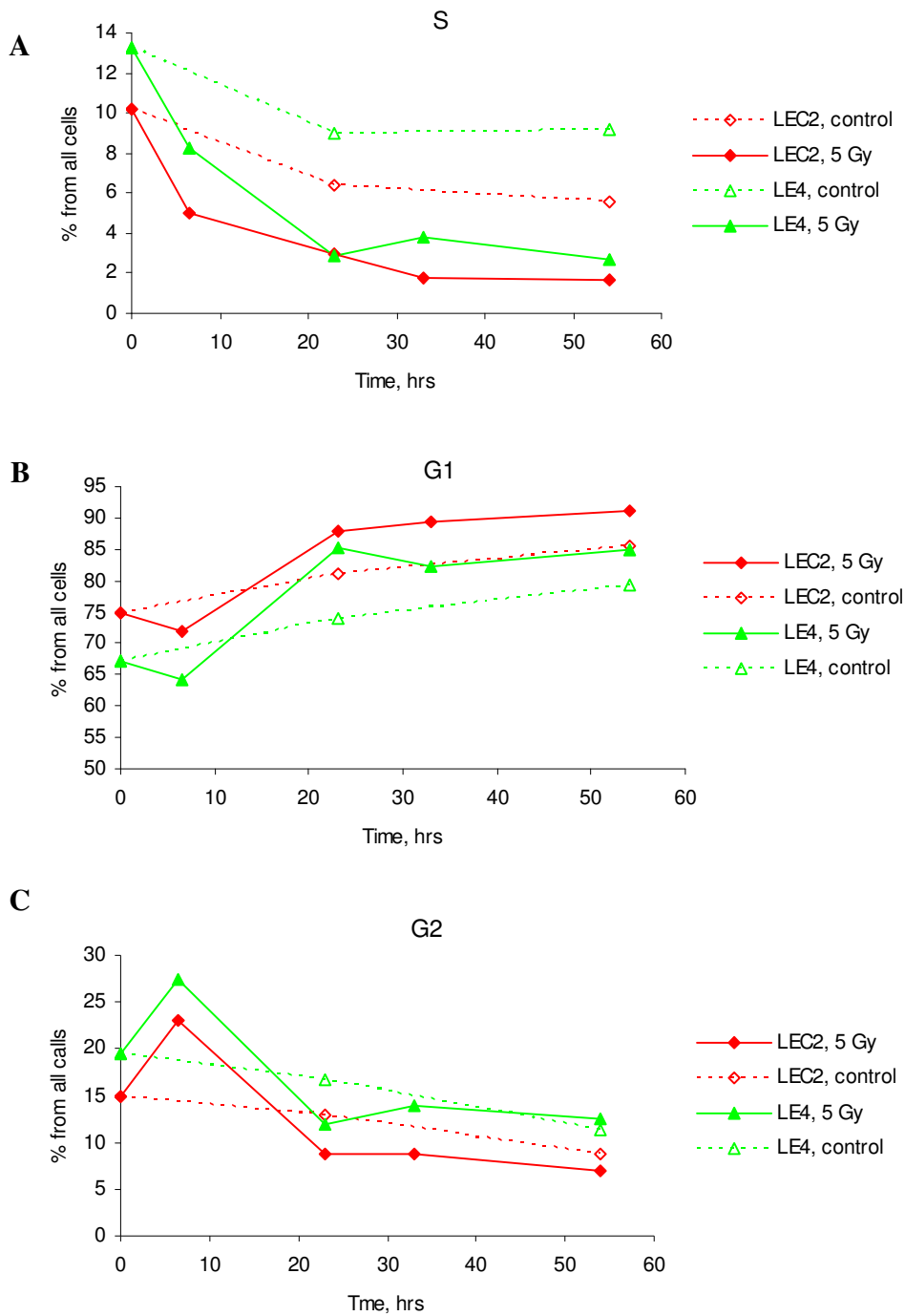


**Figure 3.15. Kinetics of cell cycle progression (G1, S and G2 phase) of LEC and LE fibroblasts after 5 Gy of  $\gamma$ -irradiation and in the controls**

The percentage of cells in G1, S, and G2 phase was estimated from DNA distribution histograms and plotted against time.

**A:** G1 phase, **B:** S phase, **C:** G2 phase.

### 3.7. Genetic analysis of locus of interest in LEC versus LE rat. Establishment of candidate gene(s)

#### 3.7.1 Sequencing analysis of *Rad18*, *v-Raf-1*, *XPC* and *Fancd2* genes

Considering the data published by Agui *et al.*, 2000 [83], showing linkage of LEC strain radiosensitivity to an anonymous locus on chromosome 4 (see **Figure 1.1., Introduction, 1.2.2**), the locus was further analysed. A number of genes functionally related to DNA damage response and repair is located within and include, among the others, *Rad18*, *Raf-1* and *Xpc* genes. The selection of the genes was done considering their function and knowledge of the phenotype in knock-out mice/cells.

The coding sequence of the *Rad18* gene was investigated by means of DNA sequencing, since it is known that yeast *rad18* mutants are extremely sensitive to DNA-damaging agents, including UV, IR, DNA alkylating agents, and DNA cross-linking agents [130]. RAD6/RAD18 epistasis group proteins are involved in postreplication repair by TLS. RAD18 has DNA-binding activity and a RING finger motif, common to E3 ubiquitin ligases [131].

According to the ENSEMBL Genome Browser, the rat *Rad18* gene (see **Figure 3.17.**) is located at chromosome 4 between 148.461.924 - 148.543.746 bps. The coding sequence of rat *Rad18* was analysed using the published in NCBI Database predicted mRNA sequence under GeneBank annotation XM\_342734 (gil34858303) (Rattus Norvegicus RAD18 homolog (S. cerevisiae), predicted). Firstly, the RNA was extracted from liver and brain tissues of LEC and WKAH rat (were only available at that moment) then reverse transcription was performed. Further, sequencing of cDNA was performed with a set of primers designed on the basis of the predicted *Rad18* sequence (see **Figure 3.17., A**). The results of the sequence analysis revealed the absence of a part of the predicted mRNA of the *Rad18* gene at position 344-471 in both cDNAs of LEC and WKAH rat (see **Figure 3.17., B**). Moreover, this region was not correctly predicted and represents a spliced out intron instead of a predicted exon. The rat genomic sequence released later under annotation NM\_001077673 confirmed this finding.

The substitution of a C-to-T nucleotide was found in LEC rat strain at position 585 of the *Rad18* coding sequence, which does not lead to aminoacid change.

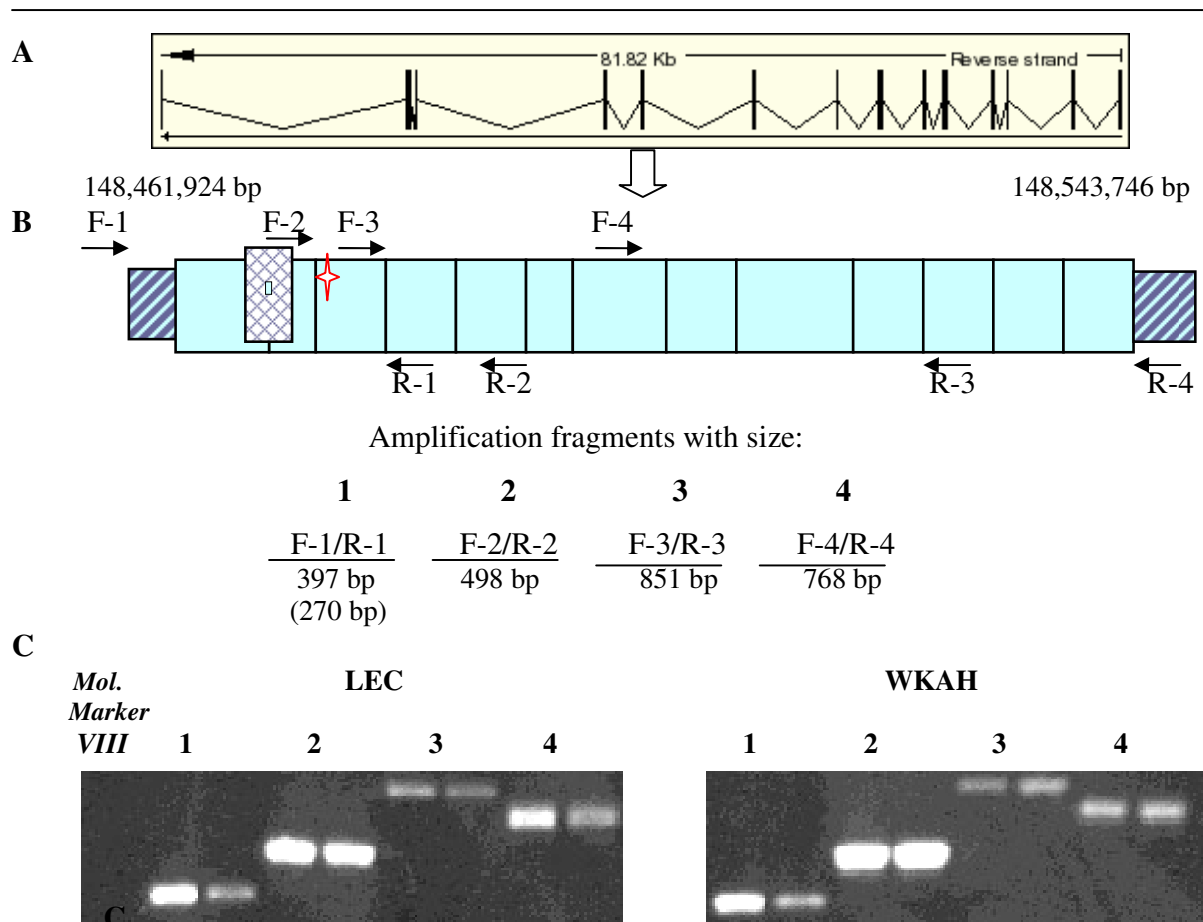


**Figure 3.17. Amplification of cDNA of Rad18 gene**

**A:** The *Rad18* gene can be found on the chromosome 4 at location between 148.461.924-148.543.746 bps. The total length of the predicted transcript is 1.491 bps. The genomic structure of *Rad18* was modified from Ensembl.

**B:** Primer design in the *Rad18* gene. Hatched bars indicate the 5' and 3' -UTR.

Further sequence analysis revealed the substitution of C=>T nucleotide in the position of 585, which does not cause changes on the amino acid level, and absence of part of predicted mRNA in the position from 344-471 (XM\_342734). F (forward) are 5'primers and R (reverse) are 3' primers. The designed primers spanned the junction of adjacent exons, what allow exclude the effect of possible contamination with genomic DNA. The sequences of respective primers are listed in **Table 2.2., Materials 2.1.** PCR amplicon sizes in base pairs (bp) are indicated. Detected SNP is shown as  $\star$ .

**C:** PCR product resulting from amplification of cDNA of LEC and WKAH was subjected to the gel electrophoresis on 2% agarose.

RAF-1 is a serine/threonine kinase signal transduction factor in the MAPK signal transduction pathway and is believed to be involved in an IR signal transduction pathway, modulating the G1/S checkpoint [132]. It was published that downregulation of Raf through antisense RNA made human cells more sensitive to IR [133], [134].

The coding sequence of *Raf-1* (see **Figure 3.18.**) was amplified with primers designed on the basis of published sequence under accession number NM\_012639, *Rattus norvegicus* murine leukemia viral (*v-raf-1*) oncogene homolog. The primers are listed in **Table 2.2., Materials, 2.1.7.** The *Raf-1* gene is located on chromosome 4 at the genetic position 151.752.583-151.775.613 bps. **Figure 3.18.** shows the genomic (**A**) and transcript (**B**) structure of *Raf-1*.

Sequencing of amplified products (**Figure 3.18., C**) of *v-raf-1* gene indicated a C=>T substitution in the 644 nucleotide, which is the third nucleotide in threonine and did not change the aminoacid sequence.

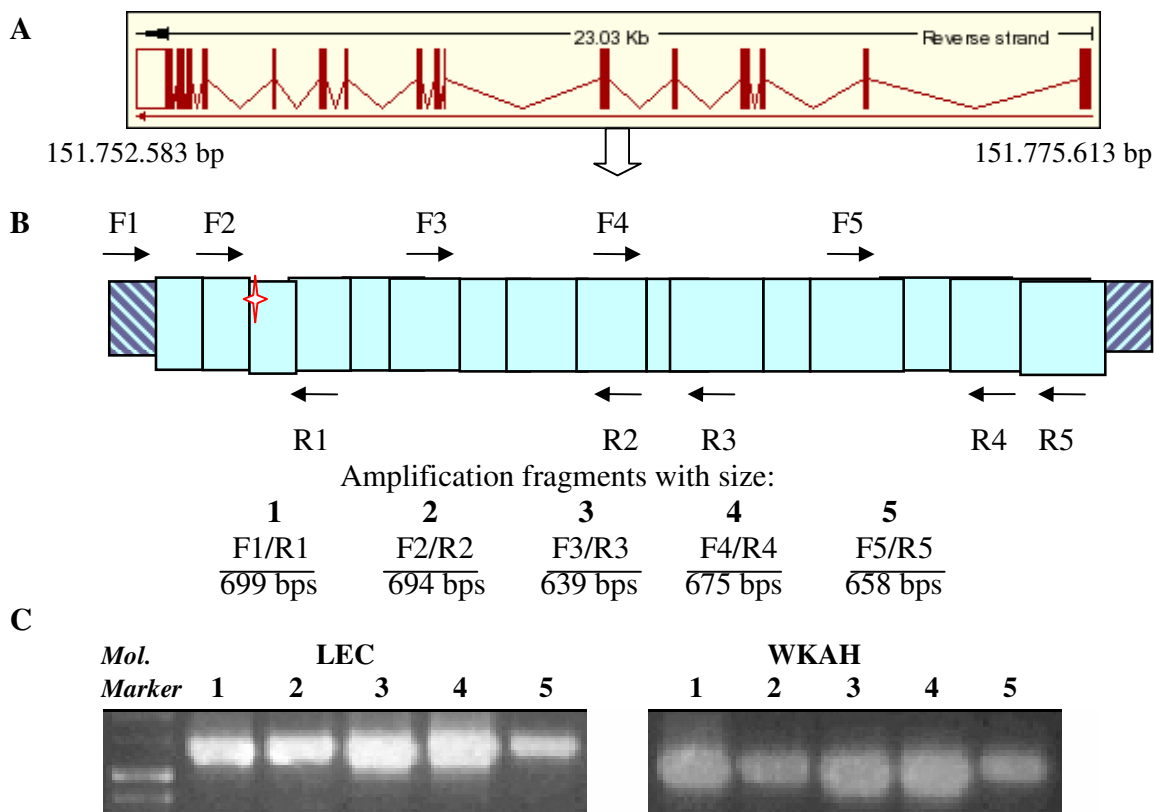


**Figure 3.18. Amplification of cDNA of Raf-1 gene**

**A:** The *Raf-1* gene can be found on the chromosome 4 at the location between 151,752,583-151,775,613 bps. The figure shows the genomic organisation of the gene with introns and exons, shown as vertical lines of different thickness, depending on their size.

**B:** Scheme of the amplification of cDNA of *Raf1* with selected primers (see **Table 2.2., Materials, 2.1.7.**). Hatched bars indicate the 5' and 3'-UTR. Further sequence analysis reveals the substitution of C=>T nucleotide at position of 644 (shown as  $\star$ ), which does not cause changes at the aminoacid level.

**C:** PCR products resulting from amplification of cDNA of LEC and WKAH was subjected to electrophoresis on a 2% agarose gel.

DNA repair Xeroderma pigmentosum group C complementing protein homolog (XPC) is involved in an early stage of sensing and the incision process of NER. An abnormally high chromosomal aberration frequency was observed after X-irradiation in XP-C skin fibroblasts [135-137].

The *Xpc* gene is found on chromosome 4 at position 125.673.446-125.699.866 bps.

Sequencing of the *Xpc* gene was performed with primers designed from sequence published in the NCBI Database under annotation XM\_232194 (Rattus norvegicus xeroderma pigmentosum, complementation group C (predicted) (XPC\_predicted) and did not reveal a difference in the coding sequence from the published data. **Figure 3.19., B** contains the schematic representation of *Xpc* transcript. The respective amplicons of PCR reaction with primer pairs for amplification of *Xpc* cDNA are pictured in **Figure 3.19., C**.

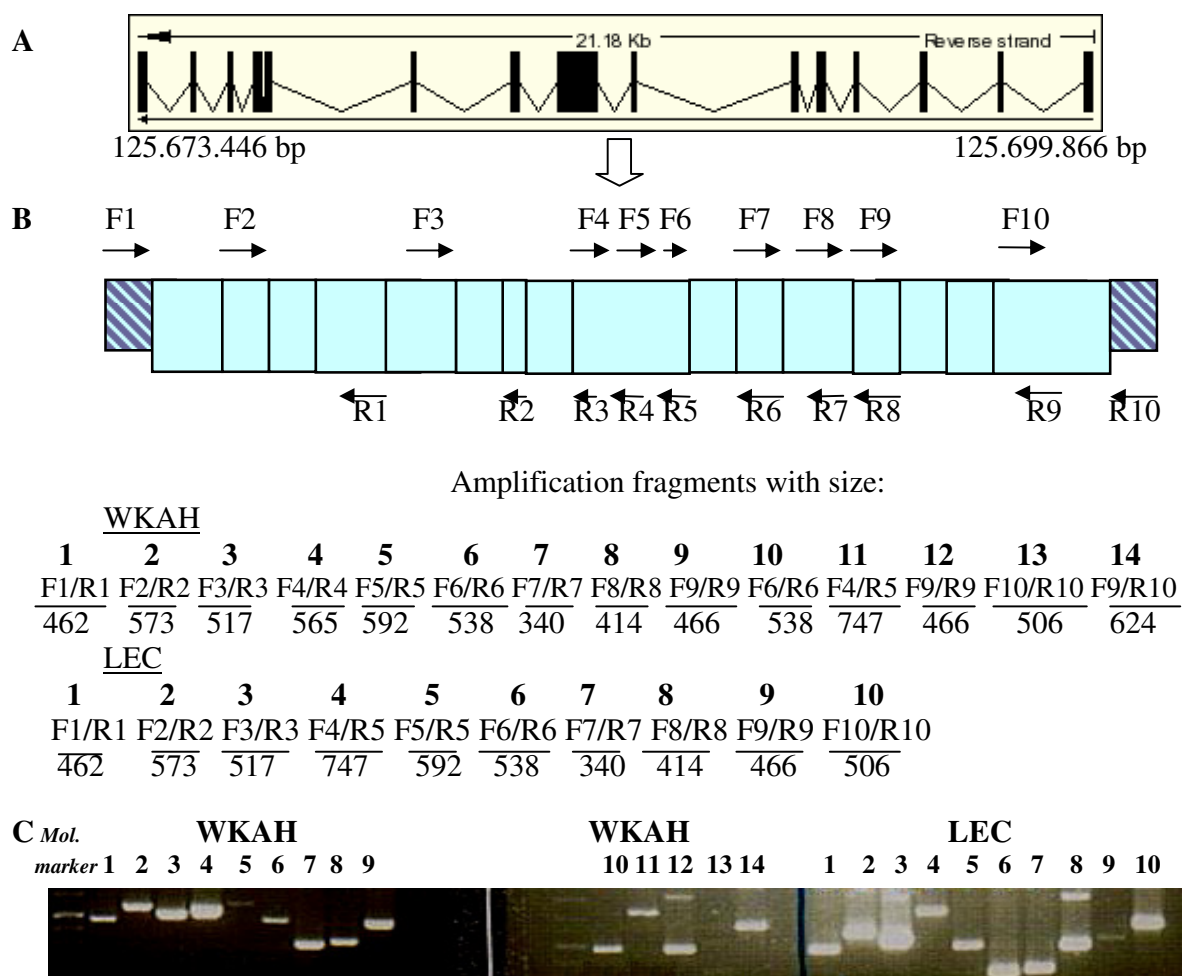


**Figure 3.19. Amplification of cDNA of *Xpc* gene**

**A:** The *Xpc* gene can be found on the chromosome 4 at position 125.673.446-125.699.866 bps. The image contains the scheme of genomic organisation of *Xpc* with introns and exons, shown as vertical lines of different thickness, depending on their size.

**B:** Scheme of the amplification of cDNA with selected primers for *Xpc* (see **Table 2.2., Materials, 2.1.7**). Hatched bars indicate the 5' and 3'-UTR.

**C:** PCR product resulting from amplification of cDNA of LEC and WKAH was subjected to the gel electrophoresis on 2% agarose.

Fanconi anemia (FA) is a rare autosomal disorder that is characterised by increased spontaneous and DNA crosslinker-induced chromosome instability. FANCD2 cells have a defect in the IR-induced S phase checkpoint and show radioresistant DNA synthesis [138].

The *Fancd2* gene is found at a chromosomal location between 149.424.558-149.500.006 bps. It has the total transcript length of 4.359 bps and is composed of 44 exons.

Sequencing of coding sequence of *Fancd2* gene revealed two amino acid substitutions in both LEC and LE rat strains (A955G (isoleucine→valine) and G1645A (glycine → arginine)) compared to the predicted sequence (*personal communications with M. Rosemann*).

A number of rat strains were genotyped for these variations (see **Table 3.10**). The designed primers were located in the introns adjacent to the exons, containing the changes. The results showed, that another two rat strains, F344 and Copper rat, were also homozygote for both polymorphisms. Therefore, the identified changes could not be the reason for the radiosensitivity in LEC rat, since it was shown by Tsuji *et al.*, 2005 [85] that LEC rat is more radiosensitive than F344 rat. The sequence information about the observed polymorphisms in the analysed rat strains was submitted to GeneBank under the annotation AY621075.

**Table 3.10. Genotyping of several rat strains for amino acid substitutions in the *Fancd2* gene**

Rat strain	Genotype	
	Nucleotide 955	Nucleotide 1645
LEC	G	A
LE	G	A
WKY	A	G
Lewis	A	G
SHR	A	G
F344	G	A
BN	A	G
Copper	G	A

Table lists the genotypes for nucleotides 955 and 1645 in the *Fancd2* gene (the reference sequence is found in NCBI database under annotation AY621075) of different rat strains.

### 3.7.2 Real-time PCR

#### Validation of the $2^{-\Delta\Delta CT}$ relative expression method

The mRNA expression levels of two candidate genes (*Fancd2* and *Gata-2*) were compared in LEC and LE fibroblasts without irradiation and at 4 and 24 hours after 5 Gy of IR by means of the  $2^{-\Delta\Delta CT}$  relative expression method [120]. For validation of the  $2^{-\Delta\Delta CT}$  method the efficiencies of primers used for amplification of target genes (*Fancd2* and *Gata-2*) were

compared to that of a reference gene - porphobilinogendeaminase (*Pbgd*) (for the list of primers see **Table 2.3., Materials 2.1.7**). The mean  $\Delta C_T$  values, ( $C_{T, Fancd2} - C_{T, Pbgd}$ ) and ( $C_{T, Gata-2} - C_{T, Pbgd}$ ), calculated for serial cDNA dilutions in three experiments were plotted against log of RNA dilutions. The slope of the linear regression fit had an absolute value of 0.073 for *Fancd2* and 0.069 for *Gata-2* (see **Figure 3.20.**). This means that efficiencies of selected primer pairs for the target (*Gata-2, Fancd2*) and the reference (*Pbgd*) genes were similar at different cDNA concentrations therefore, the  $2^{-\Delta\Delta C_T}$  method could be used [120].

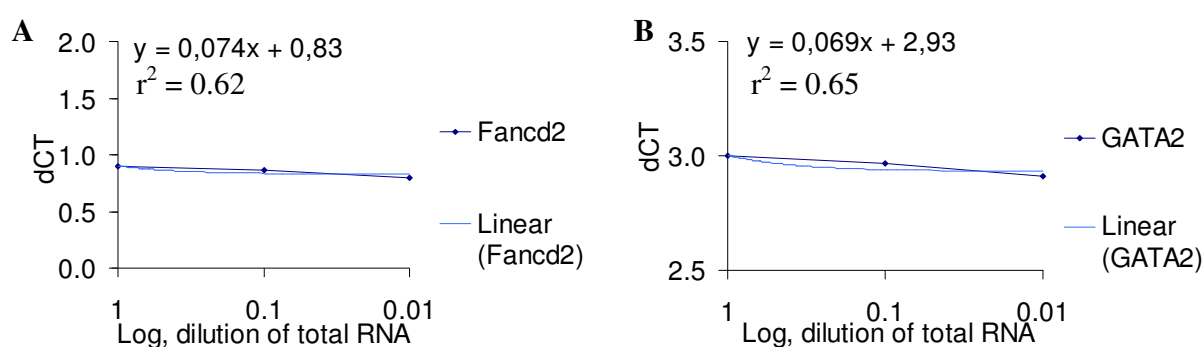


**Figure 3.20. Validation of the  $2^{-\Delta\Delta C_T}$  method**

Pooled cDNA, which was reverse-transcribed from RNA, extracted from livers several LPP rats, was serially diluted and *Pbgd*, *Gata-2* and *Fancd2* genes amplified. The efficiency of the primers was evaluated. The  $\Delta C_T$  was calculated for each cDNA dilution. The means of three measurements were fitted applying linear-regression analysis of Excel [120].

**A:**  $\Delta C_T, Fancd2 = C_{T, Fancd2} - C_{T, Pbgd}$

**B:**  $\Delta C_T, Gata-2 = C_{T, Gata-2} - C_{T, Pbgd}$

### Expression of the *Fancd2* gene in LE/LEC fibroblasts

Levels of *Fancd2* mRNA did not differ significantly between LEC and LE fibroblasts. Both basal levels and those 4 hours and 24 hours after 5 Gy of IR (see **Figure 3.21., A**) were almost identical. Irradiation of cells caused a decrease of *Fancd2* expression at 4 hours and 24 hours in both LEC and LE cells (**Figure 3.21., B**). No reproducible difference was observed between the strains.

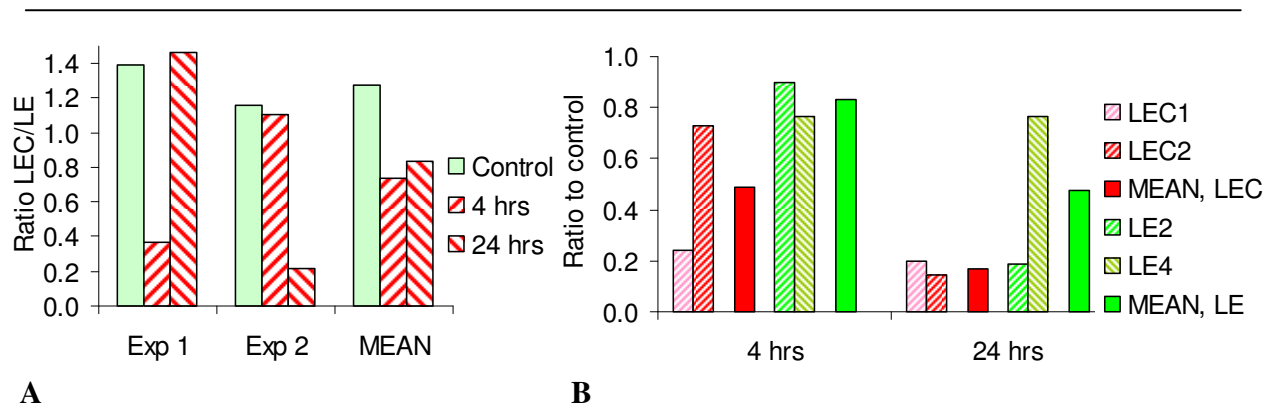


**Figure 3.21. Analysis of *Fancd2* expression with relative  $2^{-\Delta\Delta CT}$  method**

**A:** The expression of *Fancd2* was investigated in LEC fibroblasts at 4 and 24 hours after 5 Gy of IR and in controls (sham-irradiated). Expression of the target gene was normalized to that of LE by means of the relative quantification -  $2^{-\Delta\Delta CT}$  method. *Pbgd* gene was used as a calibrator.

**B:** The changes in expression over time (4 and 24 hours after 5 Gy of IR) were investigated compared to the control in LEC and LE fibroblasts respectively.

### Exclusion of analysed genes from possible candidates of the enhanced radiosensitivity of LEC rat

The data published at the end of 2005 by Tsuji *et al.*, 2005 [85] narrowed the locus of interest down to the region of the size  $\approx 1,3$  Mb between the D4Got85 and D4Got148 (**Figure 1.3., INTRODUCTION, 1.2.2**) microsatellite markers. These results excluded the analysed *Rad18*, *v-Raf-1*, *XPC* and *Fancd2* genes, since they are located outside of the updated region of interest.

### 3.7.3 Establishment of further candidate genes

A schematic presentation of the revised locus of interest is shown in **Figure 3.22**. With improved annotation of the rat genome, a number of additional genes, hypothetical proteins and predicted genes were assigned to the radiosensitivity locus, which was defined by Tsuji *et al.*, 2006 [94] to the region between the AI069943 and BF397922 SNP markers (see **Figure 3.22., B**).

Genes, which were analysed by Tsuji *et al.*, 2005 [85], and novel genes, which were assigned recently to the region, are shown. The novel genes were analyzed for homology to human and mouse genes using the UCSC Database (**Figure 3.23., APPENDIX, page 154-155**). **Figure 3.23.** was constructed with application of UCSC Genome Browser. It shows that the locus of interest is now completely annotated without any gaps (all the gaps are bridged). It also

contains the location of known genes in the locus, based on UniProt, RefSeq, GenBank mRNA (B), N-SCAN gene predictions and rat mRNAs from GenBank (D), spliced ESTs (E) and evolutionary conservation in mammalian, amphibian, bird, and fish species (F).

The novel proteins coded by the genes, located on the locus are RGD1562105\_predicted, RGD1565557\_predicted, LOC686635, RGD1307688 (similar to RIKEN cDNA 5830446M03), LOC500251, RGD1565596\_predicted, GATA-2. **Figure 3.22.** contains information about their arrangement on the locus and genetic position as derived from NCBI Database. The biological function of respective human/mouse orthologous proteins and known functional domains is listed in **Table 3.11.**

### **Genotyping of LE rat on the radiosensitivity locus**

In view of the available information about the LEC genotype *versus* F344 on the locus of interest, published by Agui *et al.*, 2001 [83], Tsuji *et al.*, 2005 [85], Tsuji *et al.*, 2006 [83, 85, 94], several LE rats were genotyped for number of microsatellite markers/SNPs and compared to LEC (see **Figure 3.22.**, A). The position of the markers is given according (where available) to the CELERA and NCBI Databases. Comparison of the analysed haplotypes shows significant genetic difference between LEC and LE rats at the locus of interest. LEC had 5 markers different from LE among 9 analysed (D4Got85, AW918941, D4Rat54, D4Nirs2, Rpn1 (1 SNP)). The *Rpn1* gene was analysed by Tsuji *et al.*, 2005 [85], Tsuji *et al.*, 2006 [94] among other candidate genes located on the locus. LEC and LE had the same genotype for the BF397992 SNP marker, belonging to the *Gata-2* gene. Such similarity was observed for another two markers, AW252115 and D4Nirs1.

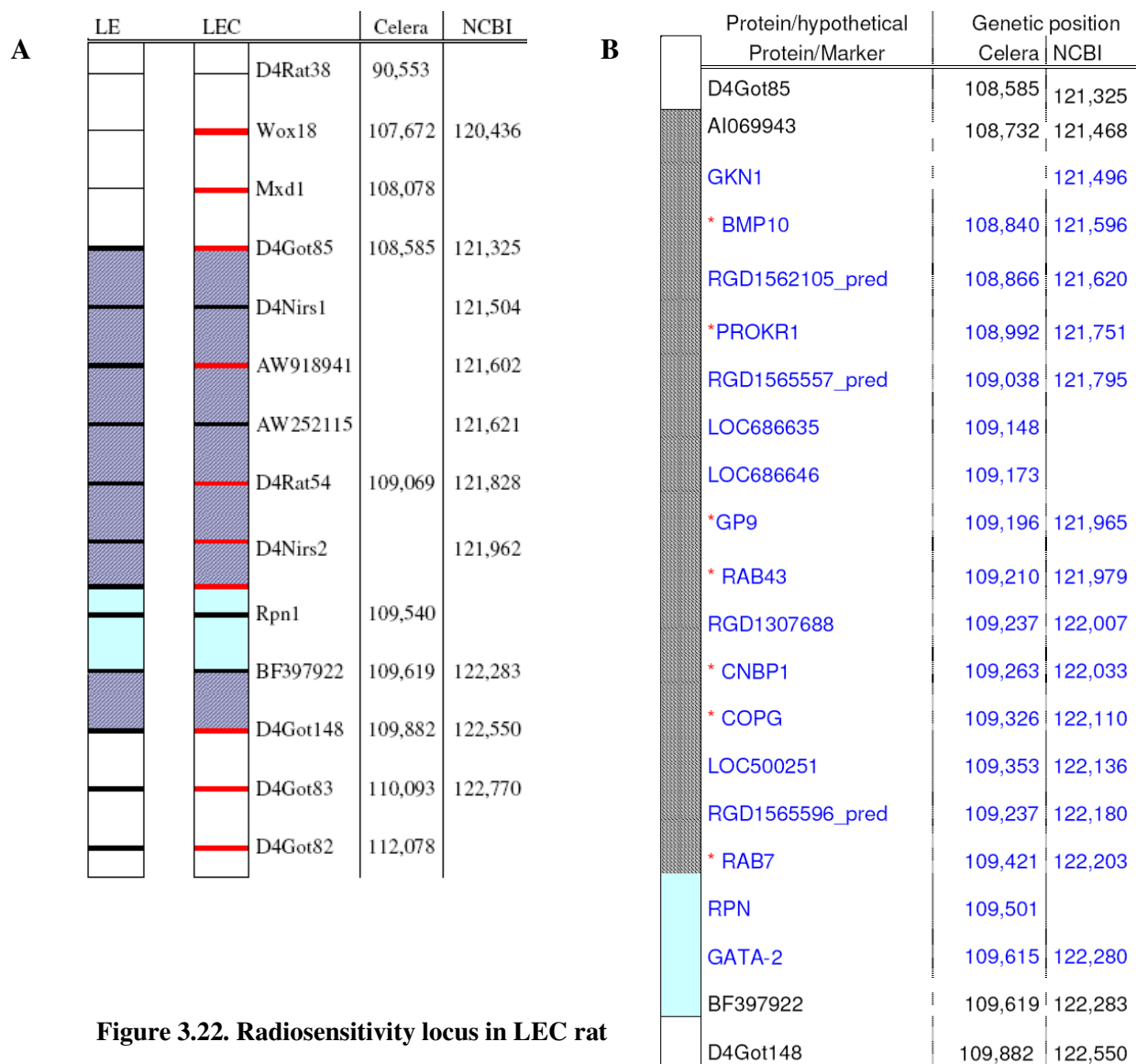


**Figure 3.22. Radiosensitivity locus in LEC rat**

**A:** Schematic representation of the LE versus LEC genotype for chosen SSLP/SNPs. Informative markers are indicated by the red ticks on the LEC scheme. Painted black ticks in LEC genotype indicate similar genotypes/haplotypes in LE as in LEC. The position of markers was derived from RGSC v3.4, released in 2004 by the Baylor College of Medicine Human Genome Sequencing Centre (BCM-HGSC) as part of the Rat Genome Sequencing Consortium (RGSC) (marker genetic positions according to NCBI/CELERA data). The titles of SNPs are written in blue colour. The hatched dark blue region between D4Got85 and BF397922 markers delineates the radiosensitivity locus [85]. Position of the BAC, partially complementing radiosensitivity in LEC rat [94] is shown as coloured light blue region.

**B:** The analysis of the locus of interest on chromosome 4, defined by AI069943 and BF397922 [85] genetic markers (hatched grey region). The position of the complementing BAC 65K18 is shown as light blue region. The known proteins and hypothetical proteins (written in blue), assigned to the region, are shown. Proteins, which coding sequences were analyzed by Tsuji *et al.*, 2005 [85], are marked by red astericks. The location (Mb) of genetic markers (written in black) and genes is shown according to the CELERA and NCBI databases (where available).

**Table 3.11. List of novel genes mapping to the radiosensitivity locus in LEC rat**

PROTEINS	KNOWN ORTHOLOGUES IN MOUSE/HUMAN	BIOLOGICAL PROCESS AND PUTATIVE FUNCTION	FUNCTIONAL DOMAINS
RGD1562105_predicted	Rho-GTPase-activating protein 25	- signal transduction - control of the actin and microtubule cytoskeleton	- Spectrin/pleckstrin-like - RhoGAP
RGD1565557_predicted	C2Orf13 (APLF)	- novel repair gene [139, 140] - interacts with XRCC1, XRCC4 and XRCC5 - activated by CK2	- FHA (forkhead-associated)
LOC686635	Hypothetical	unknown	- Calcium-binding EF-hand
LOC686646	Coiled Coil domain containing 48 (CCDC48)	unknown	- Coiled-coil
RIKEN cDNA 5830446M03 (RGD1307688)	homolog of pre-mRNA-splicing factor ISY1	- mRNA processing - splicing - cell cycle?	- Isy1-like splicing
LOC500251	C3Orf37	unknown	- DUF159
RGD1565596_predicted	histone H1X	- chromatine modification	- Histone H1/H5, histone H5 -Winged helix repressor DNA-binding
GATA-2	GATA binding protein 2	- transcriptional regulation	- Zn-finger

Table was created on the basis of UCSC and NCBI Rat Genome Browser, RGSC, v3.4, July 2006. It contains the novel loci identified in the region of interest on the chromosome 4 (see **Figure 3.23. APPENDIX**, page 154-155), the human/mouse orthologues genes, known function and functional domains as determined by <http://www.ebi.ac.uk/InterProScan/> analysis.

### 3.7.4 Analysis of the Gata-2 gene

The BAC clone 65K18, which according to the complementation analysis, performed by Tsuji *et al.*, 2006 [94] partially complements the cellular radiosensitivity phenotype in LEC, was further investigated and it was found to contain an open reading frame with high homology to human *Gata-2* (Gata binding factor 2), although authors Tsuji *et al.*, 2006 [94] only reported about the location of the *Rpn1* gene on the BAC.

GATA-2 (GATA binding protein 2) belongs to a number of Zn-finger transcription factors specifically binding the DNA sequence (A/T)GATA(A/G) in the regulatory regions of genes. Existence of numerous interaction partners of GATA-2, such as Fanconi anaemia zinc

finger, Testis zinc finger protein, promyelocytic leukaemia [141, 142], and the essential role of GATA-1 (belonging to the same family of transcription factors) in the induction of ERCC1 (NER) through the MAPK pathway [143] makes the *Gata-2* gene the promising candidate in the locus.

### **Bioinformatics analysis of *Gata-2***

*Gata-2* is highly conserved between species and (98.8% identity between rat and human GATA-2 proteins, and 98.1% identity between rat and mouse GATA-2) according to UniGene Database (Rn 34322, <http://www.ncbi.nlm.nih.gov/UniGene/clust.cgi?UGID=395875&TAXID=10116&SEARCH=gata2>).

The *Gata-2* gene has a complex genomic structure and context-dependent function and regulation as was shown in mouse and human [144-148]. **Figure 2.24.** shows enhancers, which have been identified and characterized in mouse and human (not all shown) [146]. The number of promoters are located upstream of the untranslated 1S and 1G exons respectively [149]. The 1S promoter of untranslated 1S exon in human (see **Figure 2.24.**) was shown to be active in the hematopoietic stem cell/progenitor fraction [148].

The described regulatory regions are known to be conserved between species [150, 151], and the according genomic regions regulatory in human and mouse have a high sequence similarity to that in rat. BLAST comparison of published enhancer sequences [146], revealed the presence of the enhancer regions (-3.9; -2.8; -1.8, position in kb from start of transcription of mouse *Gata-2*) in the upstream region of rat *Gata-2*, which are reflected in **Figure 2.24., A.,** lower panel. Additionally an active intronic enhancer, which was identified in mouse [145] in the intron between exons 3 and 4 (+9.5, see **Figure 2.24., A.,**) is conserved and present in many species, as shown by BLAST and UCSC conservation analysis (comparison of genomic sequences of rat, mouse, human, dog, opossum, chicken, and *X. tropicalis*). The genomic regions with high conservation between species are reflected as high regions in the histograms (**Figure 2.24, A., B.**). Pairwise alignments of each species to the rat genome are displayed below as a grayscale density plot that indicates alignment quality (The darker are the regions, the higher is the alignment quality).

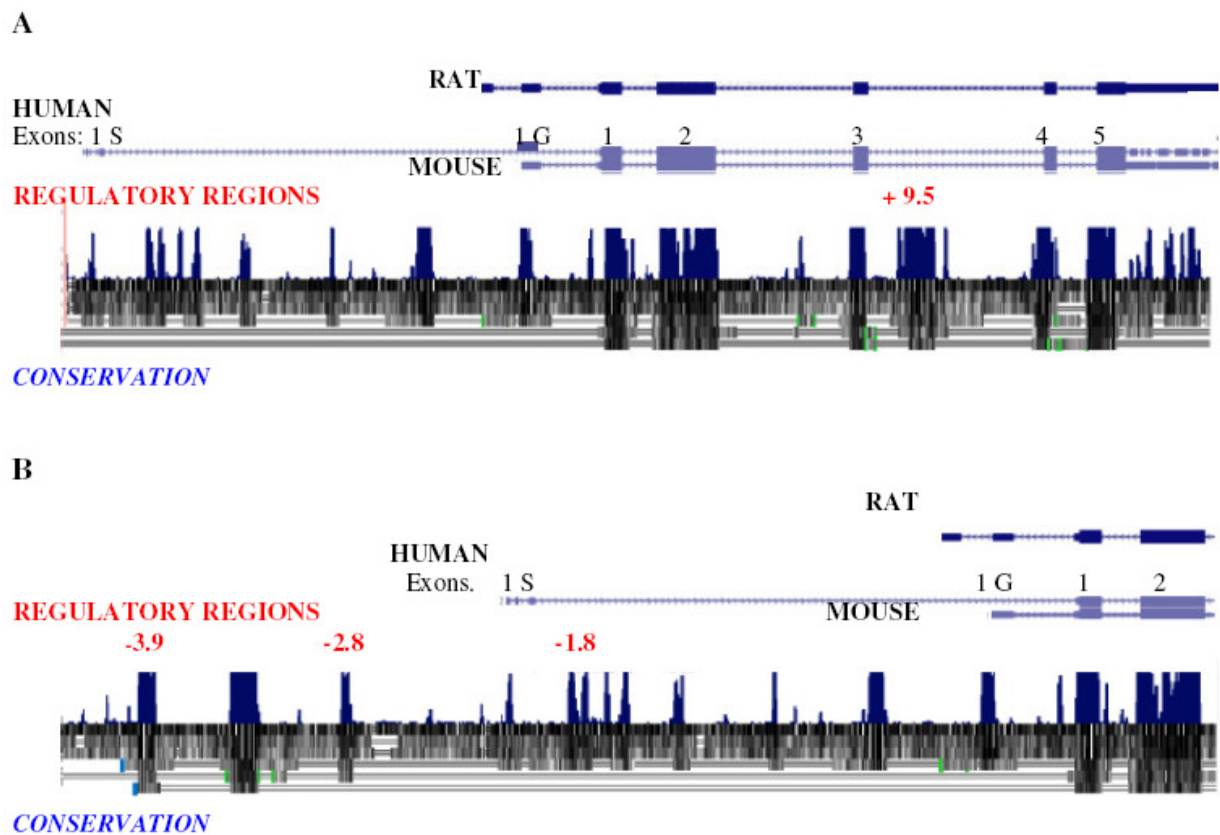


**Figure 3.24. Comparative Bioinformatics Analysis of *Gata-2* genomic structure (performed with UCSC Rat Genome Browser)**

The image contains a schematic overview of the rat *Gata-2* gene, 5' upstream region, and its known orthologous in human and mouse. The lower panels depict the conservation of genomic sequence between vertebrate species (mouse, human, dog, opossum, chicken, *X. tropicalis*)

**A:** The highly conserved parts of 5'UTR region contain enhancers. Number of them was characterized in human and mouse [145, 148].

**B:** The coding sequence of *Gata-2* gene consists of two untranslated exons and 5 protein coding exons. The comparison of homology between species shows high conservation of the promoters upstream 1S and 1G exons, the enhancer in the intron between 3<sup>rd</sup> and 4<sup>th</sup> exons, and of the protein coding region.

### Sequence analysis of *Gata-2*

Consider that *Gata-2* is one of the positional and function candidate gene, *Gata-2* coding sequence, sequence of respective exon-intron boundaries were analysed.

The published genotyping of LEC [94] included BF397922 (see **Introduction, 1.2.2, Figure 1.2.**). BF397922 is part of the EST starting in intron 2 (see **Figure 3.25.**) and includes exon 3. BF397922 was shown to limit the radiosensitivity locus in LEC [94], see **Figure 3.22.**). Considering this information, it is reasonable to assume that changes causing enhanced radiosensitivity in LEC happened in the region upstream of the BF397922 genetic marker, which includes untranslated exons and translated exons 1, 2, intronic sequences of *Gata-2* and excludes the downstream region of *Gata-2*, what means that further exons number 4 and 5 are excluded (see **Figure 3.25.**).

To compare LEC to LE the genotyping of the BF397922 was performed with primers listed in **Table 2.1, Materials 2.1.7.**

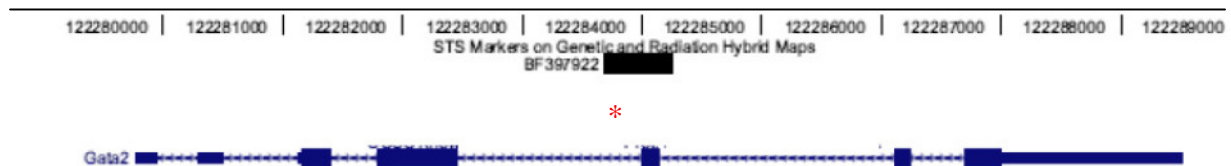


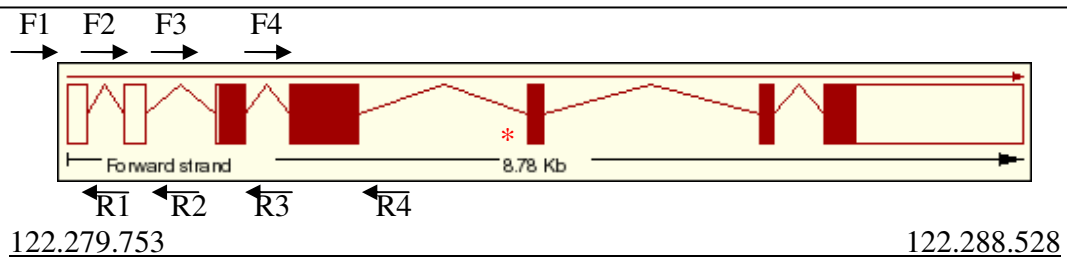
**Figure 3.25. Genomic position of BF397922. The investigated SNP is located in the intron (marked with \*).**

The results showed the similarity between LEC and LE in the genotype of BF397922, which is part of *Gata-2* gene. Both LEC and LE had a SNP (C), when in the database, WKY and SD (G).

Sequencing analysis of the coding sequence of the *Gata-2* gene was performed by M. Rosemann and no changes in LEC and LE comparing to the published predicted sequence were found (*personal communications with M. Rosemann*).

Further sequencing analysis included analysis of intron-exon boundaries. For this purpose the primers were designed in such way that sequences of at least 80 nucleotide of adjusted intron were included and analyzed (see **Figure 3.26.**). In such way analysis of the first two untranslated exons, exon 1, 2, 3 and 4 was performed.

The found changes was addition of G in the position of 26<sup>th</sup> nucleotide in the intron following after 1G exon (2<sup>nd</sup> untranslated exon) comparing to the sequence published in the NCBI Database. The genotype was present in LEC and LE, but was not observed in SD rat (see **Figure 3.27., APPENDIX, page 156.**)



Amplification fragments with size:

1	2	3	4	5
F1/R1	F2/R2	F3/R3	F4/R4	F5/R5
374	392	481	566	482

**Figure 3.26. Amplification of intron/exon boundaries of *Gata-2* gene**

The *Gata-2* gene can be found on the chromosome 4 at the location between 122.279.753-122.288.528 bps. The image contains the scheme of genomic DNA with introns and exons, shown as vertical lines of different thickness, depending on their size. Arrows show direction of primers used for the amplification of first 4 exons with intron boundaries (see **Table 2.2., Materials, 2.1.7**).

## Expression of *Gata-2* gene

Relative expression of *Gata-2* was evaluated in three independent experiments in LEC and LE fibroblasts. There was no significant difference observed in controls and at 4 and 24 hours after 5 Gy of IR (see **Figure 3.28., A**). The **Figure 3.28., B** reflects the pattern of *Gata-2* expression in irradiated cells, normalized to control values. Irradiation of cells caused slight increase (1.2 fold in LEC and 1.5 fold in LE cells), the observed difference was not significant. At 24 hours the expression of *Gata-2* had did not caused significant changes decrease of *Fancd2* expression at 4 hours and 24 hours in both LEC and LE cells. No reproducible difference was observed.

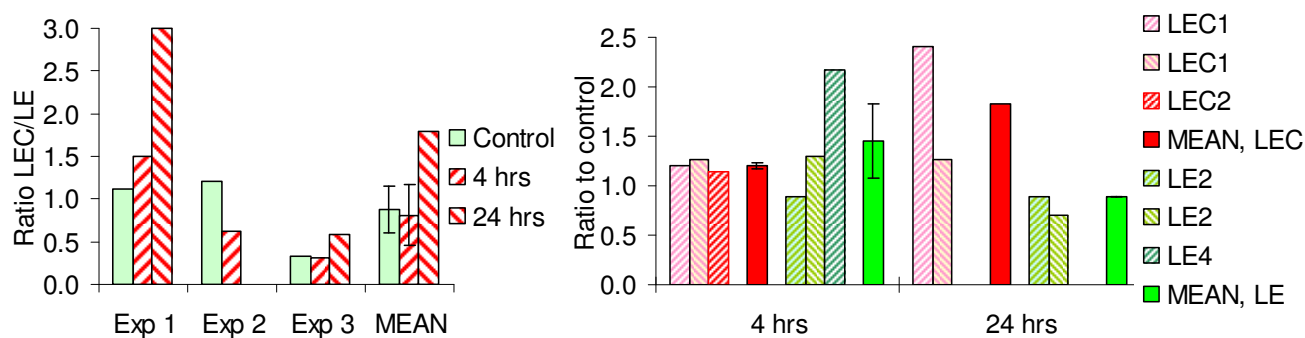


**Figure 3.28. Analysis of *Gata-2* expression with relative  $2^{-\Delta\Delta CT}$  method**

**A:** The expression of *Gata-2* was investigated in LEC fibroblasts *versus* LE at 4 and 24 hours after 5 Gy of IR and in controls (sham-irradiated). Expression of the target gene was normalized to that of LE by means of relative quantification -  $2^{-\Delta\Delta CT}$  method. *Pbgd* gene was used as a calibrator.

**B:** The changes in expression with time (4 and 24 hours after 5 Gy of IR) were investigated comparing to that of the control in LEC and LE fibroblasts respectively.

## IV. DISCUSSION

According to the data published by Hayashi *et al.*, 1992, 1993 [80, 81], the LEC rat is a rat strain that is more sensitive to total body irradiation rat than other rat strains (WKAH [80, 81], F344 [85]), and BN [83]). Published data [80, 81] show that the value of LD<sub>50/30</sub> of bone marrow death in the LEC rat was 3 Gy and that in the WKAH rat was 7 Gy, which is twice as high compared to that in LEC (dose modifying factor (DMF) is 2.38). The estimated LD<sub>50/7</sub> of intestinal death are 7.8 Gy in the LEC and 13.0 Gy in the WKAH [80, 81]. Observations by Hayashi *et al.*, 1993 [81] show that hematopoietic cells were largely recovered on 8<sup>th</sup> day after irradiation in the bone marrow of WKAH rats; in contrast, in LEC rats hematopoietic cells were not recovered and fibrous tissues increased instead.

LEC rats do not show any obvious phenotypic features characteristic of human cancer syndromes, such as premature aging, neurological phenotype, or increase in cancer incidence. Liver cancer is inherited independently from radiosensitivity and results from hepatitis, which LEC rat develop at 4-5 month of age [95] (it is caused by mutation in the *Atp7b* gene (a copper transporter)). The presence of increased radiosensitivity and absence of associated cancer phenotype [152] makes the LEC rodent model particularly valuable in the field of radiation protection, since the presence of radiosensitive individuals who do not develop cancers in an otherwise healthy population, was not studied. The only evidence to date, which might support the presence of radiosensitive, but otherwise healthy persons, are epidemiological studies of breast cancers in survivors of nuclear bombings in Japan. A 6-fold increase in excess relative risk per Sv for early onset cancer in women exposed below the age of 20 was found, which might reflect the presence of radiosensitive fraction among otherwise normal population [153].

## 4.1 Investigation of growth characteristics in LEC and LE fibroblasts

Primary fibroblasts are a common experimental model for phenotypes observed *in vivo*. Any germ-line defects in the LEC radiation response pathway would most probably operate in fibroblasts, since investigations of repair and radiosensitivity of a number of mice with disrupted genes involved in repair were performed in the fibroblasts and defects were identified and characterized [27, 28, 30, 33]

The increase in doubling time of the fibroblasts of the same cell line reflects the reduction of the growth potential of fibroblasts with passaging with approaching the crisis, observed normally in cultures of primary rodent/human fibroblasts [154-157]. The difference known between rodent and human cells is that rodent (mouse) cells have the capacity of spontaneous immortalisation after about 12 doublings in culture [154] and human fibroblasts go into senescence after some number of population doubling in culture not having the ability for such spontaneous transformation [155, 156].

Growing fibroblasts are part of a differentiating cell system composed of potentially mitotic progenitor fibroblasts and differentiated post-mitotic fibrocytes [158]. LEC and LE fibroblast cell lines had normal fibroblast culture characteristics described in the literature, such as a generation time of around 25-55 hours and the ability to be inhibited by cellular contact [157, 158], without significant difference in generation time ( $43.9 \pm 14.9$  hours for LEC and  $29.8 \pm 5.3$  hours for LE cell lines (**RESULTS 3.1, Table 3.1.**)).

There are examples showing that cell cultures derived from individuals with certain diseases, for example progeria [159] and Down syndrome [160], demonstrate increased doubling times (DT) as compared to the age-matched controls, and such observations were consistent with premature-aging phenotypes of the progeria and Down syndrome patients.

IR caused inhibition of growth in both LE and LEC fibroblasts as was measured at 23.5 hours and 54 hours after 5 Gy (see **APPENDIX, Figure 3.2.**, page 150, **RESULTS 3.1, Figure 3.3., Table 3.1.**). Data of cell cycle progression after 5 Gy of  $\gamma$ -irradiation confirm the observed growth inhibition, since the percentage of cells in S-phase decreases from 10-14% in unirradiated cells to

5-8% in irradiated cells and accumulate in the G1 phase of the cell cycle 88-85% in irradiated cells at 23.5 hours after 5 Gy of IR versus 81-73% in mock-irradiated (see **Figure 3.15.**).

Inhibition of DNA replication and cell division caused by damage induction is an important mechanism at the organism level against neoplastic transformation and cancer [161].  $\gamma$ -irradiated fibroblasts may be blocked in the G1-phase of the cell cycle by premature differentiation [15, 162, 163], by stress-induced premature senescence [164], or may undergo mitotic cell death [15]. The stress-induced premature senescence was shown [164] to be characterized by changes in morphology, positive staining for senescence-associated beta-galactosidase activity, accumulation of p53, p21, p16 and phosphorylation of p38 MAPK, although ATM activity was shown to be dispensable.

Normal human diploid fibroblasts do not show induction of the apoptotic death mode by IR (8 Gy), the same was shown for AT cells [165]. According to the work published by Rave-Fränk *et al.*, 2001 [15] in the fibroblast system *in vitro* radiosensitivity is determined not only by processes directly involved in DNA damage recognition and repair, but also by intracellular signalling cascades, which will lead to radiation-induced premature differentiation mostly mediated by TGF- $\beta$ 1. This is supported by observations of Debacq-Chainiaux *et al.*, 2005 [166], who showed an important role of TGF- $\beta$ 1 in UVB-induced premature senescence of human diploid fibroblasts. The authors [15] also show that in the studied group of fibroblasts the highest level of TGF- $\beta$ 1 was produced in radiosensitive cells and this correlated with an increase in radiation-induced excess of acentric fragments, which result mostly from unrepaired or misrepaired DSB.

## 4.2 Clonogenic assay

The first parameter evaluated from clonogenic survival experiments was plating efficiency (PE) of the different cell lines at 0, 1, 2, 3 and 4 Gy of IR. The PE of human tumour cells of various origins without irradiation may be close to 80-90%. However, the PE of normal human fibroblasts is usually very low (ranging from as low as 1 to 12-15%) [105]. Similar low values of plating efficiencies were determined in the present study and were slightly, but not significantly, lower in LEC ( $1.3 \pm 0.44\%$ ) compared to those of LE ( $1.5 \pm 0.35\%$ ). It is known

that fibroblasts from patients with genetic disorders are often not only more radiosensitive than normal fibroblasts, but also show reduced PE, as was observed by Fertil and Deschavanne, 1999 [167] for AT homo- and heterozygote fibroblasts, Cockayne syndrome, and retinoblastoma mutant fibroblasts.

The parameters used to describe survival curves ( $\alpha/\beta$ , SF2, D1) can all provide specific information about the mechanism of cell killing by IR, but have different limitations. Parameters  $\alpha$  and  $\beta$  characterize the fitting of survival curves to the linear-quadratic equation (see **RESULTS 3.2, Figure 3.5., Table 3.4.**). According to the linear-quadratic model, the biological meaning of  $\alpha$  and  $\beta$  values relate to the mechanism of cell killing.  $\alpha$ , the linear component of cell killing, results from cell death from 'one-hit' events and  $\beta$ - cell death from multiple hits. Increase in the  $\alpha$  component (0.39 in LEC as compared to 0.19 in LE) indicate the possibility of higher cell killing in LEC by the simple one hit event. The observed difference was only a statistical trend, since the t-test returned a borderline p-value of 0.058. The  $\beta$  parameter, characterizing cellular radiosensitivity in the higher dose range, did not differ between LEC and LE fibroblasts ( $0.14 \pm 0.04$  in LEC cells and  $0.16 \pm 0.04$  in LE cells), the t-test had a non-significant value of 0.72.

Often SF2 is preferred to other parameters to reflect intrinsic cellular radiosensitivity, because it was shown to be the best discriminator of cellular radiosensitivity in rodent tumour cell lines in culture and in addition represents the clinically relevant, low-dose portion of the radiation survival curve [168-171]. SF2 was significantly different between LEC and LE fibroblasts ( $0.25 \pm 0.02$  for LEC and  $0.34 \pm 0.03$  for LE (see **Table 3.3.**),  $n = 6$ , p-value of Student's t-test 0.018), therefore reflecting mildly enhanced intrinsic cellular radiosensitivity of LEC cells. Comparison of survival of LEC versus LE fibroblasts in the applied dose range with two-way ANOVA test showed significant difference in survival of fibroblasts between rat strains (p-value 0.019).

The studies published in the literature [171-173] about human fibroblasts show that their radiosensitivity is characterised by a broad variation. Dikomey *et al.*, 2000 [172], found that for normal human fibroblasts the SF2 was found to range from 15 to 36%. Zhou *et al.*, 1998 [173] have observed a different radiation sensitivity even between normal cell lines, which was correlated with the number of residual DSBs at 4 hours after irradiation.

The work of Kasten-Pisula *et al.*, 2005 [171], shows that SF2 of studied mutant cell lines (NHEJ, BER, HR, signal transduction) varied in the range between 0.013-0.49 in contrast to a variation of 0.15-0.53 for normal fibroblasts. For a dose of 2 Gy, SF2 varies from 0.14 to 0.53,

which corresponds to a coefficient of variation (CV) of 30% [122]. This variation was attributed to genetic differences. The examples of the most sensitive fibroblasts are  $ATM^{-/-}$  and  $LIG4^{-/-}$  primary fibroblasts, where SF2 was shown to be only 0.02 and 0.03 respectively. When compared to AT-fibroblasts with SF2 = 0.02, the normal fibroblast lines are much more radioresistant [12, 172].

The estimated values of SF2 of LEC and LE cells show that LE primary fibroblasts are in a normal range of radiosensitivity and LEC are slightly more radiosensitive, but not to such a degree as the highly radiosensitive  $Lig4^{-/-}$  or  $Atm^{-/-}$  fibroblasts. It is important to correlate the cellular phenotype and effect of a particular mutation on the whole animal. In the case of the  $Lig4^{-/-}$  knockout mice the fibroblasts are highly radiosensitive, but embryonic lethality of the knockout is 100%. In the case of LEC rat no significant increase in embryonic lethality was observed.

The values of DMF 2.36 for bone marrow death and 1.9 for intestinal death are derived from published data on the radiosensitivity of LEC rats in comparison to WKAH [80, 81]. They are higher than DMF of 1.3 of SF2 in primary LEC fibroblasts *versus* LE. The observed difference between in the degree of animal sensitivity and cellular sensitivity could be due to a defect in a pathway, which operates predominantly in stem cells of bone marrow and intestine, rather than in fibroblasts, or is active in the cell cycle phase different from G1 (S or G2). For example, it is known for the Fanconi Anemia (FA) syndrome, where patients show an extreme degree of radiosensitivity, that FA fibroblasts are only slightly more radiosensitive than wild type fibroblasts [129]. The difference in DMF observed between animal and cellular data could also be explained by different controls, since in animal experiments LEC was compared to WKAH and in the clonogenic assay of the present study to LE cells.

The growth curve data do not show an increase in radiosensitivity of LEC fibroblasts, as compared to LE cells. This might be explained by different approaches in these endpoints. Cell number counts for growth curves were done after 54 hours, whilst in the case of clonogenic survival colonies were harvested one or two weeks after irradiation. In addition, the dose of 5 Gy applied in growth curve measurements, causes cell killing of nearly 100% in clonogenic survival assay, where no colonies could be observed. This means that cells lose their ability to form colonies. The observations, which were done by Kalb *et al.*, 2004 [174], in FA-D2 mutants concerning reduced survival after UV-radiation exposure, were also not paralleled by the

corresponding cell growth data. Their explanation was that the 100-fold difference in plating density between clonogenic assay and survival assay, by some mechanism such as metabolic cooperation and/or a bystander effect, may have contributed to their discrepant results and/or minor degrees of sensitivity, which cannot be reliably separated from the background variation of cell culture assays [174]. This might also be the reason for experiments on growth curves LEC/LE fibroblasts failing to reflect the clonogenic sensitivity of LEC cells.

The higher sensitivity of LEC rat to IR suggests that damage induced in LEC may be less efficiently repaired or may be induced at a higher level, than that of the WKAH control rat [80, 81, 175]. Acute radiation syndromes develop due to the exhaustion of the stem cell compartment caused by DNA damage to such a degree that they fail to repopulate (see **Introduction, 1.2.2**). According to [32], defect in stem cells repopulation might result from defects in DSB repair. Diminished DNA DSB repair in the *Lig4Y288C* (hypomorphic) strain causes progressive loss of the hematopoietic stem cells and bone marrow cellularity during ageing, severely impairs stem cell function in tissue culture and transplantation, what elucidate the sensitivity of hematopoietic stem cells to NHEJ deficiency [32]. Similar proliferative exhaustion of stem cells has been reported for mice deficient in P21 and GFI-1 (Growth factor independence 1). These data [32] show that stem cells have a low threshold for damage checkpoint activation and exploit apoptosis or checkpoint arrest to limit the potential harmful impact of genetic damage.

The sensitivity of the LEC rat to whole body irradiation includes intestine syndrome and bone marrow death. This might be attributed to a defect in the stem cells repopulation in bone marrow/intestine of LEC rat. Known human cancer and immunodeficiency syndromes [11] include conditions with higher radiosensitivity resulting from variable molecular defects in DSB signalling and repair pathways (Rb, ATM, ATR, TP53, MRE11, PTCH, Ligase IV, BRCA1, BRCA2, etc), translesion synthesis (helicases RecQL4, WRN RecQ), nucleotide excision repair (XPD and XPB), which in addition to their role in repair function as part of transcription factor TFIIH [176] and mismatch repair (MLH1, MSH2, MSH6, PMS2) [11].

### **4.3 Induction of DNA damage**

The dose-response data did not reveal an enhanced sensitivity of LEC cells towards the induction of DSB under the applied experimental conditions of PFGE (**Figure 3.7., RESULTS 3.3**).

There was also no difference observed between LEC and LE fibroblasts in induction of SSB and ALS with 4 Gy of IR as shown by comet assays (see **Figure 3.12.-3.14., RESULTS 3.5**). It is known that, for example, FA fibroblasts have a higher DNA damage induction as revealed by comet assay, even not being very radiosensitive [129]. Increase in dose-response was also demonstrated for AT fibroblasts [129], which are in contrast to FA fibroblasts extremely radiosensitive. Investigations of damage induction in LEC/LE fibroblasts/lymphocytes failed to reveal any difference and clonogenic assay data do not show any pronounced radiation sensitivity of LEC cells.

### **4.4 Repair of DSB**

The molecular biology of repair processes have been studied extensively. In a number of instances, a dramatically radiosensitive mutant can result from a mutation in a single gene that functions as a repair or checkpoint gene.

Kinetics of DSB rejoining after 70 Gy of  $\gamma$ -irradiation was evaluated by the PFGE-FAR method, which does not allow estimation of how correctly they are repaired. The different capacities to rejoin DSB were shown to closely correlate with cell survival [177]. In terms of clonogenicity, 70 Gy is a huge dose that generates no surviving colonies in the studied cell lines, since only occasional colonies were observed after irradiation with much lower doses of 4-7 Gy. According to Foray *et al.*, 1999 [123] the number of DSB induced per cell is 39.1 / Gy. Applying the much higher dose of 70 Gy of  $\gamma$ -irradiation, would therefore induce around 2737 DSB per cell.

Repair of DSB, expressed in FAR, demonstrated slightly diminished efficiency in LEC cells compared to LE (see **Figure 3.8., RESULTS, 3.3**). Converting FAR values to Gy-equivalents using the induction (calibration) curves from each single experiment (see **Figure 3.9., RESULTS, 3.3**) removed the observed difference in FAR.

This methodology is known to have some limitations, especially when damage repair is mostly complete. According to Foray *et al.*, 1999 [123], underestimation of residual damage expressed as FAR is a problem when the amount of damage is small because of the threshold effect, since under the applied conditions, in the range of induction doses from 0 - 10 Gy, the number of DNA fragments, which are small enough to be able to migrate into the gel is very low. Investigating this problem, Foray *et al.*, 1999 [123], found an underestimation of damage in the range of 15%, which therefore significantly affected the evaluation of residual damage. There is also a possibility, which was not evaluated, that the same FAR values in induction curves and repair curves of mutant and controls may result from different distributions of fragments, when the less repaired, larger number of smaller fragments will give the same FAR as better repaired, smaller number of longer fragments.

#### **4.5 H2AX phosphorylation**

Evaluation of H2AX phosphorylation as a marker of repair and radiosensitivity in LEC cells was performed. Current theory, although still contradictory, suggests that  $\gamma$ H2AX is a marker of DSB induction, repair, and radiosensitivity [29].

According to [124],  $\gamma$ H2AX might be more important for processes occurring further away from the break that is required for efficient repair such as sister chromatid cohesion. Studies conducted in yeast reveal the possibility that the signal to trigger  $\gamma$ H2A loss might not be the completion of DSB repair, but rather the completion of a step that will normally lead to repair and loss of  $\gamma$ H2A occurs after synapse formation but before completion of repair [178].

Since it is known that the amount of residual damage determines cellular death, and the half-time of  $\gamma$ H2AX foci loss after IR treatment (2-3 hours post-treatment) is longer than that of DSB rejoining observed with PFGE (happens within the first 30 min) [179], the number of

residual  $\gamma$ H2AX foci was analyzed in confluent LEC and LE cells at later times at 9 and 24 hours after 1 Gy of  $\gamma$ -irradiation and in sham-irradiated controls. Basal  $\gamma$ -H2AX foci numbers did not differ between LEC and LE fibroblasts ( $0.93 \pm 0.26$  foci per cell for LEC and  $1.05 \pm 0.08$  for LE,  $n = 3$ ), but the number of foci per cell counted at 9 hours after 1 Gy of IR were consistently higher in LEC than in LE in every single experiment (see **Table 3.9., RESULTS 3.4**). The statistical evaluation of data (paired t-test) did not confirm the difference ( $4.25 \pm 1.4$  in LEC cells,  $2.04 \pm 0.26$  in LE cells) (see **Table 3.9.**), although a trend to higher foci counts in LEC cells was clearly observed. These results might confirm that LEC cells are radiosensitive and possibly have a subtle defect in DNA DSB repair.

#### **4.6 Comet assay**

The analysis of data obtained from comet assay (**Figure 3.12.-3.14., RESULTS 3.5**) allows to conclude that no significant defect in SSB/ALS repair is present in LEC comparing to that of LE, since the statistical analysis of means, medians and 75<sup>th</sup> percentiles (see **Figure 3.13.**) did not show any significant difference at the measured repair times after 4 Gy of IR, although the mean values of 75<sup>th</sup> percentiles were slightly higher in LEC and the difference was especially pronounced at 15 min after irradiation (see **Figure 3.13.**).

#### **4.7 Regulation of cell cycle progression**

Eukaryotic cells respond to DNA damage induced by IR by arresting cell cycle progression and coordinating it with DNA repair, chromatin remodelling, transcriptional programs and other metabolic adjustments or cell death, to ensure survival and propagation of accurate copies of the genome in subsequent divisions [31]. Failures in cell cycle checkpoints can lead to the acquisition and accumulation of genetic alterations and karyotype abnormalities.

These changes may result in the activation of oncogenes and/or the inactivation of tumour suppressor genes and ultimately result in tumourigenesis.

Depletion of S-phase cells was observed in both LEC and LE cells at 6.5 hours after 5 Gy of IR (**Figure 3.15., A**). Activation of the S-phase checkpoint causes inhibition of initiation of new replicons and slowing down DNA replication leading to a delay in cell cycle progression. It is mediated by the Cdc25A-degradation pathway and ATM-mediated phosphorylation of NBS1 and SMC1 proteins. A defective intra-S-phase checkpoint was also reported for cells lacking functional BRCA1, 53BP1, FANCD2 [31].

G2 arrest was induced with a dose of 5 Gy in LEC and LE cells and caused delay of cell cycle progression and accumulation of cells in the G2 phase at 6.5 hours. The number of cells in G2 increased from 15% to 24% in LEC cells and from 19% to 28% in LE cells (see **Figure 3.15., C**). The G2 checkpoint (also known as the G2/M checkpoint) prevents cells from initiating mitosis when they acquire DNA damage during G2 or if they progress into G2 with some unrepaired damage inflicted in the previous S phase or even G1 phase, what helps to avoid the segregation of damaged chromosomes. At 24 hours, the G2 checkpoint was resolved in both LEC and LE cells, and G2 cells progressed further to the G1 phase of the cell cycle, since the number of G2 cells fell to 8 - 12% and the number of G1 cells increased from 63 - 71% at 6.5 hours to 88-85% at 24 hours. The G2 checkpoint is mediated by ATM/ATR-and Chk1/Chk2 pathways, which require transcriptional targets of p53, including the p21, GADD45 and 14-3-3 $\theta$  proteins, and additional mechanisms, such as p53 independent BRCA1-stimulated expression of p21 and GADD45 [31, 180].

G1 arrest was activated both in LEC and LE cells by 5 Gy of IR. Accumulation of cells at G1 phase was especially evident 24 hours after irradiation (see **Figure 3.15., A**) and was prolonged into later time points measured. G1 arrest is also activated by ATM/ATR and Chk1/Chk2 pathway, which has two effectors, the Cdc25A phosphatase and the p53 transcription factor [31].

#### **4.8 Discrepancy in observations of the cellular radiation sensitivity phenotype and cell cycle progression of LEC cells**

The radiation sensitivity, as determined by the clonogenic assay, was expressed much less in primary LEC fibroblasts, compared to the data presented by [82]. The conducted study of DSB repair by PFGE (see **RESULTS, 3.3**) did not confirm the observations of Hayashi *et al.*, 1994 [82], where a large deficiency in DSB repair was seen in LEC fibroblasts, although the applied dose was the same (70 Gy) and FAR analysis was performed. The reason for such discrepancies in the results may be a different experimental system. The authors performed their repair experiments in SV40-transformed fibroblasts, without considering the cell cycle distribution of the studied cells and without calibrating the data by induction curves. The standardization of the initial cell cycle distribution and performing experiments in primary non-transformed fibroblasts led to different conclusions. It is known that SV40 transformation changes many cellular functional characteristics. Studies of Wachsberger *et al.*, 1999 [181], showed that immortalisation with SV40 (T antigen) leads to failure of G1 cell cycle arrest in infected cells due to its perturbation of the retinoblastoma and p53 tumour suppressor proteins. Indeed, exactly this phenomena was observed by Hayashi *et al.*, 1998 [182], who showed an absence of G1 arrest and higher accumulation of irradiated SV-transformed LEC fibroblasts in G2/M. These observations were also not confirmed by experiments performed in the present study in primary non-transformed fibroblasts (see **Figure 3.15., A-C**). Additional experiments were conducted later by Masuda, K. *et al.*, 2006 [183], in primary fibroblasts and showed normal cell cycle progression in studied primary LEC fibroblasts.

#### **4.9 Repair capacity and radiosensitivity in LEC**

The radiosensitivity in cancer patients is not always confirmed by radiosensitivity tests. For example, the study of El-Awady *et al.*, 2005 [175], failed to establish the correlation between

radiosensitivity of breast cancer patients *in vivo* and the performed *in vitro* clonogenic survival and capacity of DSB repair. The study of Budach *et al.*, 1998 [184], also did not reveal significant correlation between fibroblast radiosensitivity and acute radiation side effects.

In the LEC rat, the high radiation sensitivity to total body irradiation was observed, although the studies of cellular phenotype have shown only marginal difference considering the values of DMF. Neither PFGE, nor analysis of  $\gamma$ H2AX foci in G1 fibroblasts or G0 lymphocytes in comet assays revealed a clear repair deficiency phenotype, although the possibility that they carry a subtle defect, which is difficult to distinguish from background variation due to the methodology in the applied assays cannot be excluded.

According to the work of Kasten-Pisula *et al.*, 2005 [171], big differences in cellular radiosensitivity are caused by very small variations in DSB repair capacity. The authors [171] show, that SF2 of mutant cell lines deficient for components of NHEJ, BER, HR, signal transduction was in the range of 0.013-0.49 in contrast to a range of values between 0.15-0.53 for normal fibroblasts. The studied cells had no difference in the number of initial DSB and very small variation in the number of DSB remaining 24 h after irradiation, which correlated with the cellular sensitivity measured as SF2. After 100 Gy it was 2-5 Gy-equivalents for normal fibroblasts and 3-7 Gy-equivalents for mutated cell lines, corresponding to repair capacities of 95-98% in controls and 93-97% in mutants [171]. The values of Gy-equivalents estimated in LEC cells at 6 hours after irradiation with 70 Gy were  $8.5 \pm 1.8$  (n = 3) versus  $6.3 \pm 1.6$  (n = 3) in LE cells.

There are examples of radiosensitivity in cancer patients, where *in vitro* studies, failed to reveal a phenotype. Fibroblasts, established from highly radiosensitive FA patients, do not show a radiosensitivity phenotype, although comet assay reveals a higher dose dependent damage and slower repair [129]. Other examples of non radiosensitive repair mutants are *Rad52* and *Rad54* knock-out mice. *Rad52* and *Rad54* genes are involved in homologous repair, but show almost no radiosensitivity phenotype and no DSB repair deficiency, but misrepair of DSB, as detected with the I-SceI nuclease based assay [27]. There is also an example of an AT mutation, where extreme radiosensitivity is known, but reports about a repair defect are contradicting each other, although the data of Foray *et al.*, 1997 [185], show that A-T cells have a higher residual damage at 24 hours after doses of 5-40 Gy due to defective repair of a small fraction of DSB in A-T cells [185].

It is also possible, that such a radiosensitivity phenotype results from a hypomorphic mutation, which does not inactivate completely the function of the affected gene, but diminishes it. There are examples, described in the literature, that even SNPs, which are causing single amino acid substitution variants [186] in ATM, p53, p21, XRCC1, XRCC3, and TGF $\beta$ 1 lead to increased radiation sensitivity in human fibroblasts. An increase in radiosensitivity was also described in patients carrying SNPs (one silent, another missense) in a gene involved in DNA DSB repair and sister chromatid cohesion – hHR23A [187]. Another example was described by [188], where a SNP in a splice acceptor site of exon 4 of XPC led to a decrease of its information content and an increase of mRNA with skipped exon 4. The abnormally spliced XPC mRNA isoform had diminished DNA repair function and possibly caused cancer susceptibility.

Considering the small extend of radiosensitivity of LEC fibroblasts and lack of developmental defects/tumourigenesis it may be concluded that the NHEJ repair pathway is not affected in the LEC rat, since described NHEJ mutants show pronounced radiosensitivity (7 fold) and repair defects [28].

DNA repair experiments, conducted on G1 cells cannot evaluate efficiency of another pathway of DSB repair – HR, which operates mostly in S/G2 phase of the cell cycle. HR is considered to either act on a small fraction of IR induced DSB or to engage in the repair processes at a step after the initial end joining [189]. HR deficient cells show mild radiosensitivity (1.7 fold) and a very small or no DSB repair defect, but a high rate of chromosomal aberration. Direct measurements of DSB HR repair using I-SceI nuclease based assays revealed that deficiencies in the HR proteins XRCC2 and XRCC3 produce severe ( $\approx$  25-fold) reductions in HR repair and sensitivity to cross-linking agents, which also was not tested in LEC cells [62]. Loss of FA gene function has been associated with mild ( $\approx$ 3.5-fold) reductions in the efficiency of HR repair [62].

Cell killing is suggested to result from non- and misrepaired DSB leading to chromosomal damage such as terminal or interstitial deletions as well as dicentrics [185]. It was found that in normal human fibroblasts irradiated in the G0 phase of the cell cycle  $\approx$  25% of all initially induced breaks undergo mis-rejoining [190]. Investigation of DSB repair in LEC cells with the applied FAR-PFGE technique allowed to measure repair versus non-repair, but not misrepair. Evaluation of misrepair of DSB is possible with, for example, I-SceI nuclease assay or counting chromosomal aberrations.

Considering the sensitivity of LEC rats to DNA damaging agents, other than IR, it is only known that higher levels of chromosomal aberrations induced by BNU and MMS are observed in bone marrow of LEC and LEA rats than that of Wistar or SD rats [102]. Repair of damage, which is induced by these alkylating agents, involves BER and HR [191]. It is possible to hypothesize, that this common between LEC and LEA rat strains lesion might be caused by the same defect, which makes these rats also radiosensitive. Investigations of DNA repair on the cellular level should also include the evaluation of cross-sensitivity to other damaging agents, such as alkylating and cross-linking agents.

#### **4.10 Analysis of candidate genes**

##### **Excluding of Rad18, v-raf-1, XPC, and Fancd2 as candidate genes**

The genetic analysis of *Rad18*, *v-raf-1*, *XPC*, and *Fancd2* genes led firstly to the establishment of *Fancd2* as the main candidate, since the *Fancd2* gene carried two mutations in the coding sequence, at nucleotide 955, A→G which caused substitution of Isoleucine by valine, and at nucleotide 1645, G→A, with substitution of glycine by arginine. The observed mutations were present in the LE rat too. In FA cells, the accumulation of cells in the G2/M phase of the cell cycle was observed after MMC treatment. Deficient DNA end joining activity in extracts from FA fibroblasts has also been reported [138]. This knowledge of the function of *Fancd2* in DSB repair made *Fancd2* the best candidate for the LEC phenotype. However, the number of other rat strains were additionally genotyped for the observed mutations (see **Table 3.10., RESULTS 3.7**) and the same mutations were observed in F344 and Copper rat strains. Neither F344 or Copper rats were shown to be radiosensitive and the conclusion was done that the observed changes are common polymorphisms. The analysis of *Fancd2* expression with Real-time PCR has shown the same level and pattern of irradiation-induced changes in its expression between LEC and LE cells. The observed suppression of *Fancd2* expression at later times was also shown by Zhou *et al.*, 2006 [192].

## **GATA binding protein 2**

The gene coding for the GATA binding protein 2 might be considered as the main candidate due to its location in the 65K18 clone, which was shown by Tsuji *et al.*, 2006 [94] to partially complement the radiosensitivity phenotype in LEC cells.

The family of GATA binding proteins include six known members with a common DNA-binding domain that is highly conserved among vertebrate species. *Gata-1* expression is restricted to haematopoietic lineage, *Gata-2* expression is less restricted, with expression in haematopoietic, endothelial, and neuronal cells [193].

Although there are no evidences exist so far, which would show the role of GATA-2 in radiation response, hypothesizing about possible function of GATA-2 in radiation-induced changes in gene expression might explain differential regulation of large number of genes in LEC *versus* Fisher [85] in unirradiated and irradiated conditions. The role of GATA-2 in hemopoietic stem cells (HSC) development [149] also points o to the possibility that not-yet identified mutations in regulatory sequences might cause defects in its function in repopulation of HSCs. Although sequencing of the coding sequence did not reveal any mutations, changes in introns of the 5'UTR might affect tissue specific splicing or transcriptional regulation of this gene. There was no significant impairment of *Gata-2* expression observed in fibroblasts, but the possibility that situation is different in targeted cells (haematopoietic cells) cannot be excluded. According to the work of [194, 195] the changes in nonconding sequences may cause pathological conditions. One recently described example is the loss of 1-2 T in the poly(T) element in the intron, which causes significant missplicing of *Smad5*, leading mutant mice being unable to rapidly respond to acute anemia [194].

## **Characterisation of other candidate genes identified on the locus**

The locus of chromosome 4 (see **Figure 3.23.**, APPENDIX, page 154-155, **Figure 3.22**, **RESULTS**, 3.7.) was investigated further for novel genes. Several hypothetical genes were identified, some of them are coding for proteins functioning in DNA repair and cell cycle (see **Table 3.12.**, **RESULTS**, 3.7).

The product of the newly described gene *Aplf (C2Orf13)* was shown recently by Ilies *et al.*, 2007 [140], and Bekker-Jensen *et al.*, 2007 [139] to be a novel member of the FHA domain

family of proteins, interacting with XRCC1 *in vivo* and *in vitro* in a manner that is stimulated by CK2. The authors [147] also show interaction of APLF with the DSB repair proteins XRCC4 and XRCC5 (Ku86), phosphorylation of APLF in a DNA damage and ATM-dependent manner, and that depletion of APLF reduces the rate of chromosomal DNA strand break repair following IR [140].

There is evidence in the literature [196], which shows that another candidate, histone H1, plays a role in DNA NHEJ. It was proposed that DNA-PK may act as a linker histone kinase by phosphorylating linker histones in the vicinity of a DNA break and coupling localized histone H1 release from DNA ends with the recruitment of ligase IV/XRCC4 to carry out double-stranded ligation.

Affected function of Rho-GTPase activating protein 25 might also cause the radiosensitivity phenotype, considering the data [37] published about the *Cdc42GAP* knockout primary MEFs, which show radiosensitivity with SF2 of 30% for mutant and 70% for wild type cells (see **Introduction 1.10**). They have reduced survival as determined by survival assays after treatment with alkylating agent MMS, mitomycin C (MMC), H<sub>2</sub>O<sub>2</sub>, increased genomic abnormalities, induction of multiple cell cycle inhibitors, and premature senescence [37].

The other possible candidates, which function was not described yet, are LOC686646, Pre-mRNA-splicing factor ISY1, LOC686635 and LOC500251. Hypothetical protein LOC686646 has a known human ortholog, which is called coiled-coil domain containing 48 (CCDC48). Its function is not defined yet, but it is known that in animals and yeast, the coiled-coil motif has been identified in a variety of proteins associated with the cytoskeleton, the golgi, centromeres, centrosomes, the nuclear matrix, and chromatin. (URL: <http://www.coiled-coil.org/>). The function of Pre-mRNA-splicing factor ISY1 in *Saccharomyces cerevisiae* is related to pre-mRNA splicing [197]. Performed InterProScan analysis showed the presence of a calcium-binding EF-hand domain in the hypothetical protein LOC686635. This protein has no characterized orthologs with known function in human or mouse. Hypothetical protein LOC500251 is a homologous to Homo Sapiens C3Orf37 on chromosome 3. It codes for an uncharacterized, yet highly conserved protein with unknown function.

## FINAL SUMMARY AND CONCLUSIONS

The increased sensitivity of the LEC rat strain to total body irradiation, characterised by the bone marrow and intestinal acute radiation syndromes [80, 81], and the absence of any phenotypic features of known radiosensitivity syndromes or DNA repair deficiencies (premature aging, neurological phenotype, cancer) make LEC rat a very valuable model for the field of radiation protection and radiobiology.

- To understand the molecular basis for the increased radiation sensitivity a series of studies were performed.
- The cellular radiation sensitivity and repair of G1 phase LEC fibroblasts was studied by applying assays such as clonogenic survival, PFGE, and  $\gamma$ H2AX foci. DNA repair was also studied in quiescent LEC lymphocytes of peripheral blood by means of alkaline comet assay.
- Fibroblasts of LEC rats were slightly more radiosensitive than those of the parental LE strain in the clonogenic survival assay. Although the statistically significant difference was observed for SF at 2 and 3 Gy, no significant difference in the  $\alpha$  and  $\beta$  parameters could be detected. Dose modifying factor at 2 Gy (DMF2) (1.32) and DMF3 (1.58), both characterizing radiation sensitivity in the clonogenic assay, were lower in LEC fibroblasts compared to LEC animals themselves (DMF of 2.36 of bone marrow syndrome and 1.95 of intestinal death [80, 81]). This difference might be explained by the use of different control (WKAH in animal experiments and LE in performed *in vitro* clonogenic survival).
- A connection between impaired DNA repair capacity in non-dividing cells (G1/G0) and radiation sensitivity in LEC rats could not be established by the alkaline comet assay. The PFGE investigations of DSB repair did not reveal a significant defect in G1-accumulated fibroblasts applying conversion of FAR data into Gy equivalents, although the tendency toward slower DSB repair deficiency existed in LEC cells compared to LE. Failure to detect large differences might be caused by methodological limitations of FAR analysis in PFGE

(low sensitivity of detection of small values of DNA degradation). The possibility exists that affected pathway might operate in other phases of cell cycle (S, G2/M), and/or the difference was not significant enough to be distinguished from background with the available methods.

- The induction of damage (dose-response) was investigated by means of PFGE in fibroblasts (G1) and comet assay in lymphocytes (G0) and did not show any differences in initial damage between LEC and LE.

- It is known that the NHEJ pathway of DSB repair is operating mostly in the G1/G0 phase of the cell cycle and mutants in this pathway have a high radiosensitivity and pronounced DSB repair deficiency. The lack of profound changes excludes large defects in NHEJ, although the possibility of a mild phenotype caused by a hypomorphic mutation still exists, but may not explain the *in vivo* sensitivity. The HR pathway operates in the S/G2/M phases of the cell cycle. Mutations in its components are often lethal in animal models, although cells are not very sensitive to IR at G0/G1, without significant defect in quantity of DSB repair, but have pronounced misrepair of DSB. Mutations in HR components cause high sensitivity to alkylating agents, as well as defects in NER. The published observation of an increase in chromosomal aberrations induced by MMS and BNU alkylating agents in bone marrow of LEC rat [102] *versus* Fisher/SD rat might indicate such a defect.

- Cell cycle progression without and after IR did not differ between LEC and LE fibroblasts and exponentially growing heterogeneous fibroblast population had G1 arrest, S phase depletion, and transient G2 arrest induced by irradiation with 5 Gy. This indicates that no mutation in genes controlling cell cycle regulation is present in LEC rats.

- The results of PFGE, clonogenic, and cell cycle analysis assays do not confirm earlier reports of a defect in LEC fibroblasts, which was described by Hayashi *et al.*, 1994 [82], and Hayashi *et al.*, 1998 [182]. In these earlier studies SV40 transformation was used, which may explain the high radiosensitivity, pronounced cell cycle changes, and high DSB repair deficiency in these fibroblasts [183]. In performed experiments the more biologically relevant experimental system was studied - primary non-transformed fibroblasts, additionally the standardisation of cell cycle conditions, which is known to be particularly important for

reliability of data from clonogenic survival and PFGE, was performed. This led to a different conclusion about cellular radiosensitivity, cell cycle arrest induction and DSB repair in LEC cells [82], [182].

- The genotype of LEC and LE rats at the locus of interest was different for a number of microsatellite markers and SNPs analysed, suggesting the mutation arose at the time of separation of LEC and LE strains. The analysis of candidate genes excluded *Rad18*, *v-raf-1*, *XPC* and *Fancd2* candidate genes from being responsible for the LEC radiosensitivity phenotype.
- Further analysis of genes on the locus established GATA binding protein 2 as one of the main candidates. The expression of the GATA binding protein 2 was not significantly different between LEC and LE in either control or irradiated cells. No mutations were identified in the protein-coding region of the gene.
- The ORF with high homology to human genes: *Ap1f*, H1X histone, and Rho-GTPase activating protein 25 were found on the locus of interest too together with several other genes, which function has not been described yet. For further characterisation of LEC rat it is necessary to perform a more detailed genetic analysis of the candidate genes, which includes sequencing of exons, splice sites, introns, and 5'/3' UTR regions, which are highly conserved between species (potential regulatory regions) and expression analysis.
- Further investigations on the cellular level might include (depending on the results of the mutational analysis of candidate genes) estimation of cross-sensitivity of LEC fibroblasts to other types of damage, different from induced by IR, like alkylating and cross-linking agents, investigation of DSB misrepair and sensitivity in G2/M stages of the cell cycle, and comparison to that of LE cells.

## REFERENCES

1. Nenot, J. C., *Overview of the Radiological Accidents in the World, Updated December 1989*. International Journal of Radiation Biology, 1990. **57**(6): p. 1073-85.
2. IAEA, *Radiation, People and Environment* J. Ford, Editor. 2004.
3. Hall, E. J., *Radiobiology for the Radiologist*. 5 ed. 2000, Philadelphia: Lippincott Williams & Wilkins. 608.
4. Dizdaroglu, M., Karakaya, A., *Mechanisms of oxidative damage: lesions and repair*. 1999, New York: Kluwer Academic Publishers/plenum Press. 67-87.
5. Evans, M. D., Dizdaroglu, M., and Cooke, M., S., *Oxidative damage and disease: induction, repair and significance*. Mutation Research, 2004. **567**(1): p. 1-61.
6. Lindahl, T., *Instability and decay of the primary structure of DNA*. Nature, 1993. **362**: p. 709-15.
7. Cline, S. D., and Hanawalt, P. C., *Who's on first in the cellular response to DNA damage?* Nature Reviews Molecular Cell Biology 2003. **4**(5): p. 361-72.
8. Slupphaug, G., Kavli, B., and Krokan, H. E., *The interacting pathways for prevention and repair of oxidative DNA damage*. Mutation Research, 2003. **531**: p. 231-51.
9. Tounekti, O., Kenani, A., Foray, N., Orłowski, S., and Mir, L. M., *The ratio of single- to double-strand DNA breaks and their absolute values determine cell death pathway*. British Journal of Cancer 2001. **84**(19): p. 1272-9.
10. Ward, J. F., *The yield of DNA double-strand breaks produced intracellularly by ionizing radiation: a review*. International Journal of Radiation Biology, 1990. **57**(6): p. 1141-50.
11. Bourguignon, M. H., Gisone, P. A., Perez, M. R., Michelin, S., Dubner, D., Di, G. M., and Carosella, E. D., *Genetic and epigenetic features in radiation sensitivity. Part II: implications for clinical practice and radiation protection*. European Journal of Nuclear Medicine and Molecular Imaging, 2005. **32**(3): p. 351-68.
12. Dikomey, E., Dahm-Daphi, J., Brammer, I., Martensen, R., and Kaina, B., *Correlation between cellular radiosensitivity and non-repaired double-strand breaks studied in nine mammalian cell lines*. International Journal of Radiation Biology, 1998. **73**(3): p. 269-78.
13. Obe, G., Pfeiffer, P., Savage, J. R., Johannes, C., Goedecke, W., Jeppesen, P., Natarajan, A. T., Martinez-Lopez, W., Folle, G. A., and Drets, M. E., *Chromosomal aberrations: formation, identification and distribution*. Mutation Research, 2002. **504**(1-2): p. 17-36.
14. Bedford, J. S., Mitchell, J. B., Griggs, H. G., and Bender, M. A., *Radiation induced cellular reproductive death and chromosome aberrations*. Radiation Research, 1978. **76**(3): p. 573-86.
15. Rave-Fränk, M., Virsik-Köpp, P., Pradier, O., Nitsche, M., Grünefeld, S., and Schmidberger, H., *In vitro response of human dermal fibroblasts to X-irradiation: relationship between radiation-induced clonogenic cell death, chromosome aberrations and markers of proliferative senescence or differentiation*. International Journal of Radiation Biology, 2001. **77**(12): p. 1163 - 74.
16. Schär, P., *Spontaneous DNA damage, genome instability, and cancer - when DNA replication escapes control*. Cell, 2001. **104**(3): p. 329-32.
17. Kaplan, M. I., Limoli, C. L., and Morgan, W. F., *Perpetuating radiation-induced chromosomal instability*. Radiation Oncology Investigations, 1997. **5**(3): p. 124-8.

18. Sinclair, W. K., *X-ray induced heritable damage and small colony formation in cultured mammalian cells*. Radiation Research, 1964. **21**: p. 584-611.
19. Little, J. B., Nagasawa, H., Pfenning, T., and Vertrous, H., *Radiation-induced genomic instability: delayed mutagenic and cytogenic effects of X-rays and alpha-particles*. Radiation Research, 1997. **148** (4): p. 229-307.
20. Gorgojo, L., and Little, J. B., *Expression of the lethal mutations in the progeny of the irradiated cells*. International Journal of Radiation Biology, 1989. **55**(4): p. 619-30.
21. Seymour, C. B., Mothersill, C., and Alper, T., *High yields of lethal mutations in somatic mammalian cells that survive ionizing radiation*. International Journal of Radiation Biology and related studies in Physics, Chemistry and Medicine 1989. **50**(1): p. 167-79.
22. Hei, T. K., *Cyclooxygenase-2 as a signaling molecule in radiation-induced bystander effect*. Molecular Carcinogenesis, 2006. **45**(6): p. 455-60.
23. Burnet, N. G., Nyman, J., Turesson, I., Wurm, R., Yarnold, J. R., and Peacock, J. H., *The relationship between cellular radiation sensitivity and tissue response may provide the basis for individualising radiotherapy schedules*. Radiotherapy and Oncology, 1995. **36**(3): p. 1995.
24. Joubert, A., Zimmerman, K. M., Bencokova, Z., Gastaldo, J., Chavaudra, N., Favaudon, V., Arlett, C. F., and Foray, N., *DNA double-strand break repair defects in syndromes associated with acute radiation response: At least two different assays to predict intrinsic radiosensitivity?* International Journal of Radiation Biology, 2008. **84**(2): p. 107-25.
25. Turesson, I., Nyman, J., Holmberg, E., Oden A., *A prognostic factors for acute and late skin reactions in radiotherapy patients*. International Journal Radiation Oncology Biology Physics 1996. **36**: p. 1065-75.
26. Johansen, J., Bentzen, S.M., Overgaard, J., Overgaard, M., *Evidence for a positive correlation between in vitro radiosensitivity of normal human skin fibroblasts and the occurrence of subcutaneous fibrosis after radiotherapy*. International Journal of Radiational Biology, 1994. **66**(4): p. 407-12.
27. Smith, J., Smith, K., and Mezard, C., *Tying up Loose Ends: Generation and Repair of DNA Double-Strand Breaks*. Atlas Genet Cytogenet Oncology Haematology, 2001.
28. Rothkamm, K., Kruger, I., Thompson, L. H., and Lobrich, M., *Pathways of DNA Double-Strand Break Repair during the Mammalian Cell Cycle*. Molecular Cellular Biology, 2003. **23**(16): p. 5706-15.
29. Rothkamm, K., and Löbrich, M., *Evidence for a lack of DNA double-strand break repair in human cells exposed to very low x-ray doses*. Proceedings of the National Academy of Science U.S.A., 2003. **100**(9): p. 5057-62.
30. Kawabata, M., Kawabata, T., and Nishibori, M., *Role of recA/RAD51 family proteins in mammals*. Acta medica Okayama, 2005. **59**(1): p. 1-9.
31. Dasika, G. K., Lin, S.-C. J., Zhao, S., Sung, P., Tomkinson, A., and Lee, E. Y.-H. P., *DNA damage-induced cell cycle checkpoints and DNA strand break repair in development and tumorigenesis*. Oncogene, 1999. **18**(55): p. 7883-99.
32. Nijnik, A., Woodbine, L., Marchetti, C., Dawson, S., Lambe, T., Liu, C., Rodrigues, N., Crockford, T., Cabuy, E., Vindigni, A., Enver, T., Bell, J., Slijepcevic, P., Goodnow, C., Jeggo, P., and Cornall, R., *DNA repair is limiting for haematopoietic stem cells during ageing*. Nature, 2007. **447**(7145): p. 686-90.
33. Bau, D., Mau, Y., and Shen, C., *The role of BRCA1 in non-homologous end-joining*. Cancer Letters, 2006. **240**(1): p. 1-8.
34. Goytisolo, F. A., Samper, E., Martin-Caballero, J., Finnon, P., Herrera, E., Flores, J. M., Bouffler, S. D., and Blasco, M. A., *Short Telomeres Result in Organismal*

- Hypersensitivity to Ionizing Radiation in Mammals*. Journal Experimental Medicine, 2000. **192**(11): p. 1625-36.
35. Woloschak, G. E., Rodriguez, M., and Krco, C. J., *Characterization of immunologic and neuropathologic abnormalities in wasted mice*. Journal of Immunology, 1987. **138**(8): p. 2493-9.
  36. Wang, Z. Q., Auer, B., Stingl, L., Berghammer, H., Haidacher, D., Schweiger, M., and Wagner, E. F., *Mice lacking ADPRT and poly(ADP-ribosyl)ation develop normally but are susceptible to skin disease*. Genes and Development, 1995. **9**(5): p. 509-20.
  37. Wang, L., Yang, L., Debidda, M., Witte, D., and Zheng, Y., *Cdc42 GTPase-activating protein deficiency promotes genomic instability and premature aging-like phenotypes*. Proceedings of the National Academy of Science U.S.A., 2007. **104**(4): p. 1248-53.
  38. Vodenicharov, M. D., Sallmann, F. R., Satoh, M. S., and Poirier, G. G., *Base excision repair is efficient in cells lacking poly(ADP-ribose) polymerase 1*. Nucleic Acids Research, 2000. **28**(20): p. 3887-96.
  39. Manis, J. P., van der Stoep, N., Tian, M., Ferrini, R., Davidson, L., Bottaro, A., and Alt, F. W., *Class switching in B cells lacking 3' immunoglobulin heavy chain enhancers*. Journal Experimental Medicine, 1998. **188**(8): p. 1421-31.
  40. Hoeller, U., Tribius, S., Kuhlmeier, A., Grader, K., Fehlauer, F., and Alberti, W., *Increasing the rate of late toxicity by changing the score? A comparison of RTOG/EORTC and LENT/SOMA scores*. International Journal Radiation Oncology, Biology, Physic, 2003. **55**(4): p. 1013-8.
  41. Williams, J., Chen, Y., Rubin, P., Finkelstein, J., and Okunieff, P., *The biological basis of comprehensive grading system for the adverse effects of cancer treatment*. Seminars in Radiation Oncology, 2003. **13**(3): p. 182-8.
  42. Kanaar, R., Hoeijmakers, J.H., *Recombination and joining: different means to the same ends*. Genes Function, 1997. **1**(3): p. 165-74.
  43. Cleaver, J. E., *Defective repair replication of DNA in xeroderma pigmentosum*. Nature 1968. **218**: p. 652-6.
  44. Petrini, J. H., and Theunissen, J. W., *Double strand break metabolism and cancer susceptibility: lessons from the mre11 complex*. Cell Cycle, 2004. **3**(5): p. 541-2.
  45. Demuth, I., and Digweed, M., *The clinical manifestation of a defective response to DNA double-strand breaks as exemplified by Nijmegen breakage syndrome*. Oncogene, 2007. **26**(56): p. 7792-8.
  46. Roselli, F., Briot, D., Pichierri, P., *The Fanconi anemia pathway and the DNA interstrand cross-link repair*. Biochimie, 2003. **85**(11): p. 1175-84.
  47. Howlett, N. G., Taniguchi, T., Olson, S., Cox, B., Waisfisz, Q., De Die-Smulders, C., Persky, N., Grompe, M., Joenje, H., Pals, G., Ikeda, H., Fox, E. A., and D'Andrea, A. D., *Biallelic inactivation of BRCA2 in Fanconi anemia*. Science 2002. **297**(5581): p. 606-9.
  48. Duckworth-Rysiecki G., and Taylor, A. M., *Effects of ionizing radiation on cells from Fanconi's anemia patients*. Cancer Research, 1985. **45**(1): p. 416-20.
  49. Harrigan, J. A., Bohr, V.A., *Human diseases deficient in RecQ helicases*. Biochimie, 2003. **85**(11): p. 1185-93.
  50. Wang, Y., Cortez, D., Yazdi, P., Neff, N., Elledge, S.J., Qin J., *BASC, a super complex of BRCA1-associated proteins involved in the recognition and repair of aberrant structures*. Genes and Development, 2000. **14**: p. 927-39.
  51. Wood, R. D., Mitchell, M., Sgouros, J., and Lindahl, T., *Human DNA repair genes*. Science 2001. **291**(5507): p. 1284-9.

52. Wood, R. D., Mitchell, M., and Lindahl, T., *Human DNA repair genes, 2005*. Mutation Research, 2005. **4**(577): p. 275-83.
53. Branzei, D., and Foiani, M., *Regulation of DNA repair throughout the cell cycle*. Nature, 2008. **9**: p. 297-308.
54. Aguilera, A., *The connection between transcription and genomic instability*. EMBO, 2002. **21**: p. 195–201.
55. Branzei, D., and Foiani, M., *The DNA damage response during DNA replication*. Current Opinion in Cell Biology, 2005. **17**(6): p. 568-75.
56. Pike, B. L., and Heierhorst, J., *Mdt1 Facilitates Efficient Repair of Blocked DNA Double-Strand Breaks and Recombinational Maintenance of Telomeres*. Molecular Cellular Biology, 2007. **27**(18): p. 6532-45.
57. Karagiannis, T. C., and El-Osta, A., *Chromatin modifications and DNA double-strand breaks: the current state of play*. Leukemia, 2007. **21**: p. 195-200.
58. Tsuzuki, T., Fujii, Y., Sakumi, K., Tominaga, Y., Nakao, K., Sekiguchi, M., Matsushiro, A., Yoshimura, Y., and Morita, T., *Targeted disruption of Rad51 gene leads to lethality in embryonic mice*. Proceedings of the National Academy of Science U.S.A., 1996. **93**(13): p. 6236-40.
59. Pittman, D. L., Cobb, J., Schimenti, K. J., Wilson, L. A., Cooper, D. M., Brignull, E., Handel, M. A., and Schimenti, J. C., *Meiotic prophase arrest with failure of chromosome synapsis in mice deficient for Dmc1, a germline-specific RecA homolog*. Molecular Cell, 1998. **1**(5): p. 697-705.
60. Luo, G., Yao, M. S., Bender, C. F., Mills, M., Bladl, A. R., Bradley, A., and Petrini, J. H., *Disruption of mRad50 causes embryonic stem cell lethality, abnormal embryonic development, and sensitivity to ionizing radiation*. Proceedings of the National Academy of Science U.S.A., 1999. **96**(13): p. 7376-81.
61. Barnes, D. E., Stamp, G., Rosewell, I., Denzel, A., and Lindahl, T., *Targeted disruption of the gene encoding DNA ligase IV leads to lethality in embryonic mice*. Current Biology, 1998. **8**(25): p. 1395-8.
62. Ouyang, Y., Kwon, Y. T., An, J. Y., Eller, D., Tsai, S. C., Diaz-Perez, S., Troke, J. J., Teitell, M. A., and Marahrens, Y., *Loss of Ubr2, an E3 ubiquitin ligase, leads to chromosome fragility and impaired homologous recombinational repair*. Mutation Research 2006. **596**(1-2): p. 64-75.
63. Hendry, J. H., Hoyes, K. P., Wadeson, P., and Roberts, S. A., *Role of damage-sensing/processing genes in the radiation response of haemopoietic in vitro colony-forming cells*. International Journal of Radiation Biology, 2002. **78**(7): p. 559 - 66.
64. Ahel, I., Ahel, D., Matsusaka, T., Clark, J. A., Pines, J., Boulton, S. J., and West, S. C., *Poly(ADP-ribose)-binding zinc finger motifs in DNA repair/checkpoint proteins*. Nature, 2008. **451**(3): p. 81-5.
65. Dantzer, F., Amé, J.-C., Schreiber, V., Nakamura, J., Ménissier-de Murcia, J., and de Murcia, G., *Poly(ADP-ribose) Polymerase-1 Activation During DNA Damage and Repair*. Methods in Enzymology, 2006. **409**: p. 493-510
66. Khanna, K. K., Jackson, S.P., *DNA double-strand breaks: signalling repair and the cancer connection*. Nature Genetics, 2001. **27**(3): p. 247-54.
67. Jeggo, P. A., Tesmer, J., and Chen, D. J., *Genetic analysis of ionising radiation sensitive mutants of cultured mammalian cell lines*. Mutation Research, 1991. **254**(2): p. 125-33.
68. Smith-Ravin, J., and Jeggo, P. A., *Use of damaged plasmid to study DNA repair in X-ray sensitive (xrs) strains of Chinese hamster ovary (CHO) cells*. International Journal Radiation Biology, 1989. **56**(6): p. 951-61.

69. Sado, K., Ayusawa, D., Enomoto, A., Sugauma, T., Oshimura, M., Sato, K., and Koyama, H., *Identification of a Mutated DNA Ligase IV Gene in the X-ray-hypersensitive Mutant SX10 of Mouse FM3A Cells*. Journal Biological Chemistry, 2001. **276**(13): p. 9742-8.
70. Sasaki, M., Yoshida, M. C., Kagamori, K., Takeichi, N., Kobayashi, H., Dempo, K., and Mori, M., *Spontaneous hepatitis in an inbred strain of Long-Evans rats*. Rat News Letters, 1985. **38**(11): p. 1369-75.
71. Li, Y., Togashi, Y., Sato, S., Emoto, T., Kang, J. H., Takeichi, N., Kobayashi, H., Kojima, Y., Une, Y., and Uchino, J., *Spontaneous hepatic copper accumulation in Long-Evans Cinnamon rats with hereditary hepatitis. A model of Wilson's disease*. Journal Clinical Investigations, 1991. **87**(5): p. 1858-61.
72. Wu, J., Forbes, J. R., Chen, H. S., and Cox, D. W., *The LEC rat has a deletion in the copper transporting ATPase gene homologous to the Wilson disease gene*. Nature Genetics, 1994. **7**(4): p. 771-4.
73. Masuda, R., Yoshida, M. C., Sasaki, M., Dempo, K., and Mori, M., *Hereditary hepatitis of LE rats is controlled by a single autosomal recessive gene*. Laboratory Animals, 1988. **22**: p. 166-9.
74. Sakai, T., Agui, T., and Matsumoto, K., *Maturational arrest from CD4+8+ to CD4+8- thymocytes is caused by the bone marrow-derived cells in LEC mutant rats*. Immunology Letters, 1993. **38**(2): p. 145-52.
75. Agui, T., Oka, M., Yamada, T., Sakai, T., Izumi, K., Ishida, Y., Himeno, K., and Matsumoto, K., *Maturational arrest from CD4+8+ to CD4+8+ thymocytes in a mutant strain (LEC) of rat*. Journal Experimental Medicine, 1990. **172**(6): p. 1615-24.
76. Yamada, T., Natori, T., Izumi, K., Sakai, T., Agui, T., and Matsumoto, K., *Inheritance of T helper immunodeficiency (thid) in LEC mutant rats*. Immunogenetics, 1991. **33**(3): p. 216-9.
77. Kose, H., Sakai, T., Tsukumo, S.-i., Wei, K., Yamada, T., Yasutomo, K., and Matsumoto, K., *Maturational arrest of thymocyte development is caused by a deletion in the receptor-like protein tyrosine phosphatase [kappa] gene in LEC rats*. Genomics, 2007. **89**(6): p. 673-7.
78. Nakajima, M., Kato, J., Kohgo, Y., Takeichi, N., and Nitsu, T., *Point mutation of aldehyde dehydrogenase-2 gene in mutant strains of Long-Evans rats*. Alcohol Alcohol Suppl, 1994. **29**(1): p. 39-43.
79. Wei, K., Izumi, K., Hino, A., Wei, S., Sasaki, Y., Yamada, T., and K., M., *Identification of a locus for susceptibility to renal cell carcinoma in the Long-Evans Cinnamon rat*. Journal of Veterinary Medical Science, 1999. **61**(11): p. 1261-4.
80. Hayashi, M., Endoh, D., Kon, Y., Yamashita, T., Hashimoto, N., Sato, F., Kasai, N., Namioka, S., *Higher sensitivity of LEC strain rat in radiation-induced acute intestinal death*. Journal of Veterinary Medical Science, 1992. **54**(2): p. 269-73.
81. Hayashi, M., Endoh, D., Kon, Y., Yamashita, T., Sato, F., Kasai, N., Namioka, S., *Hypersensitivity of LEC strain rats in radiation-induced acute bone-marrow death*. Journal of Veterinary Medical Science, 1993. **55**(1): p. 13-8.
82. Hayashi, M., Okui, T., Endoh, D., Sato, F., Kasai, N., and Namioka, S., *Radiation hypersensitivity of LEC strain rats controlled by a single autosomal recessive gene*. Mutation Research, 1994. **314**(2): p. 135-42.
83. Agui, T., Miyamoto, T., Jung, C., Tsumagari, T., Masuda, K., and Manabe, T., *Genetic linkage analysis of X-ray hypersensitivity in the LEC mutant rat*. Mammalian Genome, 2000. **11**: p. 862-5.

84. Wei, K., Muramatsu, Y., Sakai, T., Yamada, T., and Matsumoto, K., *Chromosomal mapping of the T-helper immunodeficiency (thid) locus in LEC rats*. Immunogenetics, 1997. **47**(1): p. 99-102.
85. Tsuji, A. B., Sugyo, A., Ogiu, T., Sagara, M., Kimura, T., Ishikawa, A., Sudo, H., Ohtsuki, M., Aburatani, H., Imai, T., and Harada, Y.-n., *Fine mapping of radiation susceptibility and gene expression analysis of LEC congenic rat lines*. Genomics, 2005. **86**(3): p. 271-9.
86. Urayama, K., Guillini, C., Messaddeq, N., Hu, K., Steenman, M., Kurose, H., Ert, G., and Nebigil, C. G., *The prokineticin receptor-1 (GPR73) promotes cardiomyocyte survival and angiogenesis*. FASEB J., 2007. **21**(11 ): p. 2980-93.
87. Chen, H., Ahi, S., Acosta, L., Li, W., Lu, J. P., Bao, S., Chen, Z., Yang, Z., Schneider, M. D., Chien, K. R., Conway, S. J., Yoder, M. C., Haneline, L. S., Franco, D., and Shou, W., *BMP10 is essential for maintaining cardiac growth during murine cardiogenesis*. Development, 2004. **131**(9): p. 2219-31.
88. David, I., Mallet, C., Mazerbourg, S., Feige, J. J., and Bailly, S., *Identification of BMP9 and BMP10 as functional activators of the orphan activin receptor-like kinase 1 (ALK1) in endothelial cells*. Blood, 2007. **109**(5): p. 1953-61.
89. Elsasser, S., Gali, R. R., Schwickart, M., Larsen, C. N., Leggett, D. S., Müller, B., Feng, M. T., Tübing, F., Dittmar, G. A., and Finley, D., *Proteasome subunit Rpn1 binds ubiquitin-like protein domains*. Nature Cell Biology, 2002. **4**(9): p. 725-30.
90. Vitelli, R., Santillo, M., Lattero, D., Chiariello, M., Bifulco, M., Bruni, C. B., and Bucci, C., *Role of the small GTPase Rab7 in the late endocytic pathway*. Journal Biological Chemistry, 1997. **272**(7): p. 4391-7.
91. Kasirer-Friede, A., Ware, J., Leng, L., Marchese, P., Ruggeri, Z. M., and Shattil, S. J., *Lateral clustering of platelet GP Ib-IX complexes leads to up-regulation of the adhesive function of integrin alpha IIb beta 3*. Journal Biological Chemistry, 2002. **277**(14): p. 11949-56.
92. Chen, W., Wang, Y., Abe, Y., Cheney, L., Udd, B., and Li, Y. P., *Haploinsufficiency for Znf9 in Znf9+/- mice is associated with multiorgan abnormalities resembling myotonic dystrophy*. Journal of Molecular Biology, 2007. **368**(1): p. 8-17.
93. Futatsumori, M., Kasai, K., Takatsu, H., Shin, H. W., and Nakayama, K., *Identification and characterization of novel isoforms of COP I subunits*. Journal of Biochemistry, 2000. **128**(5): p. 793-801.
94. Tsuji, A. B., Sugyo, A., Sudo, H., Sagara, M., Ishikawa, A., Ohtsuki, M., Kimura, T., Ogiu, T., Miyagishi, M., Taira, K., Imai, T., and Harada, Y.-n., *Defective repair of radiation-induced DNA damage is complemented by a CHORI-230-65K18 BAC clone on rat chromosome 4*. Genomics, 2006. **87**(2): p. 236-42.
95. Ogiu, T., Nishimura, M., Watanabe, F., Ukai, H., Ishii-Ohba, H., Shimada, Y., Tsuji, H., Sakurai, J., and Hino, O., *Absence of Linkage between Radiosensitivity and the Predisposing Atp7b Gene Mutation for Heritable Hepatitis in the LEC Rat*. Radiation Research, 2000. **154**(1): p. 113-6.
96. Hayashi, M., Nagata, A., Endoh, D., Arikawa, J., and Okui, J., *High sensitivity of thymocytes of LEC strain rats to induction of apoptosis by x-irradiation*. Journal of Veterinary Medical Science, 2002. **64**(7): p. 597-601.
97. Hayashi, M., Uehara, K., Kirisawa, R., Endoh, D., Arai, S., and Okui, T., *Abnormal G1 arrest in the cell lines from LEC strain rats after X-irradiation*. Journal Veterinary Medical Science, 1997. **59**(9): p. 769-73.

98. Okui, T., Endoh, D., Kon, Y., and Hayashi, M., *Deficiency in nuclear accumulation of G22p1 and Xrcc5 proteins in hyper-radiosensitive Long-Evans Cinnamon (LEC) rat cells after X irradiation*. Radiation Research, 2002. **157**(5): p. 553-61.
99. Okui, T., Endoh, D., and Hayashi, M., *Deficiency in fast repair process of potentially lethal damage induced by X-irradiation in fibroblasts derived from LEC strain rats*. Mutation Research, 1999. **435**(1): p. 81-8.
100. Hayashi, M., Ichikawa, Y., Arai, S., Endoh, D., and Okui, T., *Higher sensitivity in LEC rat cells to a topoisomerase II inhibitor, ellipticine*. Journal of Veterinary Medical Science, 1998. **60**(8): p. 969-71.
101. Agui, T., Miyamoto, T., and Tsumagari, T., *X-ray Hypersensitivity in the LEA Rat: Genetic Linkage Analysis of Responsible Loci*. Experimental Animal/ Japanese association for Laboratory Animal Science 2001. **50**(2): p. 147-51.
102. Ito, Y., Fujie, K., Matsuda, S., Takahashi, R., and Maeda, S., *Long-Evans A and C rat strains susceptible to clastogenic effects of chemicals in the bone marrow cells*. Japanese Journal of Cancer Research, 1994. **85**(1): p. 26-31.
103. Ungaro, P., Casola, S., Vernucci, M., Pedone, P. V., Bruni, C. B., and Riccio, A., *Relaxation of insulin-like growth factor-2 imprinting in rat cultured cells*. Molecular and Cellular Endocrinology, 1997. **135**: p. 153-63.
104. Puck, T. T., and Marcus, P. I., *Action of x-rays on mammalian cells*. Journal of Experimental Medicine, 1956. **103**(5): p. 653-66.
105. Munshi, A., Hobbs, M., and Meyn, R. E., *Clonogenic cell survival assay* Methods in Molecular Medicine ed. R.D. Blumenthal. Vol. 110. 2005. 21-8.
106. Buffa, F. M., Davidson, S. E., Hunter, R. D., Nahum, A. E., and West, C. M. L., *Incorporating biological measurements (SF2, CFE) into a tumor control probability model increases their prognostic significance: a study in cervical carcinoma treated with radiation therapy*. International Journal of Radiation Oncology, Biology, Physic, 2001. **50**(5): p. 1113-22.
107. Friedl, A., Kraxenberger, A., and Eckardt-Schupp, F., *An electrophoretic approach to the assessment of the spatial distribution of DNA double-strand breaks in mammalian cells*. Electrophoresis, 1995. **16**(10): p. 1865-74.
108. Cedervall, B., Wong, R., Albright, N., Dynlacht, J., Lambin, P., and Dewey, W., *Methods for the quantification of DNA double-strand breaks determined from the distribution of DNA fragment sizes measured by pulsed-field gel electrophoresis*. Radiation Research, 1995. **143**(1): p. 8-16.
109. Woudstra, E., Roesink, J., Rosemann, M., Brunsting, J., Driessen, C., Orta, T., Konings, A., Peacock, J., and HH, K., *Chromatin structure and cellular radiosensitivity: a comparison of two human tumour cell lines*. Radiat Research, 1996. **70**(6): p. 693-703.
110. Singh, N. P., McCoy, M. T., Tice, R. R., and Schneider, E. L., *A simple technique for quantitation of low levels of DNA damage in individual cells*. Experimental Cell Research, 1988. **175**(1): p. 184-91.
111. Singh, N., Graham, M., Singh, V., and Khan, A., *Induction of DNA single-strand breaks in human lymphocytes by low doses of gamma-rays*. International Journal Radiation Biology, 1995. **68**(5): p. 563-9.
112. Schindewolf, C., Lobenwein, K., Trinczek, K., Gomolka, M., Soewarto, D., Fella, C., Pargent, W., Singh, N., Jung, T., and Hrabé de Angelis, M., *Comet assay as a tool to screen for mouse models with inherited radiation sensitivity*. Mammalian Genome, 2000. **11**(7): p. 552-4.

113. Chuang, C.-H., and Hu, M.-L., *Use of whole blood directly for single-cell gel electrophoresis (comet) assay in vivo and white blood cells for in vitro assay*. Mutation Research, 2004. **564**(1): p. 75-82.
114. Zeller, W., Weber, H., Panoussis, B., Bürge, T., and Bergmann, R., *Refinement of blood sampling from the sublingual vein of rats*. Laboratory Animals, 1998. **32**(4): p. 369-76.
115. Duez, P., Dehon, G., Kumps, A., and Dubois, J., *Statistics of the Comet assay: a key to discriminate between genotoxic effects*. Mutagenesis, 2003. **18**(2): p. 159-66.
116. Pavloda, O., Polanska, J., Wygoda, A., and Rzeszowska-Wolny, J., *DNA damage and repair in lymphocytes of normal individuals and cancer patients: studies by the comet assay and micronucleus tests* Acta Biochimica Polonica, 2003. **50**(1): p. 181-90.
117. Nusse, M., and Kramer, J., *Flow cytometric analysis of micronuclei found in cells after irradiation*. Cytometry, 1984. **5**(1): p. 20-5.
118. Sanger, F., and Coulson, A., *A rapid method for determining sequences in DNA by primed synthesis with DNA polymerase*. Journal Molecular Biology, 1975. **94**(3): p. 441-8.
119. Pfaffl, M., *A new mathematical model for relative quantification in real-time RT-PCR*. Nucleic Acids Research 2001. **29**(9): p. e45.
120. Livak, K. J., and Schmittgen, T. D., *Analysis of Relative Gene Expression Data Using Real-Time Quantitative PCR and the 2- $[\Delta\Delta]CT$  Method*. Methods, 2001. **25**(4): p. 402-8.
121. Das, M., Dempsey, E. C., Reeves, J. T., and K.R., S., *Selective expansion of fibroblast subpopulations from pulmonary artery adventitia in response to hypoxia*. American Journal of Physiology, Lung Cellular and Molecular Physiology, 2002. **282**: p. L976-86.
122. Dikomey, E., Borgmann, K., Brammer, I., and Kasten-Pisula, U., *Molecular mechanisms of individual radiosensitivity studied in normal diploid human fibroblasts*. Toxicology, 2003. **193**(1-2): p. 125-35.
123. Foray, N., Arlett, C. F., and Malaise, E. P., *Underestimation of the small residual damage when measuring DNA double-strand breaks (DSB): is the repair of radiation-induced DSB complete?* International Journal of Radiation Biology, 1999. **75**(12): p. 1589-95.
124. Lowndes, N. F., and Toh, G. W. L., *DNA Repair: The Importance of Phosphorylating Histone H2AX*. Current Biology, 2005. **15**(3): p. R99-R102.
125. Rogakou, E. P., Boon, C., Redon, C., and Bonner, W. M., *Megabase Chromatin Domains Involved in DNA Double-Strand Breaks In Vivo*. Journal Cell Biology, 1999. **146**(5): p. 905-16.
126. Suzuki, M., Suzuki, K., Kodama, S., and Watanabe, M., *Phosphorylated histone H2AX foci persist on rejoined mitotic chromosomes in normal human diploid cells exposed to ionizing radiation*. Radiation Research, 2006. **165**(3): p. 269-76.
127. MacPhail, S. H., Banath, J. P., Yu, Y., Chu, E., and Olive, P. L., *Cell cycle-dependent expression of phosphorylated histone H2AX: Reduced expression in unirradiated but not X-irradiated G1-phase cells*. Radiation Research, 2003. **159**: p. 759-67.
128. Böcker, W., and Iliakis, G., *Computational Methods for Analysis of Foci: validation for radiation-induced g-H2AX foci in human cells*. Radiation Research, 2006. **165**(1): p. 113-24.
129. Djuzenova, C. S., and Flenje, M., *Characterization of Fanconi anemia fibroblasts in terms of clonogenic survival and DNA damage assessed by the Comet assay* Medical Science Monitor, 2002. **8**(10): p. 421-30.
130. Verkade, H., Teli, T., Laursen, L., Murray, J., and O'Connell, M., *A homologue of the Rad18 postreplication repair gene is required for DNA damage responses throughout the fission yeast cell cycle*. Molecular Genetics and Genomics, 2001. **265**(6): p. 993-1003.

131. Yukiko, M. Y., Takashi, O., Takahiro, M., Eiichiro, S., Guang, Y. Z., Kasumi, A., Satoshi, T., Masaru, Y., and Shunichi, T., *RAD18 and RAD54 cooperatively contribute to maintenance of genomic stability in vertebrate cells*. EMBO, 2002. **21**(20): p. 5558–66.
132. Sewing, A., Wiseman, B., Lloyd, A. C., and Land, H., *High-intensity Raf signal causes cell cycle arrest mediated by p21Cip1*. Molecular Cellular Biology, 1997. **17**(9): p. 5588-97.
133. Kasid, U., Pfeifer, A., Brennan, T., Beckett, M., Weichselbaum, R., Dritschilo, A., and Mark, G. E., *Effect of antisense c-raf-1 on tumorigenicity and radiation sensitivity of a human squamous carcinoma*. Science, 1989. **243**: p. 1354-6.
134. Gokhale, P. C., McRae, D., Monia, B. P., Bagg, A., Rahman, A., Dritschilo, A., and Kasid, U., *Antisense raf oligonucleotide is a radiosensitizer in vivo*. Antisense Nucleic Acid Drug Development, 1999. **9**: p. 199-201.
135. Sanford, K., Parshad, R., Price, F., Tarone, R., and Lehmann, A., *G2 phase repair of X-ray-induced chromosomal DNA damage in trichothiodystrophy cells*. Mutation Research, 1995. **346**(2): p. 107-14.
136. Gratchev, A., Strein, P., Utikal, J., and Sergij, G., *Molecular genetics of Xeroderma pigmentosum variant*. Experimental Dermatology, 2003. **12**(5): p. 529-36.
137. Li, L., Peterson, C., and Legerski, R., *Sequence of the mouse XPC cDNA and genomic structure of the human XPC gene*. Nucleic Acids Research, 1996. **24**(6): p. 1026-8.
138. Bogliolo, M., Cabre, O., Callen, E., Castillo, V., Creus, A., Marcos, R., and Surralles, J., *The Fanconi anaemia genome stability and tumour suppressor network*. Mutagenesis, 2002. **17**(6): p. 529-38.
139. Bekker-Jensen, S., Fugger, K., Danielsen, J. R., Gromova, I., Sehested, M., Celis, J., Bartek, J., Lukas, J., and Mailand, N., *Human XIP1 (C2Orf13) is a novel regulator of cellular responses to DNA strand breaks*. Journal of Biological Chemistry, 2007. **282**(27): p. 19638-43.
140. Iles, N., Rulten, S., El-Khamisy, S. F., and Caldecott, K. W., *APLF (C2orf13) Is a Novel Human Protein Involved in the Cellular Response to Chromosomal DNA Strand Breaks*. Molecular Cellular Biology, 2007. **27**(10): p. 3793-803.
141. Tsuzuki, S., and Enver, T., *Interactions of GATA-2 with the promyelocytic leukemia zinc finger (PLZF) protein, its homologue FAZF, and the t(11;17)-generated PLZF-retinoic acid receptor alpha oncoprotein*. Blood, 2002. **99**(9): p. 3404-10.
142. Tsuzuki, S., Towatari, M., Saito, H., and Enver, T., *Potentiation of GATA-2 Activity through Interactions with the Promyelocytic Leukemia Protein (PML) and the t(15;17)-Generated PML-Retinoic Acid Receptor alpha Oncoprotein*. Molecular Cellular Biology, 2000. **20**(17): p. 6276-86.
143. Andrieux, L. O., Fautrel, A., Bessard, A., Guillouzo, A., Baffet, G., and Langouet, S., *GATA-1 Is Essential in EGF-Mediated Induction of Nucleotide Excision Repair Activity and ERCC1 Expression through ERK2 in Human Hepatoma Cells*. Cancer Research, 2007. **67**(5): p. 2114-23.
144. Minegishi, N., Ohta, J., Suwabe, N., Nakauschi, H., Ishihara, H., Hayashi, N., and Yamamoto, M., *Alternative promoters regulate transcription of the mouse GATA-2 gene*. The Journal of Biological Chemistry, 1996. **273**(6): p. 3625-34.
145. Khandekar, M., Brandt, W., Zhou, Y., Dagenais, S., Glover, T. W., Suzuki, N., Shimizu, R., Yamamoto, M., Lim, K.-C., and Engel, J. D., *A Gata2 intronic enhancer confers its pan-endothelia-specific regulation*. Development, 2007. **134**(9): p. 1703-12.

146. Wozniak, R. J., Boyer, M., Grass, J., Youngsook, L., and Bresnick, E. H., *Context-dependent GATA factor function*. Journal of Biological Chemistry, 2007. **282**(19): p. 14665-74.
147. Khandekar, M., Suzuki, N., Lewton, J., Yamamoto, M., and Engel, J. D., *Multiple, distant Gata2 enhancers specify temporally and tissue-specific patterning in the developing urogenital system*. Molecular and Cellular Biology, 2004. **24**(23): p. 10263-76.
148. Pan, X., Minegishi, N., Harigae, H., Yamagiwa, H., Minegishi, M., Akine, Y., and Yamamoto, M., *Identification of human GATA-2 gene distal IS exon and its expression in hematopoietic stem cell fractions*. Journal of Biochemistry, 2000. **127**(1): p. 105-12.
149. Suzuki, N., Ohneda, O., Minegishi, N., Nishikawa, M., Ohta, T., Takahashi, S., Engel, J. D., and Yamamoto, M., *Combinatorial Gata2 and Sca1 expression defines hematopoietic stem cells in the bone marrow niche*. Proceedings of the National Academy of Science U.S.A., 2006. **103**(7): p. 2202-7.
150. Tagle, D. A., Koop, B. F., Goodman, M., Slightom, J. L., Hess, D. L., and Jones, R. T., *Embryonic epsilon and gamma globin genes of a prosimian primate (Galago crassicaudatus). Nucleotide and amino acid sequences, developmental regulation and phylogenetic footprints*. Journal of Molecular Biology, 1988. **203**(2): p. 439-55.
151. Sosinsky, A., Barry, H., Mann, R. S., and Califano, A., *Discovering transcriptional regulatory regions in Drosophila by a nonalignment method for phylogenetic footprinting*. Proceedings of the National Academy of Science U.S.A., 2007. **104**(15): p. 6305-10.
152. Mori, M., Yoshida, M. C., Takeichi, N., and Taniguchi, N., *The LEC Rat -A New Model for Hepatitis and Liver Cancer* ed. Sugimura. 1991, Tokyo Springer-Verlag. 356.
153. ICRP, A., *Genetic susceptibility to cancer, ICRP publication 79*. 1998.
154. Todaro, G. J., and Green, H., *Quantitative studies of the growth of mouse embryo cells in culture and their development into established lines*. Journal of Cellular Biology, 1963. **17**: p. 299-313.
155. Macieira-Goelho, A., *Growth inhibition of human fibroblasts in vitro*. Progress in Molecular Subcellular Biology, 1998. **20**: p. 249-70.
156. Macieira-Goelho, A., *Comparative biology of cell immortalisation*. Progress in Molecular Subcellular Biology, 2000. **20**: p. 249-70.
157. Tolstonog, G. V., Belichenko-Weitzmann, I. V., Lu, J. P., Hartig, R., Shoeman, R. L., Traub, U., and Traub, P., *Spontaneously immortalized mouse embryo fibroblasts: growth behaviour of wild-type and vimentin-deficient cells in relation to mitochondrial structure and activity*. DNA and Cell Biology, 2005. **24**(11): p. 680-709.
158. Rasheed, S., Freeman, A. E., Gardner, M. B., and Huebner, R. J., *Acceleration of transformation of rat embryo cells by rat type C virus*. Journal Virology, 1976. **18**(2): p. 776-82.
159. Goldstein, S., *Lifespan of cultured cells in progeria*. Lancet, 1969. **1**(7591): p. 424.
160. Segal, D. J., and McCoy, E. E., *Studies on Down's syndrome in tissue culture. I. Growth rates and protein contents of fibroblast cultures*. Journal of Cell Physiology, 1974. **83**: p. 85-90.
161. Chen, Q., and Ames, B. N., *Senescence-Like Growth Arrest Induced by Hydrogen Peroxide in Human Diploid Fibroblast F65 Cells*. Proceedings of the National Academy of Science U.S.A., 1994. **91**(10): p. 4130-4.
162. Linke, S. P., Clarkin, K. C., and Wahl, G. M., *P53 mediates permanent arrest over multiple cell cycles in response to gamma-irradiation*. Cancer Research, 1997. **57**: p. 1171-9.

163. Herskind, C., and Rodemann, H. P., *Spontaneous and radiation-induced differentiation of fibroblasts*. *Experimental Gerontology*, 2000. **35**(6-7): p. 747-55.
164. Naka, K., Tachibana, A., Ikeda, K., and Motoyama, N., *Stress-induced premature senescence in hTERT-expressing ataxia telangiectasia fibroblasts* *Journal of Biological Chemistry*, 2004. **279**(3): p. 2030-7.
165. Enns, L., Barley, R. D., Paterson, M. C., and Mirzayans, R., *Radiosensitivity in ataxia telangiectasia fibroblasts is not associated with deregulated apoptosis*. *Radiation Research*, 1998. **150**(1): p. 11-6.
166. Debacq-Chainiaux, F., Borlon, C., Pascal, T., Royer, V., Eliaers, F., Ninane, N., Carrard, G., Friguet, B., de Longueville, F., Boffe, S., Remacle, J., and Toussaint, O., *Repeated exposure of human skin fibroblasts to UVB at subcytotoxic level triggers premature senescence through the TGF-beta1 signaling pathway*. *Journal of Cell Science*, 2005. **118**(4): p. 743-58.
167. Fertil, B., and Deschavanne, P., *Relationships between colony forming efficiency and parameters of intrinsic radiosensitivity*. *International Journal Radiation Biology*, 1999. **75**(10): p. 1275-82.
168. Chloi, N., Baumann, M., Flentje, M., Kellokumpu-Lehtinen, P., Senan, S., Zamboglou, N., and Kosmidis, P., *Predictive factors in radiotherapy for non-small cell lung cancer: present status*. *Lung Cancer*, 2001. **31**(1): p. 43-56.
169. Deschavanne, P. J., and Fertil, B., *A review of human cell radiosensitivity in vitro*. *International Journal of Radiation Oncology, Biology, Physics*, 1996. **34**(1): p. 251-66.
170. Suit, H. D., Baumann, M., Skates, S., and Convery, K., *Clinical interest in determinations of cellular radiation sensitivity*. *International Journal Radiation Biology*, 1989. **56**(5): p. 725-37.
171. Kasten-Pisula, U., Tastan, H., and Dikomey, E., *Huge differences in cellular radiosensitivity due to only very small variations in double-strand break repair capacity*. *International Journal of Radiation Biology*, 2005. **81**(6): p. 409-19.
172. Dikomey, E., Brammer, I., Johansen, J., Bentzen, S., and Overgaard, J., *Relationship between DNA double-strand breaks, cell killing, and fibrosis studied in confluent skin fibroblasts derived from breast cancer patients* *International Journal of Radiation, Oncology, Physics*, 2000. **46**(2): p. 481-90.
173. Zhou, P.-K., Sproston, A. R. M., Marples, B., West, C. M. L., Margison, G. P., and Hendry, J. H., *The radiosensitivity of human fibroblast cell lines correlates with residual levels of DNA double-strand breaks*. *Radiotherapy and Oncology*, 1998. **47**(3): p. 271-6.
174. Kalb, R., Duerr, M., Wagner, M., Herterich, S., Gross, M., Digweed, M., Joenje, H., Hoehn, H., and Schindler, D., *Lack of Sensitivity of Primary Fanconi Anemia Fibroblasts to UV and Ionizing Radiation*. *Radiation Research*, 2004. **161**(3): p. 318-25.
175. El-Awady, R. A., Mahmoud, M., Saleh, E. M., El-Baky, H. A., Lotayef, M., Dahm-Daphi, J., and Dikomey, E., *No correlation between radiosensitivity or double-strand break repair capacity of normal fibroblasts and acute normal tissue reaction after radiotherapy of breast cancer patients*. *International Journal of Radiation Biology*, 2005. **81**(7): p. 501-8.
176. Jeggo, P., Carr, A., and Lehmann, A., *Cloning human DNA repair genes*. *International Journal of Radiation Biology*, 1994. **66**(5): p. 573-7.
177. El-Awady, R. A., Dikomey, E., and Dahm-Daphi, J., *Heat effects on DNA repair after ionising radiation: hyperthermia commonly increases the number of non-repaired double-strand breaks and structural rearrangements*. *Nucleic Acids Research*, 2001. **29**(9): p. 1960-6.

178. Keogh, M.-C., Kim, J.-A., Downey, M., Fillingham, J., Chowdhury, D., Harrison, J. C., Onishi, M., Datta, N., Galicia, S., Emili, A., Lieberman, J., Shen, X., Buratowski, S., Haber, J. E., Durocher, D., Greenblatt, J. F., and Krogan, N. J., *A phosphatase complex that dephosphorylates [gamma]H2AX regulates DNA damage checkpoint recovery*. *Nature*, 2006. **439**(7075): p. 497-501.
179. Bouquet, F., Muller, C., and Salles, B., *The loss of gammaH2AX signal is a marker of DNA double strand breaks repair only at low levels of DNA damage*. *Cell Cycle*, 2006. **5**(10): p. 1116-22.
180. O'Connell, M. J., and Cimprich, K. A., *G2 damage checkpoints: what is the turn-on?* *Journal of Cell Science*, 2005. **118**(1): p. 1-6.
181. Wachsberger, P. R., Li, W. H., Guo, M., Chen, D. J., Cheong, N., Ling, C. C., Li, G., and Iliakis, G., *Rejoining of DNA double-strand breaks in Ku80-deficient mouse fibroblasts*. *Radiation Research*, 1999. **151**(4): p. 398-407.
182. Hayashi, M., Uehara, K., Ichikawa, Y., Arai, S., Isogai, E., and Okui, T., *Higher sensitivity in induction of apoptosis in fibroblasts cell lines derived from LEC strain rats to UV-irradiation*. *Journal of Veterinary Medical Science*, 1998. **60**(2): p. 207-12.
183. Masuda, K., Miyamoto, T., Cho, A., and Agui, T., *Analysis of the cell cycle of fibroblasts derived from the LEC rat after X-irradiation*. *Japanese Journal of Veterinary Research*, 2006. **53**(3-4): p. 141-8.
184. Budach, W., Classen, J., Belka, C., and Bamberg, M., *Clinical impact of predictive assays for acute and late radiation morbidity*. *Strahlentherapie Oncologie*, 1998. **174**: p. 20-4.
185. Foray, N., Priestley, A., Alsbeih, G., Badie, C., Capulas, E. P., Arlett, C. F., and Malaise, E. P., *Hypersensitivity of ataxia telangiectasia fibroblasts to ionizing radiation is associated with a repair deficiency of DNA double-strand breaks*. *International Journal of Radiation Biology*, 1997. **72**(3): p. 271-83.
186. Ghazi, A., Medhat, E.-S., Najla, A.-H., Muneera, A.-B., Khaled, A.-H., and Naser, A.-R., *Radiosensitivity of human fibroblasts is associated with amino acid substitution variants in susceptible genes and correlates with the number of risk alleles*. *International Journal of Radiation Oncology*, 2006. **68**(1): p. 229-35.
187. Severin, D. M., Leong, T., Cassidy, B., Elsaleh, H., Peters, L., Venter, D., Southey, M., and McKay, M., *Novel DNA sequence variants in the hHR23 DNA repair gene in radiosensitive cancer patients*. *International Journal Radiation Oncology Biology Physics*, 2001. **50**(5): p. 1323-31.
188. Khan, S., G., Muniz-Medina, V., Shahlavi, T., Baker, C. C., Inui, H., Ueda, T., Emmert, S., Schneider, T. D., and Kraemer, K. H., *The human XPC DNA repair gene: arrangement, splice site information content and influence of a single nucleotide polymorphism in a splice acceptor site on alternative splicing and function*. *Nucleic Acid Research*, 2002. **30**(16): p. 3624-31.
189. Iliakis, G., Wang, H., Perrault, A. R., Boecker, W., Rosidi, B., Windhofer, F., Wu, W., Guan, J., Terzoudi, G., and Pantelias, G., *Mechanisms of DNA double strand break repair and chromosome aberration formation*. *Cytogenetics Genome Research*, 2004. **104**(1-4): p. 14-20.
190. Löbrich, M., Rydberg, B., and Cooper, P. K., *Repair of x-ray-induced DNA double-strand breaks in specific Not I restriction fragments in human fibroblasts: Joining of correct and incorrect ends*. *Proceedings of the National Academy of Science U.S.A.*, 1995. **92**(26): p. 12050-4.

191. Wyatt, M. D., and Pittman, D. L., *Methylating Agents and DNA Repair Responses: Methylated Bases and Sources of Strand Breaks*. Chemical Research in Toxicology, 2006. **19**(12): p. 1580-94.
192. Zhou, T., Chou, J. W., Simpson, D. A., Zhou, Y., Mullen, T. E., Medeiros, M., Bushel, P. R., Paules, R. S., Yang, X., Hurban, P., Lobenhofer, E. K., and Kaufmann, W. K., *Profiles of global gene expression in ionizing-radiation-damaged human diploid fibroblasts reveal synchronization behind the G1 checkpoint in a G0-like state of quiescence*. Environmental Health Perspectives, 2006. **114**(4): p. 553-9.
193. Ranganath, S., and Murphy, K. M., *Structure and specificity of GATA proteins in Th2 development*. Molecular and Cellular Biology, 2001. **21**(8): p. 2716-25.
194. Hegde, S., Lenox, L. E., Lariviere, A., Porayette, P., Perry, J. M., Yon, M., and Paulson, R. F., *An intronic sequence mutated in flexed-tail mice regulates splicing of Smad5*. Mammalian Genome, 2007. **18**(12): p. 852-60.
195. Buratti, E., Baralle, M., and Baralle, F. E., *Defective splicing, disease and therapy: searching for master checkpoints in exon definition*. Nucleic Acids Research, 2006. **34**: p. 3494-510.
196. Kysela, B., Chovanec, M., and Jeggo, P. A., *Phosphorylation of linker histones by DNA-dependent protein kinase is required for DNA ligase IV-dependent ligation in the presence of histone H1*. Proceedings of the National Academy of Science U.S.A., 2005. **102**(6): p. 1877-82.
197. Dix, I., Russell, C., Yehuda, S. B., Kupiec, M., and Beggs, J. D., *The identification and characterization of a novel splicing protein, Isyp1, of Saccharomyces cerevisiae*. RNA, 1999. **5**: p. 360-8.

## ABBREVIATIONS

AR	acute radiation
AT	ataxia telengeactasia
ALS	alkali labile sites
BER	base excision repair
DMF	dose modifying factor
DSB	double strand breaks
EST	expressed sequence tag
FAR	fraction of activity released
GGR	global genome repair
GI	genomic instability
HR	homologous repair
IR	ionizing radiation
LD <sub>50/30</sub>	dose, necessary to kill 50% of animals in 30 days
LD <sub>50/7</sub>	dose, necessary to kill 50% of animals in 7 days
LE	Long Evance
LEA	Long Evance Agouti
LEC	Long Evance Cinnamon
LMP	low melting point
MEF	mouse embryonic fibroblasts
MMR	mismatch repair
MMS	methyl methansulfonate
MN	micronuclei
NHEJ	non-homologous end joining
PARP	poly(ADP-ribose) polymerase 1
PCNA	proliferating cellular nuclear antigen
PE	plating efficiency
PBGD	porphobilinogen deaminase
PFGE	pulsed field gel electrophoresis
ROS	reactive oxygen species
RT	room temperature
SEM	standard error of the mean
SF2	surviving fraction at 2 Gy
SNP	single nucleotide polymorphism
SSB	single strand breaks
SSLP	single-sequence length polymorphism
TCR	transcription coupled repair
TLS	translesion synthesis
UV	ultraviolet
UTR	untranslated region
XP	xeroderma pigmentosum
XRCC	x ray cross complementing
DMEM	Dulbecco's modified Eagle's Media
FCS	fetal calf serum
PS	penicillin/streptomycin

## APPENDIX

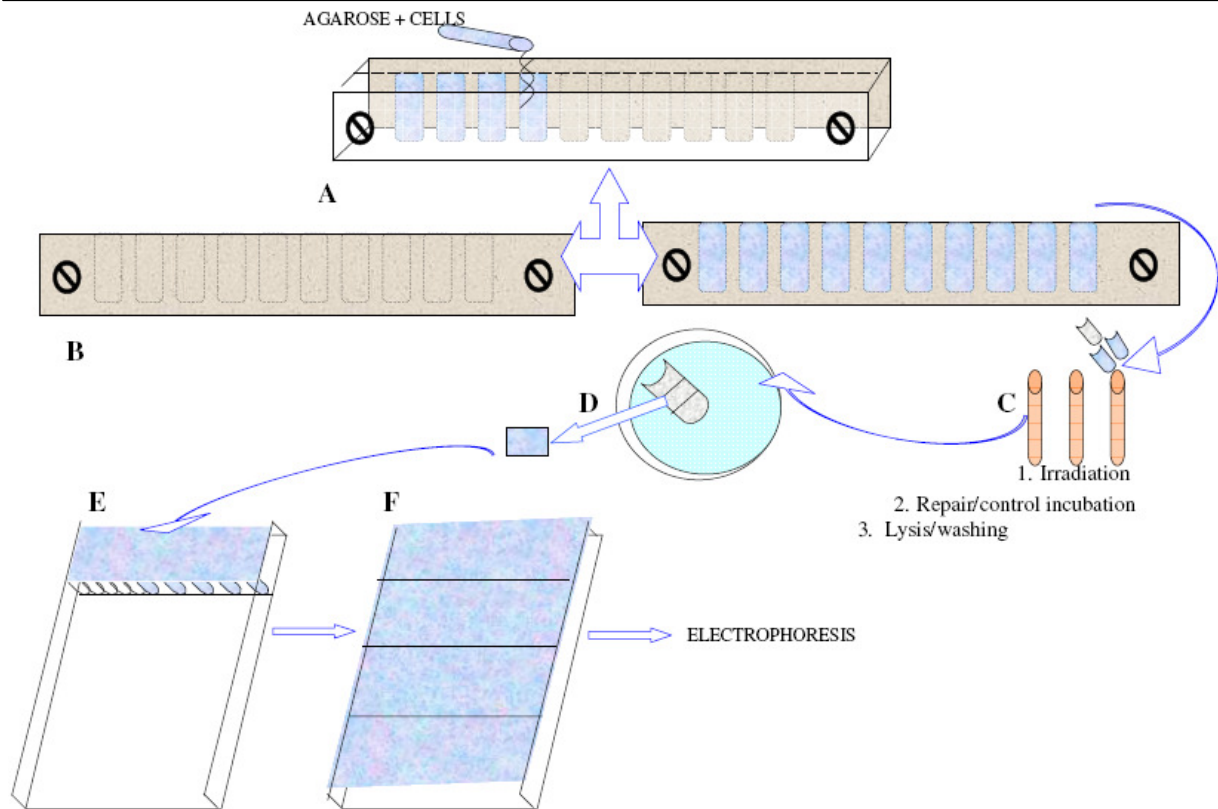


**Figure 2.2. The scheme of preparation of samples and gel for PFGE**

**A:** The procedure of preparation of PFGE samples included pouring of LMP agarose/cells mixture into the prepared custom-designed moulds

**B:** After agarose solidification the moulds were opened and prepared plugs were transferred into 50 ml Falcons filled with ice-cold media (repair and controls); induction plugs to 15 ml Falcons filled with ice-cold media

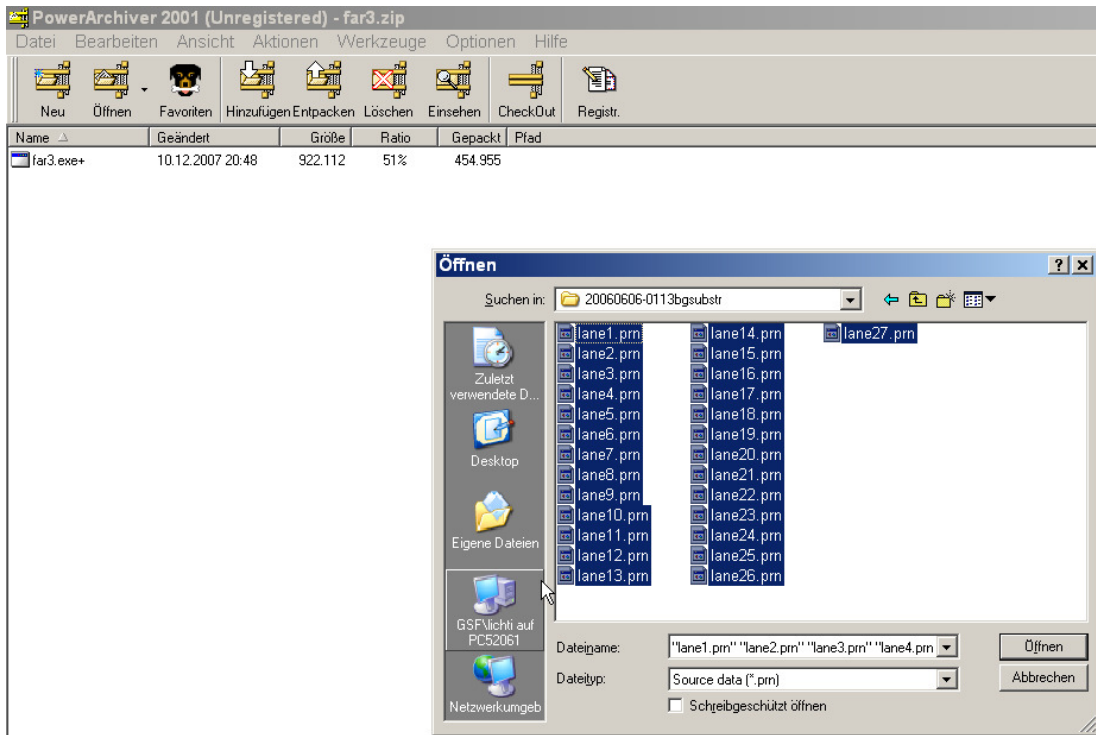
**C:** Samples were irradiated and left for incubation (repair and controls). Induction samples were equilibrated with ice-cold EDTA and further lysed. At repair time intervals the procedure was repeated with respective repair/control plugs

**D:** Samples were cutted to have pieces of 5 mm x 10 mm x 1 mm size.

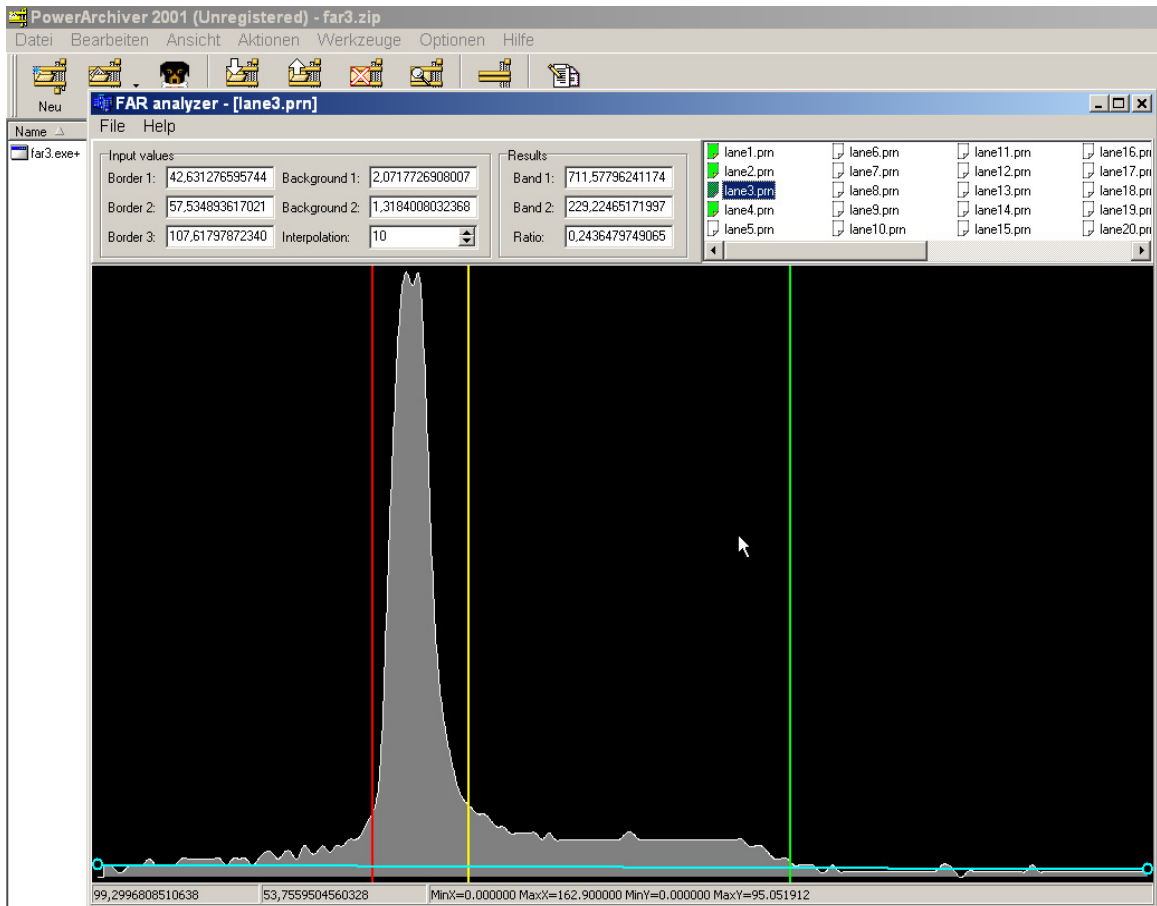
**E:** The custom-designed comb was applied. Boiled and pre-cooled agarose was poured into the chamber, forming the niches for the first row. The prepared plugs were inserted, comb was applied lower on the gel and agarose was further poured into the space between previous row and the comb.

**F:** After the gel was completed, rest of the agarose was poured over the chamber. Solidified gel was subjected to electrophoresis.

A



B



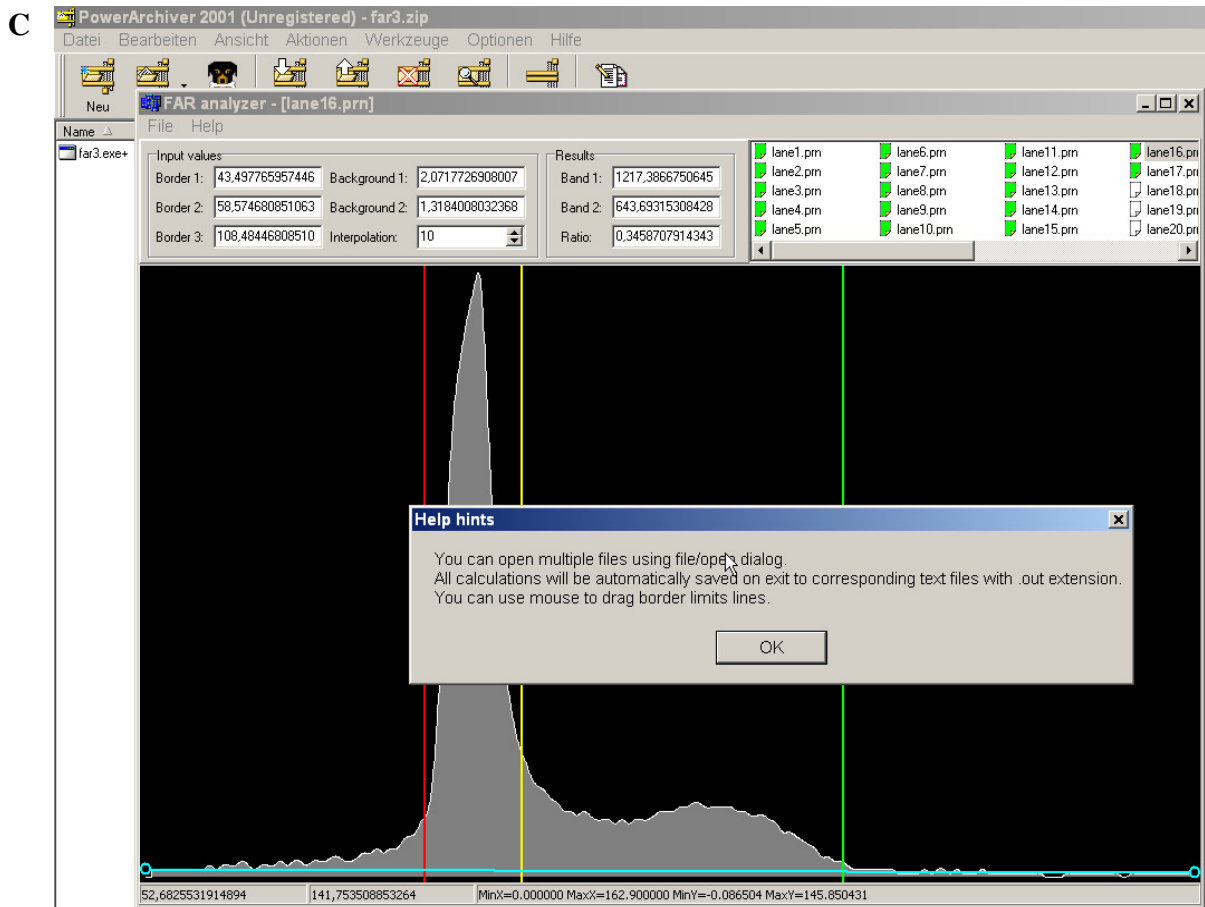


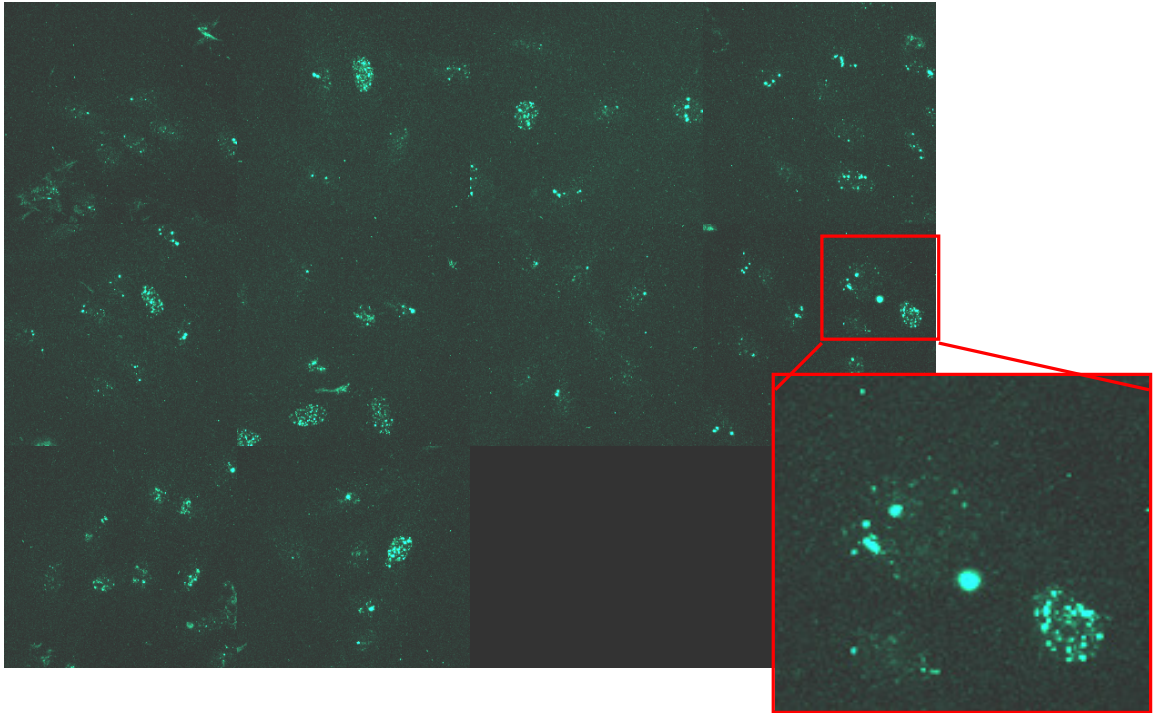
**Figure 2.4. The interface features of the FAR3 Software for analysis of FAR values in PFGE**

**A:** Starting the program and opening of one of the experimental data sets. As image indicate, all lines on the gel might be selected

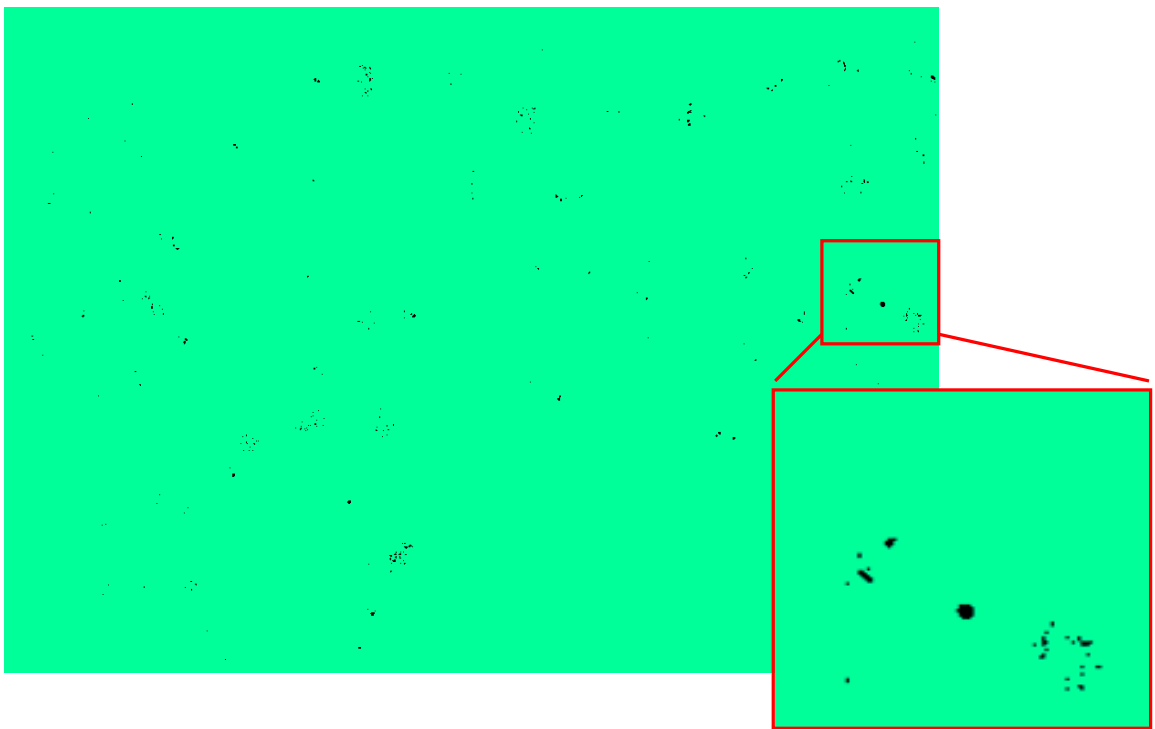
**B:** The definition of the band borders and background subtraction is performed. The value of DNA migrated into the plug is determined automatically

**C:** The program includes ‘user-friendly’ features like saving of measured values and depicting them when the user returns to the file

**A**



**B**



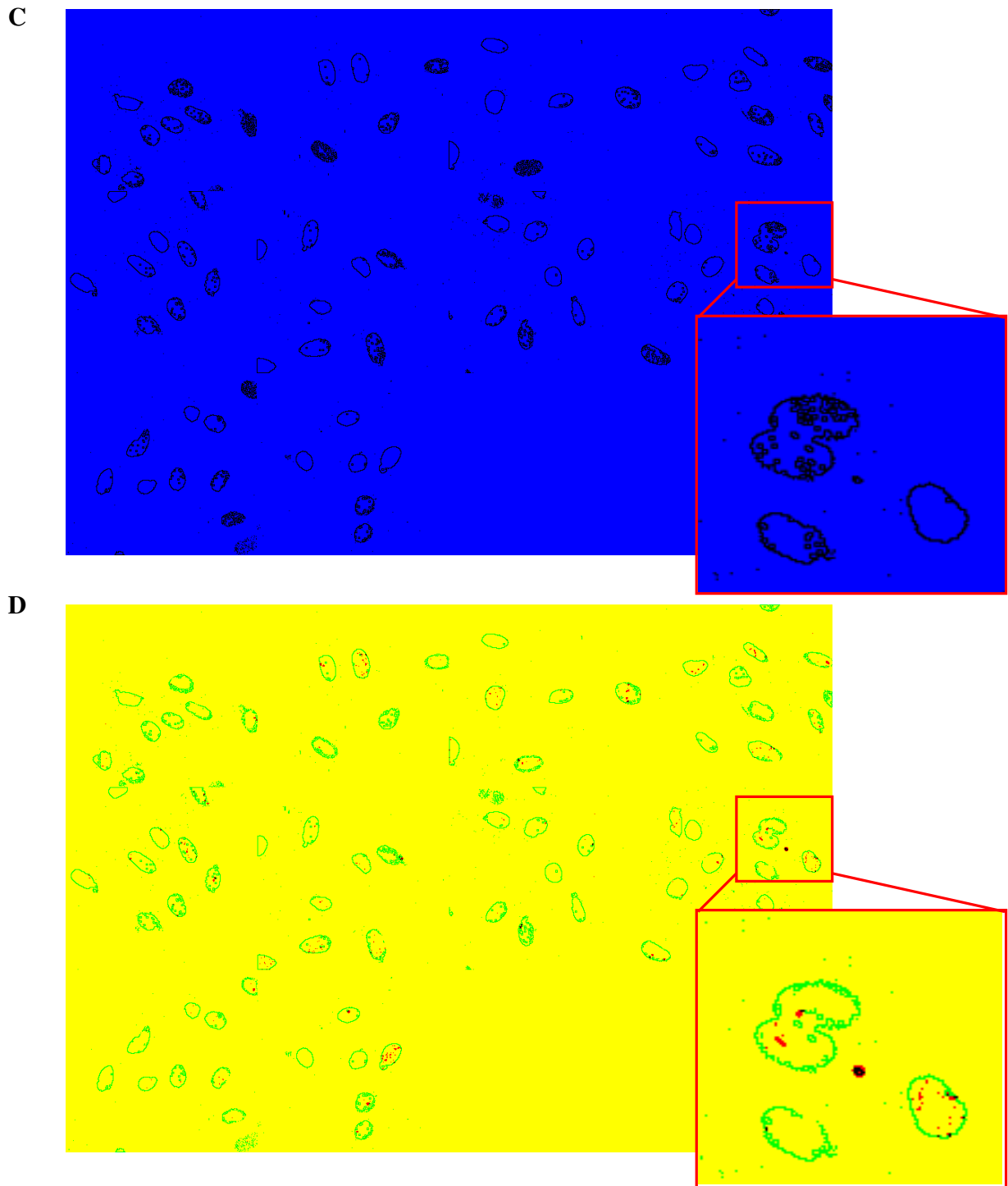


**Figure 2.7. Computerized image analysis**

**A:** stacking together 10 images with Alexa488 signal ( $\gamma$ H2AX) into one picture.

**B:** setting signal threshold and converting image to binary for further automatic quantification of foci number and size, which is performed by ImageJ Software.

**C:** outlining of DAPI signal (nuclear stain) to have nuclear shape and counting number of cells per analyzed image.

**D:** DAPI outlines (C) were merged with thresholded  $\gamma$ H2AX image (B).

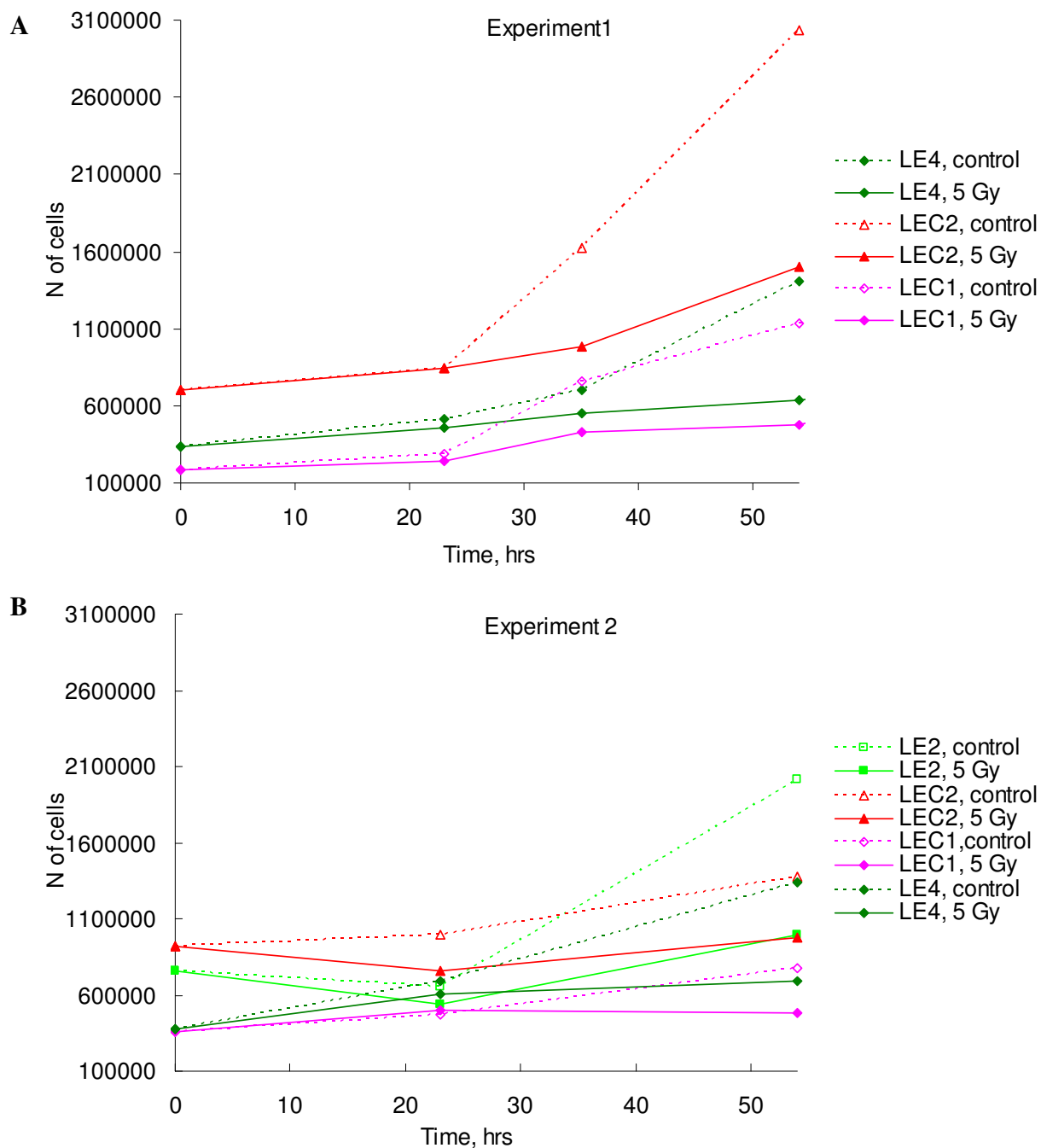


**Figure 3.2. Growth curves derived from two independent experiments with controls and irradiated with 5 Gy LEC and LE fibroblasts**

For growth curves analysis at least two counts were taken from two - three plates of each irradiated with 5 Gy and control (sham-irradiated) LEC and LE cell lines at 0, 23,5, and 54 hrs. Mean values of counts were plotted against time for measured controls and irradiated cells.

**A:** data evaluated in Experiment 1; **B:** data evaluated in Experiment 2.

**Table 3.7. PFGE experimental data**

Repair, FAR Time, min	EXP1, LEC2	EXP2, LEC1	EXP3, LEC1	EXP4, LEC2	EXP5, LEC1	EXP6, LEC1	mean	SEM	n	mean	SEM	n
0	62.5	61.7	51.9	62.4	44.8	55.9	56.5	2.9	6.0	54.4	5.2	3.0
0.25	n.d.	39.2	34.4	n.d.	n.d.	n.d.	36.8	n.d.	2.0	n.d.	n.d.	n.d.
0.5	50.0	40.7	29.5	43.5	26.6	n.d.	38.1	4.4	5.0	38.3	n.d.	n.d.
1	n.d.	19.8	18.2	n.d.	21.4	31.2	22.7	2.9	4.0	26.3	n.d.	n.d.
1.5	34.8	19.6	15.0	26.8	20.7	n.d.	23.4	3.4	5.0	27.8	n.d.	n.d.
2	29.6	12.2	13.7	23.0	17.7	23.9	20.0	2.7	6.0	23.7	3.4	3.0
3	27.6	8.1	n.d.	20.8	17.5	n.d.	18.5	4.1	4.0	22.6	n.d.	2
4	22.2	n.d.	n.d.	17.3	15.7	23.3	19.6	1.8	4.0	20.4	2.4	3.0
6	25.6	n.d.	n.d.	15.2	14.2	26.0	20.3	3.2	4.0	21.9	3.9	3.0
<hr/>												
Control, FAR Time, min	EXP1, LEC2	EXP2, LEC1	EXP3, LEC1	EXP4, LEC2	EXP5, LEC1	EXP6, LEC1	mean	SEM	n	mean	SEM	n
0	2.9	3.0	3.0	4.9	4.0	8.0	4.3	0.8	6.0	5.0	1.5	3.0
0.25	n.d.	5.9	3.9	n.d.	n.d.	n.d.	4.9	n.d.	2.0	n.d.	n.d.	n.d.
0.5	3.8	2.7	4.9	5.3	5.1	2.3	4.0	0.5	6.0	3.7	0.8	3.0
1	n.d.	4.1	3.1	5.6	6.2	4.2	4.6	0.6	5.0	5.2	n.d.	n.d.
1.5	5.5	4.1	4.2	7.5	7.8	2.3	5.2	0.9	6.0	5.2	1.6	3.0
2	7.1	3.5	5.3	9.3	8.0	5.6	6.5	0.9	6.0	6.9	0.7	3.0
3	8.5	5.3	n.d.	11.7	8.7	5.2	7.9	1.2	5.0	7.5	1.1	3.0
4	10.0	4.8	n.d.	10.7	9.7	13.0	9.6	1.3	5.0	10.9	1.1	3.0
6	7.7	n.d.	n.d.	8.4	11.6	16.3	11.0	2.0	4.0	11.9	2.5	3.0
<hr/>												
Induction Dose, Gy	EXP1, LEC2	EXP2, LEC1	EXP3, LEC1	EXP4, LEC2	EXP5, LEC1	EXP6, LEC1	mean	SEM	n	mean	SEM	n
0	4.7	1.8	3.5	4.5	1.5	6.0	3.7	0.7	6.0	4.07	1.34	3.00
5	7.9	5.1	6.1	8.5	5.1	9.5	7.0	0.8	6.0	7.50	1.29	3.00
10	n.d.	6.3	9.5	14.1	11.6	15.3	11.4	1.6	5.0	13.45	n.d.	n.d.
15	21.6	n.d.	8.3	n.d.	n.d.	19.3	16.4	4.1	3.0	20.45	n.d.	n.d.
20	22.2	n.d.	19.5	n.d.	17.7	22.8	20.6	1.2	4.0	20.90	1.61	3.00
30	32.1	27.5	n.d.	22.2	n.d.	32.5	28.6	2.4	4.0	32.30	n.d.	n.d.
40	47.2	40.3	n.d.	45.6	18.4	42.9	38.9	5.3	5.0	36.17	8.97	3.00
50	51.5	45.7	n.d.	62.6	28.0	64.2	50.4	6.6	5.0	47.90	10.60	3.00
60	n.d.	52.4	n.d.	63.5	41.4	n.d.	52.4	6.4	3.0	41.40	n.d.	n.d.
70	n.d.	68.5	n.d.	n.d.	53.6	55.2	59.1	4.7	3.0	54.40	n.d.	n.d.
<hr/>												
Repair, Gy-eqv Time, min	EXP1, LEC2	EXP2, LEC1	EXP3, LEC1	EXP4, LEC2	EXP5, LEC1	EXP6, LEC1	mean	SEM	n	mean	SEM	n
0.0	56.5	61.0	n.d.	43.5	63.0	54.0	55.6	3.4	5.0	57.8	2.7	3.0
0.3	n.d.	35.5	n.d.	n.d.	n.d.	n.d.	35.5	n.d.	1.0	n.d.	n.d.	n.d.
0.5	39.1	36.5	n.d.	32.5	28.5	n.d.	34.2	2.3	4.0	33.8	n.d.	2.0
1.0	n.d.	17.5	19.0	n.d.	16.0	31.5	21.0	3.6	4.0	23.8	n.d.	2.0
1.5	25.3	20.5	15.8	16.0	14.5	n.d.	18.4	2.0	5.0	19.9	n.d.	2.0
2.0	20.3	16.0	13.0	12.5	14.0	22.5	16.4	1.7	6.0	18.9	n.d.	3.0
3.0	17.0	7.0	n.d.	10.7	11.0	n.d.	11.4	2.1	4.0	14.0	n.d.	2.0
4.0	n.d.	n.d.	n.d.	7.8	9.5	10.5	9.3	0.8	3.0	10.0	n.d.	2.0
6.0	n.d.	n.d.	n.d.	9.5	11.0	5.0	8.5	1.8	3.0	8.0	n.d.	2.0

Repair, FAR Time, min	EXP1, LE2	EXP2, LE2	EXP3, LE4	EXP5, LE1	EXP6, LE2	mean	SEM	n	mean	SEM	n
0.0	57.2	63.6	44.6	52.3	47.5	53.0	3.4	5.0	52.3	2.8	3.0
0.3	43.2	50.3	35.1	n.d.	n.d.	42.9	4.4	3.0	43.2	n.d.	1.0
0.5	33.3	35.0	25.9	30.4	n.d.	31.2	2.0	4.0	31.9	n.d.	2.0
1.0	23.6	27.5	17.7	n.d.	n.d.	22.9	2.8	3.0	23.6	n.d.	1.0
1.5	n.d.	22.4	13.1	18.3	n.d.	17.9	2.7	3.0	18.3	n.d.	1.0
2.0	22.3	n.d.	15.3	n.d.	15.8	17.8	2.3	3.0	19.1	n.d.	2.0
3.0	15.9	n.d.	3.8	n.d.	n.d.	9.8	n.d.	2.0	15.9	n.d.	1.0
4.0	9.6	n.d.	n.d.	7.1	16.5	11.1	2.8	3.0	11.1	2.8	3.0
6.0	12.5	n.d.	n.d.	15.0	17.2	14.9	1.4	3.0	14.9	1.4	3.0
Control Time, min	EXP1, LE2	EXP2, LE2	EXP3, LE4	EXP5, LE1	EXP6, LE2	mean	SEM	n	mean	SEM	n
0.0	3.5	5.8	6.5	4.2	5.6	5.1	0.6	5.0	4.4	0.6	3.0
0.3	1.8	6.7	6.3	n.d.	n.d.	4.9	1.6	3.0	1.8	n.d.	1.0
0.5	5.1	7.5	6.2	2.0	n.d.	5.2	1.2	4.0	3.6	n.d.	2.0
1.0	4.7	7.0	7.7	n.d.	3.1	5.6	1.1	4.0	3.9		
1.5	4.2	6.5	7.3	5.5	n.d.	5.9	0.7	4.0	4.9	n.d.	2.0
2.0	3.3	7.1	8.2	9.0	6.6	6.8	1.0	5.0	6.3	1.7	3.0
3.0	2.8	n.d.	6.5	n.d.	n.d.	4.7	n.d.	2.0	2.8	n.d.	1.0
4.0	5.5	4.2	n.d.	9.3	8.2	6.8	1.2	4.0	7.7	1.1	3.0
6.0	6.9	n.d.	n.d.	9.2	10.4	8.8	1.0	3.0	8.8	1.0	3.0
Repair, Gy-eq Time, min	EXP1, LE2	EXP2, LE2	EXP3, LE4	EXP5, LE1	EXP6, LE2	mean	SEM	n	mean	SEM	n
0.0	58.2	60.5	57.0	51.0	43.0	53.9	3.2	5.0	50.7	4.4	3.0
0.3	39.0	n.d.	42.5	n.d.	n.d.	40.8	n.d.	2.0	39.0	n.d.	1.0
0.5	24.0	28.0	33.5	40.0	n.d.	31.4	3.5	4.0	32.0	n.d.	2.0
1.0	19.0	22.8	18.0	n.d.	26.0	21.5	1.8	4.0	22.5	n.d.	2.0
1.5	n.d.	19.0	11.0	19.0	n.d.	16.3	2.7	3.0	19.0	n.d.	1.0
2.0	14.5	n.d.	13.5	n.d.	15.6	14.5	0.6	3.0	15.1	n.d.	2.0
3.0	11.5	n.d.	n.d.	n.d.	14.3	12.9	n.d.	2.0	12.9	n.d.	2.0
4.0	3.0	n.d.	n.d.	0.0	12.6	5.2	3.8	3.0	5.2	3.8	3.0
6.0	4.0	n.d.	n.d.	5.5	9.3	6.3	1.6	3.0	6.3	1.6	3.0
Induction Dose, Gy	EXP1, LE2	EXP2, LE2	EXP3, LE4	EXP5, LE1	EXP6, LE2	mean	SEM	n	mean	SEM	n
0	0.1	2.2	5.1	4.0	6.8	3.6	1.2	5.0	3.63	1.94	3.00
5	3.8	6.9	4.7	7.4	10.0	6.6	1.1	5.0	7.07	1.80	3.00
10	10.5	12.0	9.4	9.6	13.6	11.0	0.8	5.0	11.23	1.21	3.00
15	15.3	n.d.	11.3	19.8	n.d.	15.5	2.5	3.0	17.55	2.25	2.00
20	25.3	19.1	n.d.	26.8	18.3	22.4	2.1	4.0	23.47	2.62	3.00
30	33.4	30.9	n.d.	30.4	n.d.	31.6	0.9	3.0	31.90	1.50	2.00
40	41.9	n.d.	24.9	51.1	41.6	39.9	5.5	4.0	44.87	3.12	3.00
50	52.5	52.3	34.5	56.7	57.6	50.7	4.2	5.0	55.60	1.57	3.00
60	55.7	n.d.	42.0	n.d.	64.2	54.0	6.5	3.0	59.95	4.25	2.00
70	64.6	68.2	n.d.	48.3	n.d.	60.4	6.1	3.0	56.45	8.15	2.00

Table contains the data from the respective PFGE experiments and gel images evaluation. The number of respective experiment and evaluated cell line (p7-p12) is shown **A, B, C, D** – LEC data set; **E, F, G, H** – LE data set. Red colour indicates the respective experimental data, which subsequently show statistically significant difference in repair as expressed in FAR. **A, E**: fraction of activity released (FAR) values of repair; **B, F**: FAR values of control; **C, G**: FAR values of induction; **D, H**: Gy-equivalents.

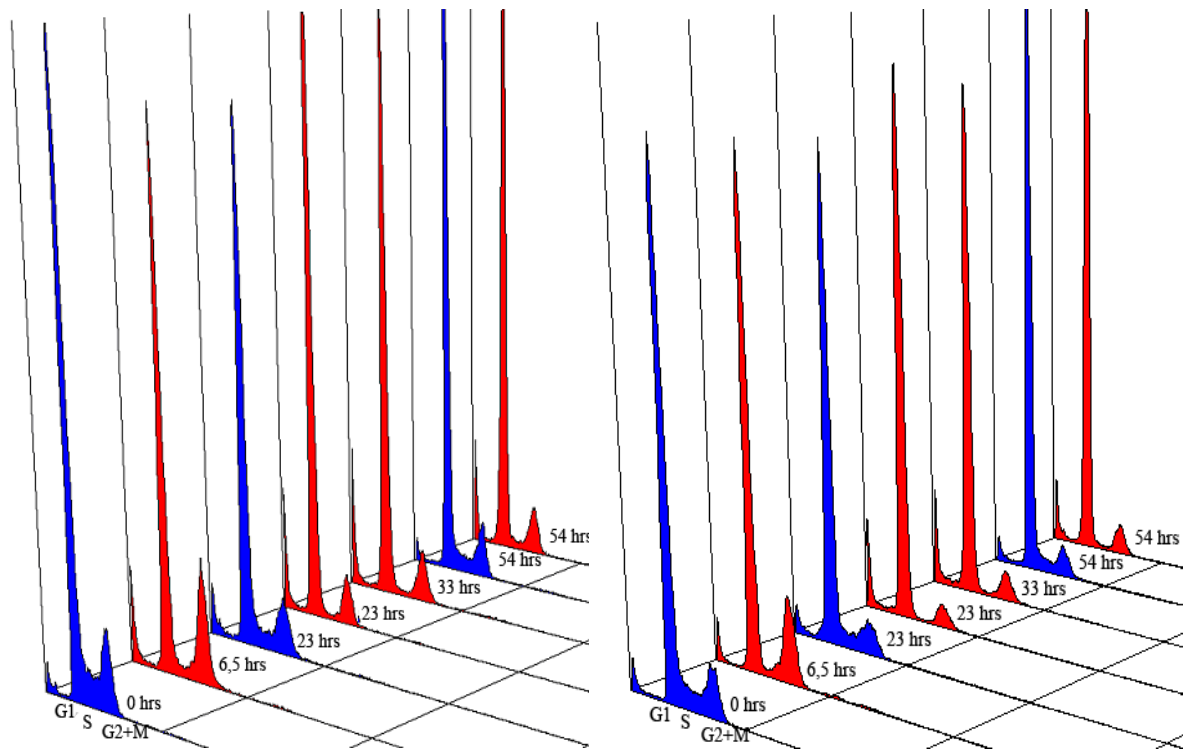


**Figure 3.16. Overlaid DNA distribution histograms showing cell cycle progression of LE-4 and LEC-1 cells after 5 Gy of IR**

Plates with cells in exponential growth were harvested at 6,5 hours, 23 hours, 33 hours, 54 hours after 5 Gy (LEC-1-filled red colour) of ionizing radiation as well as controls (LE4-filled blue colour) at 0 hours, 23 hours, 54 hours.



**Figure 3.23. The genetic map of the locus was constructed with UCSC Genome Browser (<http://genome.ucsc.edu/>)**

**A:** gaps in the assembly;

**B:** Known genes based on UniProt, RefSeq, GenBank mRNA;

**C:** orthologous RefSeq genes (not all are shown);

**D:** N-Scan gene predictions, Rat mRNAs from GeneBank;

**E:** spliced ESTs;

**F:** conservation in vertebrates



**Figure 3.27. The sequencing electropherograms of the intron-exon boundaries with insertion of extra G**

The intron-exon boundaries of Gata-2 were analysed. The SNP was detected (marked yellow). The arrow sign shows the exon/intron boundary.

## CURRICULUM VITAE

### PERSONAL DATA

Name Alesia N. Ivashkevich  
Date of birth 13.10.1978  
Nationality Belarussian  
Business address 9 Princes Street Fitzroy, Victoria 3065 Australia  
Private address 52/9 Arthur Street South Yarra, Victoria 3141 Australia  
Telephone + 61 3 9288 2480  
Fax + 61 3 9416 2676  
Email: aivashkevich@svi.edu.au olesya\_ivashkevich@hotmail.com

### CURRENT POSITION

05.01.2008- present Research Officer, St Vincent's Institute, Molecular Genetic Group  
09. 2004- 10.2008 PhD student, Institute for Pathology, GSF- National Research Center for Environment and Health, Neuherberg, Germany (LMU)  
Research project: Characterization of the cellular radiosensitivity phenotype in LEC rats (publication in preparation)

### WORK EXPERIENCE

09.2003-09.2004 Research Assistant, Institute of Pathology, GSF, Germany. Study of mutation in EYL (eyeless) mouse (publication in preparation)  
10.2002-06.2003 Research assistant, including teaching at Laboratory of Molecular Markers, International Sakharov Environmental University, Minsk, Belarus

### EDUCATION

09.2001-09.2002 MSc from University College of London, London, UK. European Master of Science Course in Radiation Biology for postgraduates (<http://www.graylab.ac.uk/usr/mscourse/home.html>)  
Practical project 'Mutation frequency in human mitochondria following treatment with ionizing radiation' was done at Institute of Radiobiology, GSF; National Research Center for Environment and Health, Neuherberg, Germany  
09.1996-07.2001 Masters degree in Environmental Medicine and Radiobiology International Sakharov Environmental University, Minsk, Belarus (<http://www.iseu.by/eng/index.html>)  
Chair of Environmental Medicine and Radiobiology  
Specialization Medical Ecology

Title of Diploma work 'Study of glycosylation of isoforms of thyroxin-binding globulin in ecologically induced pathologies'.  
Supervisor: Associate Professor, Ph.D. Anna G. Lapko

09.1986-07.1996

Primary/Secondary School, Luninetz, Belarus

## **ATTENDED MEETINGS**

Lorne Genome Conference, February, 2008, Australia

Workshop 'Responses to DNA damages' (Environmental Health Programme) March, 2007, GSF, oral presentation

53<sup>rd</sup> Radiation Research Society Meeting, 2006, Philadelphia, Pennsylvania, USA, poster presentation

2<sup>nd</sup> EU-USA Workshop 'System level understanding of DNA damage responses', 2005, Stowe, Vermont, USA, poster presentation

## **PUBLICATIONS**

Bull Exp Biol Med, 2001. May; 131 (5): 487-9. Isoforms of thyroxin-binding globulin as markers of ecologically induced pathologies. Lapko AG, Golovaty AS, Kononko ON (Ivashkevich), Torbashevich ES, Milyutin AA.

## **AWARDS AND SCHOLASHIPS**

2001

First Diploma for student work, ISEU, Minsk

09.2001-09.2002

FRIEDERICUS FOUNDATION travel scholarship covering expenses on MSc in Radiobiology

## **ADDITIONAL TRAININGS AND COURSES**

PCR training course, Fast - Real-time PCR, Applied Biosystems, 2005 – Primer design, Set-up, optimisation and troubleshooting Real-Time PCR

European School of Genetic Medicine, 7<sup>th</sup> Course in Bioinformatics for Molecular Biologist, Bertinoro, Italy, 2007 – included lectures on pathway analysis, transcriptional regulation, available databases, machine learning, expression analysis, ncRNA and practical workshops

'Clear writing for Science Publications', May 2007, GSF

Dateiname: INVESTIGATION INTO THE CELLULAR  
RADIOSENSITIVITY OF THE LEC RAT AND ANALYSIS OF CANDIDATE  
GENES.doc

Verzeichnis: C:\Dokumente und Einstellungen\Alesia\Desktop

Vorlage: C:\Dokumente und  
Einstellungen\Alesia\Anwendungsdaten\Microsoft\Templates\Normal.dot

Titel: INVESTIGATION INTO THE CELLULAR  
RADIOSENSITIVITY OF THE LEC RAT AND ANALYSIS OF CANDIDATE  
GENES

Thema:

Autor: Alesia Ivashkevich

Stichwörter:

Kommentar:

Erstelldatum: 12.03.2009 1:10

Änderung Nummer: 2

Letztes Speicherdatum: 12.03.2009 1:10

Zuletzt gespeichert von: Alesia

Letztes Druckdatum: 12.03.2009 1:12

Nach letztem vollständigen Druck

Anzahl Seiten: 165

Anzahl Wörter: 108,898 (ca.)

Anzahl Zeichen: 579,342 (ca.)